NANYANG TECHNOLOGICAL UNIVERSITY

MOLECULAR STUDIES OF THE SEVERE ACTUE RESPIRATORY SYNDROME CORONAVIRUS ENVELOPE PROTEIN

LIAO YING

SCHOOL OF BIOLOGIAL SCIENCES

2007

Molecular Studies of the Severe Acute Respiratory Syndrome Coronavirus Envelope Protein

Liao Ying

School of Biological Sciences

A thesis submitted to the Nanyang technological University
in fulfillment of the requirement for the degree of
Doctor of Philosophy

2007

MOLECULAR STUDIES OF THE SEVERE ACTUE RESPIRATORY SYNDROME CORONAVIRUS ENVELOPE PROTEIN

LIAO YING

SCHOOL OF BIOLOGIAL SCIENCES

NANYANG TECHNOLOGICAL UNIVERSITY

2007

This dissertation is dedicated to those people in my life who have made it possible, especially to my parents, my husband, and my son.

Acknowledgements

When I sat down to decide who to acknowledge for their help with this work, I began to realize just how much help and encouragement I had received during the past five years. I am certainly indebted to a number of people in more ways than I can adequately recognize here. However, I would like to express my heartfelt thanks to those who have helped me to reach this point.

There are number of people who have helped me both personally and professionally over the years. Their help has taken me to complete my Ph.D. First of all, I would like to express my deepest appreciation to my supervisor, Dr. Dingxiang Liu, for his excellent scientific and technical guidance. His patience and remarkable insight into the scientific enterprise have been invaluable to me over the years. I have special thanks to my co-supervisor Prof. James P. Tam. He gave me the opportunity to pursue research work and provided me with an environment that fostered independent work and thought. I will be always be grateful the help he has given to me. I would also like to thank Dr. Alex Gong for his help with scientific discussion. I have greatly benefited from his collaborative work and friendly encouragement.

There were a number of pals and colleagues in Dr. Liu's lab and Prof. Tam's lab with whom I worked closely and would like to acknowledge here. They are Chen Bo, Frank Li Qisheng, Ji Zhe, Lv Yanning, Wang Jibin, Wang Li and Yuan Quan. I deeply appreciate their constant help and friendship over the past five years.

My family is the source of all my strength, without them I could not have achieved my goal. They have always encouraged me to do my best. Thanks to them for their emotional support and encouragement throughout the long process. My husband has done more than anyone else to help me complete this work. He led me walk into the biological scientific door and gave me much help in the beginning stage of this work. He gave me confidence and strength when I depressed. Without his support, I cannot image I will reach this point.

Finally, thanks to all members in my dissertation committee for their valuable comments and suggestions.

This work was supported by the Agency for Science, Technology and Research, Singapore, and grants from the Biomedical Research Council, Agency for Science, Technology and Research, Singapore.

ABSTRACT

To promote viral entry, replication, release, and spread to neighboring cells, many cytolytic animal viruses encode small hydrophobic transmembrane proteins termed viroporins with potential to form hydrophilic ion channels in host cell membranes and to modify host cell membrane permeability during virus life cycles. In this study, we demonstrate that the envelope (E) protein of severe acute respiratory syndrome coronavirus (SARS-CoV) possessed viroporin activities. Initially, the SARS-CoV E protein was inducibly expressed in *E. coli* cells, leading to the arrest of bacterial growth and cell permeabilization to different compounds, such as a translation inhibitor hygromycin B, and the substrate of β-galactosidase, ONPG. Mammalian cells were also readily permeabilized to hygromycin B by the expression of E protein. Immunofluorescent staining and cell fractionation studies demonstrated that this protein was an integral membrane protein and mainly located to the perinuclear region. No obvious positive immunofluorescent staining was observed on the cell surface. Cross-linking study showed that E protein could self-associate to form dimers, trimers, tetramers, and pentamers by both disulfide bond formation and hydrophobic interaction. Systematic mutagenesis studies confirmed that the putative N-terminal transmembrane domain (9-37 amino acids) was essential for the membrane-permeabilizing activity. SARS-CoV E protein contains three cysteine residues (C40, C43 and C44) adjacent to the C-terminal end of the transmembrane domain. In *E. coli* cells, C40 and C44 residues were able to form disulfide bond, thus helped E protein to oligomerize and played a crucial role in membrane-permeabilizing activity. However, in mammalian cells, all three cysteine residues were modified by palmitates, removal of them rendered no effect on the

ion channel activity, although they also participated in disulfide bond formation. It suggested that the cysteine residues could stabilize the E protein oligomers in mammalian cells. N-linked glycosylation was also found on asparagine 66 at the C-terminal region. The disulfide bond, the palmitoylation and the N-linked glycosylation didn't play a role in the E protein viroporin activity, suggesting the N-terminal transmembrane domain was sufficient to oligomerize to form ion channels in mammalian cells. This finding endows E protein a new function in addition to its well known role in virion assembly and morphogenesis. Further exploration of E protein ion channel activity by introducing deletion or systematic mutations of E protein into SARS-CoV genome may help characterize the role of E protein in virus life cycle and screen anti-SARS drugs.

Table of contents

List of Tables

List of Figures

List of abbreviations

aa……..…amino acids

A…….alanine

C……cysteine

BCoV……...bovine coronavirus

bp…….base pair

CCoV……...canine coronavirus

CoV…….coronavirus

CPEs…….....cytopathic effects

DMEM…….. ...dulbecco's modified eagle medium

DTT……...dithiothreitol

E protein……..coronavirus envelope protein

ER……..endoplasmic reticulum

FBS…….. fetal bovine serum

FCoV…….feline enteric coronavirus

HCV…….. .....heptatis C virus

HCoV……..human coronavirus

HE…….haemagglutinin

HIV-1……..…….human immunodeficiency virus type 1

HR…….heptad repeat

IBV……...infectious bronchitis virus

Kb……kilo-base

kDa……...kilo-dalton

M protein……..membrane protein

MHV…….mouse heptatis virus

ml…….miniliter

mM……. minimolar

N48……..asparagine 48

N66……. asparagine 66

N protein……...coronavirus nucleocapsid protein

nsp…….....non-structural protein

nt……nucleotide

µl……microliter

ONPG……..orth-nitro-phenyl-beta-D-galactopyranoside

ORFs……..open reading frames

PAGE…….polyacrylamide gel electrophoresis

PBS……. **…….**phosphate buffered saline

PFU……plaque forming unit

S protein……spike protein

SARS …….severe acute respiratory syndrome

SARS-CoV…….severe acute respiratory syndrome coronavirus

SDS……...sodium dodecyl sulfate

TCoV……...turkey coronavirus

TGEV……...transmissible gastroenteritis virus

TRSs……transcription regulating sequences

UTR.……...untranslated region

v/v…….volume/volume

w/v……..weight/volume

vTF7-3…….. vaccinia virus-T7

CHAPTER 1

INTRODUCTION AND LITERATURE REVIEW

1.1. The *coronaviridae*

1.1.1. Coronavirus and disease

Coronaviruses are a group of enveloped, large positive-stranded RNA viruses. They are classified as a genus, Coronavirus, which, together with the genus Torovirus, constitutes the family *Coronaviridae* (Siddell, 1995).

Coronaviruses were first isolated from chickens in 1937. There are now approximately 28 species in this family, which infect not only human but also a wide range of animals, including pigs, cows, rats, mice, dogs, cats, chicken, and turkeys. Some are serious veterinary pathogens and a threat to the farming industry, especially in chickens. Economically significant coronaviruses of farm animals include infectious bronchitis coronavirus (IBV), porcine coronavirus (transmissible gastroenteritis, TGEV) and bovine coronavirus (BCoV). IBV is the first coronavirus to be discovered in 1937. It causes respiratory disease in young chickens that can progress to fatal bacterial infection and causes a sudden drop in egg production, which rarely returns to normal in mature egg-layers. Both TEGV and BCoV cause diarrhea in young animals. Canine coronavirus (CCoV) causes a highly contagious intestinal disease worldwide in dog. The murine coronavirus mouse hepatitis virus (MHV) A59 strain causes diseases in mice including diarrhea, hepatitis, splenolysis, immunological dysfunction, and acute or chronic neurological disorders in mice. It causes frequent enzootics in colonies of laboratory mice.

For many years, only two human coronaviruses (HCoV-229E and HCoV-OC43) were known. They are responsible for upper respiratory tract infections in children, and more than 30 % of reported common colds in the winter and early spring seasons (Estola, 1970; Tyrrell *et al.*, 1993; Engel, 1995; Vabret *et al.*, 2003; van Elden *et al.*, 2004). Recently, 3 novel human coronaviruses have been discovered, which added the human coronaviruses list to 5. SARS-CoV was identified and characterized as the etiological agent of severe acute respiratory syndrome (SARS) of human in 2003 (Peiris *et al.*, 2003; Rota *et al.*, 2003), following the worldwide outbreak of SARS initially in Asia. Compared to other members of the coronavirus family, this contagious isolate was uniquely dangerous. A fourth human coronavirus named HCoV-NL63, was discovered in 2004 in a young child with bronchitis in the Netherlands (Hoek *et al.*, 2004; Pyrc *et al.*, 2004). Recent reports from several countries including Australia, Belgium, Japan, France, Canada and China indicate that the virus has spread worldwide (Bastien *et al*., 2005a, b). This virus uses ACE2 as the cellular receptor just like SARS-CoV (Hofmann *et al.*, 2005), and is found mainly in young children, elderly and immunocompromised patients with acute respiratory illness during the winter season (Arden *et al.*, 2005; Bastien *et al.*, 2005a; Bastien *et al.*, 2005b; Chiu *et al.*, 2005; Ebihara *et al.,* 2005; Moes *et al.*, 2005; Suzuki *et al.*, 2005; Vabret *et al.*, 2005; Zhu *et al.*, 2006). Early in 2005, a research team from the University of Hong Kong reported the finding of the fifth human coronavirus belonging to group 2 in two pneumonia patients, and subsequently named it HKU1 (Woo *et al.*, 2005a; Woo *et al.*, 2005b).

1.1.2. Classification of coronavirus

Over the past decades, coronavirus were mainly regarded as veterinary importance until the emergence of SARS caused by a coronavirus. It alerted people to take the coronavirus more seriously since the deadly SARS-CoV in human is probably originated from a wild animal reservoir. The SARS epidemic puts the animal coronaviruses in the spotlight and stimulates a burst of new research to understand the basic replication mechanisms of this family. Coronavirology has advanced significantly in the past few years.

Three groups of coronaviruses have been classified by sequence homology (Table 1-1). Almost all group 1 and group 2 viruses have mammalian hosts. Viruses of group 3, by contrast, have been isolated solely from avian hosts. HCoV-229E and HCoV-NL63 belong to group 1 (Hoek *et al.*, 2004), whereas HCoV-OC43 and the newly identified HKU1 belongs to group 2 (Woo *et al.*, 2005b). Group 3 contains all the avian coronaviruses. On the basis of the analysis of a subset of structural gene sequences (Eickmann *et al.*, 2003), the regions of gene 1a and of RNA secondary structures in the 3' untranslated regions (3' UTRs) of the genome (Goebel *et al.*, 2004) supported that SARS-CoV belongs to group 2. As of March 2005, most virologists who study coronaviruses would classify SARS-CoV as under group 2 or as closely related to group 2 coronaviruses.

Three distinct bat coronaviruses have also been isolated following SAR outbreak: two are members of group 1, and the third, in group 2, is a likely precursor of the human SARS-CoV (Lau *et al.*, 2005; Li *et al.*, 2005; Poon *et al.*, 2004). In addition, new IBV-like viruses have been found to infect geese, pigeons, and ducks (Jonassen

et al., 2005). With each group, viruses are identified by their natural hosts and by nucleotide sequence and serological relationships. Most coronaviruses naturally infect only one species or several closely related species.

Table 1-1. Coronavirus groups, their main representatives, hosts, and principal associated diseases.

Group	Virus	Host	Disease
1	Feline enteric coronavirus (FCoV)	Cat	systemic enteritis
	Feline infectious peritonitis coronavirus (FIPV)	Cat	peritonitis
	Canine coronavirus (CCoV)	Dog	Enteritis
	Transmissible gastroenteritis virus (TGEV)	Pig	Enteritis
	Porcine epidemic diarrhea virus (PEDV)	Pig	Enteritis
	Porcine respiratory coronavirus (PRCoV)	Pig	Respiratory infection
	Human coronavirus (HCoV)-NL63	Human	Respiratory infection
	Human coronavirus (HCoV)-229E	Human	Respiratory infection
	Bat-CoV-61	Bat	
	Bat-CoV-HKU2	Bat	
2	Murine hepatitis virus (MHV)	Mouse	Respiratory infection/enteritis/hepatitis/encephalitis
	Rat coronavirus (RCoV)	Rat	Respiratory infection
	Sialodacryoadenitis coronavirus (SDAV)	Rat	
	Bovine coronavirus (BCoV)	Cow	Respiratory infection/enteritis
	Hemagglutinating encephalomyelitis virus (HEV)	Pig	Enteritis
	Human coronavirus (HCoV)-OC43	Human	Respiratory infection
	Human coronavirus –HKU1	Human	Respiratory infection

	SARS coronavirus (SARS-CoV)	Human	Severe acute respiratory syndrome
	Bat-SARS-CoV	Bat	
	Puffinosis coronavirus (PCoV)	Puffin	
	Equine coronavirus (ECoV)	Horse	
	Canine respiratory coronavirus (CRCoV)	Dog	
3	Infectious bronchitis virus (IBV)	Chicken	Respiratory infection/enteritis
	Turkey coronavirus (TCoV)	Turkey	Enteritis
	Pheasant coronavirus (PhCov)	Pheasant	
	Goose coronavirus (GCoV)	Goose	
	Pigeon coronavirus (PCoV)	Pigeon	
	Duck coronavirus (DCoV)	Duck	

1.1.3. Coronavirus genome and virion structure

Coronaviruses contain the largest single-stranded positive-sense RNA genome of 27 to 31 kb. The 5' end of the coronavirus genome is capped, and the RNA starts with a leader sequence of 65-98 nucleotides, which is also present at the 5' end of subgenomic mRNAs, followed by 200-400 nucleotides UTR that harbors several *cis*-acting sequences and structural elements functioning in viral replication and transcription. At the 3' end of the genome is the 3' UTR of 200-500 nucleotides followed by a poly (A) tail. Almost two-thirds of the entire RNA genome is occupied by the polymerase gene, which comprises two overlapping ORFs, 1a and 1b. The downstream ORF 1b is translated by translational read through, using a ribosomal frame-shifting mechanism. The result of the ribosomal frame-shifting mediated translation of the polymerase gene is the synthesis of two large polyproteins, pp1a and pp1ab. They range from 440 to 500 kDa and from 740 to 810 kDa, respectively, and they are co-translationally processed by two or three internally contained proteases. The final products of the autoproteolytic cleavage of pp1a and pp1ab are 16 nonstructural proteins, designated nsp1-nsp16. Nsp1- nsp11 are derived from pp1a, whereas nsp1-nsp10 and nsp12-nsp16 are derived from pp1ab. All products processed from pp1a are common to those processed from pp1ab except for nsp11, which is an oligopeptide generated when ribosomal frameshifting does not occur. For IBV, which lacks a counterpart of nsp1, there are 15 final cleavage products with numbering beginning with nsp2. They are responsible for RNA replication and transcription. The products of pp1a appear to function to prepare the cell for infection and to assemble the machinery for RNA synthesis. Then, the products that are unique to pp1ab carry out the actual catalysis of RNA replication and transcription.

The coronavirus main genes are arranged in the order 5'-pol-S-E-M-N-3'. The genes located downstream of pol1b are expressed from a 3'-coterminal nested set of subgenomic RNAs. Besides the polymerase gene and the genes encoding structural proteins, coronavirus have additional genes encoding accessory proteins that are located among genes encoding S, E, M and N. These accessory genes differ distinctly in their nature and genomic positions among coronavirus groups, and are group-specific. In all cases examined, through natural or engineered mutants, accessory genes have been found to be nonessential for viral replication in tissue culture. This dispensability has been determined for the 2a and HE genes of MHV (de Hann *et al*., 2002; Schwarz *et al*., 1990), genes 4 and 5a of MHV (de Hann *et al*., 2002; Weiss *et al*., 1993; Yokomori and Lai, 1991), the I gene of MHV (Fisher *et al*., 1997), gene 7 of TGEV (Ortego *et al*., 2003), genes 7a and 7b of FIPV (Haijema *et al*., 2003, 2004), and genes 5a and 5b of IBV (Casais *et al*., 2005; Yount *et al*., 2005). For gene 4 (Ontiveros *et al*., 2001) and the I gene (Fischer *et al*., 1997) of MHV, and for gene 7b of FIPV (Haijema *et al*., 2003), selective knockout produced no detectable effect on pathogenesis in mice or cats, respectively. By contrast, disruption of gene 7 of TGEV greatly reduced viral replication in the lung and gut of infected piglets (Ortego *et al*., 2003). In the same manner, viruses with knockouts of either the 3abc gene cluster or genes 7a and 7b in FIPV produced no clinical symptoms in cats at doses that were fatal with wild-type virus (Haijema *et al*., 2004). The deletion of genes 2a and HE, or of genes 4 and 5a, in MHV completely abrogated the lethality of intracranial infection in mice (de Hann *et al*., 2002). Even a single point mutation in MHV ORF 2a, which had no effect in tissue culture, was found to greatly attenuate virulence *in vivo* (Sperry *et al*., 2005). In a study that took the opposite approach to assessing accessory protein

function, it was discovered that engineered insertion of gene 6 of SARS-CoV greatly enhanced the virulence of an attenuated variant of MHV (Pewe *et al*., 2005).

Coronavirus particles are enveloped, spherical, 80-120 nm in diameter, with approximately 20-nm-long spikes protruding from their envelope that contribute to a corona appearance under the electron microscope. The envelope carries three structural proteins: S protein, M protein and E protein. In a few species of group 2 coronaviruses, there is an additional structural protein: haemagglutinin (HE) (esterase). The RNA genome is associated with a basic phosphoprotein, N protein. The long, flexible, helical nucleocapsid lies within the envelope obtained by budding from intracellular membranes (Lai and Cavanagh, 1997). The schematic representation of the coronavirus virion was shown in Fig.1-1**.**

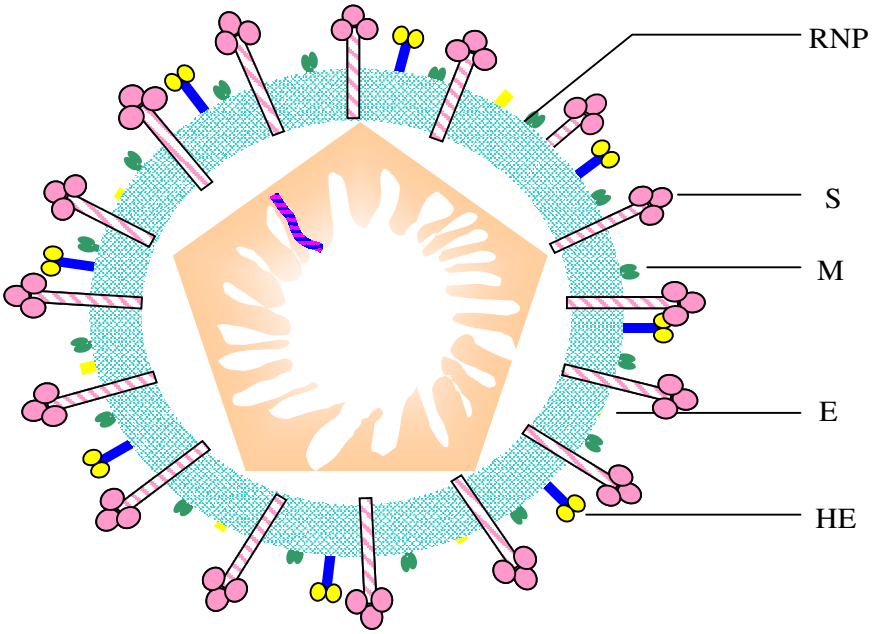
RNP
S
M
E
HE

1.1.4. Coronavirus structural proteins

1.1.4.1. Spike (S) protein

Entry of enveloped animal viruses into host cells requires fusion between the viral membrane and a cellular membrane, either the plasma membrane or an internal membrane. Coronavirus rely on the membrane-bound S protein to bind and enter host cells. The S protein is the structural protein which inserts into the envelope and constitutes the petal-shaped spikes. It is large, ranging from some 1160 (IBV) to 1452 amino acids (FCV) and has many N-linked glycosylation sites (21 to 35). Co-translational N-linked glycosylation is an essential requirement for proper folding, oligomerization, and transport of the S protein. Inhibition of this modification resulted in the production of spikeless, noninfectious virion (de Hann and Rottier, 2005). Folding of the S protein involves in the addition of oligosaccharides and the formation of many intracellular disulfide bonds. Sufficiently folded S protein monomers were associated in the endoplasmic reticulum (ER) to form trimers (Delmas and Laude, 1990; Lin *et al*., 2004).

In infected cells, S protein trimers interact with M protein (Opstelten *et al*., 1995) and perhaps also interacted with E protein, and migrate to the virus assembly site. A proportion of the S protein is transported to the plasma membrane where it causes cell-cell fusion. The S protein can be cleaved in the middle site of the protein by furin-like enzyme into amino-terminal S1 subunit and carboxy-terminal S2 subunit. The cleavage has been demonstrated for S proteins from group 2 and group 3 coronaviruses (MHV, BCoV, IBV and TCoV), but not for group 1 coronaviruses (HCoV-229E, TGEV, FCoV and CCoV) (Lai and Cavanagh, 1997). The resulting S1

and S2 subunits remain noncovalently linked, S1 subunit constitutes the globular head, whereas S2 subunit forms stalk-like region of the spike. The variable S1 subunit is responsible for receptor binding, which is the major determinant for virus entry and host range restriction. The conserved S2 subunit anchors in membrane by the transmembrane domain and contains two coiled-coils heptad repeat (HR) regions at the ectodomain. The two HRs are capable of self-assembly into stable antiparallel oligomeric complex and are involved in the membrane fusion process (de Hann and Rottier, 2005).

1.1.4.2. Membrane (M) protein

The M protein is the most abundant protein in the viral envelope and is essential for virus maturation. It is 221-260 aa in length and is glycosylated at its amino-terminal region. The M protein spans the viral membrane three times, leaving the small N-terminal domain on the outside of the virion. The glycan provides the virion with a diffuse, hydrophilic cover on its outer surface. The C-terminal half of the protein is inside the virion. In TGEV virions some of the M proteins have their cytoplasmic tail exposed to the outside. In infected cells, the M protein was observed to accumulate in the membranes of the budding compartment as well as in the Golgi compartment. It interacts with every other virion component, such as E protein, S protein, HE protein and N protein and self-interacts to drive the coronavirus envelope assembly. The group 1 and group 3 coronaviruses and SARS-CoV M proteins contain N-linked sugars, the group 2 coronaviruses M protein are O-glycosylated (Rottier, 1995), whereas the MHV-2 M protein carries both O- and N-linked sugars (Yamada *et al*., 2000). The distinct conservation of N-linked and O-linked glycosylation among

the M protein of different groups of coronaviruses suggests that the presence of particular type of carbohydrates is beneficial to the interaction between the virus and the host cells. The M protein of MHV and TGEV has an additional biological activity in induction of α-interferon and may play a role in viral pathogenesis (Charley and Laude, 1988; de Hann, *et al*., 2003; Laude *et al.*, 1992).

1.1.4.3. Envelope (E) protein

The E protein is a small hydrophobic protein (76-109 aa) and was identified as a virion component relatively late, due to its low abundance and small size (Godet *et al*., 1992; Liu and Inglis, 1991; Yu *et al*., 1994). Despite the low homology in the primary amino acid sequence, the E proteins from different coronaviruses share similarities in biochemical properties and biological functions. The N-terminal portion of E protein consists of a short 7-9 aa hydrophilic region and a 21-29 aa hydrophobic region spanning the membrane once or twice, followed by a cysteine-rich region, an absolutely conserved proline residue, and a hydrophilic tail. In the coronavirus-infected cells, E protein was localized to intracellular membranes as well as plasma membrane (Godet *et al*., 1992; Yu *et al*., 1994). Functionally, coronavirus E protein plays a pivotal role in viral morphogenesis, assembly and budding. It has been shown that E and M proteins are the only two viral proteins absolutely required for virion assembly. Co-expression of E and M proteins, from MHV (Bos *et al*., 1996; Vennema *et al*., 1996), TGEV, BCoV (Baudoux *et al*., 1998), IBV (Corse and Machamer, 2000, 2003; Lim and Liu, 2001) and SARS-CoV (H V*et al*., 2004) resulted in nucleocapsid independent formation of virus-like particles (VLPs), roughly the same size and shape as virions. Additionally, MHV and IBV E protein expressed alone resulted in the

release of vesicles containing the E protein, while expression of M protein alone did not produce vesicles containing the M protein (Corse and Machamer, 2000; Lim and Liu, 2001; Maeda *et al*., 1999). IBV M protein and E protein have been found to interact *via* their cytoplasmic domain in pre-Golgi compartments (Lim and Liu, 2001). Recently, MHV infectious clone was constructed with the entire E gene deleted. The virus was able to replicate to low titer and had a small plaque phenotype, indicating that E protein although important, is not essential for MHV replication *in vitro* (Kuo and Masters, 2003). In contrast, E protein expression was essential for TGEV replication, as deletion of the TGEV E protein was lethal and replication of the mutant virus could be rescued by TGEV E protein expressed *in trans* (Ortego *et al*., 2002). The E protein most likely functions to generate the required membrane curvature or serve to close the neck of the budding particle as it pinching off the membrane (Vennema *et al*., 1996). Furthermore, MHV and SARS-CoV E proteins were shown to induce apoptosis in E protein-expressing cells (An *et al*., 1999, Yang *et al*., 2005). Over-expression of Bcl-2 oncoprotein suppresses MHV E-protein-induced apoptosis, indicating that initiation of the apoptotic pathway began upstream of Bcl-2 (An *et al*., 1999). Over-expression of anti-apoptotic protein Bcl-xL also inhibited SARS-CoV E protein induced apoptosis by the interaction between Bcl-xL and E protein C-terminal BH3-like region (Yang *et al*., 2005).

Furthermore, coronavirus E protein shares structural similarities with small hydrophobic membrane proteins found in other enveloped viruses. Examples are HIV-1 Vpu protein, alphavirus 6K protein, and influenza virus M2 protein. These proteins belong to viroporin family and can modify membrane permeability, help the efficient release of progeny virus (Gonzalez and Carrasco, 2003).

1.1.4.4. Haemagglutinin (HE) protein

The HE protein is found in group 2 coronavirus and little is known about the functions of this protein. This 60-69 kDa glycoprotein exists as a disulfide-linked dimer anchored in the viral membrane by C-terminal transmembrane domain region, leaving a short cytoplasmic tail of about 10 residues inside the virion. It binds to 9-O-acetyl groups from sialic acid-containing cellular receptor glycoproteins and cleaves the acetyl group from the neuraminic acid. It is believed that the HE protein may mediate viral adherence to the intestinal wall through the specific yet reversible binding to mucopolysaccharide. Several studies have indicated the HE protein may play a role in pathogenicity (Brian *et al.*, 1995).

1.1.4.5. Nucleocapsid (N) protein

The N protein is the most abundantly expressed viral protein in infected cells (Laude and Masters, 1995). They vary from 377 to 455 aa in length. Consistent with its role as an RNA binding protein, it is abundant of arginine and lysine residues therefore it is highly basic. N protein is the only coronavirus structural protein known to become phosphorylated. This modification does not seem to play a critical role in the regulation of virus assembly. Three structural domains in the N protein have been identified. The functions of the N-terminal conserved domains are not yet clear. The middle domain is an RNA-binding domain. The C-terminal domain may be involved in self-association to form the oligomers. Although the primary function of the N protein is the formation of the viral ribonucleoprotein complex, several studies indicate the protein may be multifunctional. In infected cells N protein was observed to be localized throughout the cytoplasm as well as the nucleolus. The IBV N protein

was found to interact with nucleolar antigens to affect the cell cycle (Chen *et al*., 2002). Recently, SARS-CoV N protein was shown to undergo posttranslational modification by sumoylation, which play certain roles in N protein self-oligomerization and in N protein-mediated interference of host cell division (Li *et al*., 2005). Although N protein lacks membrane-spanning domain, it was found to be associated with membrane and interacted with cellular proteins that play a role in coronavirus RNA replication and transcription. Therefore, N protein is a likely component of coronavirus replication and transcription complex. N protein can also interact with leader/TRS sequences and 3' UTR, suggesting it may play a role in the discontinuous transcription process (de Hann and Rottier, 2005).

The properties and functions of coronavirus structural proteins were summarized in Table 1-2.

Table 1-2. Properties and functions of coronavirus structural proteins

Spike glycoprotein (S)	Forms large spikes on virion surfaces Binds to specific cellular receptors Induces fusion of viral envelope with cell membranes May induce cell-cell fusion Binds to 9-O-acetylated neuraminic acid or N-glycolylneuraminic acid Induces neutralizing antibody Elicits cell-mediated immunity
Membrane glycoprotein (M)	Triggers virus particle assembly Determine virus budding site An integral membrane protein in the Golgi Interact with viral nucleocapsid Associate with virus envelope Forms the shell of internal viral core (of TGEV and MHV) Induces α-interferon
Envelope protein (E)	Triggers virus particle assembly Associates with viral envelope May cause apoptosis
Hemagglutinin-esterase glycoprotein (HE)	Forms small spikes on the virion surface of some coronaviruses Binds to 9-*O*-acetylated neuraminic acid

	Cause hemagglutination May cause hemadsorption Esterase cleaves acetyl groups from 9-*O*-acetyl neuraminic acid
Nucleocapsid phosphoprotein (N)	Binds to viral RNA Forms nucleocapsid Elicits cell-mediated immunity

1.1.5. Coronavirus replication cycle and virion assembly

The replication cycle starts with attachment of the virion by binding of the S1 subunit to cellular receptors. This interaction leads to fusion of the viral envelope with a cellular membrane. The coronavirus genomic RNA is then released by uncoating and becomes available for protein translation and subsequent RNA transcription. The positive-sense genome is translated into two large precursors (Pol1a and Pol1ab). The cleavage products (replicases) of the two precursors collectively constitute the functional replication–transcription complex. In the replication-transcription complex, the replicases use the genome as the template for the RNA synthesis, via negative-strand intermediates, of both progeny genomes and a set of subgenomic mRNAs. Genes located downstream of the pol1b gene are expressed from a 3′-coterminal nested set of subgenomic mRNAs, each of which additionally contains a short 5′ leader sequence derived from the 5′ end of the genome. The sites of leader-to-body fusion in the subgenomic RNAs occur at loci in the genome that contain a short run of sequences termed transcription regulating sequences (TRSs). TRSs are fairly well conserved within each coronavirus group and located upstream of each gene serve as signals for the transcription of the subgenomic RNAs. The leader sequence is joined at a TRS to all genomic sequence distal to that TRS by discontinuous transcription, most likely during the synthesis of negative-strand subgenomic RNAs. The negative-strand subgenomic RNA exists at a rate of a tenth to a hundredth as abundant as their positive-sense counterparts. In most cases, only the 5′-most gene of each positive-strand subgenomic RNA is translated.

After translation, multiple copies of the N protein package the progeny genomic RNA into a helical nucleocapsid in the cytoplasm. The structural proteins S, M, and E are inserted into the membrane of the rough endoplasmic reticulum (RER), from where they meet the nucleocapsid and assemble into particles by budding. The M protein plays a central role in this process through interactions with all viral assembly partners. It gives rise to the formation of the basic matrix of the viral envelope generated by homotypic and lateral interactions between M molecules, and it interacts with the envelope proteins E, S, and HE (if present), as well as with the nucleocapsid, thereby directing the assembly of the virion. Virions are transported out of the cell through the constitutive secretory pathway. The glycoproteins on their way being modified in their sugar moieties, whereas the S proteins of some but not all coronaviruses are cleaved into two subunits by furin-like enzymes. Finally, progeny virions are exported from infected cells by transport to the plasma membrane in smooth-walled vesicles, or Golgi sacs. The new infectious virions are enveloped with a lipid membrane containing three to four structural proteins, S protein, M protein, E protein and HE protein (in some coronaviruses of group 2). During infection of some coronaviruses, a fraction of S protein that has not been assembled into virions ultimately reaches the plasma membrane. At the cell surface S protein can cause the fusion of an infected cell with adjacent, uninfected cells, leading to the formation of large, multinucleate syncytia. This enables the spread of infection independent of the action of extra-cellular virus, thereby providing some measure of escape from immune surveillance.

The life cycle of coronavirus was shown in Fig. 1-2.

1.2. Severe acute respiratory syndrome (SARS)

Severe acute respiratory syndrome (SARS) was an atypical pneumonia that first appeared in November 2002 in Guangdong Province, the People's Republic of China. It was first reported in Asia in February 2003. Over the next few months, the illness spread rapidly to 29 countries in Asia, North America, South America, and Europe, via international travellers. According to the World Health Organization (WHO), within a matter of 8 months, a total of 8098 people worldwide became sick with SARS; 774 of these died (a mortality rate of near 10 %) (World Health Organization, http://www.who.int/csr/sars/country/en/). Fortunately, the spread of SARS was effectively prevented through global efforts, including quarantine, patient isolation, travel restrictions, and contact precautions. This highly contagious disease also called on the collaboration of the worldwide virologists.

Within four months after the first documented case, aggressive laboratory techniques, including microscopy, virus-specific microarray technology, RT-PCR and serological tests, identified the causative agent of SARS as a newly emerged coronavirus (Drosten *et al.*, 2003; Ksiazek *et al.*, 2003; Peiris *et al.*, 2003a). On April 7, 2003, WHO announced that it was agreed that a newly identified coronavirus is the major causative agent of SARS. On April 12, 2003, scientists working at the Michael Smith Genome Sciences Center in Vancouver, British Columbia, finished mapping the genetic sequence of the new coronavirus (Marra *et al.*, 2003). This was followed by an announcement on April 16, scientists at Erasmus University in Rotterdam, Netherlands confirmed that the virus causing SARS is indeed the new coronavirus. The sequence of the SARS coronavirus (SARS-CoV) was also confirmed by other

independent groups. By July of 2003, the WHO declared that the SARS epidemic had been officially controlled.

After the outbreak of SARS, much research efforts have been directed to understanding the SARS-CoV including characterization of the evolution of the virus in the human population, isolation of the virus from wild animals, the development of vaccines and the establishment of animal models suitable for evaluation of pathogenesis and immunity (Berger *et al.*, 2004; Christian *et al.*, 2004; Donnelly *et al*., 2004; Osterhaus *et al.*, 2004; Peiris *et al.*, 2004; Poon *et al.*, 2004; Ziebuhr, 2004; Cinatl *et al.*, 2005; Groneberg *et al*., 2005; Jiang *et al*., 2005; Tan *et al*., 2005; Weiss and Navas- Martin, 2005).

SARS-CoV infection results in an atypical pneumonia, characterized by a wide spectrum of symptoms, including fever, myalgia, malaise, dyspnea, lymphopenia and lower tract respiratory infection (Navas-Martin *et al*., 2004; Nie *et al*., 2003; Peiris *et al*., 2003b). Although the exact mechanism of death caused by SARS-CoV infection is unclear, Tsui *et al*. (2003) proposed a SARS disease model, consisting of three phases: (1) viral replication, (2) immune hyperactivity and (3) pulmonary destruction (Tsui *et al*., 2003). It has been strongly suggested that the hyperactive immune response to SARS-CoV infection may largely contribute to the advanced stages of SARS.

1.3. Severe acute respiratory syndrome coronavirus (SARS-CoV)

The genome of SARS-CoV is a 29727 nucleotide, positive-strand RNA. It contains 14 potential open reading frames (ORFs). Some of these ORFs encode for

proteins that are homologous to proteins found in all known coronaviruses, namely the polymerase proteins (ORFs 1a and 1b) and the four structural proteins: nucleocapsid protein, spike protein, membrane protein and envelope protein, and these proteins are expected to be essential for the replication of the virus. The remaining eight ORFs code for accessory proteins, varying in length from 39 aa to 274 aa, which are unique to SARS-CoV. The two strains, Urbani (Rota *et al*., 2003) and Tor2 (Marra *et al*., 2003), sequenced by two independent groups, differed by only 8 nucleotides. Likewise, when compared to the genome sequences of additional SARS-CoV isolates, little variations were observed, suggesting that the viral genome is highly stable during human transmission (Ruan *et al*., 2003). In contrast, when each gene of the SARS-CoV was compared to the corresponding genes of known coronavirus, there existed only 70 % or less identity (Holmes, 2003a). Analysis of human sera collected prior to the emergence of SARS showed no SARS-CoV-specific antibodies, indicating that SARS-CoV was new to the human population (Ksiazek *et al*., 2003; Peiris *et al*., 2003a; Peiris *et al*., 2003b).

The available data suggest that SARS-CoV did not arise by mutation of a human coronaviruses or by recombination between other coronaviruses; rather, SARS-CoV most likely evolved from a common coronavirus ancestor, remaining unidentified in an animal reservoir for an unknown period time prior to infecting human (Holmes, 2003b). Although the natural animal reservoir of SARS-CoV has yet to be formally identified, SARS-CoV like viruses have been isolated from Himalayan palm civets (*Payuma laravta*), raccoon dogs (*Nycereutes procynonoides*), Chinese ferret badgers (*Melogale moschata*) and bats (Guan, *et al*., 2003; Kan *et al*., 2005; Li, 2005; Lau, *et al*., 2005). When compared to the human SARS-CoV genome, all the animal isolates

retain a 29-nucleotide sequence that is not found in most human isolates; 5'-CCTACTGGTTACCAACCTGA ATGGAATAT-3', (residue 27869 to 27897) that is 246 nucleotides upstream of the start codon of the N gene (Guan *et al*., 2003). This deletion in the SARS-CoV strains results in two new ORFs (ORF 10 and ORF 11, encoding 8a, 8b), as compared to the one ORF present in the animal viruses. Furthermore, more recent studies report that ferrets and domestic cats are susceptible to SARS-CoV infection and capable of transmitting the virus to uninfected animals (Martina *et al*., 2003). These studies strongly suggest a possible route by which the first infected humans may have come in contact with animal SARS-CoV.

Epidemiological studies also revealed that it is likely that the SARS-CoV was transmitted from an animal source to the human population and this has happened at least twice, once in Guangdong (China) in November 2002, leading to the outbreak in the human population, and a second time in Guangzhou (China) in December 2003 to January 2004 (Song *et al*., 2005; Wang *et al*., 2005). The latter refers to the infection of four people who did not have any contact history with previously documented SARS cases, and no subsequent human-to-human transmission was reported (Liang *et al*., 2004). Sequence analysis of viruses isolated from these patients showed that they were not derived from the preceding epidemic in 2003 but rather suggested that these cases represented new zoonotic transmissions (Song *et al*., 2005; Wang *et al*., 2005). These findings indicate that the SARS-CoV is of animal origin and that its precursor is still present in animal populations, and underscore the potential for the re-emergence of SARS and the need for continuing research on the virus.

As shown in Fig. 1-3, the genome organization of SARS-CoV is typical of coronavirus, having a characteristic gene order 5'-poly-S-E-M-N-3' and short untranslated regions at both termini (Marra *et al*., 2003). Upon virus entry into cells, a 3′-coterminal nested set of 9 mRNAs is produced (Thiel, *et al*., 2003). The genome-length mRNA, mRNA1, somewhat resembled the polymerase encoded by group 2 MHV and BCoV and the group 3 IBV, expresses two overlapping replicase proteins in the form of polyproteins 1a (486 kDa) and 1a/b (790 kDa) (Thiel, *et al*., 2003). The polyproteins are subsequently processed into at least 16 putative nonstructural proteins (nsp1–nsp16) by virus-encoded proteases. The mature proteins comprise proteases, RNA-dependent RNA polymerase, and helicase, involving in the replication of viral genome and generating a nested set of subgenomic mRNAs to express all the other ORFs in the genome (Ziebyhr, 2004). Similar to group 3 coronavirus, SARS-CoV encodes a single papain-like protease.

Unlike group 2 coronavirus, SARS-CoV has no HE gene. The four structural proteins, arranged in the order 5′-S-E-M-N-3′, are encoded by subgenomic mRNA 2, 4, 5, and 9, respectively. The basic functions of these structure proteins are similar to those of other coronaviruses (Table 1-2). Spike protein of SARS-CoV can bind to two receptors, which are ACE2 (angiotensin-converting enzyme 2) and CD209L (also called L-SIGN, DC-SIGNR and DCSIGN2) (Li *et al*., 2003; Jeffers *et al*., 2004). Nucleocapsid protein of SARS-CoV was found to induce actin reorganization and apoptosis in Cos-1 cells in the absence of growth factors (Surjit *et al*., 2004), and inhibits the activity of Cyclin-Cyclin-dependent kinase complex and blocks S phase progression in mammalian cells (Surjit *et al*., 2006).

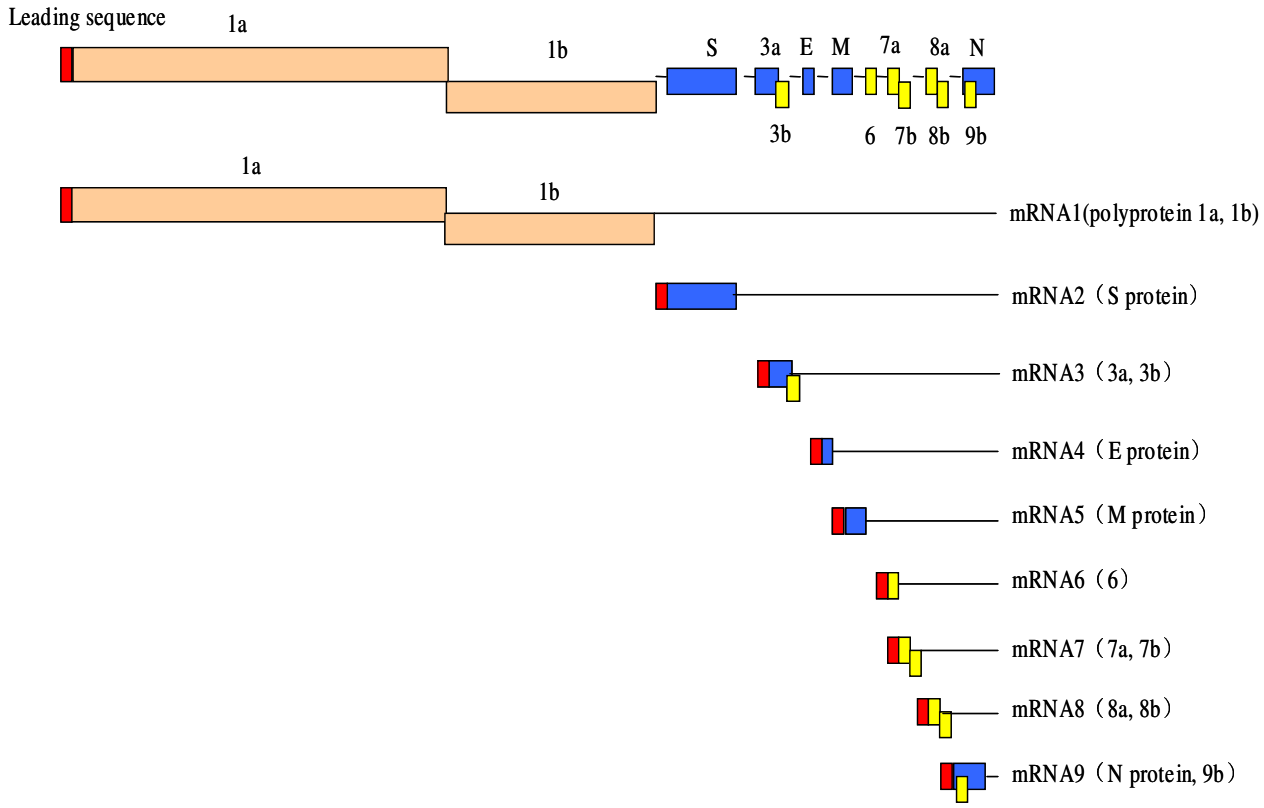

Fig. 1-3. The RNA genome organization and mRNAs of SARS-CoV. The SARS-CoV ORFs, genomic and subgenomic mRNAs are shown. Red box represent the 72-nucleotides leader sequence located at the 5' end of each viral mRNA. Like other coronaviruses, SARS-CoV uses a transcription attenuation mechanism to synthesize both full-length and subgenomic-length negative-strand RNAs which then function as templates for synthesis of full-length genomic mRNA and subgenomic mRNAs (Thiel *et al*., 2003; Yount *et al*., 2005). The first ORF is translated from the full-length genomic mRNA, while the remaining ORFs are translated from eight subgenomic RNAs synthesized as a nested set of 3-coterminal RNA species in which the leader RNA sequences on the 5-end of the genome are joined to the body sequences at distinct transcription regulatory sequences containing a highly conserved consensus sequence. Consequently, a total of nine mRNA species of different length were detected in SARS-CoV-infected cells and the SARS-CoV accessory proteins are encoded by subgenomic RNAs 3, 6, 7, 8 and 9. While subgenomic RNA 6 is mono-cistronic, subgenomic RNA 3, 7, 8 and 9 are bicistronic with the second ORFs (i.e. 3b, 7b, 8b and 9b) being expressed via an internal ribosomal entry mechanism or by a leaky ribosomal scanning mode of translation.

Each coronavirus encodes different number of accessory proteins and the predicted sequences of these proteins do not share high level of homology although there may be some degree of conservation within each subgroup of coronaviruses (Brown and Brierly, 1995). The SARS-CoV genome encodes eight putative accessory proteins (3a, 3b, 6, 7a, 7b, 8a, 8b and 9b) varying in length from 39 aa to 274 aa. Antibodies against all of the SARS-CoV accessory proteins were detected in the sera of SARS patients, suggesting that these proteins were expressed during infection *in vivo* (Chow *et al*., 2006; Guan *et al*., 2004a, Guan *et al*., 2004b; Guo *et al*., 2004; Qiu *et al*., 2005; Tan *et al*., 2004b; Yu *et al*., 2004; Zeng *et al*., 2004). While the SARS-CoV polymerase genes and structural proteins share some degree of sequence homology with those of other coronaviruses, the accessory proteins do not show significant homology, at the amino acid level, to viral proteins of known coronaviruses. These SARS-CoV accessory proteins, may offer clues to why SARS-CoV causes such a severe and rapid attack in humans. SARS was attenuated by deletion of 3a, 3b, 6, 7a and 7b suggesting that these proteins may function in modulating the intracellular environment for efficient virus replication or host response to infection (Yount *et al*., 2005).

SARS-CoV 3a protein is a group-specific accessory protein of 274 aa in length. It undergoes O-linked glycosylation and is incorporated into virus particles (Ito *et al*., 2005; Oostra *et al*., 2006). It is triple-spanning membrane protein with N-terminal ectodomain and a C-terminal endodomain (Tan *et al*., 2004c) and was located in Golgi complex and plasma membrane in infected cells and interacted with many structural proteins, such as S, M, E, and another newly defined structural protein 7a (Tan *et al*., 2004a). It was reported that 3a protein can form homo-tetramer complex

through interprotein disulfide bridges and form a potassium selective channel. Virus release is inhibited when 3a protein expression is blocked by the SiRNA (Lu *et al*., 2006).

The characteristics of SARS-CoV accessory proteins and their effects on cellular functions were summarized in Table 1-3.

Table 1-3. Characteristics of SARS-CoV accessory proteins and their effects on cellular functions

Viral gene	Genome position (bp)	No.of amino acids	Cellular localization	Characteristics of proteins and its effects on cellular functions
3a	25252-26076	274	Golgi apparatus and cell surface (Tan *et al*., 2004c; Ito *et al*., 2005)	Undergoes efficient endocytosis (Tan *et al*., 2004c) Interacts with structural proteins S, E and M, and accessory protein 7a (Tan *et al*., 2004c; Zeng *et al*., 2004) Is a structural protein inserted into the viral envelope with N terminal outside (Huang *et al.,* 2006; Ito *et al*., 2005; Shen *et al*., 2005) Is secreted out of the cell (Huang *et al*., 2006) Is O-linked glycosylated (Oostra *et al*., 2006) Up-regulates the expression of fibrinogen in lung cells (Tan *et al*., 2004c) Induce apoptosis via a caspase-8 dependent pathway (Law *et al*., 2005)
3b	25673-26137	154	Nucleus (Yuan *et*	Induce cell cycle arrest at the G0/G1

			al., 2005 c); Mitochondrial (Yuan *et al*., 2006)	phase and apoptosis (Yuan *et al*., 2005b)
6	27058-27249	63	Throughout cytoplasm and somewhat concentrated in the ER and Golgi apparatus (Geng *et al*., 2005; Pewe *et al*., 2005)	Enhance the virulence of an attenuated murine coronavirus (Pewe *et al*., 2005)
7a	27257-27625	122	Intermediate compartments between the ER and Golgi apparatus (Fielding *et al*., 2004; Nelson *et al*., 2005)	Is a viral structural protein (Huang *et al*., 2006) Has an Ig-like fold and showed structural similarity to D1 domain of ICAM-1 (Hanel *et al*., 2006; Nelson *et al*., 2005) Induces apoptosis (Kopecky-Bromberg *et al*., 2006; Tan *et al*., 2004a) Inhibits cellular protein synthesis (Kopecky-Bromberg *et al*., 2006) Induces the phosphorylation and activation of p38 mitogen-activated protein kinase (Kopecky-Bromberg *et al*., 2006) Blocks cell cycle progression at G0/G1 phase (Yuan *et al*., 2006b)

				Interacts with host protein SGT and viral structural proteins, E and M (Fielding *et al*., 2006)
7b	27622-27756	44	Not determined	Not determined
8a	27763-27882	39	Punctuate vesicle-like structures through the cytoplasm (unpublished data)	Not determined
8b	27848-28102	84	Punctuate vesicle-like structures through the cytoplasm (unpublished data)	Not determined
9b	28114-28410	98	Not determined	Not determined

1.4. viroporin

1.4.1. General introduction of viroporin

Viruses inflict a number of injuries as they infect susceptible cells. Injury to the cellular plasma membrane, such as alteration of plasma membrane permeability, is a common feature observed with most of animal viruses. Three groups of virus-encoded proteins are capable enhancing cell membrane permeability: (1) viroporins, which include a number of small, very hydrophobic integral membrane proteins (Carrasco *et al*., 1995; Gonzalez and Carrasco, 2003); (2) viral pore forming glycoproteins, some of them are endowed with membrane fusion activity (Carrasco *et al*., 1995; Nieva *et al*., 2004; Arroyo *et al*., 1995). In viruses which lack typical viroporin, the function could be replaced by the pore-forming glycoprotein. For instance, HIV-2 does not encode the viroporin Vpu, while its glycoprotein gp41 is endowed with membrane-permeabilizing capacity (Arroyo *et al*., 1995); (3) proteases, such as HIV-1 protease (Blancoet *et al*., 2003). The mechanism for the protease-induced effects on membrane permeability may be degradation of one or more proteins involved in maintenance of plasma membrane architecture.

Virus infection modifies membrane permeability at two well-defined stages, early and late in the lytic cycle (Carrasco *et al*., 1995). Early membrane modifications are induced by the process of virus entry and uncoating, and cause structural and functional changes in the membrane, resulting in an imbalance of ions in the cytoplasm, thus block host protein synthesis and lead to cell lysis. Usually it is caused by virion glycoprotein or viroporin located in the virus envelope. The extent and degree of these modifications vary with virus-cell system and with the multiplicity of

infection. Late membrane modifications require viral genes expression and are manifested as a general increase in permeability to ions and small molecules, but not to macromolecules, suggesting the formation of hydrophilic pores by viroporin in the intracellular membrane and plasma membrane.

Animal viruses could be divided into two groups according to the presence or absence of typical viroporin gene in their genome. Those viruses that code for a viroporin may also contain a glycoprotein with the capacity to alter membrane permeability. In this case, glycoprotein may exhibit their permeabilization capacity at either early or late stages of infection, while viroporin alters membrane permeability at late stage of infection. In virus species with no evident viroporin gene, other viral molecules such as glycoprotein or protease might take on its function.

Viroporins are small, highly hydrophobic, virus-encoded proteins which can modify the cell membrane permeability to ions or other small molecules. These proteins contain at least one transmembrane domain that interacts with and expands the lipid bilayer. Upon their insertion into membranes, the transmembrane domain tends to oligomerize to create a hydrophilic pore. The hydrophilic channels would allow low molecular weight hydrophilic molecules to cross the membrane barrier, leading to the disruption of membrane potential, collapse of ionic gradients, and release of essential compounds from the cell. Alterations in ion concentration would promote translation of viral *versus* cellular mRNAs, as translation of mRNAs from many cytolytic animal viruses is fairly resistant to high sodium concentrations (Carrasco *et al*., 1995; Gonzalez and Carrasco, 2003). Progressive membrane damage during viral replication cycles would also result in cell lysis, promote viral budding

and release, and facilitate virus spread to surrounding cells. A major activit

phosphorylated at serine residue 64 and palmitoylated at cysteine 50, penetrates the membrane to generate a N_{out}-C_{in} topology. Hydrophobic interaction and disulfide bond (Cysteine 17 and 19) link the monomers into homo-tetramer to create a proton conducting channel in the cell membrane (Holsinger and Lamb, 1991; Sakaguchi *et al.*, 1997). Histidine-37 and tryptophan-41 within the transmembrane domain has been found to be involved in the pH induced channel opening, acting as the gate that open and closes the pore (Okada *et al.*, 2001; Takeuchi *et al.*, 2003; Tang *et al.*, 2002). The main role of M2 protein is to serve as proton channel and is responsible for lowering the interior pH of the virion. The lower internal virion pH is thought to weaken protein-protein interactions between the viral matrix protein (M1), the ribonucleoprotein (RNP) core, and lipid bilayer, thereby freeing the viral genome from interactions with viral proteins and enabling the viral RNA segments to migrates to the host nucleus (the process of uncoating).

A second role for the M2 protein of some subtypes of virus is to shunt the pH gradient of the Golgi apparatus and prevent premature conformation change of the HA protein (Lamb *et al.*, 1994). Moreover, M2 protein impairs the correct glycosylation of the viral glycoprotein and slows traffic along the secretory pathway (Henkel and Weisz, 1998). The antiviral compound amantadine, which blocks the entry of influenza virus, selectively interacts with the M2 channel, inhibits the proton conductivity function of M2, and prevents virus uncoating, therefore inhibits virus infection. This drug also hinders the proper budding of virus particles (Wang *et al.*, 1993).

1.4.3. Human immunodeficiency virus type 1 (HIV-1) Vpu protein

HIV-1 Vpu is another viroporin well characterized. It is an 81 aa accessory protein and most likely to inserts into the membrane (N_{out}-C_{in}) to form a homo-pentamer pore. It has phosphorylation sites at serine residues 52 and 57. Two biological functions have been attributed to the Vpu protein: degradation of the viral receptor CD4 molecules in the ER and enhancement of virus release from infected cells. These two functions of Vpu are mechanistically independent. The rapid degradation of surface receptor CD4 in Vpu-expressing cells is caused by the formation of a multiprotein complex consisting of Vpu, CD4 and β-TrCP. CD4 was directed by β-TrCP into the proteasome-degradation pathway. Consequently, Vpu enhances the degradation of the CD4-gp160 complex and the release of gp160 (Willey *et al*., 1992a, b.). More gp160 cleavage products gp120 and gp41, which are required for the production of new virus particle, are produced.

Another function of Vpu is to increase progeny virus secretion from the infected cells (Schubert *et al*., 1996). This role is allocated to the N-terminal transmembrane domain, which can form ion channel with preference for cations and a minor indication of permeability of divalent (Ewart *et al*., 1996; Marassi *et al*., 1999; Schubert *et al*., 1996). Expression of Vpu in BHK cells leads to an increase of permeability of the cells to hydrophilic molecules, leading to the suggestion that Vpu may also act as a viroporin (Gonzalez and Carrasco, 1998). The Trp-22 within the transmembrane domain may functions as gate (Fischer and Sansom, 2002; Fischer, 2003; Gonzalez and Carrasco, 2003; Montal, 2003). However, there is still some questions remaining about the specificity of Vpu ion channel activity and it is unclear how Vpu as an ion channel could regulate the release of viral particles. Nevertheless, the fact that amiloride derivatives 5-(*N, N,* -hexamethylene) amiloride and 5-(*N, N,* -

dimethyl) amiloride block ion channel activity and inhibit enhancement of viral-like particles release provide further evidence for linking ion channel activity to virus release (Ewart *et al*., 2002).

Vpu may enhance viral release by counteracting human host cell restriction factors that interfere with HIV-1 particle release. Interestingly, Vpu was found to form heter-oligomers with an acid-sensitive K^+ channel-forming protein called TASK-1, whose expression inhibits HIV-1 release (Hsu *et al*., 2004). Functionally, Vpu expression suppressed TASK-1-specific current in a dose dependent manner. Intriguingly, the suppressing effect of Vpu on TASK-1 conductance appears to result not only from the formation of defective hetero-complexes between Vpu and TASK-1 but also from an acceleration of TASK-1 degradation during HIV-1 infection. Taken together, these findings raise the possibility that Vpu might enhance HIV-1 release by altering the activity of the TASK-1 K^+ channel and not form its reported intrinsic ion channel activity as previously thought.

1.5. Post-translational modifications

1.5.1. Palmitoylation

In eukaryotic cells, membrane proteins are synthesized in the rough ER. Here they enter the exocytic pathway along which they are transported to different locations in the cell or to the plasma membrane. During their synthesis and while being transported through compartments of the biosynthetic pathway, the proteins undergo various modifications including proteolytic cleavage, disulfide bond formation, glycosylation, and acylation.

There are three classes of protein fatty acylation in eukaryotic cells: N-myristoylation, S-palmitoylation, and N-palmitoylation. Protein N-myristoylation refers to the covalent attachment of myristate, a 14-carbon saturated fatty acid, to the N-terminal glycine of proteins. In most cases, N-myristoylation occurs cotranslationally and is a stable modification. S-palmitoylation is the reversible addition of 16-carbon saturated fatty acid palmitate or other long chain fatty acids to protein at cysteine residues via a thioester linkage. N-palmitoylation is the addition of palmitate via amide linkage to the N-terminal cysteine residues or glycine residues of proteins. While the biology and enzymology of protein N-myristoylation have been extensively characterized, the process is less well understood for protein palmitoylation.

Palmitoylation is known as a post-translational modification, it has been reported to occur at various subcellular sites, such as the ER, Golgi apparatus, and plasma membrane (Bijlmakers and Marsh, 2003; Veit and Schmidt, 1993), and is an enzymatic process, involving a palmitoyltransferases (PATs), enzymes that catalyze the attachment of palmitate to protein substrates (Dunphy *et al*., 2000; Leventis *et al*., 1997). Several palmitoyltransferase activities have been partially or completely purified (Resh, 1999), but their involvement in the palmitoylation of proteins under physiologic conditions remains to be established. It also has been observed that palmitoylation can occur spontaneously *in vitro* in the absence of cellular factors. It is believed that the initial attachment of palmitate occurs through a thioester linkage, followed by bond rearrangement to generate an amide-linked palmitate (N-palmitoylation). Thioester-linked palmitate can be removed from palmitoylated proteins by palmitoyl thioesterase.

Palmitoylation occurs on a wide variety of viral and cellular proteins, many of which play key roles in regulating cellular structure and function. The family of proteins modified with thioester-linked palmitate is large and diverse including cell receptors, viral membrane proteins, and a number of proteins involved in cell signaling or metabolic regulation. In transmembrane proteins, palmitoylation occurs on cysteine residues located in the border region between the transmembrane region and the cytoplasmic domain, helping protein to target to lipid membranes. In cytosolic proteins, palmitoylation occurs primarily at cysteine residues near the N- and C-terminus, although modification of cysteines located at internal sites or at sites adjacent to other hydrophobic lipids has also been documented.

The palmitoylated proteins were broadly classified into four types (Fig. 1-4) (Resh, 1999). Type I proteins consist of plasma membrane receptors and other membrane proteins that are typically palmitoylated on one or several cysteine residues located to or adjacent to or just within the transmembrane domain. Type II proteins are proteins modified with palmitate at N- or C- terminus. Type III proteins include members of the Ras family that are first modified with a farnesyl moiety in their C-terminal CAAX box. Prenylation of Ras is required for subsequent palmitoylation of the nearby cysteines in the C-terminal region. Type IV proteins are acylated with myristate and palmitate and nearly all contain the consensus sequence Met-Gly-Cys at their N-terminus. Myristoylation of Gly-2 facilitates palmitoylation of Cys-3.

The function of palmitoylation depends on the protein that is being considered. In general, it increases the hydrophobicity of proteins and contributes to their membrane association. However, the function of palmitoylation, ranges beyond a simple

membrane anchor. Trafficking of lipidated proteins from the early secretory pathway to the plasma membrane is dependent upon palmitoylation in many cases. In addition, modification with fatty acids impacts the lateral distribution of proteins on the plasma membrane by targeting them to lipid rafts. This process relies on the ability of the palmitate to fit well in an ordered lipid environment, and is not simply a function of hydrophobicity. Palmitoylation also plays an important role in subcellular trafficking of proteins between membrane compartments or subdomains with the same membrane, as well as in modulation protein-protein interactions and regulation of protein activity. Removal of palmitate from proteins occurs both constitutively and in response to signals. The reversibility of palmitoylation makes it an attractive mechanism for regulating protein activity. The regulation of palmitoylation occurs through the actions of protein acyltransferases and protein acythioesterases. This regulated modification acts much like protein phosphorylation. Depalmitoylation and repalmitoylation could provide a mechanism to regulate the binding of cytosolic proteins to membranes, or the segregating of proteins to microdomains, or the mediating of protein-protein interaction. For proteins involved in signal transduction, palmitate cycling is linked to proteins activation, or involved in controlling the access to specific substrates. In addition to cellular protein, a number of viral proteins have been found to be modified by palmitoylation.

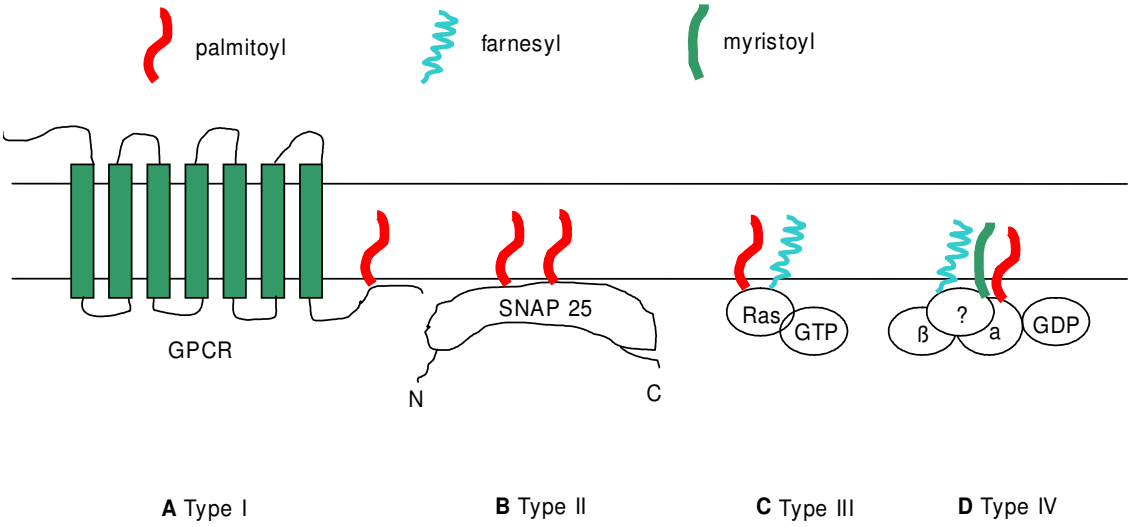

Fig. 1-4. Schematic representation of different types of palmitoylated proteins. (A) G-protein coupled receptors (GPCRs) are palmitoylated on cysteine residues close to their transmembrane domains. (B) Peripheral membrane proteins such as SNAP25 are modified with palmitate only. (C) The Ras family of proteins is farnesylated at a C-terminal CAAX box and also modified near the C-terminus. (D) Gα subunits are myristoylated at an N-terminal glycine residue and also palmitoylated near their N-terminus.

1.5.2. Glycosylation

Glycosylation is the most common post-translational modification for many of the soluble and membrane bound proteins, including those destined for transport to the Golgi apparatus, lysosomes, plasma membrane, or extra cellular space. It is a dynamic process involving additions, removals, and modifications of oligosaccharides by compartment-specific enzymes. According to Spiro's report in 2002, there are 41 different types of glycosylation, which involve a total of 13 different kinds of monosaccharides and 8 amino acids residues (Spiro, 2002). Although there are many kinds of glycosidic bond, N- and O-linked glycans still remain the most abundant.

The N-linked glycosylation, typified by the attachment of the glycan to an asparagine of the protein, is by far the most common. The consensus sequence for N-glycosylation is Asn-Xaa-Ser/Thr, where Xaa is any amino acid other than proline. Primary processing of the N-glycan occurs mainly in the ER. It starts with the co-translational transfer of a 14-sugar precursor from a lipid-linked intermediate to the nascent polypeptide chain in the ER. The structure of this precursor is common to most eukaryotes, and contains 3 glucose, 9 mannose, and 2 N-acetylglucosamine molecules. After attachment, once the protein is correctly folded, the three glucose residues are removed from the chain and the protein is available for export from the ER. The glycoprotein thus formed is then transported to the Golgi complex where removal of further mannose residues may take place. Mature glycoproteins contain a 'core' structure containing 3 mannose, and 2 N-acetylglucosamine residues, which may then be elongated with a variety of different monosaccharides including galactose (Gal), N-acetylglucosamine (GlaNAc), fucose，and sialic acid (SA).

There are two major types of N-linked saccharides found in mature glycoprotein: high-mannose oligosaccharides and complex oligosaccharides. High-mannose is just two N-acetylglucosamines with many mannose residues, often almost as many as are seen in the precursor oligosaccharides before it is attached to the protein. Complex oligosaccharides are so named because they contain almost any number of the other types of saccharides, including more than the original two N-acetylglucosamines and three mannoses. Whether an oligosaccharide is high-mannose or complex is thought to depend on its accessibility to saccharide-modifying proteins in the Golgi complex.

O-linked glycosylation occurs at a later stage during protein processing, probably in the Golgi apparatus. There are several O-linked glycans such as O-N-acetylgalactosamine (O-GalNAc), O-fucose, O-glucose.

Statistical analyses of reported eukaryotic glycoproteins show that there are 883 N-glycosylation proteins and 188 O-glycosylated proteins (Http: //www. cbs.dtu.dk/databases /OGLYCBASE/). The observations that so many eukaryotic proteins are glycosylated and that N-linked glycosylation is more frequently observed in proteins suggest that N-linked glycans are a prime requisite for structure and function in many proteins. The polysaccharide chains attached to the target proteins serve various functions. For instance, some proteins do not fold correctly unless they are glycosylated first. N-linked glycan confers stability on some secreted glycoproteins and the unglycosylated protein degrades quickly. Removal of the glycan from some folded proteins has no effect on their activity but their stability and folding kinetics are altered. This implies that glycan could affect the folding process and stability of a protein without affecting the biological function, similar to protein

chaperones. In addition, the glycan attached to some cell surface proteins can be recognized by transmembrane lectins called selectins, which function in cell-cell adhesion. Thus, glycosylation may play a role in cell-cell adhesion as well.

Glycosylation can also have important regulatory roles. Signal through the cell-surface signaling receptor Notch is important for proper cell fate determination in development. The O-linked glycosylation of Notch can sensitize the Notch receptor, and allows these cells to respond selectively to activating stimuli. In this way, glycosylation has become important to the establishment of spatial boundaries in developing tissues.

1.6. Aim of the dissertation study

The existence of viroporin has been reported for many enveloped and non-enveloped viruses but not for coronavirus until 2004 (Liao *et al*., 2004). In this study, we aimed to identify and characterize SARS-CoV proteins that may induce membrane permeability. Among five proteins tested, the E protein can obviously permeabilize cell membrane. Thus, the overall objective of this dissertation is to characterize the SARS-CoV E protein, the potential viroporin of SARS-CoV. This objective was met through the following specific aims:

1. To demonstrate the SARS-CoV E protein can enhance membrane permeability in both *E. coli* cells and mammalian cell systems.

2. To examine the membrane association, subcellular localization and oligomerization of the SARS-CoV E protein.

3. To examine the role of cysteine residues of the SARS-CoV E protein in its modification of membrane permeability and oligomerization.

4. To examine the role of transmembrane domain of the SARS-CoV E protein in its modification of membrane permeability and oligomerization.

5. To characterize the post-translational modifications of the SARS-CoV E protein.

CHAPTER 2

MATERIALS AND METHODS

2.1. Virus and Cells

2.1.1. Recombinant vaccinia virus

Vaccinia virus harboring the T7 polymerase cDNA (VTF7-3) was described by Fuerst (Fuerst *et al*, 1986). Briefly, DNA coding for bacteriophage T7 RNA polymerase was ligated to a vaccinia virus transcriptional promoter and integrated within the vaccinia virus genome. The recombinant vaccinia virus retains infectivity and stably expresses T7 RNA polymerase in mammalian cells. When cells are infected with the recombinant vaccinia virus and transfected with plasmid containing the target gene inserted at unique restriction site separating a T7 promoter from a T7 terminator, the target gene can acquire very high expression. The recombinant vaccinia virus was propagated in HeLa cells.

2.1.2. HeLa cells

HeLa cell is an immortal cell line derived from cervical cancer cells taken from Henrietta Lacks, who died from her cancer in 1951. References for this cell line are from Masters (2002), Landecker and Hannah (2000), Van *et al.* (1991). HeLa cells were grown at 37 ºC in 5 % CO_2 and maintained in Glasgow's modified Eagle's medium supplemented with 10 % fetal calf serum.

2.1.3. BSR T7/5 cells

BSR *T7/5* cell is a cell line derived from Baby Hamster Kidney cells. It can stably express T7 RNA polymerase (Buchholz *et al*., 1999). BSR *T7/5* cells were grown at 37 ºC in 5 % CO_2 and maintained in Glasgow's modified Eagle's medium supplemented with 10 % fetal calf serum and 1 mg/ml of G418.

2.1.4. Sf9 cells

Sf9 cells were obtained from BD Bioscience (Cat. No.554762). The Sf9 cell line was cloned by Gale E. Smith from the parent line, IPLB-SF21 AE2, which was derived from pupal ovarian tissue of the fall armyworm *Spodoptera frugiperda*.2. The Sf9 cell line is highly susceptible to infection with *Autographa california nuclear polyhedrosis virus* (AcNPV baculovirus), and can be used with all baculovirus expression vectors. Healthy sf9 cells generally double every 18-24 hours when frown in TNM-FH media.

2.1.5. Bacterial strains

DH5α: DH5α is a common host for gene cloning. It was used to propagate all the plasmids used in this study.

BL21 (DE3): BL21 (DE3) is an expression cell clone with DE3 and transcriptional repressor pLysS. It was used to express proteins in this study.

2.2. Plasmid vectors

pET-24a-d (+): pET-24a-d (+) was *E. coli* expression vector obtained from Novagen. pET-24a-d (+) carries T7 promoter and terminator. There are an N-terminal T7 tag

sequence plus an optional C-terminal His-tag sequence. Multiple clone sites are between the N-terminal T7-tag sequence and the C-terminal His-tag sequence. Its selectable marker is kanamycin.

pKT0: pKT0 is a mammalian expression vector containing T7 promoter. It was obtained from Department of Pathology, University of Cambridge, UK. Its selectable marker is ampicillin.

pVL1392: pVL1392 was obtained from BD bioscience. It is a baculovirus transfer vector and was derived from the plasmid PVL941. It contains the complete polyhedron gene locus including flanking regions of AcNPV cloned into the PUC8 vector, but it lacks part of the polyhedrin gene coding region. A MCS region has been inserted 37 nucleotides downstream of the ATG polyhedrin start codon, which has been changed into an ATT. The insert of choice must provide its own ATG start signal at the 5' end of the gene. The vector may be used for high level expression of non-fused foreign proteins under the strong polyhedrin promoter of AcNPV. It is used in conjunction with PharMingen's BaculoGoldTM Baculovirus DNA to get recombination baculovirus.

pFlag: pFlag was derived from pKT0 by inserting a Flag-tag (MDWKDDDDK) sequence between the T7 promoter and the first multiple clone site.

2.3. Immunoreagents

His-tag (H20) Antibody: His-tag (H20) antibody was obtained from DELTA BIOLABS (DB063). It is an affinity purified rabbit polyclonal antibody, raised against a peptide

containing the 6x histidine tag. His-tag (H20) was used for Western blot at 1:1000 dilutions in this study.

Flag M2 antibody: Monoclonal Flag M2 antibody was obtained from Sigma-Aldrich (F3165). It is raised in mouse against a peptide containing the Flag-tag MDWKDDDDK. It was used for Western blot at 1:2000 dilutions and for immunoprecipitation or immunofluorescence at 1:200 dilutions, respectively.

GM130 antibody: Monoclonal GM130 antibody produced in mouse was bought from Abcam (ab1299). It was raised against rat recombinant full length GM130. It reacts with rat GM130, does not react with Human GM130. It was used for immunofluorescence at 1:200 dilutions and for Western blot at 1:1000 dilutions.

SARS-CoV E antibody: Polyclonal SARS-CoV E antibody was raised in rabbit using the C-terminus of SARS-CoV E protein as antigen. It was obtained from Institute of Molecular and Cell Biology, Singapore. It was used for Western blot at 1:1000 dilutions and for immunoprecipitation and immunofluorescence at 1:200 dilutions, respectively.

SARS-CoV N antibody: Polyclonal SARS-CoV N antibody was raised in rabbit using SARS-CoV N protein as antigen. It was obtained from Institute of Molecular and Cell Biology, Singapore. It was used for Western blot at 1:1000 dilutions and for immunoprecipitation and immunofluorescence at 1:200 dilutions, respectively.

Polyclonal Goat anti-Rabbit immunoglobulins HRP: Polyclonal Goat anti-Rabbit immunoglobulins HRP was bought from DAKO (P0448) and was used for Western blot as secondary antibody at 1:2000 dilutions.

Polyclonal rabbit anti-Mouse immunoglobulins HRP: Polyclonal rabbit anti-Mouse immunoglobulins HRP was bought from DAKO (P0161) and was used for Western blot as secondary antibody at 1:2000 dilutions.

Polyclonal Goat anti-Mouse immunoglobulins FITC: Polyclonal Goat anti-Mouse immunoglobulins FITC was bought from DAKO (F0479) and was used for immunofluorescence as secondary antibody at 1:100 dilutions.

Polyclonal Swine anti-Rabbit immunoglobulins FITC: Polyclonal Swine anti-Rabbit immunoglobulins FITC was bought from DAKO (F0054) and was used for immunofluorescence as secondary antibody at 1:100 dilutions.

Polyclonal Rabbit anti-Mouse immunoglobulins TRITC: Polyclonal Rabbit anti-Mouse immunoglobulins TRITC was bought from DAKO (R0270) and was used for immunofluorescence as secondary antibody at 1:100 dilutions.

Polyclonal Swine anti-Rabbit immunoglobulins TRITC: Polyclonal Swine anti-Rabbit immunoglobulins TRITC was bought from DAKO (R0156) and was used for immunofluorescence as secondary antibody at 1:100 dilutions.

2.4. Fluorescence Probes

R6 (rhodamine B hexyl-ester chloride): R6 was obtained from Invitrogen. It is a short chain carbocyanine dye for labeling specifically the ER of mammalian cells.

2.5. Commercial Kits

QIAquick PCR Purification Kits: Obtained from QIAGEN. Cat. No. 28106.

QIAquick Gel Extraction Kits: Obtained from QIAGEN. Cat. No. 28706.

*QIAprep Miniprep Kits***:** Obtained from QIAGEN. Cat. No. 27104.

HiSpeed Plasmid Midi Kits: Obtained from QIAGEN. Cat. No. 12643.

Effectene Transfection Reagent Kit: Obtained from QIAGEN. Cat. No. 301427.

BD BaculoGold™ Transfection kit: Obtained from BD Bioscience. Cat. No. 554740.

Amersham ECL Plus Western blotting Detection System: Obtained from Amersham. Cat. No. RPN2132.

2.6. Chemicals, radioactivity materials and antibiotics

2.6.1. 2-Nitrophenyl β-D-galactopyranoside(ONPG)

ONPG was obtained from Sigma-Aldrich (Cat. No.N-1127). It is a colorimetric substrate for β-galactosidase and is hydrolyzed to o-nitrophenol by the enzyme. *O*-Nitrophenol is yellow in alkaline solution and can be quantitated at 410-420 nm. The

activity of β-galactosidase was determined by the absorbance reading at 420 nm using this ONPG as the substrate.

2.6.2. Hygromycin B solution from Streptomyces hygroscopicus

The 50 mg/ml hygromycin B solution was obtained from Sigma-Aldrich (Cat. No.H-5527). Hygromycin B is an antibiotic substance isolated from *Streptomyces hygroscopicus*. Its mode of action is the inhibition of protein synthesis by inducing the misreading of the mRNA template in the prokaryote, (*E. coli*, at 100 μg/ml), lower eukaryotes (e.g., yeast, at 200 μg/ml) and higher eukaryotes (e.g., mammalian cells in culture). It selectively penetrates cells that have been rendered permeable by virus infection and combined with its potency to inhibit translation. In this study, it was used for detection of the alteration of cell membrane permeability upon protein expression.

2.6.3. G418 sulfate solution

The 50 mg/ml G418 sulfate solution was obtained from Sigma-Aldrich (Cat. No.G-8168). G418 is an aminoglycoside antibiotic similar in structure to gentamycin. It exhibits toxicity towards both eukaryotic and prokaryotic cells. The optimal concentration for selection and maintenance must be determined for each cell line. Resistance is typically conferred by one of two dominant genes of bacterial origin, which can be expressed in eukaryotic cells. Cells that are multiplying will be affected sooner than those are not. Cells in log phase may require three to seven days for selection. In general, approximately concentrations of 400 μg/ml for selection and 200 μg/ml for

maintenance are required for mammalian cells, respectively. In this study, it was used for maintaining BSR T7/5 cell line in 1 mg/ml concentration.

2.6.4. Alkylating Reagent, Iodoacetamide

The iodoacetamide was order from Sigma-Aldrich (Cat. No.A-3221). It is an alkylating reagent for cysteine and histidine residues in protein and is used in peptide sequencing as well as an irreversible enzyme inhibitor. In this study, it was used to prevent the artificial formation of disulfide bond during cell lysis.

2.6.5. Glutaraldehyde

The cross-linking reagent glutaraldehyde was ordered from Sigma.

2.6.6. Protein A agarose

The protein A agarose (Cat. No. 223-50-00) was ordered from KPL (kirkegarrd and perry laboratories). It was used for immunoprecipitation.

2.6.7. DAKO cytomatin Fluorescent Mounting medium

The cytomatin Fluorescent Mounting medium was ordered from DAKO (Cat. No. S3023) and was used to stabilize the fluorescence in indirect immunofluorescence experiment.

2.6.8. Hydroxylamine

The hydroxylamine was ordered from Sigma-aldrich (Cat. No. A-5131) and was used for cleaving the palmitate from E protein in this study.

2.6.9. [9, 10 (n)-^{3}H] Palmitic acid

The [9, 10 (n)-^{3}H] palmitates was ordered from Amersham Bioscience (Cat. No. TRK909).

2.6.10. Redivue pro-mix L-[35S] in vitro cell labeling mix

The redivue pro-mix L-[^{35}S] *in vitro* cell labeling mix was ordered from Amersham Bioscience (Cat. No. AGQ0080).

2.6.11. Low-Range Rainbow Molecular Weight Markers

The Low-Range Rainbow Molecular Weight Markers were ordered from Amersham Bioscience (Cat. No. RPN756) and were labeled with ^{14}C.

2.6.12. Dulbecco's Modified Eagle Medium (without L-Methionine and L-cysteine)

The Dulbecco's Modified Eagle Medium (without L-Methionine and L-cysteine) was ordered from Gibico (Cat. No.21013-024) and was used for ^{35}S methionine and cysteine labeling.

2.7. Enzymes

Pfu: Obtained from New England Biolab.

T4 ligase: Obtained from New England Biolab.

Restriction Enzymes: Obtained from New England Biolab.

2.8. Molecular Biology and Cloning

2.8.1. Polymerase chain reaction and site-directed mutagenesis

Amplification of respective template DNAs with appropriate primers was performed with pfu DNA polymerase (New England Biolab) with 2 mM $MgCl_2$. The PCR reaction was carried out in 200 µl thin-wall Gene-Amp tubes (Axygen) containing a 50 µl mixture of 1 × pfu DNA polymerase reaction buffer (New England Biolab), 0.125 mM each of the deoxynucleoside triphosphate (dNTPs: dATP, dCTP, dGTP and dTTP, Gibco BRL], 0.5 pM of both forward and reverse primers, 5 units of pfu DNA polymerase and 50 ng of DNA template. The PCR conditions were 5 minutes at 94 ^{o}C for initial DNA denaturation, followed by 35 cycles of 94 ^{o}C for 45 seconds, 46-58 ^{o}C for 45 seconds, and 72 ^{o}C for 30 seconds. The annealing temperature and extension time were subjected to adjustments according to the melting temperatures of the primers used (5 ^{o}C below the melting temperatures of the primers) and the lengths of the PCR fragments synthesized. After cycles, a 5 minutes final extension was programmed. The melting temperature Tm value of primers was calculated according to the following equation: Tm (^{o}C) = 4 X (G+C) + 2 X (A+T).

Site-directed mutagenesis was carried out with two rounds of PCR and two pairs of primers. Two pairs of primers were designed, the first pair being the cloning primers

(Primer 1 and 2), were used to amplify the full-length fragment, while the second pair carried the respective mutations (primer 3 and 4). The first round of PCR was performed in 2 separate reactions. Each tube contains the appropriate DNA template and primer combinations of primer 1/primer 4 or primer 3/primer 2. The two PCR fragments were subjected to electrophoresis, the desired band was excised using a sterile razor blade, and the desired fragment was extracted by gel extraction kit according the protocol provided by the manufacturer. Full length PCR fragment containing the mutation was obtained after equal amount of the gel exaction PCR product were mixed and subjected to a second round of PCR using primer 1 and 2.

2.8.2. Agarose gel electrophoresis and gel purification of nucleic acid fragments

2 % agarose gels containing 0.5 µg/ml ethidium bromide (Sigma) were prepared by dissolving agarose powder (Biorad) in 1 × TAE buffer (40 mM Tris base, 10 mM EDTA-, 20 mM acetic acid, pH 8.5). Gel were submerged in a running tank of TAE buffer, appropriate amounts of DNA were mixed with 6 × DNA loading buffer [0.25 % bromophenol blue and 40 % sucrose (w/v)], and run horizontally at 120 V, at constant voltage for 30 minutes. Fragment sizes were compared with that of 100 bp DNA marker (New England biolab). If it is necessary, the desired band was excised using a sterile razor blade, and the desired fragment was extracted by gel extraction kit according the protocol provided by the manufacturer.

2.8.3. Restriction endonuclease digestion of PCR products and DNA fragments

In a reaction volume of 100 µl, up to 5 µg of plasmid DNA or half of the purified PCR products was digested with 10 units (U) of the appropriate restriction endonuclease for 2 hours, using the buffer provided and conditions recommended by the manufacturer. "1U will completely digest 1 µg of substrate DNA in a 50 µL reaction in 60 minutes (New England Biolabs)." Glycerol concentrations did not exceed 10 % (v/v) of total reaction volume (enzymes stored in 50 % glycerol). Double digestion with two enzymes was performed either sequentially with intervening to remove the enzymes and salts by PCR purification kit or simultaneously, if the condition of each reaction was compatible. Subsequently the sample was purified by spin-column chromatography using PCR purification kit to remove enzymes and salts.

2.8.4. Ligations

Typically, ligations of 3' hydroxyls and 5' phosphates into phospodiester bonds were performed with 5 U T4 DNA ligase in the presence of ATP and divalent cation cofactor. Intermolecular ligations were performed by mixing 50 ng of plasmid vector with a 3-fold molar excess of insert fragments in a minimal total volume along with ligation buffer (containing polyethylene glycol) and T4 DNA ligase (New England Biolab).

2.8.5. Transformations of plasmids into bacterial cells

Competent cells (100 µl) were thawed on ice, and pre-chilled plasmid (minimum 5 ng) was added and incubated with cells for 30 minutes on ice followed by heat shock for 2 minutes at 42 ^{o}C. Cells were subsequently chilled on ice for 5 minutes followed by addition of 1 ml of LB medium (no antibiotics) and incubated at 1 hour at 37 ^{o}C. Cells

were spun down at 500 × g for 2 minutes, 900 µl supernatant LB was removed, the remnant 150 µl cells were spread onto appropriate selective solid medium and incubated overnight for growth of colonies.

2.8.6. Preparation of competent E. coli cells

A single clony of *E. coli* on the LB plate was inoculated into 2 ml LB medium [1 % tryptone (w/v), 0.5 % yeast extract (w/v), 1 % NaCl (w/v), pH 7.0] and grown overnight (approximately 15 hours) at 37 ºC, at 250 rpm on the shaking platform. 150 µl of the overnight culture was diluted 100 fold into 15 ml fresh LB medium, and was incubated at 37 ºC , shaking at 250 rpm, until the OD 600 is around 0.5 (about 2 hours). Put the *E. coli* cells on ice for 10 minutes and centrifuge them at 2500 × g for 5 minutes. Remove the supernatant and gently resuspend the pellet in 10 ml of sterile ice cold 50 mM $CaCl_2$ and chill the cells on ice for 30 minutes. Pellet the cells again, resuspend the cells in 1 ml of ice-cold 20 % glycerol in 50 mM $CaCl_2$ and chill on ice for further 5 minutes, aliquot the cells by 50 µl per tube and store them at -80 ºC.

2.8.7. Construction of plasmids

Plasmids pET24a-E, pET24a-3a, pET24a-3b, pET24a-6, pET24a-7a, and pET24a-HCVE1 were constructed by cloning an *Nde*I/*Xho*I-digested PCR fragment into *Nde*I/*Xho*I-digested pET24a vector. All the constructs have a His-tag fused to the 3' end of the genes.

The two primers for SARS-CoV E protein are:

5′-CGGGATATCCCATATGTACTCATTCGTTTCGGAA-3′

and 5′-CGGAATTCTTACTCGAGGACCAGAAGATCAGGAACTCC-3′.

The two primers for SARS-CoV 3a protein are:

5′-CGGGATATCCCATATGGATTTGTTTATGAGATTT-3′

and 5′-CGGAATTCTTACTCGAGCAAAGGC-ACGCTAGTAGTTCGT-3′.

The two primers for SARS-CoV 3b protein are:

5′-CGGGATATCCCATATGATGCCAACTACTTTGTTT-3′

and 5′-CGGAATTCTTACTCGAGACGTACCTGTTTCTTCCGAA-A-3′.

The two primers for SARS-CoV 6 protein are:

5′-CGGGATATCCCATATGTTTCATCTTGTTGACTTC-3′

and 5′-CGGAATTCTTACTCGAGTGGATAATCTAACTCCATAGG-3′.

The two primers for SARS-CoV 7a protein are:

5′-CGGGATATCCCATATGAAAATTATTCTCTTCCTG-3′

and 5′-CGGAATTCTTACTCGAGTTCTGTCTTTCTCTTAATGGT-3′.

The two primers for HCV E1 protein are:

5′-CGGGATATCCCATATGTACCAAGTGCGCAATTCCTCG-3′

and 5′-CCGGAATTCTTAGCGGCCGCCGCGTCGACGCCGGCAAATAG-3′.

Plasmid pFlag-E was constructed by cloning an *EcoR*V- and *EcoR*I-digested PCR fragment into *EcoR*V- and *EcoR*I-digested pFlag. The Flag tag is fused to the N-terminus of the E protein.

The two primers used are: 5′-CGGGATATCCTACTCATTCGTTT CGGAA-3′

and 5′-CCGGAATTCTTAGACCAGAAGATCAGGAAC-3′.

Mutations were introduced into the E gene by two rounds of PCR. The PCR amplified fragments were cloned into *EcoR*V- and *EcoR*I-digested pFlag. All plasmids and the introduced mutations were confirmed by automated DNA sequencing. All the sequencings were performed by Research Biolab, Singapore.

2.8.8. Plasmid preparation

Plasmid preparation was performed using QIAprep Spin Miniprep kit or Hispeed plasmid midi kit (Qiagen) according the protocols provided by the manufacturer.

2.9. Cell culture and virus infection

2.9.1. Preparation and resuscitation of frozen mammalian cell line stock

HeLa cells or BSR T7/5 cells cultured in 175 cm^2 flasks were subjected to trypsinization, and centrifugation at 500 rpm for 5 minutes. 10 ml of cell freezing

medium (50 % DMEM, 10 % DMSO and 40 % FBS) was used to resuspend the cell pellet. Cells were aliquoted into plastic cryogenic polypropylene vials (Iwaki) and were subjected to slow freezing to -20 ºC and -80 ºC for 1 hour each, prior to long term storage at -154 ºC. To resuscitate the frozen cell line stock, a vial of frozen Vero or Cos-7 cells was thawed at 37 ºC and carefully transferred to a 25 cm^2 culture flask (Nunc) containing 6 ml of complete DMEM prewarmed to 37 ºC. Resuscitated cells were incubated at 37 ºC in humidified 5 % CO_2 for 24 hours, before the culture medium was replaced with fresh complete DMEM.

2.9.2. Preparation of recombinant vaccinia virus-T7 (vTF7-3) working stock

HeLa cells were grown to confluency in 4 × 175 cm^2 and infected with 0.1 PFU/cell of a recombinant vaccinia/virus (vTF7-3) for 24 hours, before fresh medium was used to replace the inoculum. After 40 hours, when cytopathic effects were observed, the infected cells were harvested together with the culture medium by scraping. The viruses were released from cells via three rounds of freeze-thaw (at -80 ºC and room temperature respectively), before they were aliquoted in 1.5 ml screw-cap vials (Iwaki) and stored at -80 ºC.

2.9.3. Passage of continuous mammalian cell line

Rinse the confluent cells in 75 cm^2 flasks (Nunc) with tissue culture grade Phosphate Buffered-Saline [PBS, 0.8 % NaCl (w/v), 0.02 % KCL (w/v), 0.144 % Na_2HPO_4 (w/v) and 0.024 % KH_2PO_4 (w/v) adjusted to pH 7.4 by HCl] containing 0.02 % EDTA. Then detach the adhered cells from the polystyrene surface by adding 2 ml of trypsin (0.05 %

trypsin, 0.023 % EDTA, Gibco BRL) to the culture and incubation at room temperature for 5 minutes. 10 ml of complete DMEM medium containing 10 % FBS was added to stop the proteolytic process and the cells were subjected to 500 rpm centrifugation for 5 minutes. Then the cell pellets were resuspended in 36 ml of fresh complete DMEM, and were seeded into 75 cm^2 flasks in an appropriate density. For protein expression, the cells were seeded 35 mm, 60 mm or 100 mm culture dishes (Falcon) in an appropriate density.

2.9.4. Passage of continuous insect cell line

sf9 cells can grow well both in monolayer cultures and suspension cultures.

In monolayer cultures, sf9 cells were grown at 27 °C and maintained in TNM-FH media using 75 cm^2 flasks (Nunc). The cells attach the flask wall loosely. When doing the passage, a stream of medium from 10 ml pipette was used and the cells were gently dislodged from the flask wall. Strongly attached cells require persistence and more forceful pipetting. Two volumes of fresh medium were added into the cell suspension to make the initial cell density about 30 % and cells were splitted to 75 cm^2 flasks.

In suspension cultures, sf9 cells were grown at 27 °C and maintained in TNM-FH media using spinner flasks under constant stirring at 50-60 rpm. Routine maintenance of spinner cultures requires subculturing when the cell density reaches approximately 2 × 10^6 cells/ml (2-3 times a week). The cell density was determined using hemocytometer. 65 %-75 % of the cell suspension was removed and replaced with fresh medium. The culture was re-seeded into a clean sterile spinner flask every 2 weeks to prevent build-up of by-products or other contaminants.

2.9.5. Freezing and thawing insect cells

Spin down sf9 from a healthy, log-phase culture at 1000 × g for 10 minutes. Decant supernatant and keep cell pellet on ice. Resuspend pellet in 90 % TNM-FH medium, 10 % DMSO. The cell density should be at least 4 × 10^6 cell/ml. Dispense 1 ml aliquots quickly into freezing vials, keeping the cells cold at all times. The cells were placed at -20 ºC for 1 hour and - 80 ºC overnight to freeze, prior to long term storage at -154 ºC.

To thaw the frozen sf9 cells stock, a vial of cells was thawed at 37 ºC and carefully transferred to a 25 cm^2 culture flask (Nunc) containing 8 ml fresh TNM-FH medium and incubated at 27 ºC. After 24 hours, the old medium was removed and replaced with fresh TNM-FH.

2.10. Protein expression and analysis

2.10.1. Expression of proteins in E. coli

Plasmids were transformed into *E. coli* strain BL21 (DE3) pLysE and grown on LB plate with appropriate antibiotics. A single colony was picked into LB medium from the LB plate. Shake the culture overnight at 250 rpm, at 37 ºC. Dilute the overnight culture 100-fold in LB medium or M9 medium (supplemented with 0.2 % glucose) containing appropriate antibiotics. When the absorbance of the cultures reached 0.6 at 600 nm, 1 mM IPTG (Sigma) was added to the medium to induce protein synthesis.

At indicated times post-induction, the cell density of bacterial cultures was determined by measuring the light scattering at 600 nm.

For the detection of the protein expression, 1 ml of cell culture was harvested at 3 hour post-induction. Cells were pelleted and lyszed in 2× Laemmli sample buffer [100 mM Tris-Cl (pH 6.8), 4 % (w/v) SDS, 0.2 % (w/v) bromophenol blue, 20 % (v/v) glycerol] in the presence or absence of 2 % β-mercaptoethanol or 200 mM DTT plus 10 mM of iodoacetamide, heated at 100 ºC for 5 minutes, centrifugated, then subjected to 15 % SDS-PAGE and Western blot.

2.10.2. SDS-PAGE

Separating gels of 15 % acrylamide concentrations and 3 % stacking gels were cast between two glass plates. After the protein samples were loaded into the wells, gels were run vertically in a reservoir filled with running buffer 2.88 % glycine (w/v), 0.6 % Tris (w/v) and 0.1 % SDS (v/v)] at constant voltage of 150V for 1 hour.

2.10.3. Western blot analysis

Post SDS-PAGE, proteins were transferred to PVDF membrane (Stratagene) by wet transfer or semi-dry transfer, and blocked overnight at 4 °C in blocking buffer (5 % fat free milk powder in TBST buffer, 20 mM Tris-HCl PH 7.4, 150 mM NaCl, 0.1 % Tween 20). The membrane was incubated with 1:1000 or 1:2000 diluted primary antibodies in blocking buffer for 2 hours at room temperature. After washing three times with TBST, the membrane was incubated with 1:2000 diluted anti-mouse or anti-rabbit IgG antibodies conjugated with horseradish peroxidase (DAKO) in blocking buffer for 1 hour at room temperature. After washing three times with PBST, the polypeptides were detected with a chemiluminescence detection kit (ECL, Amersham Biosciences)

according to the manufacturer's instructions. The excess detection reagent was drained off from the membranes and saran wrap was used to wrap the membranes before exposure to X-ray film.

2.10.4. Hygromycin B assays in E. coli cells

To detect the entry of hygromycin B into bacterial cells, 2 mM of hygromycin B was added to the medium 50 minutes post-induction. After incubation for 30 minutes, 1 μCi of [^{35}S] methionine per ml was added to the medium and incubated at 37 °C for 15 minutes. The bacterial cells were then harvested and subjected to SDS-PAGE. The proteins were detected by autoradiography.

2.10.5. Autoradiography

After SDS-PAGE, polyacrylamide gels were fixed in fixative buffer (10 % v/v glacial acetic acid, 25 % v/v methanol) for 30 minutes by gently shaking, and subsequently soaked in an enhancement reagent such as "Amplify" (Amersham Bioscience) for 30 minutes. Gels were dried onto filter paper under vacuum at 64 ºC for 1 hour followed by exposure of gels to X-ray film (Amersham Bioscience) overnight or longer time at -70 ºC. The X-ray film was developed by the Kodak film developing machine.

2.10.6. β-Galactosidase assay

To measure the entry of ONPG into bacterial cells, 1 ml of bacterial cultures was removed at indicated times post-induction. After centrifugation, cells were re-suspended

in 1 ml of fresh M9 medium containing 2 mM ONPG, a β-galactosidase substrate. Cells were incubated for 10 minutes at 30 °C, and the reaction was stopped by addition of 0.4 ml of 1 M sodium carbonate. Samples were centrifuged, and the absorbance of the supernatant was measured at 420 nm to estimate the degree of the cleavage of ONPG.

2.10.7. Transient expression of SARS-CoV sequence in mammalian cells

HeLa cells were grown at 37 ℃ in 5 % CO_2 and maintained in Dulbecco's modified Eagle's medium supplemented with 10 % fetal calf serum. SARS-CoV E and mutants were cloned into vector pFlag or pKT0 under the control of a T7 promoter and transiently expressed in mammalian cells using a vaccinia virus-T7 expression system. Briefly, 60 – 80 % confluent monolayer of HeLa cells grown on dishes (Falcon) were infected with 10 plaque-forming units/cell of a recombinant vaccinia virus (vTF7-3) that expressed T7 RNA polymerase. 2 hours later, cells were transfected with plasmid DNA mixed with Effectene according to the manufacturer's instructions (Qiagen). Cells were harvested at 12 to 24 hours post-transfection.

2.10.8. Preparation of cell lysates

The cells were washed twice before they were harvested. Cells were scrapped off the dishes, resuspended in PBS and removed by centrifugation at 14000 rpm for 1 minute and stored at - 80 ℃ until for further use. For Western blot, the cells were directly lysised in 2 × Laemmli sample buffer [100 mM Tris-Cl (pH 6.8), 4 % (w/v) SDS, 0.2 % (w/v) bromophenol blue, 20 % (v/v) glycerol] in the presence or absence of 2 % β-

mercaptoethanol or 200 mM DTT plus 10 mM of iodoacetamide, heated at 100 ºC for 5 minutes, centrifuged, then subjected to 15 % SDS-PAGE and Western blot.

2.10.9. Hygromycin B assay in mammalian cells

Membrane permeability of cells expressing SARS-CoV E or mutants to hygromycin B was determined as described below. Briefly, HeLa cells in 100 mm dish were transfected with plasmids as described above, the cells were pretreated with different concentrations of hygromycin B (Sigma) for 30 minutes in methionine–cysteine free medium at 12 hours post-transfection, and then 25 μCi/ml of [^{35}S] methionine–cysteine (Amersham) was added to the culture medium. The cells were incubated at 37 ℃ for 3 hours in the presence or absence of hygromycin B, harvested, and lysed in 1× radioimmune precipitation assay buffer (RIPA, 20 mM Tris-HCl pH 7.4, 5 mM EDTA, 150 mM NaCl, 0.5 % SDS, 0.1 % sodium deoxycholate, 0.5 % NP-40) containing 1.0 mM phenylmethylsulfonyl fluoride (PMSF, Sigma) and 10 μg/ml each of aprotinin and leupeptin (Sigma). The cell extracts were clarified for 10 minutes at 13,000 rpm at 4 ℃, and the proteins were immunoprecipitated with appropriate antibodies for 1 hour at 4 ℃, followed by incubation with 20 μl of protein A agarose overnight at 4 ℃. Immunoprecipitated beads were washed three times with RIPA buffer. The proteins were analyzed on 15 % SDS-PAGE and subjected to autoradiography.

2.10.10. Expression and purification of the SARS-CoV E protein expressed in insect cells

A cDNA fragment covering the SARS-CoV wild-type E protein or the mutant E protein with a His-tag at the C-terminus was cloned to the transfer vector pVL1392

(Pharmingen). A recombinant baculovirus expressing the His-tagged SARS-CoV E protein was generated by cotransfection of the pVL1392-E-His construct together with Baculogold DNA (Pharmingen) into sf9 cells according to the instruction of the manufacturer. Fresh Sf9 cells were infected with the recombinant virus and harvested at 72 hours postinfection. The His-tagged E protein was purified using Ni-NTA purification system (Qiagen) according to the instruction of the manufacturer.

2.10.11. Cross-linking experiment

His-tagged E protein was incubated with 0.1, 0.25, 0.5, 0.75 and 1 mM glutaraldehyde, respectively at room temperature for 1 hour. The reaction was quenched by adding 100 mM glycine. Polypeptides were separated by 15 % SDS-PAGE in the presence or absence of 1 % β-mercaptoethanol, and subjected Western blot with anti-His antibody.

2.10.12. Indirect immunofluorescence

Baby hamster kidney (BHK-21) cells carrying T7 polymerase gene (BSR T7/5) or HeLa cells were grown on 4-wells chamber slides (Iwaki) and were transfected with plasmids. HeLa cells were infected with recombinant vaccinia virus-T7 (vTF7-3) prior to transfected with plasmids. After 3 washes with PBS, the cells were fixed with 4.0 % paraformaldehyde (in PBS, Sigma) for 15 minutes at 12 hours post-transfection. For immunofluorescence of permeabilized cells, cells were incubated with 0.2 % Triton X-100 for a further 10 minutes at room temperature, before they were rinsed three times with 1 x PBS. For untagged or Flag-tagged E protein and mutants, rabbit anti-E

polyclonal antibodies were used to detect E protein, and mouse anti-GM130 monoclonal antibody (Abcam) were used to detect GM130, a Golgi marker, or mouse anti-calnexin monoclonal antibodies (Abcam) were used detect calnexin, an ER marker. Mouse anti-Flag monoclonal antibodies were also used to detect Flag-tagged E protein and mutants. Cells were incubated with primary antibody diluted in 1:100 fluorescence blocking buffer (5 % FBS in PBS) for 2 hours at room temperature, washed three times with 1x PBS, then incubate with FITC or TRITC-conjugated secondary antibody (DAKO) diluted in 1:100 fluorescence blocking buffer (5 % FBS in PBS) for 2 hours at 4 ^{o}C. After three washes with PBS, cells were mounted with glass coverslips using fluorescent mounting medium containing 15 mM NaN3 (DAKO).

2.10.13. Subcellular fractionation

HeLa cells were resuspended in hypotonic buffer (1 mM Tris–HCl pH 7.4, 0.1 mM EDTA, 15 mM NaCl) containing 10 μg each of leupeptin and aprotinin (Sigma) per ml and 0.4 mM phenylmethylsulfonyl fluoride (PMSF, Sigma) and broken by 20 strokes with a Dounce cell homogenizer. Cell debris and nuclei were removed by centrifugation at 1500 × *g* for 10 minutes at 4 °C. The cytosol fraction and membrane fraction (postnuclear fraction) were separated by ultracentrifugation through a 6 % sucrose cushion at 150,000 × *g* for 30 minutes at 4 °C. Membrane pellets were resuspended in hypotonic buffer, treated with 1 % Triton X-100, 100 mM Na_2CO_3 or 1 M KCl for 30 minutes, and further fractionated into supernatant (S) and pellet (P) fractions by ultracentrifugation at 150,000 × *g* for 30 minutes at 4 °C. Membrane pellets were resuspended in immunoprecipitation buffer (20 mM Tris-HCl pH7.4, 5 mM EDTA, 150

mM NaCl, 0.5 % SDS, 0.1 % sodium deoxycholate, 0.5 % NP-40), and the supernatants were also adjust to the same volume with 2 × immunoprecipitation buffer. Samples were incubated with appropriate antibody for 1 hour at 4 ºC, followed incubated with 20 µl protein A agarose overnight at 4 ºC. Immunoprecipitated beads were washed three times with the immunoprecipitation buffer and subjected to 15 % SDS-PAGE and Western blot.

2.10.14. Palmitoylation study of E protein

To verify if the SARS-CoV E protein is palmitoylated, two independent experiments were performed.

For the hydroxylamine treatment, total cell lysates prepared from HeLa cells expressing the Flag-tagged SARS-CoV E protein and IBV E protein were treated with 1M hydroxylamine at pH 7.4 for 1 hour at room temperature. Controls were incubated in the presence of 1 M Tris-HCl, pH 7.4. Hydroxylamine can cleave the thioester bond between the fatty acid and cysteine side chain. These techniques are significantly more sensitive than metabolic labeling with [9, 10-^{3}H] palmitates and can be used quantitatively to measure levels of protein palmitoylation (Drisdel and Green, 2004). Polypeptides were separated by 15 % SDS-PAGE and subjected to Western blot using the anti-Flag antibody.

For the [9, 10-^{3}H] palmitates labeling, HeLa cells in 60 mm dish were infected with 10 plaque-forming units/cell of a recombinant vaccinia virus (vTF7-3) that expressed T7 RNA polymerase. Two hours later, cells were transfected with plasmid DNA mixed with Effectene according to the manufacturer's instructions (Qiagen). Four hours later, cells

were labeled with 1 mMCi/ml of [9, 10-^{3}H] palmitates (50 Ci/mmol; Amersham) for 10 hours. A duplicate dish of cells was labeled with 25 μCi/ml of [^{35}S] methionine/cysteine (Amersham) for 10 hours at 4 hours post-transfection. Cells were harvested and proteins were immunoprecipitated as described above.

2.10.15. Glycosylation study of E protein

HeLa cells expressing E protein were treated with glycoprotein denaturing buffer (0.5 % SDS and 1 % β-mercaptoethanol) at 100 °C for 10 minutes. The denaturing proteins were incubated with 1 μl glycosidase PNGase F (Research Biolabs) in G7 reaction buffer (50 mM sodium phosphate, pH 7.5) supplemented with 1 % NP40 at 37 °C for 1 hour. The deglycosylated proteins were analyzed on 15 % SDS-PAGE and Western blot.

CHAPTER 3

RESULTS

3.1. Introduction

Coronavirus infection of cultured cells causes typical cytopathic effects (CPEs). The typical CPEs of coronavirus infection are fusion of the infected cells, formation of giant syncitial cells, cells detachment from the culture dishes, and cells lysis. Among them, formation of giant syncitial cells is the hallmark of early CPE in cells infected with most coronaviruses. However, SARS-CoV infection seldom causes syncytia formation. The main CPEs are cell ballooning, detachment and lysis (Ksiazek *et al*., 2003). These phenomena are clearly related to cell membrane perturbation. Typically, three groups of virus-encoded proteins are capable perturbing cell membrane permeability: viroporins, viral pore-forming glycoproteins and proteases.

In this study, we aimed to identify and characterize SARS-CoV proteins that related to cell membrane perturbation. Among five proteins tested, the E protein could obviously enhance membrane permeability to *O*-nitrophenyl-β-D-galactopyranoside (ONPG), a β-galactosidase substrate, and hygromycin B, an antibiotic which can inhibit protein synthesis. E protein was demonstrated to be an integral membrane protein and was localized to perinuclear region. It could self-associate to form oligomers. The membrane-permeabilizing activity was associated with the transmembrane domain but not cysteine

residues. Further characterization of the E protein showed that C40, C43 and C44 were modified by palmitoylation and N66 was modified by N-linked glycosylation.

3.2. SARS-CoV E protein alters membrane permeability both in *E. coli* and HeLa cells

3.2.1. Retardation of bacterial growth by SARS-CoV E, 6 and 7a proteins

SARS-CoV E, 3a, 3b, 6, and 7a proteins contain potential transmembrane domain, seem to be good candidates for membrane-active proteins. Usually, the membrane-active protein can cause cell lysis. The effect of over-expression of these proteins on bacterial cells growth was initially tested. To assess the membrane perturbation of the SARS-CoV proteins, we used an inducible *E. coli* BL21 (DE3) pLysE expression system. This system has been demonstrated to be suitable for the characterization of other membrane-active viral proteins. *E. coli* BL21 (DE3) pLysE carries the T7 RNA polymerase gene integrated in the chromosome under the control of a lac UV5 promoter. The lac UV5 promoter can be induced by IPTG. The PlysE plasmid constitutively expresses high levels of the T7 phage lysozyme. In the case the alteration of membrane permeability allows the passage of T7 lysozyme to the periplasmic space where it could exert its lytic activity on bacterial wall.

As a first approach to analyze the effect of the SARS-CoV proteins on bacterial membrane, nucleotide sequences covering the SARS-CoV E, 3a, 3b, 6, 7a and HCV E1 proteins, respectively, were cloned into pET24a vector with His-tag at C-terminus. The resultant plasmids were used to transform *E. coli* BL21 (DE3). HCV E1 protein was

chosen as a positive control, as it has been shown to be able to increase membrane permeability when over-expressed in *E. coli* cells. The growth rates of the transformed bacterial cells were analyzed spectrophotometrically by measurement of optical density at 600 nm. As shown in Fig. 3-1, expression of 3a and 3b proteins rendered no obvious effects on the growth of bacterial cells, compared with cells carrying the empty plasmid pET24a. Certain degrees of retardation of bacterial growth were observed in cells expressing the E, 6, 7a and HCV E1 proteins (Fig. 3-1). The result indicated that, like HCV E1, E, 6 and 7a was toxic to bacterial cells and could cause cell lysis. It was reported that protein 6 could enhance the virulence of an attenuated murine coronavirus (Pewe *et al.,* 2005). Over-expression of 7a protein could induce apoptosis via caspase-dependent pathway (Tan *et al*., 2004a) and inhibit cell growth and block cell cycle procession at G0/G1 phase via cyclin D3/Rb pathway in mammalian cells (Yuan, *et al*., 2006b).

The expression of these proteins was then checked by labeling with [^{35}S] methionine in the presence of rifampicin. Rifampicin blocks *E. coli* mRNA transcription, which leads to diminished synthesis of host cell proteins. This allows an easier detection of the cloned protein. Fig. 3-2 showed the presence of protein bands with apparent molecular masses of 14 (lane 1), 32 (lane 2), 18.5 (lane 3), 14.8 (lane 5), and 21.7 kDa (lane 6), corresponding to the expected His-tagged E, 3a, 3b, and 7a and HCV E1 proteins, respectively. Interestingly, E protein migrated slower than the theoretical molecular weight (about 9.3 kDa). This is not an unusual phenomenon for small hydrophobic peptides, where it is thought that the uniform binding of SDS may be affected, altering the relative rate of

migration through polyacrylamide gels. No band corresponding to the His-tagged protein 6 (8.5 kDa) was detected (Fig. 3-2, lane 4). To confirm the expression and identities of these proteins, Western blot analysis was conducted using anti-His antibody. The 14 kDa E protein (lane 7), 32 kDa 3a protein (lane 8), 14.8 kDa 7a protein (lane 11), and 21.7 kDa HCV E1 protein (lane 12) were detected, confirming the expression of these proteins. However, the antibody failed to react with the 3b protein (Fig. 3-2, lane 9). The reason for the failure to detect the His-tagged 3b protein is currently uncertain. Once again, no obvious band corresponding to protein 6 was detected (Fig. 3-2, lane 10), indicating that this protein expressed at a very low level in the bacterial cells. As significant inhibition of the growth of bacterial cells carrying gene 6 was observed (Fig. 3-1), suggesting that the protein might be highly toxic to bacteria. It was also noted that induction of the empty vector, pET24a, affected the growth of bacterial cells, compared with bacterial cells carrying pET24-3a and pET24-3b (Fig. 3-1). This reflected the fact that over-expression of the multiple cloning sites His-tag region in pET24a might affect bacterial growth.

First time	E	3a	3b	protein 6	7a	HCV E1	pET24a
0h	0.6	0.601	0.594	0.601	0.611	0.603	0.599
1h	0.785	0.924	0.986	0.776	0.63	0.765	0.763
2h	0.91	1.002	1.155	0.753	0.666	0.823	0.94
3h	0.923	1.096	1.367	0.746	0.687	0.834	1.027
4h	0.965	1.11	1.403	0.72	0.689	0.833	1.031

Second time	E	3a	3b	protein 6	7a	HCVE1	pET24a
0h	0.597	0.59	0.604	0.757	0.612	0.596	0.608
1h	0.825	0.845	1.002	0.746	0.653	0.808	0.987
2h	0.867	0.903	1.119	0.744	0.67	0.835	1.09
3h	0.901	0.967	1.197	0.709	0.684	0.879	1.167
4h	0.937	1.098	1.291	0.691	0.698	0.897	1.224

Third time	E	3a	3b	protein 6	7a	HCVE1	pET24a
0h	0.612	0.6	0.594	0.655	0.581	0.602	0.599
1h	0.822	1.045	1.023	0.838	0.648	0.787	0.908
2h	0.853	1.037	1.164	0.849	0.652	0.802	0.996
3h	0.899	1.041	1.17	0.813	0.672	0.834	0.988
4h	0.921	1.054	1.22	0.712	0.687	0.876	1.002

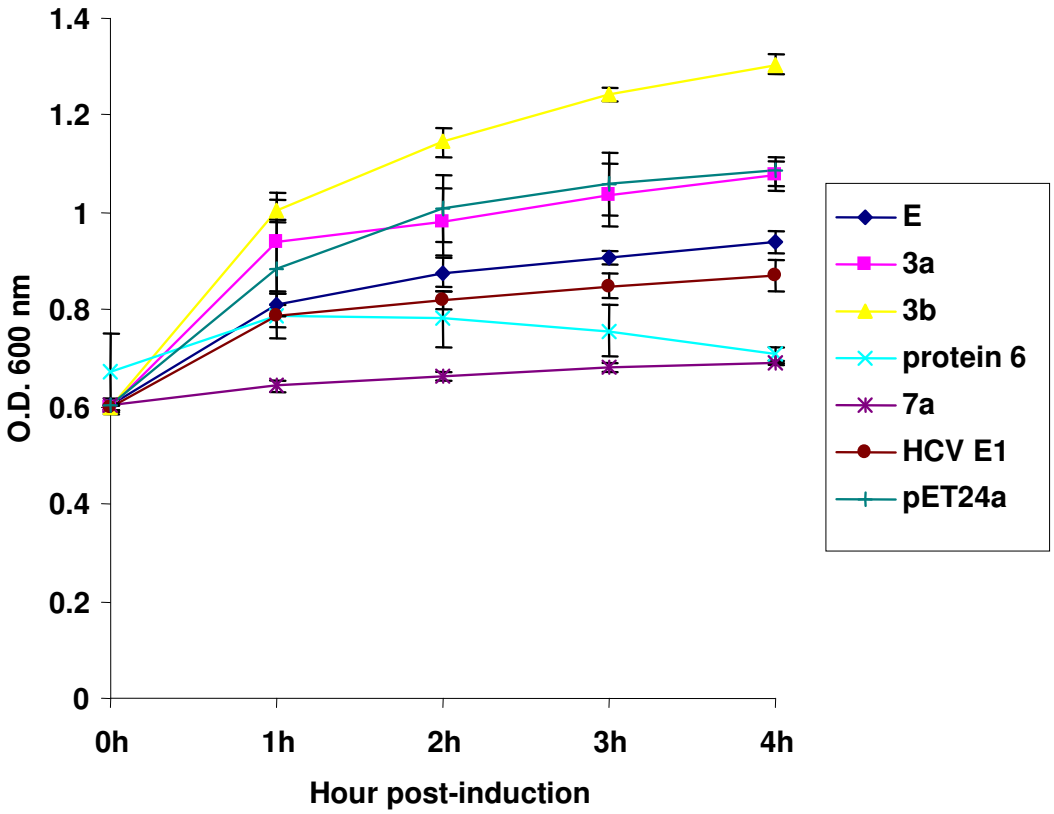

Fig. 3-1. Retardation of bacterial growth by SARS-CoV 6, 7a, and E proteins. *E. coli* strain BL21 (DE3) pLysE cells carrying pET24a-E, pET24a-3a, pET24a-3b, pET24a-6, pET24a-7a, pET24a-HCVE1, and pET24a were induced with 1 mM IPTG. The cell densities were measured at 600 nm at indicated times post-induction. Cells carrying pET24a-HCVE1 were used as positive control, and cells carrying pET24a were used as negative control.

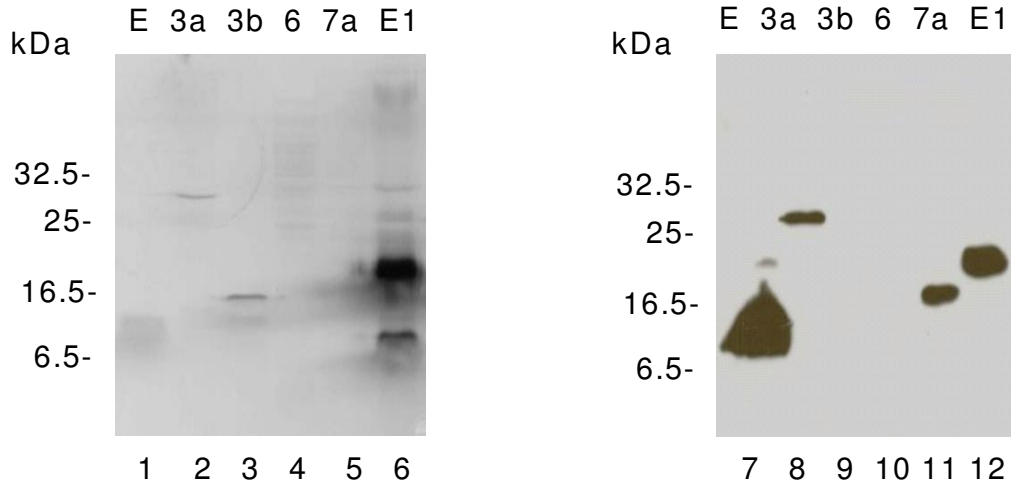

Fig. 3-2. Analysis of the expression of SARS-CoV proteins. BL21 (DE3) pLysE cells carrying plasmid pET24a-E, pET24a-3a, pET24a-3b, pET24a-6, pET24a-7a, and pET24a-HCVE1 were induced with 1 mM IPTG. To detect the proteins expression directly, 150 μg/ml of rifampicin was added 30 minutes post-induction. After incubation for 2 hours, cells were labeled with [^{35}S] methionine for 15 minutes. Electrophoresis of cell extracts was carried out on 15 % SDS-PAGE (lanes 1–6) and subjected to autoradiography. SARS-CoV E, 3a, 3b, 7a, and HCV E1 proteins were presented on the SDS-PAGE. No band corresponding to the SARS-CoV protein 6 was detected. To further confirm the expression and identities of the proteins, the unlabeled bacterial cells were harvested at 2 hours post-induction. The cell extracts were subjected to 15 % SDS-PAGE and analyzed by Western blotting using anti-His monoclonal antibody (lanes 7–12). SARS-CoV E, 3a, 7a, and HCV E1 were recognized by anti-His monoclonal antibody. No bands corresponding to the SARS-CoV protein 3b and protein 6 were detected. Numbers on the left indicate molecular masses in kilodaltons.

3.2.2. Alteration of membrane permeability in E. coli cells is associated with SARS-CoV E protein expression

Since expression of 3a and 3b proteins rendered no obvious effects on the growth of bacteria, these two proteins were excluded in the subsequent studies. To test if the observed inhibition of bacterial growth by the expression of E, 6 and 7a proteins is caused by the modification of membrane permeability, hygromycin B was added to the culture medium after induction of proteins expression with IPTG. Hygromycin B is an antibiotic which can inhibit host cell protein synthesis but is normally impermeable to cells within a short period of time. When the cell membrane permeability is altered, hygromycin B can entry into cells to block cellular proteins translation. Cells were metabolically labeled with [^{35}S] methionine for 15 minutes after addition of hygromycin B. Result revealed that expression of SARS-CoV E protein allowed the entry of hygromycin B into cells, as host protein synthesis was completely blocked (Fig. 3-3, lanes 1-2). Similar inhibitory effect on host protein synthesis was observed in bacterial cells expressing the positive control protein, HCV E1 protein (Fig. 3-3, lanes 5-6). No obvious effect on membrane permeability was observed in cells expressing 6 or 7a protein (Fig. 3-3, lanes 3-4).

To further confirm the observation that expression of SARS-CoV E protein could enhance membrane permeability, entry of ONPG into bacterial cells was analyzed. ONPG (2-Nitrophenyl-b-D-galactopyranoside), a colorimetric and spectrophotometric substrate for detection of β-galactosidase activity, is normally excluded by the membrane of intact cells. The enhancement of membrane permeability will increase the entry of ONPG. The entry

of ONPG into bacterial cells can be easily monitored by measuring its conversion to a colored compound (O.D. at 420 nm) by the β-galactosidase activity present in bacterial cells. As shown in Fig. 3-4, induction of the expression of E protein caused a clear increase in the entry of ONPG into bacterial cells. The similar effect was also observed upon the expression of positive control HCV E1 protein. These results confirmed that expression of SARS-CoV E protein could increase membrane permeability in bacterial cells.

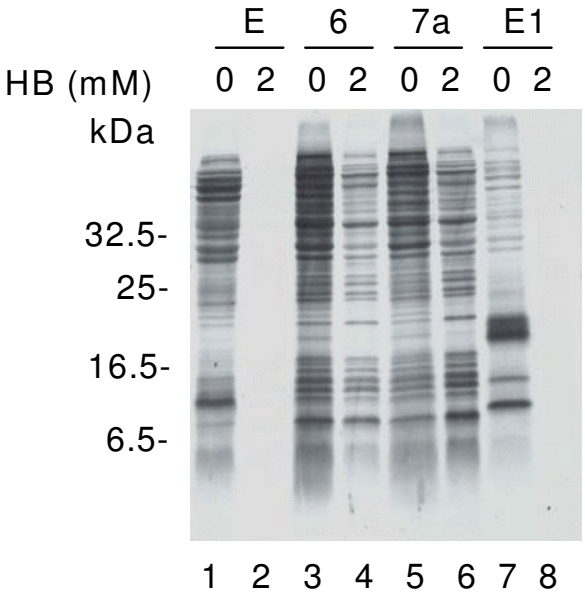

Fig. 3-3. Bacterial cells expressing SARS-CoV E protein allow the entry of hygromycin B. BL21 (DE3) pLysE cells transformed with individual pET24a-E, pET24a-6, pET24a-7a, and pET24a-HCVE1 were induced with 1 mM IPTG. At 1 hour post-induction, 2 mM hygromycin B was added. After incubation for 15 minutes, proteins were metabolically labeled with [^{35}S] methionine for 15 minutes. Cell extracts were analyzed on 15 % SDS–PAGE and subjected to autoradiography. Cells carrying HCV E1 protein were used as positive control. Numbers on the left indicate molecular masses in kilodaltons. Protein synthesis inhibition was observed in bacterial cells expressing SAR-CoV E protein and HCV E1 protein.

First time	E	7a	HCV E1	pET24a
0h	0.011	0.006	0.012	0.007
1h	0.114	0.044	0.067	0.054
2h	0.277	0.124	0.1	0.101
3h	0.35	0.209	0.154	0.124
4h	0.525	0.242	0.312	0.142

Second time	E	7a	HCV E1	pET24a
0h	0.012	0.002	0.005	0.008
1h	0.156	0.123	0.143	0.024
2h	0.226	0.172	0.195	0.085
3h	0.245	0.184	0.219	0.094
4h	0.289	0.215	0.254	0.097

Third time	E	7a	HCV E1	pET24a
0h	0.017	0.014	0.011	0.005
1h	0.149	0.053	0.098	0.115
2h	0.289	0.078	0.134	0.132
3h	0.347	0.16	0.243	0.151
4h	0.56	0.175	0.298	0.165

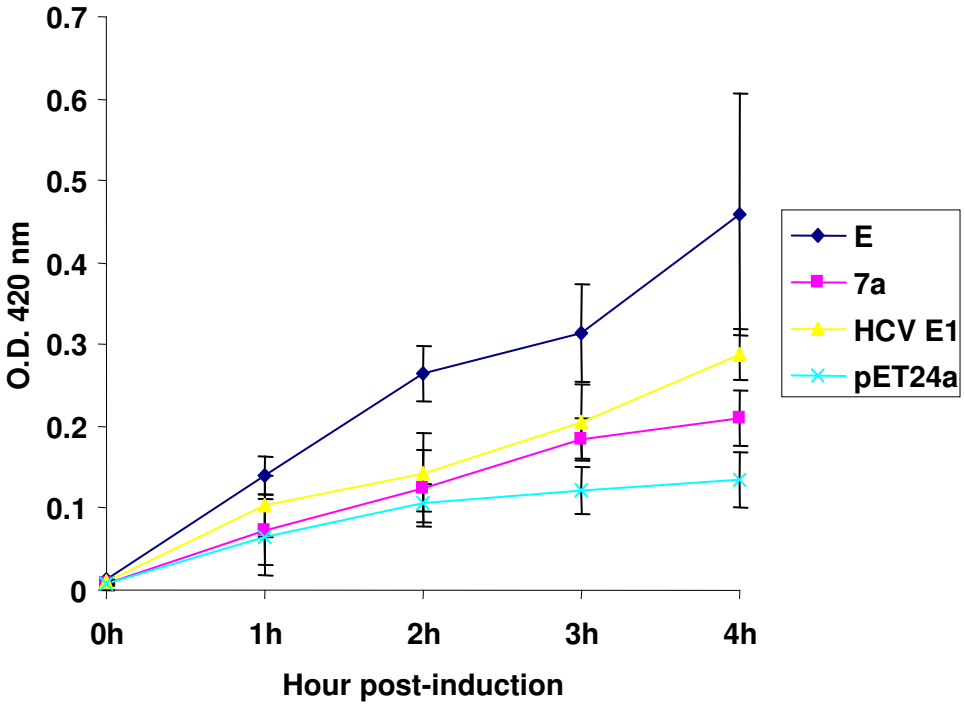

Fig. 3-4. Bacterial cells expressing SARS-CoV E protein allow the entry of ONPG. BL21 (DE3) pLysE cells carrying individual pET24a-E, pET24a-7a, pET24a-HCV E1, and pET24a were induced with 1 mM IPTG. 2 mM ONPG was added at the indicated times post-induction and incubated at 30 °C for 10 minutes. The β-galactosidase activity was determined by measuring the absorbance at O.D. 420 nm. Cells carrying pET24-HCV E1 were used as positive control and cells carrying pET24a were used as negative control. The entry of ONPG was observed in bacterial cells expressing SARS-CoV E protein and HCV E1 protein.

3.2.3. Alteration of membrane permeability to hygromycin B upon expression of SARS-CoV E protein in HeLa Cells

To gather more evidence on the membrane-permeabilizing activity of SARS-CoV E protein, we next tested the ability of E protein to induce membrane leakiness in mammalian cells. SARS-CoV N protein was included in this experiment as a control because N protein has good expression in HeLa cells and was easily detected. The SARS-CoV E gene or N gene was cloned into pFlag, an eukaryotic expression vector with Flag epitope tag (D-Y-K-D-D-D-D-K) fused at N-terminus. The expression of Flag-tagged E protein or Flag-tagged N protein was under the control of T7 promoter. Recombinant vaccinia virus (vTF7-3) offers the T7 RNA polymerase. HeLa cells were transfected by pFlag-E or pFlag-N after vTF7-3 infection. At 12 hours post-transfection, cells were treated with two different concentrations (1 mM and 2 mM) of hygromycin B for 30 minutes, and then radiolabeled with [^{35}S] methionine–cysteine for 3 hours in methionine–cysteine free medium. As the transfection efficiency cannot reach 100 %, the inhibitory effect on host protein synthesis in cells expressing E protein or N protein was disguised by the untransfected cells. To avoid this problem, only the E protein or N protein synthesis was analyzed. Cell extracts were prepared and the Flag-tagged E protein or N protein was immunoprecipitated by anti-Flag antibody under mild washing conditions. After immunoprecipitation, the Flag-tagged E protein or N protein was subjected 15 % SDS-PAGE and autoradiography.

As shown in Fig. 3-5, extracts prepared from cells without treatment of hygromycin B showed the detection of the Flag-tagged E protein migrating at about 14 kDa, which is

larger than the calculated molecular mass of approximately 10 kDa of the Flag-tagged E protein. The slightly aberrant migration may be due to the highly hydrophobic nature of the E protein. Meanwhile, some other cellular proteins were also detected. In cells treated with 1 and 2 mM of hygromycin B, the expression of the Flag-tagged E protein was reduced to 6 and 2 %, respectively (Fig. 3-5). However, in cells expressing SARS-CoV N protein, a similar amount of the Flag-tagged N protein was detected in presence or absence of hygromycin B (Fig. 3-5). The expression of the Flag-tagged N protein was only reduced to 90 and 85 %, respectively (Fig. 3-5). These data revealed that hygromycin B could readily penetrate cells expressing Flag-tagged E protein, but it was unable to cross the plasma membrane of cells expressing Flag-tagged N protein. It further confirmed that expression of E protein in mammalian cells enhanced the membrane permeability to hygromycin B.

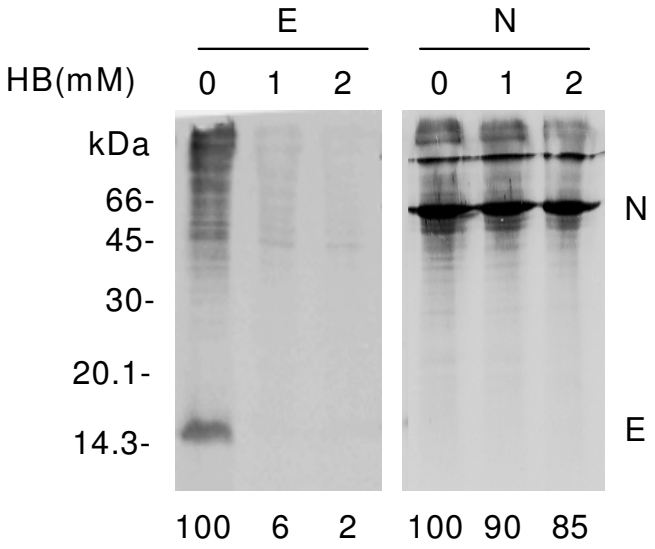

Fig. 3-5. Modification of the mammalian cell membrane permeability by SARS-CoV E protein. HeLa cells expressing the Flag-tagged SARS-CoV E protein or N protein were treated with 0, 1, and 2 mM of hygromycin B for 30 minutes at 12 hours post-transfection, and were radiolabeled with [^{35}S] methionine–cysteine for 3 hours. Cell lysates were prepared and the expression of Flag-tagged E protein or N protein was detected by immunoprecipitation with anti-Flag monoclonal antibody under mild washing conditions. Polypeptides were separated by 15 % SDS-PAGE and visualized by autoradiography. Cells expressing Flag-tagged SARS-CoV N protein were included as control. The percentages of Flag-tagged E protein or N protein detected in the presence of hygromycin B were determined by densitometry and indicated at the bottom. Numbers on the left indicate molecular masses in kilodaltons. Obvious protein synthesis inhibition was observed in cells expressing E protein but not in cells expressing N protein.

3.3. Membrane association of SARS-CoV E protein

3.3.1. SARS-CoV E protein is an integral membrane protein

SARS-CoV E protein contains long hydrophobic domain and enhances cell membrane permeability like a viroporin. It is believed that E protein is associated with cell membrane. In order to characterize the membrane association property of the SARS-CoV E protein in detail, solubilized studies were performed using buffers that allow differentiation between peripheral and integral membrane proteins.

HeLa cells expressing the Flag-tagged E protein were disrupted by Dounce homogenization. Nuclei and cell debris were removed by centrifugation (1000 × g for 10 minutes). The cytosol fraction and membrane fraction were separated by ultracentrifugation (45000 × g for 30 minutes), and the presence of the E protein in each fraction was analyzed by Western blot. As shown in Fig. 3-6, the Flag-tagged SARS-CoV E protein was almost exclusively located in the membrane fraction. The IBV E protein was included as a control as it has been demonstrated as an integral membrane protein. Fractionation of HeLa cells expressing the Flag-tagged IBV E protein showed exclusive detection of the protein in the membrane fraction. This result demonstrated that SARS-CoV E protein was associated with cellular membrane.

Western blot analysis of the same fractions with anti-GM130 antibody (Abcam, GM130 antigen is from mouse) showed the detection of an unknown host protein of approximately 60 kDa that was exclusively located in the membrane fraction (Fig. 3-6). During experiment process, it was found the biochemical characteristic of this 60 kDa

host protein was perfect integral membrane protein. The 60 kDa host protein was released out of cellular membrane under Triton X-100 treatment, however, it was still associated with the cellular membrane under high pH or high salt treatment. Triton X-100 is a detergent that can solubilize the cellular membrane therefore release integral membrane protein and peripheral membrane protein from membranes (Helenuis and Simons, 1975). High pH treatment disrupts membrane vesicles, releasing the peripheral membrane proteins from these vesicles but not integral membrane protein (Fujiki *et al*., 1982; Tiganos *et al*., 1998). High salt buffer also releases membrane-associated but not integral membrane proteins from the membrane fraction. It would be expected that integral membrane proteins would be solubilized and thus be found in the supernatant fraction after Triton X-100 treatment but not high salt or high pH treatment. Therefore, this 60 kDa host protein was used as an integral membrane protein control, to ensure that the procedures and conditions used to treat the cell lysates were appropriate.

To determine if SARS-CoV E protein was embedded into the cellular membrane or attached to the membrane, the membrane fraction was treated with either 1 % Triton X-100, 1 M KCl (high salt), or 100 mM Na_2CO_3 (high pH, pH 11), before centrifugation to separate the soluble content (S) from the pellet (P). As Fig. 3-6 shown, treatment of the membrane pellets with 1 % Triton X-100 and high pH led to the detection of SARS-CoV and IBV E proteins in both the supernatants and the pellets, whereas treatment of the membrane fraction with 1 M KCl (high salt) showed that both E proteins were solely detected in the pellets. In the same membrane fraction treated with Triton X-100, anti-GM130 antibodies detected the 60 host kDa protein exclusively in the supernatants,

whereas in samples treated with both high pH and high salt, the 60 kDa host protein was detected in the pellets only (Fig. 3-6), confirming that all the experiment procedures were appropriate.

These results demonstrated that SARS-CoV E protein was associated with membrane as an integral membrane protein similar to IBV E protein but was slightly different from the 60 kDa host integral membrane protein. Under 1 % Triton X-100 treatment, the SARS-CoV and IBV E proteins were partially released out of the cellular membrane, whereas the 60 kDa host protein was fully released out of the cellular membrane. Under high pH treatment, the SARS-CoV and IBV E proteins were also partially released out of the membrane, while the 60 kDa host protein was absolutely associated membrane. The resistance to Triton X-100 treatment of SARS-CoV and IBV E protein indicated that a proportion of E protein might be associated with specific site in the cell membrane such as lipid rafts that were partial insoluble in Triton X-100. The partially presence of E protein in the supernatant fractions of the high pH treatment could be attributed to its inherent ability to permeabilize and destabilize membranes. The membrane perturbation probably caused E protein containing vesicle disruption and fragmentation under high pH treatment. Based on this explanation, SARS-CoV E protein should be an integral membrane protein.

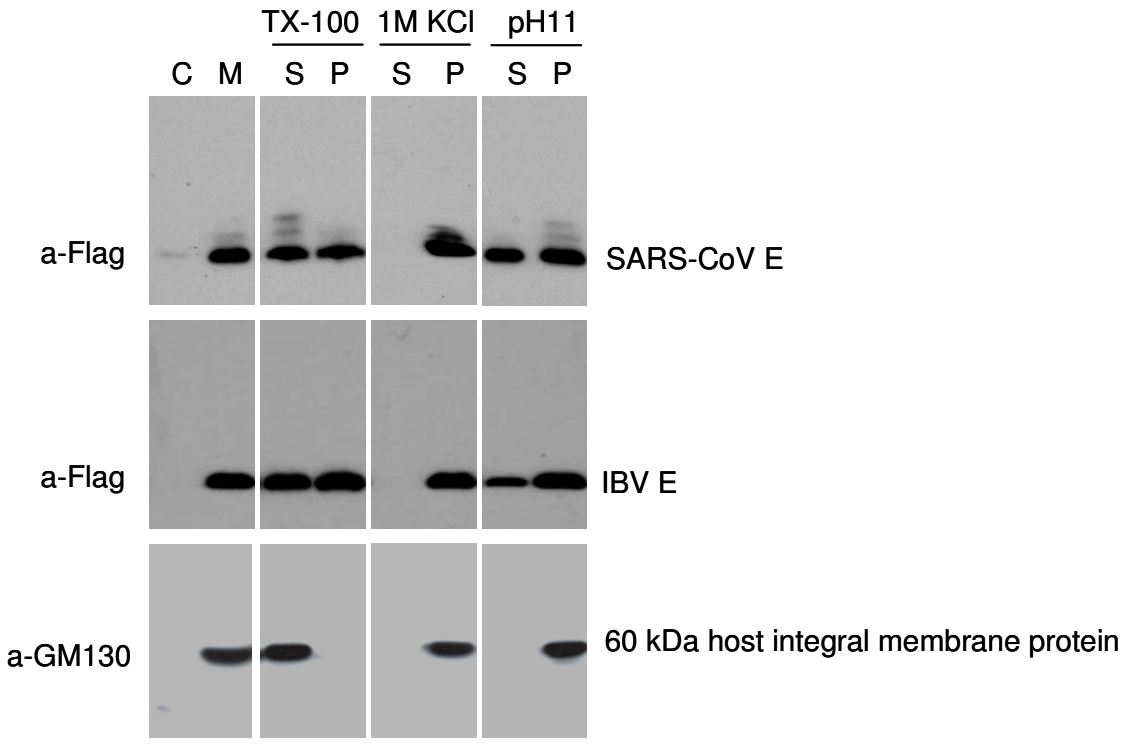

Fig. 3-6. SARS-CoV E protein is associated with cell membrane. HeLa cells expressing the Flag-tagged SARS-CoV and IBV E proteins, respectively, were harvested at 12 hours post-transfection, broken by 20 stokes with a Dounce cell homogenizer, and fractionated into cytosol (C) and membrane (M) fractions after removal of cell debris and nuclei. The membrane fraction was treated with 1 % Triton X-100, 1 M KCl (high salt), and 100 mM Na_2CO_3 (pH 11) at room temperature, respectively, and further fractionated into soluble (S) and pellet (P) fractions. Polypeptides were separated by 15 % SDS-PAGE and subjected to Western blot using either anti-Flag antibody (Sigma) or anti-GM130 antibody (Abcam). Numbers on the left indicate molecular masses in kilodaltons.

3.3.2. Subcellular localization of SARS-CoV E protein

To further analyze the membrane association properties of the SARS-CoV E protein, its subcellular localization was studied by indirect immunofluorescence. HeLa cells over-expressing the Flag-tagged E protein using vTF7-3 system were fixed with 4 % paraformaldehyde at 12 hours post-transfection and stained with anti-Flag monoclonal antibody (Fig. 3-7). In cells permeabilized with 0.2 % Triton X-100, the Flag-tagged E protein was mainly localized to the perinuclear regions of the cells (Fig. 3-7, panel A). The staining patterns largely overlap with calnexin, an ER resident protein (panels B and C). It was also noted that some granules and punctated staining patterns are not well merged with the calnexin staining patterns. They may represent aggregates of the E protein.

The exact subcellular localization of a coronavirus E protein is an issue of debate in the current literature. Although clear ER localization of the coronavirus IBV E protein was observed at early time points in a time course experiment using an over-expression system (Lim and Liu, 2001), no such localization patterns were observed as reported by Corse and Machamer (2001, 2002). To clarify that the above observed ER localization pattern may be due to the high expression level of the protein in HeLa cells using the vTF7-3 system, the subcellular localization of the SARS-CoV E protein in BSR *T7/5* cells with lower expression efficiency was carried out. BSR *T7/5* cells can stably express T7 RNA polymerase (Buchholz *et al*., 1999) and doesn't rely on vTF7-3 to provide T7 RNA polymerase. As shown in Fig. 3-7, the Flag-tagged SARS-CoV E protein exhibited typical Golgi localization patterns in BSR *T7/5* cells as the E protein staining patterns

merged well with Golgi resident protein GM130 (panels D–F). The untagged SARS-CoV E protein also co-localized with GM130 in BSR *T7/5* cells (Fig. 3-7, panels G–I). These results suggested that the predominant ER localization patterns in HeLa cells observed above might be due to the cell type used and the very high expression levels in individual cells with the vTF7-3 expression system. The main localization of E protein should be Golgi apparatus.

Cell surface expression is a prerequisite for SARS-CoV E protein to alter the cell membrane permeability. Over the course of this study, it was observed that SARS-CoV E protein exhibited weak cell surface staining even in cell over-expressing the protein (Yuan *et al.,* 2006). The reason for this observation is that the epitopes were inaccessible to the antibody under non-permeable condition as the majority of the E protein adopts $N_{cyto}C_{cyto}$ topology (Yuan *et al.,* 2006).

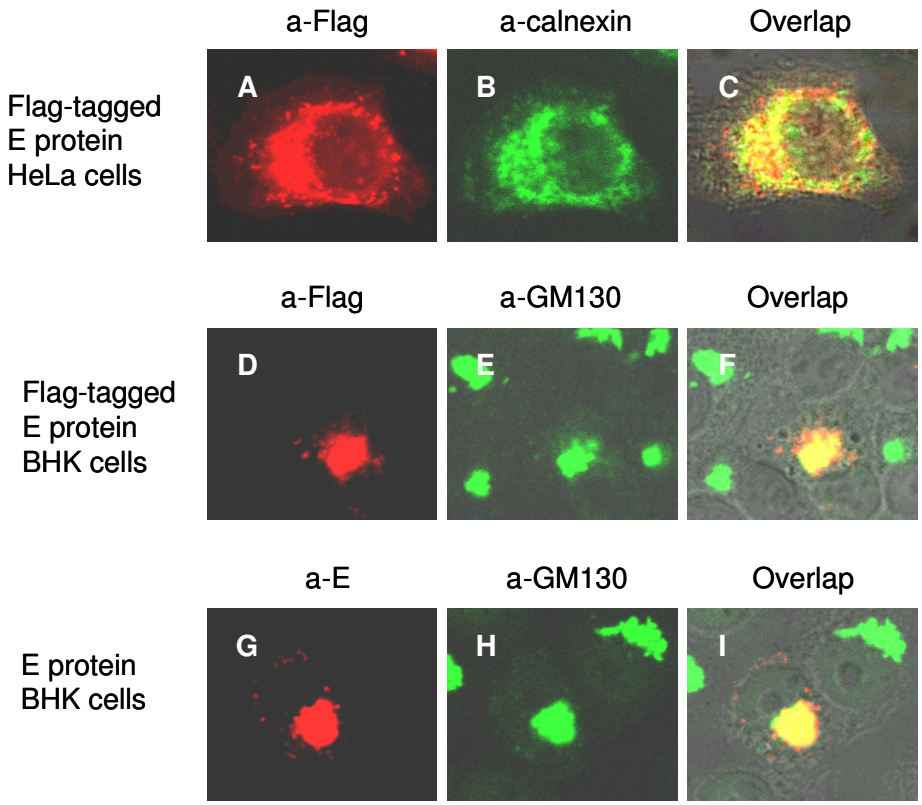

Fig. 3-7. Subcellular localization of SARS-CoV E protein. HeLa cells expressing the Flag-tagged SARS-CoV E protein (A–C), and BSR *T7/5* cells expressing the Flag-tagged (D–F) and untagged (G–I) E protein were stained with either anti-Flag (A–F) or anti-E (G–I) antibodies at 12 hours post-transfection after permeabilizing with 0.2 % Triton X-100. The same HeLa cells were also stained with anti-calnexin antibody (B), and the same BSR *T7/5* cells were also stained with anti-GM130 antibodies (panels E and H). Panels C, F, and I showed the overlapping images. In HeLa cells, the over-expressed SARS-CoV E protein using the vTF7-3 system was co-localized to with ER resident protein calnexin (A-C). However, in BSR *T7/5* cells stably-expressing the T7 RNA polymerase, the E protein with lower expression level was co-localized with Golgi resident protein GM130 (D-I).

3.4. Oligomerization of SARS-CoV E protein

3.4.1. Examination of the oligomeric status of SARS-CoV E protein in bacterial cells

Virtually all of the viroporins identified to date possess the ability to oligomerize and form aggregates in mammalian cells. Oligomerization of these viral proteins is thought to be critical for the formation and expansion of the hydrophilic pore in lipid bilayers. This study sought to determine whether SARS-CoV E protein was able to oligomerize in cells.

Initially, the ability of SARS-CoV E protein to form oligomers was examined in bacterial cells. After induction with IPTG, the bacterial cells were harvested and lysed with the protein loading buffer in the presence (reducing condition) or absence (non-reducing condition) of 100 mM DTT. DTT can disrupt the disulfide bonds and dissociated oligomers formed by disulfide bonds. The protein loading buffer also contains 10 mM of iodoacetamide. Iodoacetamide was used to irreversibly block the free cysteinyl thiols to form disulfide bonds. Under such conditions, electrophoresis of the bacterial expressed E protein on reducing 15 % SDS–PAGE showed the detection of a 14 kDa band, representing the monomer of the E protein (Fig. 3-8, lane 2). In addition to the 14 kDa protein band, analysis of the same sample on non-reducing SDS–PAGE showed the detection of an additional protein band migrating at the position of 28 kDa (Fig. 3-8, lane 1), representing a putative homo-dimer of the SARS-CoV E protein. This result suggested that E protein might form homo-dimers by disulfide bonds in bacterial cells.

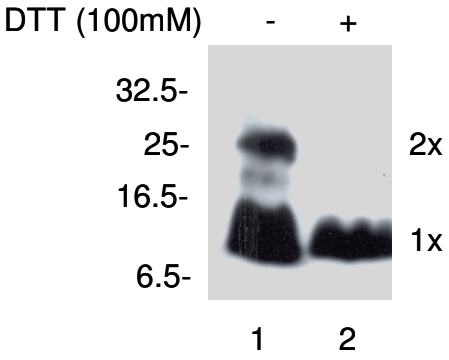

Fig. 3-8. Oligomerization of SARS-CoV E protein in bacterial cells. The His-tagged SARS-CoV E protein expressed in bacterial cells (lanes 1-2) was separated by 15 % SDS-PAGE under reducing (lane 2) and non-reducing (lane 1) conditions, and analyzed by Western blot using anti-His monoclonal antibodies. Dimer and monomer of the E protein are indicated on the right. Numbers on the left indicate molecular masses in kilodaltons. E protein dimer was observed in the absence of DTT and was invisible in the presence of DTT.

3.4.2. Examination of the oligomeric status of SARS-CoV E protein in HeLa cells

We also examined the oligomeric status of SARS-CoV E protein in HeLa cells. To detect the protein expression, Flag-tag was fused to the N-terminus of the E protein. HeLa cells expressing Flag-tagged E protein were harvested and lysed with the protein loading buffer (contains 10 mM of iodoacetamide) in the presence or absence of 100 mM DTT. Analysis of the E protein on the reducing SDS-PAGE showed the detection of the 14 kDa monomer. Both the 14 kDa monomer and the 28 kDa dimer were observed under non-reducing conditions (Fig. 3-9). This result confirmed that E protein could form dimer by disulfide bonds in HeLa cells. In addition to the 14 kDa and 28 kDa species, additional bands (between 14 kDa and 18 kDa) were detected under both reducing and non-reducing conditions, suggesting that E protein may undergo post-translational modification (Fig. 3-9). The post-translational modification of E protein would be characterized later. More detailed characterization of the oligomeric status of the SARS-CoV E protein was hampered by the low expression efficiency of the protein in the HeLa cell system.

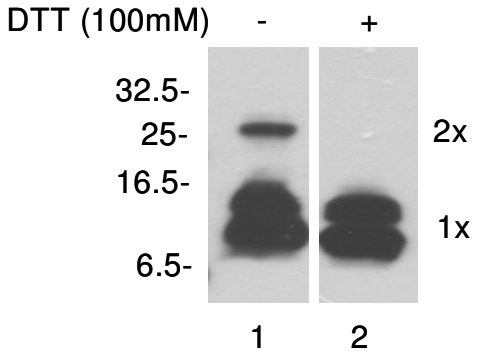

Fig. 3-9. Oligomerization of SARS-CoV E protein in HeLa cells. The Flag-tagged SARS-CoV E protein expressed in HeLa cells were separated by 15 % SDS-PAGE under reducing and non-reducing conditions, and analyzed by Western blot using anti-Flag antibody. Dimer and monomer of the E protein are indicated on the right. Numbers on the left indicate molecular masses in kilodaltons. E protein dimer was observed in the absence of DTT and invisible in the presence of DTT.

3.4.3. Examination of the oligomeric status of SARS-CoV E protein in insect cells by cross-linking

To further explore the oligomeric nature of SARS-CoV E protein, glutaraldehyde, a short self-polymerizing reagent that reacts with lysine, tyrosine, histidine, and tryptophan, was used. In this study, the baculovirus expression system was chosen to express SARS-CoV E protein as this system can produce large amount of E protein with correct folding as well as disulfide bond formation, oligomerization and other important post-translational modifications. The E protein with a His-tag at the C-terminus was expressed in insect cells by recombinant baculovirus and purified by Ni-NTA purification system. The purified E protein was concentrated and subjected to cross-linking with three different concentrations of glutaraldehyde (0.1 mM, 0.25 mM, and 0.5 mM). As shown in Fig. 3-10, cross-linking with glutaraldehyde showed the detection of dimer, trimer, tetramer, and other higher-order oligomers/aggregates of the E protein under either non-reducing (Fig. 3-10, lanes 1–3) or reducing (Fig. 3-10, lanes 4–6) conditions. It was noted that more higher-order oligomers/aggregates were detected under non-reducing conditions when higher concentrations of the cross-linking reagent were used (Fig. 3-10, lanes 1–3). Some of these higher-order oligomers/aggregates were dissociated into trimer, dimer and monomer under reducing conditions, indicating that these higher oligmers were linked by glutaraldehyde as well as interchain disulfide bonds. This result confirmed that the SARS-CoV E protein could form higher-order oligomers. Both the interchain disulfide bonds formation and hydrophobic interaction might contribute to this.

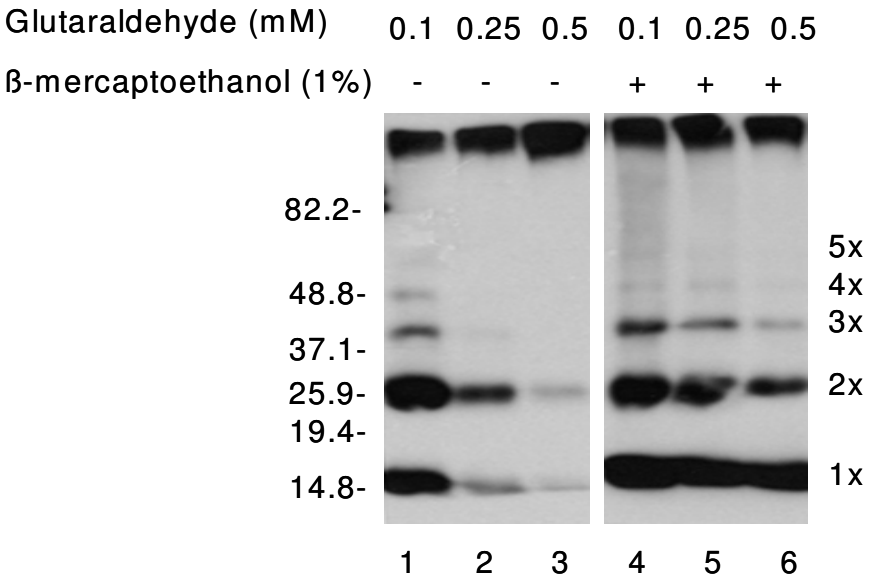

Fig. 3-10. Oligomerization of SARS-CoV E protein in insect cells. The His-tagged SARS-CoV E protein expressed in Sf9 insect cells was purified using Ni-NTA purification system (Qiagen), and incubated with three different concentrations of glutaraldehyde (0.1, 0.25, and 0.5 mM) for 1 hour at room temperature. The reaction was quenched by adding 100 mM glycine. Polypeptides were separated by 15 % SDS-PAGE in the presence or absence of 1 % β-mercaptoethanol, and analyzed by Western blot with anti-His antibody. Dimer, trimer, tetramer and higher order oligomers were observed. Different oligomers of the E protein are indicated on the right. Numbers on the left indicate molecular masses in kilodaltons.

3.5. The role of cysteine residues of SARS-CoV E protein in its membrane-permeabilizing activity and oligomerization

3.5.1. The essential role of C40 and C44 of SARS-CoV E protein in its oligomerization and membrane-permeabilizing activity in E. coli cells

SARS-CoV E protein contains three cysteine residues at amino acid positions 40, 43, and 44, respectively. These residues are located 3–7 aa downstream of the C-terminus of the transmembrane domain. To evaluate the role of these cysteine residues in disulfide bonds and oligomer formation, the cysteine residues were converted by site-specific mutagenesis to alanine residues either individually or in combination of two or three. A schematic diagram showing the single- or double- or triple-cysteine mutants is shown in Fig. 3-11A. The mutants were then expressed in *E. coli* cells and polypeptides were analyzed under non-reducing conditions on 15 % SDS-PAGE. As can be seen in Fig 3-11B, there were mutant-specific differences in electrophoretic mobility patterns. Both the 14 kDa monomer and the 28 kDa dimer were detected in bacteria expressing individual wild-type E protein C43-A under non-reducing conditions (lanes 1-3). Only the 14 kDa monomer was detected in bacterial cells expressing individual C40-A, C44-A, C40/44-A and C40/43/44-A (lanes 2, 4, 5 and 6). These results confirmed that both C40 and C44 were involved in oligomerization of the E protein by formation of interchain disulfide bonds between C40 and C44.

Since the C40 and C44 are involved in the oligomerization of E protein, they might affect the membrane-permeabilizing activity of E protein. To analyze the involvement of

these cysteine residues in the membrane-permeabilizing activity of E protein in bacterial cells, hygromycin B assay was performed in *E. coli* cells expressing individual mutants. As can be seen in Fig. 3-11C, expression of wild-type E protein and mutant C43-A showed obvious induction of membrane permeability, as significant inhibition of protein synthesis by hygromycin B was observed (Fig. 3-11C, lanes 1-2; and lanes 5-6). In contrast, expression of mutants C40-A, C44-A, C40/44-A and C40/43/44-A showed no obvious enhancement of membrane permeability to hygromycin B (Fig. 3-11C, lanes 3-4, and 7–12), indicating that these mutations might abolish the membrane-permeabilizing activity of E in *E. coli* cells. These results demonstrated that C40 and C44 could link E protein together to form a pore in the membrane, therefore enhanced membrane permeability in the bacterial cells.

A

```
                1         10        20        30        40        50        60        70
E               MYSFVSEETGTLIVNSVLLFLAFVVFLLVTLAILTALRLCAYCCNIVNVSLVKPTVYVYSRVKNLNSSEGVPDLLV
C40-A           ----------------------------------------A---------------------------------
C43-A           -----------------------------------------A--------------------------------
C44-A           ------------------------------------------A-------------------------------
C40/44-A        ----------------------------------------A---A-------------------------------
C40/43/44-A     ----------------------------------------A--AA-------------------------------
```

B

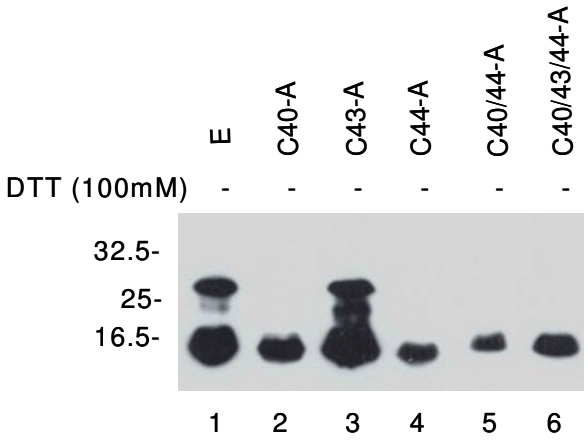

C

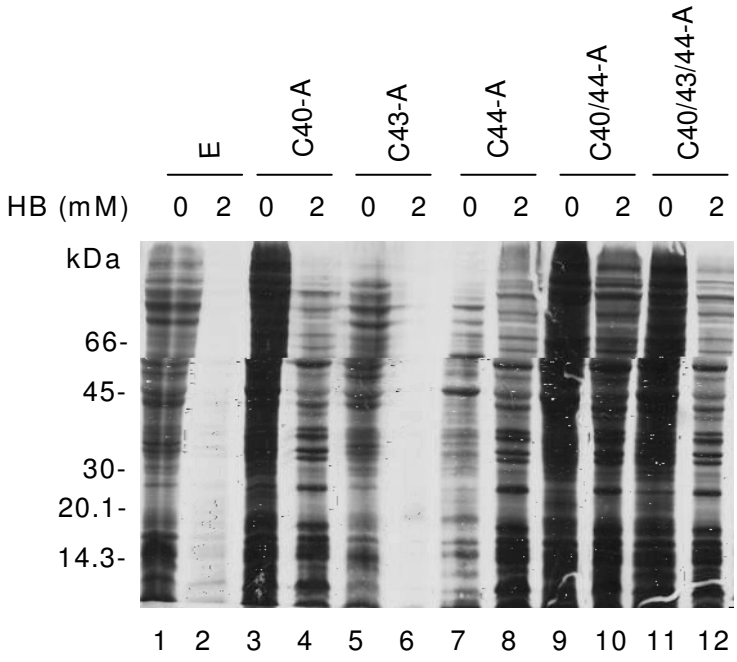

Fig. 3-11. The essential role of C40 and C44 of SARS-CoV E protein in its oligomerization and membrane-permeabilizing activity in *E. coli* cells. (A) Schematic diagram of cysteine mutants. The putative transmembrane domain is underlined. For each mutant, the cysteine residues at amino acid positions 40, 43 and 44 are indicated as C (cysteine) or the altered residue A (Alanine). The designation of the mutants C40-A, C43-A, C44-A, C40/44-A and C40/43/44-A is shown on the left. (B) Oligomerization of wild-type and mutant E proteins in *E. coli* cells. The His-tagged wild-type and mutant E proteins expressed in *E. coli* cells were separated by 15 % SDS-PAGE under non-reducing conditions, and analyzed by Western blot using anti-His antibody. Numbers on the left indicate molecular masses in kilodaltons. Only wild-type E protein and C43-A can form dimer. The C40-A, C44-A, C40/44-A and C40/43/44-A cannot form dimer. (C) Entry of hygromycin B into bacterial cells expressing wild-type and mutant E proteins. BL21 (DE3) pLysE cells transformed with wild-type or mutant E proteins were induced with 1 mM IPTG. At 1 hour post-induction, 2 mM hygromycin B was added. After incubation for 15 minutes, proteins were metabolically labeled with [^{35}S] methionine for 15 minutes. Cell extracts were analyzed on 15 % SDS–PAGE and subjected to autoradiography. Numbers on the left indicate molecular mass in kilodaltons. Bacterial cells expressing wild-type E protein or mutant C43-A are permeable to hygromycin B, whereas bacterial cells expressing mutant C40-A, C44-A, C40/44-A and C40/43/44-A are impermeable to hygromycin B.

3.5.2. The C40 and C44 residue are not essential in the membrane-permeabilizing activity of SARS-CoV E protein in mammalian cells

The first and third cysteine residues, at amino acid positions 40 and 44, respectively, were shown to play a certain role in oligomerization of the SARS-CoV E protein in bacterial cells (Fig. 3-11B). They were also involved in the E protein-induced alteration of membrane permeability in bacterial cells (Fig. 3-11C). Since the membrane system and protein folding in bacterial cells and mammalian cells are quite different, the role of cysteine residues need to be further explored in mammalian cells. To systematically test the effects of these cysteine residues on the oligomerization and the membrane-permeabilizing activities of SARS-CoV E protein in mammalian cells, five mutants C40-A, C43-A, C44-A, C40/44-A, and C40/43/44-A were cloned into mammalian cells expression vector pFlag, with Flag-tag fused at N-terminus of them. Wild-type and mutant E proteins were expressed in HeLa cells using a vTF7-3 expression system. Western blotting analysis of cells expressing wild-type and mutant constructs showed specific detection of three species migrating at the range of molecular masses from 14 to 18 kDa under reducing conditions and representing different isoforms of E protein (Fig. 3-13A). These isoforms might be derived from post-translational modifications of the protein. No 28 kDa dimers for these mutants were observed under non-reducing condition (data not shown). It may due to the cysteine residues mutation or low protein concentration.

In the membrane permeability assay, cells were treated with two different concentrations (1 mM and 2 mM) of hygromycin B for 30 minutes, and then radiolabeled

with [^{35}S] methionine–cysteine for 3 hours. Cell extracts were prepared and the expression of E protein was detected by immunoprecipitation with anti-Flag antibody. As shown in Fig. 3-12B, expression of wild-type and mutant E proteins showed that similar levels of inhibition of protein synthesis by hygromycin B were obtained (Fig. 3-12B). These results suggested that, contrary to the previous results observed in bacterial cells, these cysteine residues do not render significant effects on the membrane-permeabilizing activity in mammalian cells. The observation that disulfide bond formation was not essential for E protein membrane-permeabilizing activity in mammalian cells was unexpected. This discrepancy may reflect differences in post-translational modifications, membrane association, subcellular localization, and translocation of the E protein in prokaryotic cells and eukaryotic cells. In mammalian cells, oligomerization was specified mainly by the transmembrane domain and the cysteine residues might play a role in stabilization of the oligomers. The role of cysteine residues in E protein oligomerization would be analyzed in insect cells expression system in which E protein can acquire higher expression level.

A

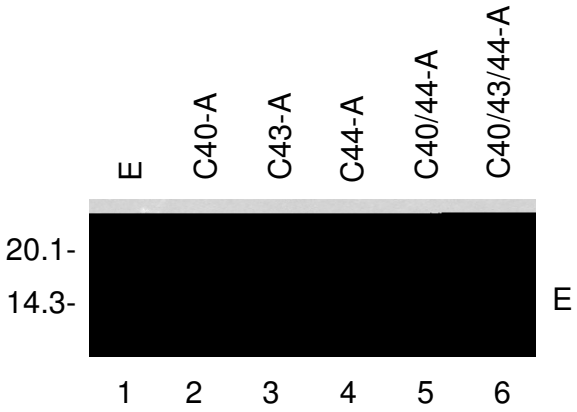

B

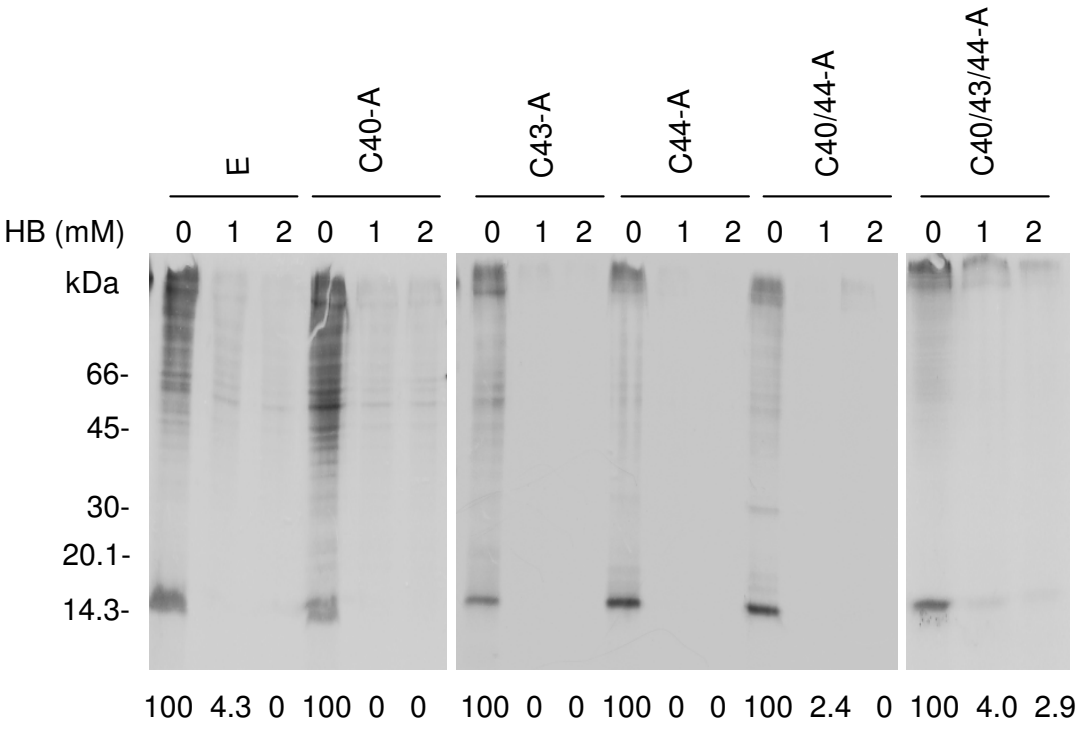

Fig. 3-12. Mutational analysis of the three cysteine residues of SARS-CoV E protein in mammalian cells. (A) The expression of wild-type and mutant SARS-CoV E proteins. HeLa cells were transfected with the Flag-tagged wild-type and mutant E protein constructs containing mutations of either a single (C40-A, C43-A, and C44-A), combination of two (C40/44-A) or all three (C40/43/44-A) cysteine residues. Cell lysates were prepared at 12 hours post-transfection, polypeptides were separated by 15 % SDS-PAGE and analyzed by Western blot using the anti-Flag antibody. Numbers on the left indicate molecular masses in kilodaltons. (B) Entry of hygromycin B into HeLa cells expressing wild-type and mutant E proteins. HeLa cells expressing the Flag-tagged wild-type or mutant E proteins were treated with 0, 1, and 2 mM of hygromycin B for 30 minutes at 12 hours post-transfection, and radiolabeled with [^{35}S] methionine–cysteine for 3 hours. Cell lysates were prepared and the expression of E protein was detected by immunoprecipitation with anti-Flag antibody under mild washing conditions. Polypeptides were separated by 15 % SDS-PAGE and visualized by autoradiography. The percentages of E proteins detected in the presence of hygromycin B were determined by densitometry and indicated at the bottom. Numbers on the left indicate molecular masses in kilodaltons. The wild-type and mutant E proteins showed similar levels of inhibition of protein synthesis by hygromycin B.

3.5.3. The role of cysteine residues on oligomeric status of SARS-CoV E protein in insect cells

Why cysteine mutants of SARS-CoV E protein still retained the membrane-permeabilizing activity in mammalian cells? To answer this question, mutant C40/43/44-A with His-tag at C-terminus was constructed to examine their roles in the oligomeric status of SAS-CoV E protein in insect cells. This mutant was constructed into baculovirus and expressed in insect cells. After purifying from the insect cell lysates by Ni-NTA beads, the mutant E protein C40/43/44-A was concentrated and subjected to SDS-PAGE and Western blot. As shown in Fig. 3-13 A, under non-reducing condition, the trimer, tetramer and pentamer of mutant protein C40/43/44-A were almost undetectable, the dimer was still formed. Compare with wild-type E protein, less dimer of this mutant was observed and the dimer of this mutant was resistant to the 1 % β-mercaptoethanol treatment (Fig. 3-13A). The β-mercaptoethanol resistant dimer might be formed by hydrophobic interaction as no disulfide bond could be formed in the absence of cysteine residues. This mutant could be linked into high molecular weight species after cross-linking (3-13B), confirming that E protein still could form oligomers in the absence of cysteine residues. The cysteine residues might be not essential in the formation of the E protein oligomers but could stabilize the oligomeric structure. This result might explain that why cysteine mutants of E protein still retained the membrane-permeabilizing activity in eukaryotic cells.

A

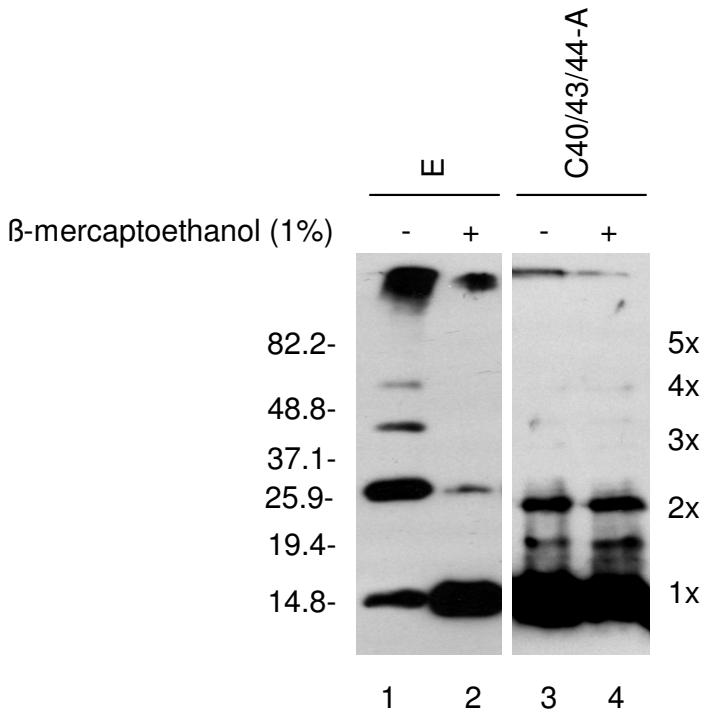

B

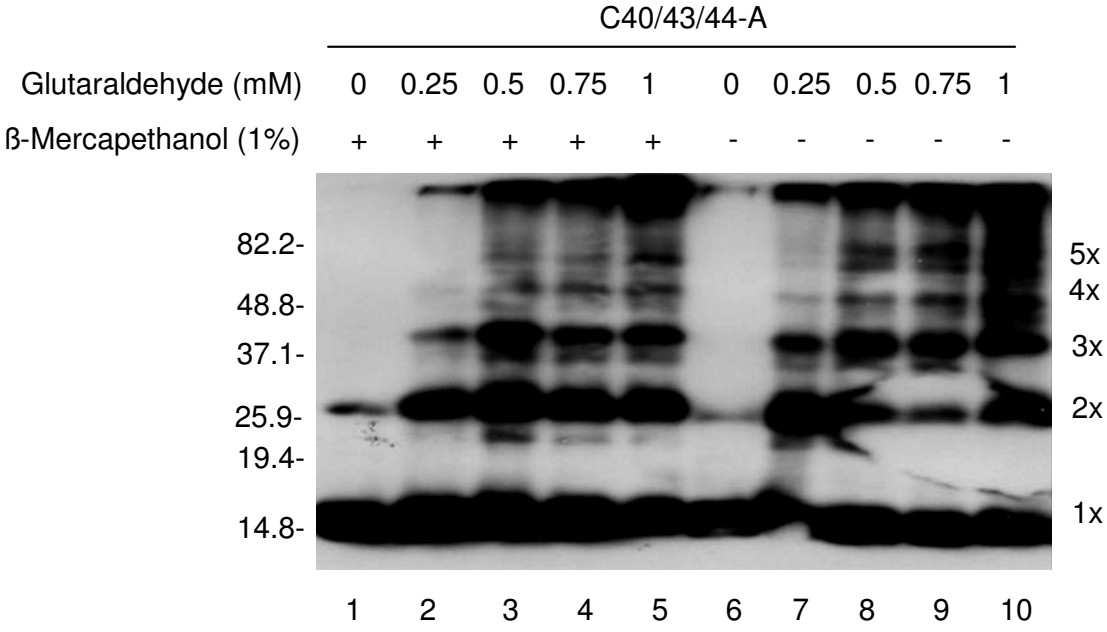

Fig. 3-13. Mutational analysis of the role of three cysteine residues of SARS-CoV E protein in its oligomerization in insect cells. (A) The His-tagged wild-type and mutant SARS-CoV E protein expressed in Sf9 insect cells was purified using Ni-NTA purification system (Qiagen). Polypeptides were concentrated and separated by 15 % SDS-PAGE in the presence or absence of 1 % β-mercaptoethanol, and analyzed by Western blot with anti-His antibody. Different oligomers of the E protein are indicated on the right. Compared to wild-type E protein, the trimer, tetramer and pentamer of C40/43/44 were almost undetectable, but the dimer was still formed and it was resistant to the 1 % β-mercaptoethanol. Numbers on the left indicate molecular masses in kilodaltons. (B). The purified mutant E protein C40/43/44-A was incubated with five different concentrations of glutaraldehyde (0, 0.25, 0.5, 0.75 and 1 mM) for 1 hour at room temperature. The reaction was quenched by adding 100 mM glycine. Polypeptides were separated by 15 % SDS-PAGE in the presence or absence of 1 % β-mercaptoethanol, and analyzed by Western blot with anti-His antibody. Different oligomers of the E protein are indicated on the right. The mutant E protein C40/43/44 still can form dimer, trimer, tetramer, pentamer, and higher molecular weigh species after cross-linking. Numbers on the left indicate molecular masses in kilodaltons.

3.6. The role of transmembrane domain of SARS-CoV E protein in its membrane-permeabilizing activity and oligomerization

3.6.1. Effects of mutations introduced into the transmembrane domain on the membrane-permeabilizing activity of the SARS-CoV E protein

SARS-CoV E protein contains an unusually long putative transmembrane domain of 29 aa with a high leucine/isoleucine/valine content (55.17 %). Recent molecular simulation and biochemical evidence showed that this domain may be involved in the formation of ion channel by oligomerization. In this study, mutations of the putative transmembrane domain were carried out to study its functions in membrane association and membrane-permeabilizing activity of the E protein. As shown in Fig. 3-14A, four mutants, Em1, Em2, Em3, and Em4, were initially made by mutation of 3–7 leucine/valine residues to charged amino acid residues in the transmembrane domain. These mutants were generated because F23 has been suggested to have a central role in the formation of a putative short hairpin of the transmembrane domain, and L18, L19, F20, L21, A22, V24, V25, F26, L27 and L28 form palindrome with the inversion point F23 (Arbely *et al*., 2004). These mutants might perturb the hairpin structure of the transmembrane domain. Em5, which contained mutation of N15 to E, was constructed because N15 might provide stabilization for the oligomers *via* interchain hydrogen bonds (Arbely *et al*., 2004; Torres *et al*., 2006). All these mutants were cloned into vector pFlag, with Flag-tag at the N-terminus. Expression of these mutants showed the detection of polypeptides with apparent molecular masses ranging from 10 to 18 kDa (Fig. 3-14B). Interestingly, mutations introduced into Em2, Em3, and Em4 significantly change the

migration rate of the corresponding mutant E protein on 15 % SDS-PAGE. The apparent molecular mass of these mutant proteins were approximately 10 kDa, which was consistent with the predicted molecular weight for the Flag-tagged E protein (Fig. 3-14B). The fact that substitutions of the hydrophobic amino acid residues in the transmembrane domain of the E protein with charged amino acids significantly altered the migrating properties of the E protein reflected that the slower migration of wild-type E protein on SDS-PAGE was due to its hydrophobic property. All the Em mutants could still form dimers or trimers in non-reducing conditions. The dimers and trimers were dissociated into monomer after DTT treatment (Fig. 3-14B). This result indicated the cysteine residues might be involved in the oligomerization of these Em mutants. When the transmembrane domain of E protein was disrupted, the cysteine might help E protein to form disulfide bond by disulfide bonds.

In the membrane permeability assay, 0.5 and 1 mM of hygromycin B were used. The use of lower concentrations of hygromycin B is to ensure the detection of subtle changes on membrane permeability induced by the mutant constructs. Meanwhile, Flag-tagged SARS-CoV N protein was co-transfected with wild-type or mutant E proteins into HeLa cell to aid assessment of the inhibitory effect of protein synthesis by hygromycin B. As Fig. 3-14C shown, all mutant E proteins still increased the cell membrane permeability to hygromycin B. However, the ability of the mutant proteins to induce these alterations varied for the different mutations. In cells expressing individual Em1, Em2, and Em5 showed a similar degree of inhibition on protein synthesis compared to in cells expressing wild-type E protein (Fig. 3-14C). However, in cells expressing more dramatic

mutants Em3 and Em4, much less inhibition of protein synthesis by hygromycin B was observed compared to cells expressing wild-type E protein (Fig. 3-14C), indicating that Em3 and Em4 allowed less hygromycin B to enter into cell than wild-type E protein. These results confirmed that the transmembrane domain is essential for the membrane-permeabilizing activity of E protein and further suggested that more dramatic or precise mutations in the transmembrane domain were required to disrupt membrane-permeabilizing function. None of these mutants could totally block the entry of hygromycin B. It revealed that although transmembrane domain was disrupted, the cysteine residues might still link SARS-CoV E protein together to alter the membrane permeability.

A

```
          1         10         20         30         40         50         60         70
E         MYSFVSEETGTLIVNSVLLFLAFVVFLLVTLAILTALRLCAYCCNIVNVSLVKPTVYVYSRVKNLNSSEGVPDLLV
Em1       ----------------EK-E-----------------------------------------------------------
Em2       ------------------------E-KE-----------------------------------------------------
Em3       ----------------EK-----E-KE-----------------------------------------------------
Em4       ----------------EKEKEKE-------------------------------------------------------
Em5       --------------E----------------------------------------------------------------
```

B

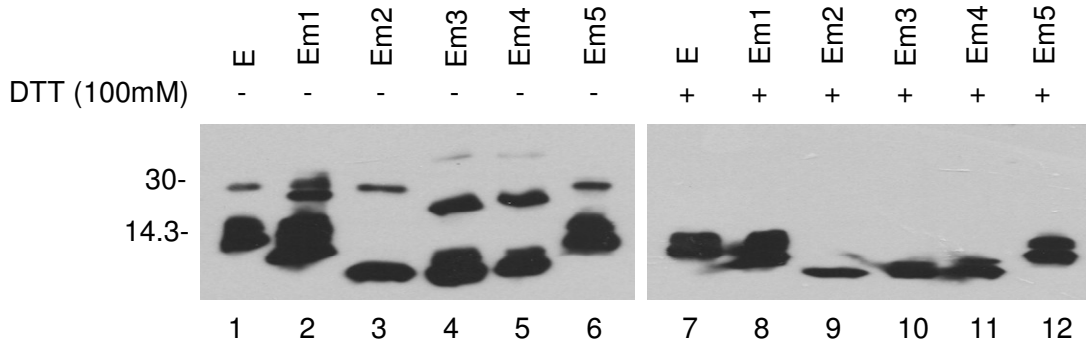

C

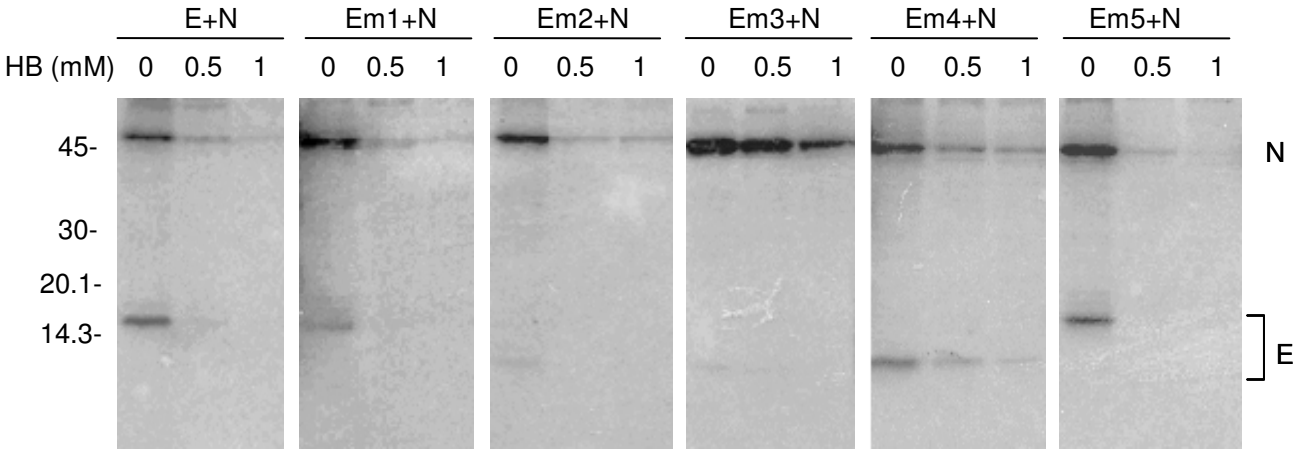

N	100	15	4	100	8	6	100	14	9	100	74	39	100	54	21	100	6	1
E	100	3	0	100	0	0	100	0	0	100	2	0	100	39	13	100	0	0

Fig. 3-14. Mutational analysis of the transmembrane domain of SARS-CoV E protein. (A) Amino acid sequences of wild-type and mutant SARS-CoV E proteins. The putative transmembrane domain is underlined. Also indicated are the amino acid substitutions in each mutant construct. (B) Analysis of the expression and oligomeric status of the transmembrane domain mutant SARS-CoV E protein. HeLa cells were transfected with the Flag-tagged wild-type and mutant constructs containing mutations in the transmembrane domain of the E protein. Cell lysates were prepared 12 hours post-transfection. Polypeptides were separated by 15 % SDS-PAGE and analyzed by Western blot using the anti-Flag antibody. All the wild-type and mutant E proteins can still form dimers or trimers in the absence of DTT. The dimmers or trimers were dissociated into monomer under DTT treatment. (C) Entry of hygromycin B into HeLa cells expressing wild-type and mutant E proteins. HeLa cells expressing the individual wild-type E and mutant E protein were treated with 0, 0.5, and 1 mM of hygromycin B for 30 minutes at 12 hours post-transfection, and radiolabeled with [^{35}S] methionine–cysteine for 3 hours. Cell lysates were prepared and the expression of E protein was detected by immunoprecipitation with anti-Flag antibody under mild washing conditions. SARS-CoV N protein fused with Flag-tag was co-expressed with E proteins, and the expression of N protein was also detected by immunoprecipitation with anti-Flag antibodies. Polypeptides were separated by 15 % SDS-PAGE and visualized by autoradiography. The percentages of E and N proteins detected in the presence of hygromycin B were determined by densitometry and indicated at the bottom. Cells expressing Em1, Em2, and Em5 showed similar degree of inhibition on protein synthesis by the entry of hygromycin B, whereas in cells expressing Em3 and Em4, much less inhibition of protein synthesis was observed.

3.6.2. The combination of mutations in the transmembrane domain and the three cysteine residues abolishes the membrane-permeabilizing activity of E protein

From above results, it showed that neither cysteine residues mutants nor transmembrane mutants can totally abolish the membrane-permeabilizing activity of E protein. This reflected that these two regions might be complementary: when the cysteine residues were removed, the transmembrane region could formed oligomers to alter the membrane permeability, or when the transmembrane region were disrupted, the cysteine residues could help E protein associate with membrane to perform its function. What will happen if both regions are disrupted? To answer this question, Em6 was made by the combination of Em4 and C40/43/44-A (Fig. 3-15A) and was placed into the vector pFlag, with Flag-tag fused at the N-terminus.

When the Em6 was subjected to membrane permeability assay, no obvious inhibition of protein synthesis was observed (Fig. 3-15C), indicating that cells expressing Em6 remained impermeable to hygromycin B. This result was reproducible and suggested that Em6 lost the membrane-permeabilizing function. Thus, amino acids position at 18 to 24 and C40, C43, C44 appear to be important. The overall hydrophobic nature of transmembrane domain and the cysteine residues were crucial for viroporin activity. Western blot shown in Fig. 3-15B confirmed the expression of Em6 in HeLa cells. Unexpectedly, trimer of Em6 was occasionally observed under reducing conditions (Fig. 3-15B).

A

```
          1         10         20         30         40         50         60         70
E         MYSFVSEETGTLIVNSVLLFLAFVVFLLVTLAILTALRLCAYCCNIVNVSLVKPTVYVYSRVKNLNSSEGVPDLLV
Em6       ------------------EKEKEKE----------------A--AA--------------------------------
```

B

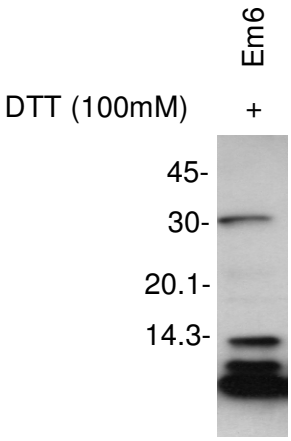

C

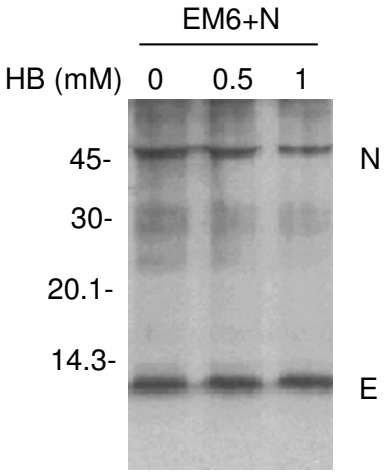

N	100	80	69
E	100	95	94

Fig. 3-15. Mutational analysis of the transmembrane domain and cysteine residues of SARS-CoV E protein. (A) Amino acid sequences of wild-type and mutant Em6 protein. The putative transmembrane domain is underlined. (B) Analysis of the expression and oligomeric status of Em6 in HeLa cells. HeLa cells were transfected with the Flag-tagged Em6 protein. Cell lysates were prepared 12 hours post-transfection. Polypeptides were separated by 15 % SDS-PAGE and analyzed by Western blot using the anti-Flag antibody. Numbers on the left indicate molecular masses in kilodaltons. Trimer of Em6 was occasionally observed under the reducing condition. (C). HeLa cells expressing the Flag-tagged Em6 construct, were treated with 0, 0.5, and 1 mM of hygromycin B for 30 minutes at 12 hours post-transfection, and radiolabeled with [^{35}S] methionine–cysteine for 3 hours. Cell lysates were prepared and the expression of Em6 protein was detected by immunoprecipitation with anti-Flag antibody under mild washing conditions. SARS-CoV N protein fused with Flag-tag was co-expressed with mutant Em6 protein, and the expression of N protein was also detected by immunoprecipitation with anti-Flag antibodies. Polypeptides were separated by 15 % SDS-PAGE and visualized by autoradiography. The percentages of E and N proteins detected in the presence of hygromycin B were determined by densitometry and indicated at the bottom. Numbers on the left indicate molecular masses in kilodaltons.

3.6.3. Subcellular localization and membrane association of SARS-CoV E protein Em mutants

To address whether the altered biological activity displayed by the various Em mutants was due to a potential change in the subcellular localization, the subcellular localization of wild-type E protein and six mutants, Em1, Em2, Em3, Em4, Em5, and Em6, was then studied in BSR *T7/5* cells by indirect immunofluorenscence. All the proteins were tagged with Flag at N-terminus. The localization patterns of Em1, Em2, and Em5 were similar to wild-type E protein, showing predominant Golgi localization patterns (Fig. 3-16A). In cells expressing Em3, Em4 and Em6, more diffuse staining patterns throughout the cytoplasm with no obvious enrichment at the Golgi apparatus were observed (Fig. 3-16A). The results suggested that these mutations might change the membrane association properties of the protein, leading to the alteration of the subcellular localization of the protein. This result was reproducible and was consistent with the finding that Em1, Em2 and Em5 functioned similarly to the wild-type E protein in the hygromycin B permeability assay, whereas Em3, Em4 and Em6 did not resemble wild-type E protein. These finding indicated that Golgi apparatus localization and membrane targeting correlated with membrane-permeabilizing activity.

The membrane association properties of wild-type and mutant E proteins were further confirmed by fractionation of HeLa cells expressing E protein into membrane fraction and cytosol fraction, and the presence of E protein in each fraction was analyzed by Western blot. As shown in Fig. 3-17B, 95.28 % of wild-type E protein was detected in the membrane fraction. The percentages of the mutant E protein detected in the similarly

prepared membrane fraction were 93.67 % for Em1, 89.85 % for Em2, 62.60 % for Em3, 58.58 % for Em4, 93.64 % for Em5, and 55.46 % for Em6 (Fig. 3-16B), less Em3, Em4 and Em6 were associated with membrane. Therefore, it was concluded that the altered biological activity of Em3, Em4 and Em6 were due to a change in the subcellular localization and membrane association.

A

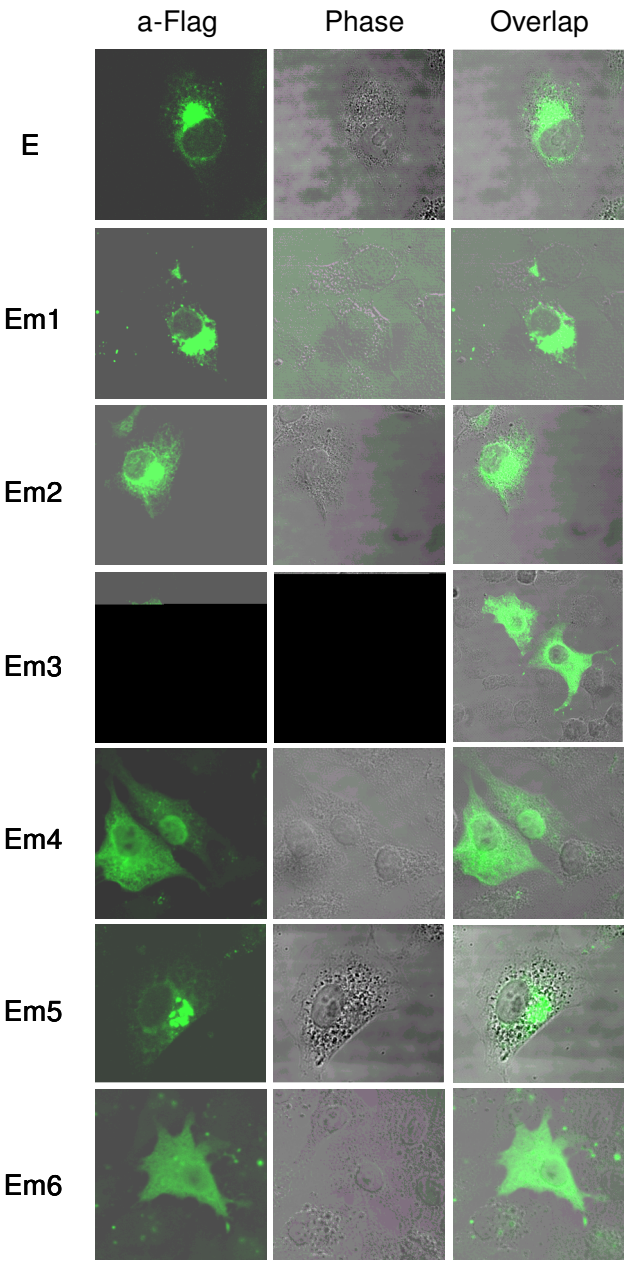

B

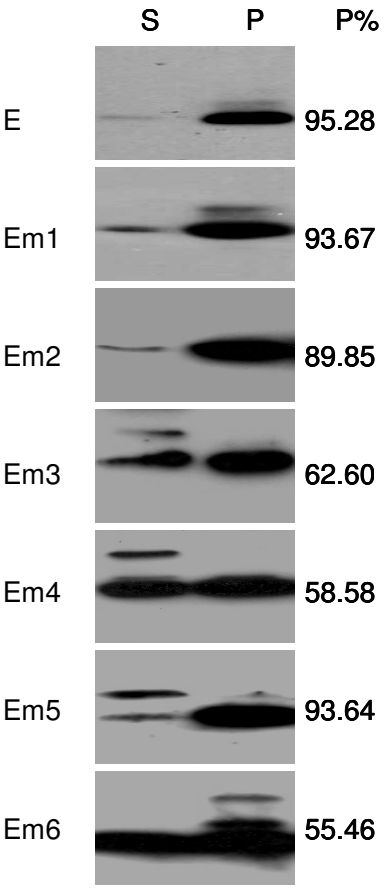

Fig. 3-16. Subcellular localization and membrane association of wide type and mutant SARS-CoV E protein. (A) Subcellular localization of SARS-CoV E protein mutants. BSR *T7/5* cells expressing the Flag-tagged wild-type (E) and mutant E protein (Em1, Em2, Em3, Em4, Em5, and Em6) were stained with anti-Flag antibody at 12 hours post-transfection after permeabilizing with 0.2 % Triton X-100. Em1, Em2, and Em5 were mainly localized to Golgi apparatus as well as wild-type E protein, where as Em3, Em4, and Em6 exhibited more diffuse pattern. (B) The membrane association properties of wild-type and mutant E proteins. HeLa cells expressing the Flag-tagged wild-type and mutant E protein were harvested at 12 hours post-transfection, disrupted with 20 stokes using a Dounce cell homogenizer, and fractionated into cytosol (C) fraction and membrane (M) fraction after removal of cell debris and nuclei. Polypeptides were separated by 15 % SDS-PAGE and analyzed by Western blot using the anti-Flag antibody. The percentages of SARS-CoV E protein detected in the membrane fraction were determined by densitometry and indicated on the right. Less Em3, Em4 and Em6 were associated with membrane than wild-type E, Em1, Em2, and Em5. Numbers on the left indicate molecular masses in kilodaltons.

3.6.4. Further analysis of residues involved in SARS-CoV E protein oligomerization.

To further examine the role of hydrophobic interaction in the oligomerization of SARS-CoV E protein, a mutant N15A/A22F/A32F/I33F with His-tag at its C-terminus was produced. The N15 in the transmembrane helices might promote dimerization and the removal of it might disrupt the dimerization. The A22, A32, I 33 are all located at the interfaces (computer prediction), replacement of them with bigger residues might perturb the transmembrane region structure. It is believed the mutation of N15, A32, A22 and I33 together will disrupt the pentamer. This mutant was constructed into baculovirus and expressed in insect cells. After purification, the mutant protein was subjected to SDS-PAGE and Western blot. The results showed that under non-reducing conditions, mutant N15A/A22F/A32F/I33F formed less dimer, trimer, tetramer and pentamer compared to wild-type E protein (Fig. 3-17B). These trimer, tetramer, pentamer and part of the dimer were dissociated into monomer while some of the dimer was still there in the presence of 1 % β-mercaptoethanol (3-17B). The β-mercaptoethanol resistant dimer may be formed by hydrophobic interaction other than disulfide bonds, while other β-mercaptoethanol sensible species were linked by both disulfide bonds and hydrophobic interaction. Mutant N15A/A22F/A32F/I33F was linked into high molecular species after cross-linking (3-17C), indicating that the mutation introduced into N15, A22, A32 and I33 did not totally destroy the interchain interaction. These residues were not essential in E protein oligomerization. Which residues were essential for the E protein oligomerization? More precise mutations for SARS-CoV E protein are necessary to address this question.

A

```
                    1         10        20        30        40        50        60        70
E                   MYSFVSEETGTLIVNSVLLFLAFVVFLLVTLAILTALRLCAYCCNIVNVSLVKPTVYVYSRVKNLNSSEGVPDLLV
N15A/A22F/A32F/I33F ----------A------F---------FF----------------------------------------
```

B

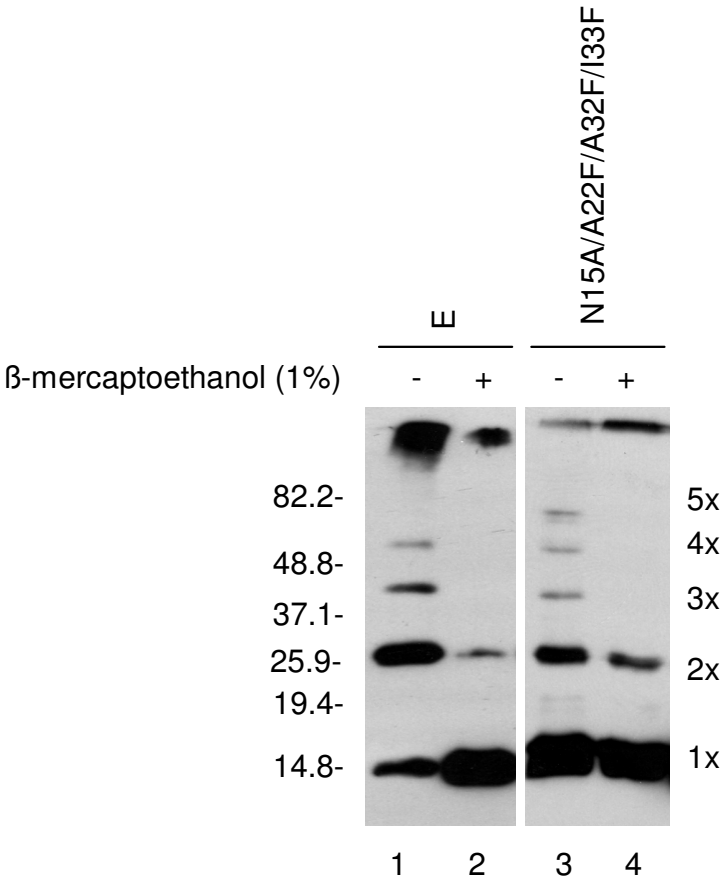

C

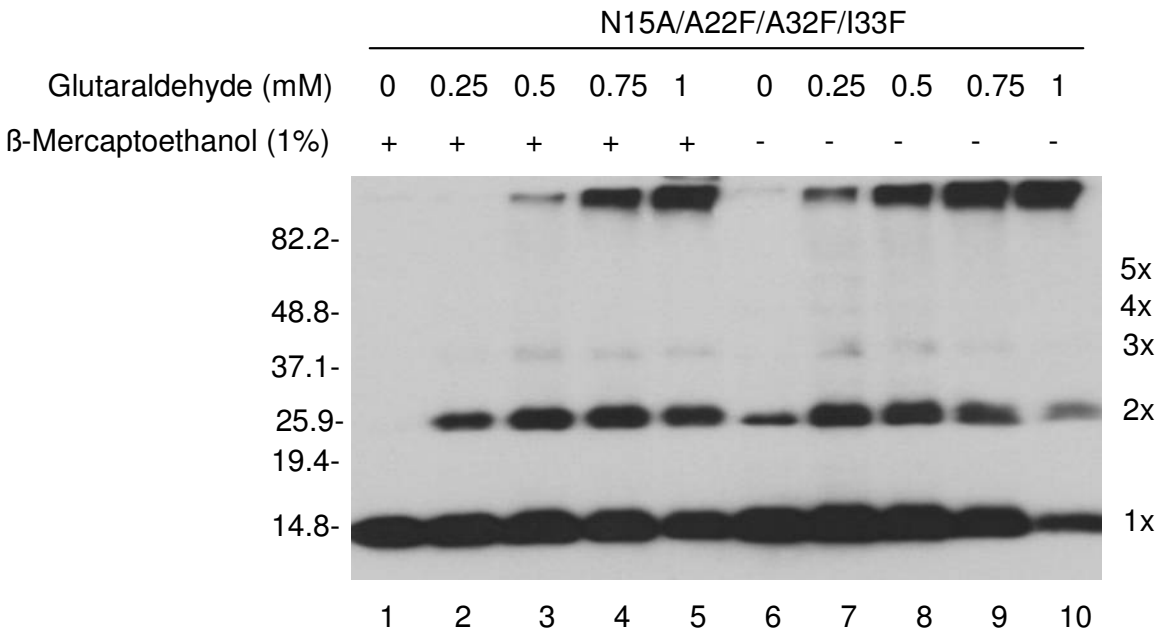

Fig. 3-17. The oligomerization of SARS-CoV E protein mutant N15A/A22F/A32F/I33F in insect cells. (A) Schematic diagram of mutant N15A/A22F/A32F/I33F. (B) The His-tagged wild-type and mutant E protein expressed in sf9 insect cells was purified using Ni-NTA purification system (Qiagen). Polypeptides were separated by 15 % SDS-PAGE in the presence or absence of 1 % β-mercaptoethanol, and analyzed by Western blot with anti-His antibody. Different oligomers of the E protein are indicated on the right. Numbers on the left indicate molecular masses in kilodaltons. Mutant E protein N15A/A22F/A32F/I33F still formed oligomers similar to wild-type E protein. (C) The purified mutant E protein N15A/A22F/A32F/I33F was incubated with five different concentrations of glutaraldehyde (0, 0.25, 0.5, 0.75 and 1mM) for 1 hour at room temperature. The reaction was quenched by adding 100 mM glycine. Polypeptides were separated by 15 % SDS-PAGE in the presence or absence of 1 % β-mercaptoethanol, and analyzed by Western blot with anti-His antibody. Different oligomers of the E protein are indicated on the right. Numbers on the left indicate molecular masses in kilodaltons. The mutant E protein N15A/A22F/A32F/I33F can be linked into oligomers by glutaraldehyde.

3.7. Post-translational modification of SARS-CoV E protein

3.7.1. Palmitoylation of SARS-CoV E protein

The E proteins from coronavirus MHV and IBV were shown to undergo modification by palmitoylation (Corse and Machamer, 2002). To verify if SARS-CoV E protein is palmitoylated, two independent experiments were performed. First, as palmitoylation occurs on cysteine residues are liable to hydroxylamine, the Flag-tagged SARS-CoV E protein was treated with 1 M hydroxylamine. Fig. 3-18A showed the reduced detection of the more slowly migrating isoforms under the hydroxylamine treatment (Fig. 3-18A, lanes 1-2), indicating that the palmitates were removed by hydroxylamine. As a control, treatment of the Flag-tagged IBV E protein with the same reagent abolished the detection of upper bands (Fig. 3-18A, lanes 3-4).

Second, the three cysteine residues in combinations of two or all three were mutated to alanine (Fig. 3-18B). Wild-type and mutant Flag-tagged E proteins were then expressed in HeLa cells and labeled with [^{35}S] methionine–cysteine or [^{3}H] palmitates overnight. At 12 hours post-transfection, cells were harvested and subjected to immunoprecipitation using anti-Flag antibody. As shown in Fig. 3-18C, Western blot analysis using anti-Flag antibody confirmed the expression of wild-type and all mutant E proteins (upper panel). All the proteins were efficiently labeled with [^{35}S] methionine–cysteine (middle panel). In cells labeled with [^{3}H] palmitates, wild-type and the three mutants with mutations of different combinations of two cysteine residues (C40/44-A, C40/43-A and C43/44-A) were efficiently detected (Fig. 3-18C, lower panel, lanes 1–4).

However, the construct with mutation of all three cysteine residues (C40/43/44-A) was not labeled (Fig. 3-18C, lower panel, lane 5) by [^{3}H] palmitates. As a positive control, the IBV E protein was also efficiently labeled by [^{3}H] palmitates (Fig. 3-18C, lower panel, lane 6). These results confirmed that SARS-CoV E protein was modified by palmitoylation at all three cysteine residues.

A

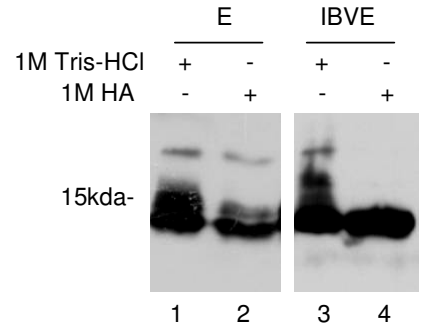

B

```
                1         10        20        30        40        50        60        70
E               MYSFVSEETGTLIVNSVLLFLAFVVFLLVTLAILTALRLCAYCCNIVNVSLVKPTVYVYSRVKNLNSSEGVPDLLV
C40/44-A        ----------------------------------------A---A--------------------------------
C40/43-A        ----------------------------------------A--A---------------------------------
C43/44-A        ----------------------------------------AA---------------------------------
C40/43/44-A     ----------------------------------------A--AA--------------------------------
```

C

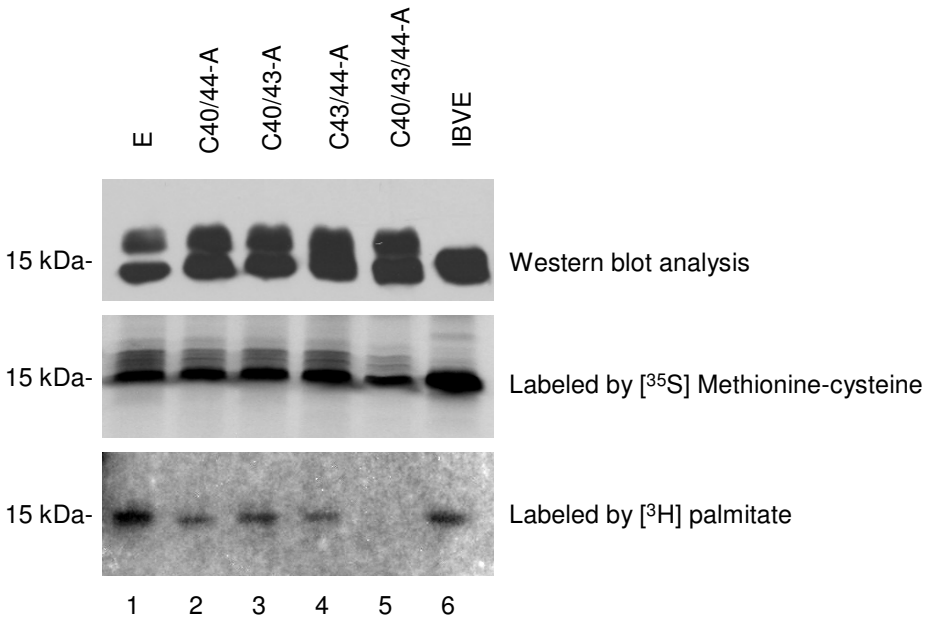

Fig. 3-18. Palmitoylation of SARS-CoV E protein. (A) Treatment of the SARS-CoV E protein with hydroxylamine showed SARS-CoV E protein was palmitoylated. Total cell lysates prepared from HeLa cells expressing the Flag-tagged SARS-CoV E protein (lanes 1-2) and IBV E protein (lanes 3-4) were treated either with 1 M Tris–HCl (lanes 1-3) or 1 M hydroxylamine (lanes 2-4). Polypeptides were separated by 15 % SDS-PAGE and analyzed by Western blot using the anti-Flag antibody. Numbers on the left indicate molecular masses in kilodaltons. (B) Amino acid sequences of wild-type and mutant SARS-CoV E proteins. (C) SARS-CoV E protein was modified by palmitoylation at all three cysteine residues. HeLa cells expressing the Flag-tagged wild-type SARS-CoV E protein (lane 1), mutant C40/44-A (lane 2), C40/44-A (lane 3), C43/44-A (lane 4), C40/43/44-A (lane 5), and IBV E protein (lane 6) were radiolabeled with [^{35}S] methionine–cysteine or [^{3}H] palmitates overnight. Cell lysates were prepared and subjected to immunoprecipitation with anti-Flag antibody. Polypeptides were separated by 15 % SDS-PAGE and subjected to Western blot or visualized by autoradiography. Western blot confirmed the expression of wild-type and mutant E proteins (upper panel), and all the proteins were efficiently labeled with [^{35}S] methionine–cysteine (middle panel). Wild-type E protein, mutant C40/44-A, C40/44-A, and C43/44-A were efficiently labeled with [^{3}H] palmitates, whereas C40/43/44-Awas not labeled by [^{3}H] palmitates (lower panel). Numbers on the left indicate molecular masses in kilodaltons.

3.7.2. Palmitoylation of SARS-CoV E protein is not involved in membrane-permeabilizing activity

As the C40, C43 and C44 have the ability to bind with palmitate, it would be interesting to test if these cysteine residues could affect the membrane-permeabilizing activity of SARS-CoV E protein. For this purpose, the Flag-tagged constructs were co-expressed with SARS-CoV Flag-tagged N protein in HeLa cells. At 12 hours post-transfection, cells were treated with 0.5 mM and 1 mM hygromycin B for 30 minutes, and then radiolabeled with [^{35}S] methionine-cysteine for 3 hours. Cell extracts were prepared and the expression of E protein was detected by immunoprecipitation with anti-Flag antibody. As shown in Fig.3-19A, all these mutation did not obviously affect the membrane-permeabilizing activity of the E protein. A very similar degree of inhibition of protein synthesis was observed in cells expressing wild-type and all the mutant E protein. Western blot shown in Fig. 3-19B demonstrated the expression of these proteins in HeLa cells. It suggesting removal of palmitoylation doesn't directly affect the membrane-permeabilizing activity of E protein.

A

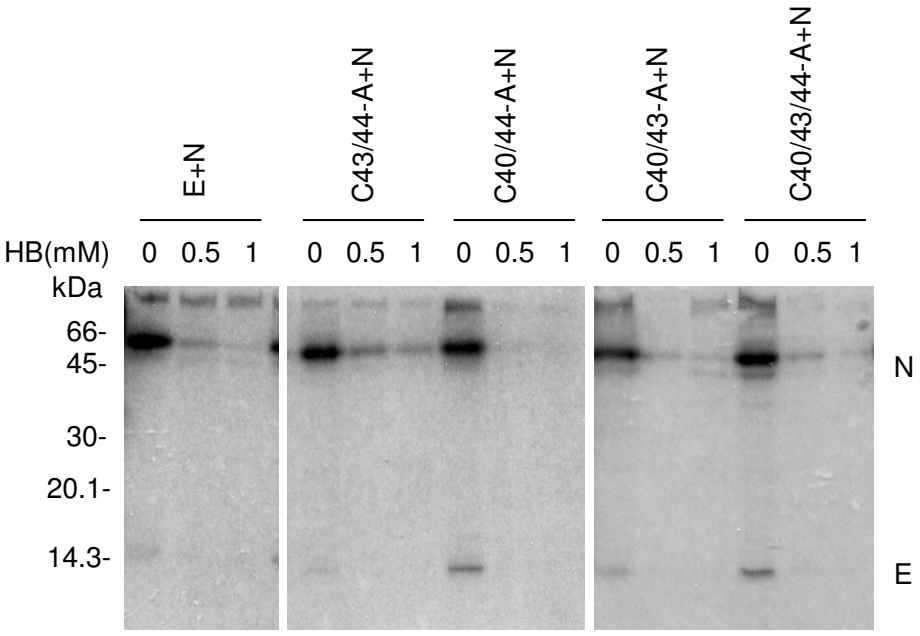

N	100	14	5	100	44	19	100	6	2	100	29	9	100	9	5
E	100	2	0	100	0	0	100	0	0	100	0	0	100	2	0

B

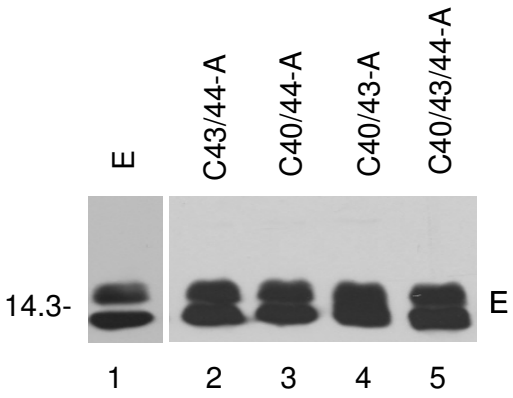

Fig. 3-19. Palmitoylation of SARS-CoV E protein is not involved in the membrane-permeabilizing activity. (A) Entry of hygromycin B into HeLa cells expressing wild-type and mutant E proteins. HeLa cells expressing the Flag-tagged wild-type E, C43/44-A. C40/44-A, C40/43-A, or C40/43/44-A were treated with 0, 0.5, and 1 mM of hygromycin B for 30 minutes at 12 hours post-transfection, and radiolabeled with [^{35}S] methionine–cysteine for 3 hours. Cell lysates were prepared and the expression of E protein was detected by immunoprecipitation with anti-Flag antibody under mild washing conditions. Flag-tagged SARS-CoV N protein was co-expressed with wild-type and mutant E protein, and the expression of N protein was also detected by immunoprecipitation with anti-Flag antibody. Polypeptides were separated by 15 % SDS-PAGE and visualized by autoradiography. The percentages of E and N proteins detected in the presence of hygromycin B were determined by densitometry and indicated at the bottom. A similar degree inhibition of protein synthesis was observed in cells expressing all the mutants as well as wild-type E protein. Numbers on the left indicate molecular masses in kilodaltons. (B). Western blot analysis of wild-type and mutant E proteins. HeLa cells were transfected with the Flag-tagged wild-type and mutant C43/44-A, C40/44-A, C40/43-A, and C40/43/44-A. Cell lysates were prepared at 12 hours post-transfection, polypeptides were separated by 15 % SDS-PAGE and analyzed by Western blot using the anti-Flag antibody. Numbers on the left indicate molecular masses in kilodaltons.

3.7.3. N-linked glycosylation of SARS-CoV E protein

Multiple bands were usually detected when SARS-CoV E protein was expressed in different system even after removing palmitoylation site C40/43/44 (Fig. 3-19C, lane 5), suggesting it may undergo other translational modification. Examination of the SARS-CoV E protein sequence showed the presence of two potential glycosylation sites on asparagines 48 (N48) and 66（N66） (Fig. 3-20A). In order to address the possibility that the protein may be modified by N-linked glycosylation, cells expressing Flag-tagged E protein were lysed. The total cell lysates were first treated with the N-linked glycosidase PNGase F, and analyzed by Western blot with anti-Flag antibody. PNGase F is an amidase which cleaves between the innermost GlcNAc and asparagine residues of high mannose, hybrid and complex oligosaccharides from *N*-linked glycoproteins. Treatment of the cell lysates by PNGase F led to the removal of the most slowly migrating species of the three isoforms (Fig. 3-20B), lanes 1-2), confirming that it represented the N-linked glycosylated form of E protein.

To further analyze the N-linked glycosylation of the SARS-CoV E protein, mutations were introduced into the predicted N-linked glycosylation sites from asparagines to aspartic acid. Two mutants, Flag-tagged N48-D and N66-D were generated and expressed (Fig. 3-20C). Western blot analysis of cells expressing wild-type and N48-D showed that the detection of three bands on 15 % SDS-PAGE (Fig. 3-20C, lanes 1-2). In cells expressing the N66-D mutant, only two bands were detected; the most slowly migrating species of the three isoforms was not observed (Fig. 3-20C, lane 3). These results demonstrated that a minor proportion of the SARS-CoV E protein was modified

by N-linked glycosylation and the N66 residue was the site for this modification. More importantly, it suggested that the C-terminal region of this glycosylated portion of the SARS-CoV E protein would be located in the lumen in the ER and the Golgi apparatus.

A

```
          1         10         20         30         40         50         60         70
E         MYSFVSEETGTLIVNSVLLFLAFVVFLLVTLAILTALRLCAYCCNIVNVSLVKPTVYVYSRVKNLNSSEGVPDLLV
N48-D     ----------------------------------------------D ----------------------------
N66-D     ------------------------------------------------------------------D ---------
```

B

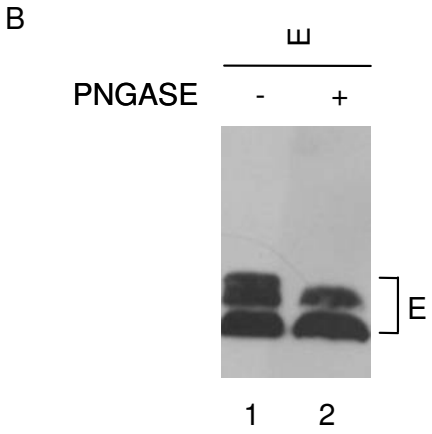

C

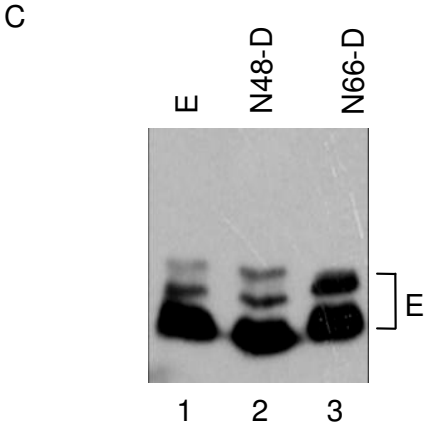

Fig 3-20. N-linked glycosylation of SARS-CoV E protein. (A) Diagram of wild-type and mutant SARS-CoV E constructs. (B) PNGase F treatment led to the removal of the most slowly migrating isoform of the E protein. Total cell lysates prepared from HeLa cells expressing the Flag-tagged SARS-CoV E protein were treated either with (lane 1) or without (lane 2) PNGase F. Polypeptides were separated by 15 % SDS-PAGE and visualized by autoradiography. (C) N-linked glycosylation occurred at the N66 residue. HeLa cells were transfected with the Flag-tagged wild-type SARS-CoV E protein (lane 1) and two constructs containing mutations of the N48-D (lane 2) and N66-D (lane 3). Cell lysates were prepared by 12 hours post-transfection. Polypeptides were separated by SDS-PAGE and analyzed by Western blot using the anti-Flag antibody. Mutant N66-D lost the most slowly migrating species of E protein.

3.7.4. Glycosylation of SARS-CoV E protein is not involved in the subcellular localization and membrane-permeabilizing activity

The effects of the N48 and N66 mutations on the subcellular localization of E protein were then analyzed. As shown in Fig. 3-21A, expressing of the Flag-tagged SARS-CoV E protein in BSR *T7/5* cells stably expressing the T7 RNA polymerase (Buchholz, *et al*., 1999) showed that the protein mainly located in the Golgi region. The two mutant proteins N48-D and N66-D also displayed very similar localization patterns (Fig. 3-21A). These results demonstrated that mutation of the glycosylation site of the protein does not affect the membrane association and localization patterns of the protein.

As the removal of N-linked site N66 did not change the subcellular localization of E protein, it would be interesting to test if this mutation could affect the membrane-permeabilizing activity of the SARS-CoV E protein. For this purpose, the Flag-constructs were co-expressed with Flag-tagged SARS-CoV N protein in HeLa cells. At 12 hours post-transfection, cells were treated with different concentration of hygromycin B for 30 minutes, and then radiolabeled with [^{35}S] methionine-cysteine for 3 hours. Cell extracts were prepared and the expression of E protein was detected by immunoprecipitation with anti-Flag antibody. As shown in Fig. 3-21B, N48-D and N66-D did not obviously affect the membrane-permeabilizing activities of the E protein. A very similar degree of inhibition of protein synthesis was observed in cells expressing the E, N48-D and N66-D (Fig. 3-21B).

A

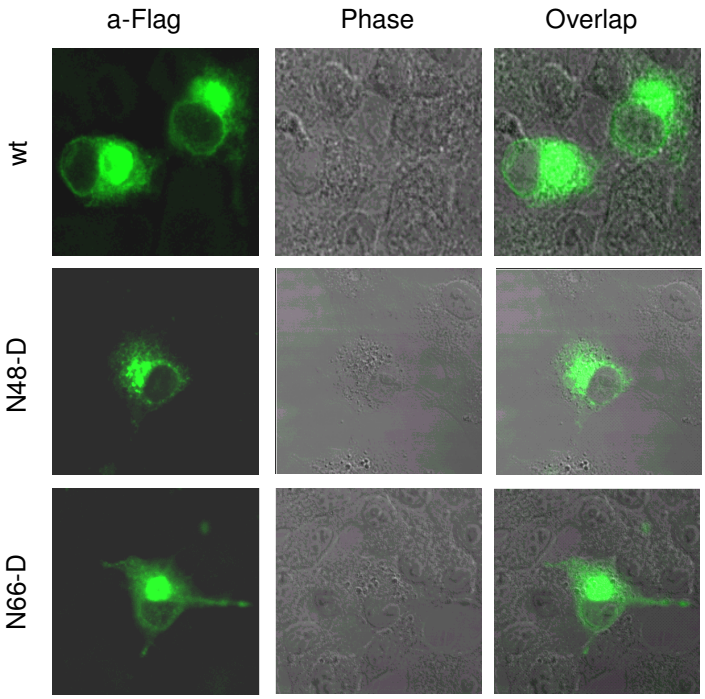

B

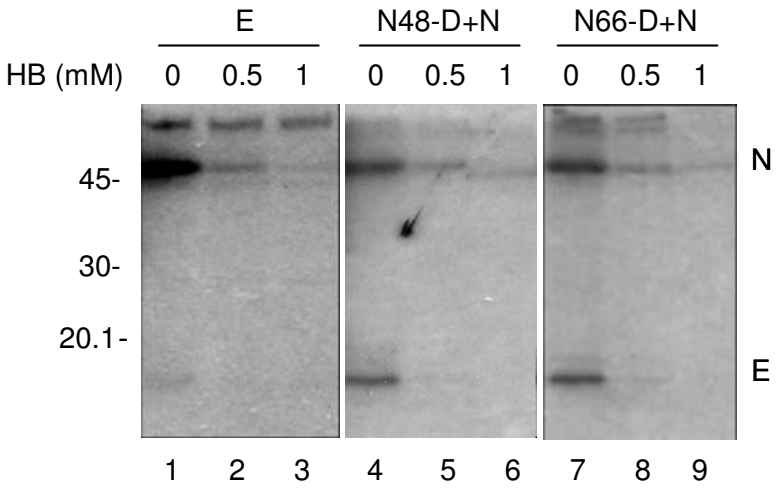

Fig. 3-21. Glycosylation of SARS-CoV E protein is not involved in the subcellular localization and membrane-permeabilizing activity. (A) Subcellular localization of wild-type SARS-CoV E protein, mutant E protein N48-D and N66-D. BSR *T7/5* cells expressing the Flag-tagged wild-type and mutant E proteins were stained with anti-Flag antibody at 12 hours post-transfection after permeablizing with 0.2 % Triton X-100. All the proteins were mainly localized to Golgi apparatus. (B) Entry of hygromycin B into HeLa cells expressing wild-type and mutant E proteins. HeLa cells expressing the Flag-tagged wild-type E proteins (lanes 1-3), mutant E protein N48-D (lanes 4-6) and N66-D (lanes 7-9) were treated with 0, 0.5 and 1 mM of Hygromycin B for 30 minutes at 12 hours post-transfection, and radiolabeled with [^{35}S] methionine-cysteine for 3 hours. Cell lysates were prepared and the expression of wild-type and mutant E protein were detected by immunoprecipitation with anti-Flag antibody under mild washing conditions. The Flag-tagged SARS-CoV N protein was co-expressed with wild-type and mutant E protein, and the expression of N protein was detected by immunoprecipitation with anti-Flag antibody. Polypeptides were separated by 15 % SDS-PAGE and visualized by autography. A similar degree of inhibition of protein synthesis was observed in cells expressing the wild-type and mutant E proteins. Numbers on the left indicate molecular masses in kilodaltons.

3.8. Summary

Viroporin interacts with membranes to increase permeability to ions and other small molecules. Their presence significantly increases cell lysis and enhances the virion release. In this study, we aimed to identify and characterize SARS-CoV proteins that may perturb cell membrane and alter cell membrane permeability. Among five proteins (3a, 3b, 6, 7a，E protein) tested, the E protein could obviously arrest bacterial cell growth and enhance membrane permeability to ONPG and hygromycin B. It suggested that E protein induced disorganization of the inner bacterial membrane and hence allowed cytoplasmic lysozyme to reach and digest the peptidoglycan layer of the outer cell wall. Similar observations were recently reported on mouse heptaitis virus E protein (Madan *et al*., 2005).

Biochemical and functional characterization of E protein in eukaryotic cells showed that the expression of SARS-CoV E protein also altered membrane permeability of mammalian cells. This protein was characterized as an integral membrane protein which could form oligomers by both disulfide bond and hydrophobic interaction, and the membrane-permeabilizing activity was associated with the transmembrane domain. Immunofluorescent staining showed E protein was localized to the perinuclear regions of the cells, near the site for virus assembly and budding. A very small portion of E protein might be translocated to the cell surface, where the permeation to hygromycin B was exerted. Cysteine residues adjacent to the C-terminus of the transmembrane domain affected membrane-permeabilizing activity in bacterial cells but not in mammalian cells.

To gain further information regarding the relationships between the structure and function of the SARS-CoV E protein, post-translational modifications of the E protein was examined. Palmitoylation was found at all the three cysteine residues adjacent to the C-terminus of the transmembrane domain. Removal of palmitoylation did not change the perinuclear localization pattern and showed no obvious effect on membrane-permeabilizing activity.

Glycosylation motif search showed SARS-CoV E protein had two N-linked glycosylation consensus sequences (Asn-Xaa-Ser) at N48 and N66 position. Enzymatic and mutational studies showed N66 residue was modified by N-linked glycosylation. This is the first finding that there is glycosylation in coronavirus E protein. Removal of the glycosylation site of E protein did not affect the membrane-association and membrane-permeabilizing activity of the SARS-CoV E protein. Further exploration of the functions and effects of these post-translational modifications on SARS-CoV E protein using an infectious cloning system may shed light on the molecular biology and pathogenesis of SARS-CoV.

CHAPTER 4

GENERAL DISCUSSION AND FUTURE DIRECTION

4.1. SARS-CoV E protein is endowed with viroporin activity

4.1.1. SARS-CoV E protein enhances the membrane permeability in both E. coli cells and mammalian cells

In this study, we demonstrated that expression of the SARS-CoV E protein in bacterial cells inhibited cell growth and increased the entry of ONPG and hygromycin B into *E. coli* cells. It could form homo-dimers by formation of disulfide bonds when expressed in *E. coli* cells. Cysteine residues, C40 and C44, were found to be involved in the dimerization and modification of the membrane permeability in *E. coli* cells. Further evidence for alteration of membrane permeability to hygromycin B of SARS-CoV E protein was obtained in HeLa cells.

Hygromycin B is a translation inhibitor that does not easily pass the membrane barrier of intact cells, but readily across the membrane of prokaryotic or eukaryotic cells after membrane modification by membrane-active agents or virus infection. Inhibition of protein synthesis by hygromycin B constitutes a very sensitive test to assay modifications of membrane permeability in intact cells. For this reason, hygromycin B is widely used for the identification and analysis of membrane-active proteins such as viroporin. Several membrane-active proteins including viroporin have been successfully analyzed by this antibiotic, such as poliovirus 2B and 3AB (Aldable *et al*., 1996; Lama and Carrasco,

1995, 1996), influenza A virus M2 (Guinea and Carrasco, 1994) and human immunodeficiency virus gp41 and Vpu (Arroyo *et al*., 1995; Gonzalez and Carrasco, 1998). Consequently, the alteration of membrane permeability to hygromycin B by expressing SARS-CoV E protein in *E. coli* cells and HeLa cells can be considered as a significant indication of membrane-permeabilizing activity of E protein.

SARS-CoV E protein is a short and hydrophobic protein of 76 aa. The putative long transmembrane domain of the E protein (amino acid 9-38) has been reported to adopt a highly unusual topology, consisting of a very short helical hairpin, with F23 as the center of inversion of the hairpin. This residue was suggested to be located at the center of the lipid bilayer (Arbely *et al*., 2004), although a recent report placed this residue adjacent to the polar head groups of the lipids (Khattari *et al*., 2006). This hairpin structure could deform lipid bilayers and cause tabulation (Arbely *et al*., 2004). However, *in silico* NMR, *in vitro* NMR and infrared dichotic data of tansmembrane domain of E protein suggested that it was a normal transmembrane helix rather than a hairpin model (Torres *et al*., 2005, 2006). Recently, it was reported that the SARS-CoV E protein had two distinct membrane topologies: 1) both the N- and C-terminal regions of the E protein face to the internal side of the virion, 2) the C-terminal region is located outside of the virion, whereas N-terminal region faces to the outside or inside of the virion (Yuan *et al*., 2006).

SARS-CoV E protein exhibits many of the characteristics of viroporin. In this study, SARS-CoV E protein exhibited membrane-permeabilizing activity both in bacterial cells and mammalian cells. In another study, the full-length and N-terminal 40 aa region of SARS-CoV E protein were shown to be able to form cation-selective ion channels on

artificial lipid bilayers (Wilson *et al*., 2004). Molecular dynamic simulations predicted that the transmembrane domain of SARS-CoV E protein could form pore in the membrane by homo-oligomerization into pentamers (Torres *et al*., 2006). In addition, SARS-CoV E protein and all reported viroporins are small hydrophobic integral membrane proteins of 50-120 aa, containing at least one transmembrane hydrophobic domain of 20-30 residues and an intracellular region rich in basic residues that is adjacent to the transmembrane domain. Furthermore, SARS-CoV E protein and some viroporins contain cysteine residues in their cytoplasmic regions, positioned proximal to their membrane-spanning domains. Usually, these cysteine residues are modified by palmitoylation. Based on these reports and the capacity of the SARS-CoV E protein to permeabilize the *E. coli* cells and HeLa cells, SARS-CoV E protein might function as a viroporin and play a crucial role in the cell lysis and virion release.

4.1.2. SARS-CoV E protein is an oligomeric integral membrane protein localized to perinuclear region

Membrane association and oligomerization of viroporin is thought to be a prerequisite for the formation of the hydrophilic pore in the lipid bilayer. In this study, it was showed SARS-CoV E protein was localized to the perinuclear region of the cells, mainly associated with Golgi apparatus. Subcellular fractionation and biochemical characterization studies demonstrated that, similar to the IBV E protein, the SARS-CoV E protein behaved as an integral membrane protein. However, it was consistently observed that, under the experimental conditions used, certain proportions of both SARS-CoV and IBV E proteins associated with cellular membranes were resistant to 1 % Triton

X-100, while some of the E proteins could be released from the membrane pellets by treatment with high pH. Two possibilities for these phenomena are considered. First, SARS-CoV E protein is partially associated with detergent resistant microdomain, lipid rafts (Liao *et al*., 2006). Lipid rafts are cholesterol-enriched microdomain in plasma membrane as well as in intracellular membranes. They function as platforms for signal transduction and as the site of budding of several enveloped viruses, including influenza virus. The lipid rafts localization of E protein may render it resistant to the treatment by Triton X-100. Second, immunofluorescent staining of cells expressing the E protein showed the detection of the protein with punctated staining patterns at perinuclear region. It would suggest that the protein may form aggregates. These aggregates may be co-fractionated with the membrane-associated E protein and can be released by high pH.

Molecular dynamic simulations predict that SARS-CoV E protein forms pentamers (Torres *et al.,* 2006). In this study, dimerization of SARS-CoV E protein was observed under non-reducing conditions both in bacterial and mammalian cells. Higher molecular species representing trimer, tetramer and pentamer were observed after E protein was purified from insect cells. Membrane association and oligomerization study demonstrated that SARS-CoV E protein could oligomerize and insert into the cell membrane, although the evidence for the real oligomeric status of the SARS-CoV E protein in virus-infected cells still lacks.

4.1.3. The differential roles of cysteine residues C40 and C44 of SARS-CoV E protein in its oligomerization and modification of membrane permeability in bacterial and mammalian cells

SARS-CoV E protein contains three cysteine residues (C40, C43, and C44) adjacent the C-terminus of the transmembrane domain. In bacterial, C40 and C44 were found to participate in interchain disulfide bond formation and linked E protein to dimer. Removal of the C40 or C44 resulted in dissociation of dimer and loss of the membrane-permeabilizing activity. However, in mammalian cells, all the three cysteine residues are not essential for the membrane-permeabilizing activity of E protein. Examination of the oligomeric status of E protein in insect cells found that mutant E protein could still form dimers, trimers, tetramers and pentamers in the absence of C40, C43 and C44, although less oligomers were formed in this C40/C43/C44-A mutant comparing with wild-type E protein. It indicated that the disulfide bond linkage was dispensable for formation of the E protein oligomers in eukaryotic cells. However, formation of this covalent bond stabilizes the E protein oligomers from dissociation by detergent, and thus it may also stabilize the E protein oligomers in membrane. Indeed, subsequent study showed that these cysteine residues were palmitoylated in HeLa cells, indicating the role of cysteine residues in mammalian cells was different from bacterial cells.

These observations are reminiscent of the finding made with the influenza A virus M2 protein. It has been found that the two cysteine residues C17 and C19 were not required for the formation of M2 tetramers but could stabilize the M2 tetramer (Holsinger and Lamb, 1991). It was also observed that the two disulfide linkages were not required for formation of the dimeric form but that formation of these disulfide linkages prevented dissociation of the noncovalently linked dimer by detergent in the transferring receptor (Alvarez *et al*., 1989). The cysteine residues of the M2 protein are not required for

influenza A virus replication (Castrucci *et al*., 1997). Thus, in viroporin, at least in influenza A virus M2 and SARS-CoV E protein, the oligomer formation might be dependent on the transmembrane domain rather than cysteine residues.

4.1.4 . SARS-CoV E protein membrane-permeabilizing activity is associated with transmembrane domain

Evidence was presented that SARS-CoV E protein N-terminal first 40 aa were sufficient for the formation of ion channels *in vitro*, with similar selectively as the full-length E protein (Wilson *et al*., 2004). This report supported that the transmembrane domain of E protein was essential and enough for pore formation and ion channel activity. Thus, E protein is an ion channel can be demonstrated if mutations introduced into the transmembrane domain of the E protein alter the membrane-permeabilizing activity.

The transmembrane domain (residues 9-38) of SARS-CoV E protein was reported to form a palindromic helical hairpin and the incorporation of the helical hairpin into lipid vesicles increased membrane curvature by deforming lipid bilayers (Arbely *et al*., 2004). Based on this report, four mutants, Em1 (L18/E, L19/K, L21/E), Em2（V25/E, L27/K, L28/E, Em5 (N15/E), Em3 (L18/E, L19/K, V25/E, L27/K, L28/E) and Em4 (L18/E, L19/K, F20/E, L21/K, A22/E, F23/K, V24/E) were generated to perturb the hairpin structure of the transmembrane domain. Em5 (N15/E), which contained mutation of N15 to E, was constructed because N15 might provide stabilization for the oligomers *via* interchain hydrogen bonds (Arbely *et al*., 2004; Torres *et al*., 2006). Several altered characteristics were measured. First, the amino acids alteration caused change in the

migration properties of Em1, Em2, Em3 and Em4. It suggested that these mutations would have significantly altered the overall folding, hydrophobicity, and membrane association properties of the E protein. Second, the amino acids alteration caused change in membrane-permeabilizing activity. Although Em1, Em2, and Em5 showed very similar properties in subcellular localization, membrane association, and membrane-permeabilizing activity as wild-type E protein, the more dramatic mutations in Em3 and Em4 caused less entry of hygromycin B into cells compared to wild-type E protein. This functional alteration might correlate to the subcellular localization and membrane association alteration. Em3 and Em4 exhibited more diffused staining pattern throughout the cytoplasm with no obvious enrichment at the Golgi apparatus and less Em3 and Em4 were associated with membrane compared to wild-type E protein. This data provide strong evidence that the transmembrane domain is essential for the membrane-permeabilizing activity and membrane association properties of the E protein.

The dramatic transmembrane mutants Em3 and Em4 still partially retained membrane-permeabilizing activity and membrane association properties may reflect more dramatic or precise mutations of the transmembrane domain are required to disrupt this function. Alternatively, palmitoylation of the Em3 and Em4 could help target the protein to the cellular membrane as the Em3 and Em4 still retained cysteine residues which were modified by palmitates. This membrane association by palmitates could, in turn, cause membrane damage, leading the increased membrane permeability to hygromycin B. To test our suspect, an E protein mutant Em6 with combination of Em4 and C40/C43/C44-A was generated. This mutant changed the amino acids that line in the pore and removed

palmitoylation at the C-terminus of transmembrane domain. The membrane-permeabilizing activity of SARS-CoV E protein was totally abolished in Em6. Less Em6 was found to associate with cellular membrane than other mutants. Similar to Em3 and Em4, Em6 also exhibited diffused cytoplasm localization with no obvious enrichment at the Golgi apparatus. It suggested that the lost of palmitoylation of Em6 failed to target the protein to the cellular membrane and failed to form functional pores in the membrane. Therefore, both transmembrane domain and the cysteine residues might play a role in the membrane-permeabilizing activity and membrane association of SARS-CoV E protein.

Oligomerization of E protein was observed in our study. Transmembrane domain was demonstrated to be essential for the membrane-permeabilizing activity of E protein. However, a plausible pore model for the E protein is still lacking. According to Arbely's model, the E protein transmembrane domain formed a palindromic helical hairpin (Arbely *et al*., 2004). Therefore, E protein traversed the membrane twice, the N-terminus and C-terminus faced to the same side of the membrane. Torres *et al*. (2006) showed E protein transmembrane domain was a regular α-helix and formed homo-pentamer in the membrane using the orientational parameters derived from infrared dichroic data. In Torres' model, E protein traversed membrane once, the N-terminus and C-terminus of faced to different side of the membrane. E protein viroporin activity appears to be more compatible with a pentameric α-helix bundle model (Torres *et al*., 2006) than with hairpin model (Arbely *et al.,* 2004). But the hairpin model may explain better the role of E protein in viral morphogenesis. In Yuan's report (Yuan *et al*., 2006), immunofluorescent staining of cells differentially permeabilized with detergents and

proteinase K protection assay revealed that the majority of E protein is inserted into membrane with an $N_{cyto}C_{cyto}$ topology, which is consistent with hairpin model. However, a small proportion of E protein was modified by N-linked glycosylation and inserted into the membrane with the C-terminus exposed to the luminal side. It is possible E protein adopt more than one topology due to its multiple functions. Different structural models could arise in different environments and are responsible for distinct functions.

4.1.5. The mechanism of SARS-CoV E protein viroporin activity

The exact mechanism for the alteration of plasma membrane permeability by SARS-CoV E protein is unknown yet. There are two possibilities to account for E protein's action: direct permeabilization by E protein at the plasma membrane, or an indirect mechanism that E protein functions as a regulator to trigger the opening of a cellular ion channel at the plasma membrane.

According to the first model, cell surface expression should be a prerequisite for SARS-CoV E protein to alter the membrane permeability of cells. In this study, it was observed that SARS-CoV E protein was mainly localized to Golgi apparatus and almost no signal could be detected on plasma membrane under non-permeabilizing conditions (Yuan *et al.,* 2006). It is puzzling that little signal was detected on the cell surface. The reason for this observation could be the unique topology of the SARS-CoV E protein. The $N_{cyto}C_{cyto}$ topology might make the epitopes (N-terminus or C-terminus) of E protein inaccessible to antibodies under non-permeablilizing conditions (Yuan *et al*., 2006).

Alternatively, it could because the low proportion of E protein at the plasma membrane. It is quite certain that SARS-CoV E protein must be transported to the cell surface.

Immunolocalization studies show most of the viroporins are located in intracellular membrane, while little or none is detected at the plasma membrane. This might suggest that viroporin acts by releasing a signal from an intracellular compartment to the plasma membrane, where viroporin activity is detected. In this study, it was observed that the SARS-CoV E protein was mainly localized to the Golgi apparatus, a place near the virus budding site. How can Golgi apparatus localized protein permeabilize plasma membrane to hygromycin B? Is it possible that E protein functions as a regulator which triggers the opening of cellular channels on the plasma membrane by alteration of subcellular ion homeostasis? There are some examples that small integral membrane proteins are able to regulate endogenous channels of the host cells (Shimbo *et al*., 1995). For example, HIV-1 Vpu was found to interact with the mammalian cell K^+ channel, CASK-1, which can inhibit HIV-1 release. The interaction between Vpu and CASK-1 suppressed conductance of TASK-1, therefore enhanced HIV-1 release (Hsu *et al*., 2004).

According to our experiment results, it is impossible that SARS-CoV E protein functions as a regulatory protein which actives a normally silent endogenous channel. This conclusion is based one observation: the structure of the pore region of an ion channel determines the properties of the channel. Even a change of a few amino acids in the pore region of an ion channel can change the properties of the ion channel. This is unlikely to happen for a regulator. It was found that the membrane-permeabilizing activity was changed in cells expressing transmembrane mutants Em3, Em4, and Em6

compared to the wild-type E protein, indicating that the membrane-permeabilizing activity depend on the transmembrane domain amino acid sequence of the E protein. Therefore, SARS-CoV E protein functions as an ion channel per se and is not a regulatory protein that triggers the opening of a normally silent endogenous channel. The Golgi apparatus localization implied that E protein might perform multiple functions other than permeabilized plasma membrane. The ability of E protein to permeabilize the Golgi membrane also remains to be determined.

4.1.6. Coronavirus E protein is a new group of viroporin

Is induction of the membrane permeability a general feature of coronavirus E protein? Although the E proteins from different coronaviruses share a low homology in their primary amino acid sequences, the general structural features, such as consisting of transmembrane domain, are conserved. It suggests that the E proteins from different coronaviruses may have similar function and play similar role in virus life cycle. Comparative studies of E proteins from different coronaviruses would help delineate the molecular and structural basis of their potential of membrane-permeabilizing activity.

MHV E protein also has been demonstrated to enhance membrane permeability both in *E. coli* cells and mammalian cells in a separate study (Madan *et al*., 2005). In our study, IBV E protein could permeabilize membrane to hygromycin B similar to SARS-CoV E protein (Data not shown). Recently, the E proteins from HCoV-229E, MHV, and IBV were demonstrated to form cation-selective channels (Wilson *et al*., 2006), conducting the flux of sodium or potassium. Therefore, it is possible that ion channel function is

common to all coronaviruses E proteins. Coronavirus E proteins are now new members of viroporin.

Hexamethylene amiloride (HMA), which could inhibit the HIV-1 virus Vpu ion channel, was found to inhibit the HCoV-229E and MHV E protein ion channel conductance in bilayer (Wilson *et al*., 2006). Moreover, HMA was found to inhibit budding or release of the parent coronaviruses in cultured cells (Wilson *et al*., 2006). It was demonstrated that disruption of the function of E protein impaired the virus replication and the virus release, rendering this group of viral proteins suitable targets for the development of antiviral drugs.

4.2. Palmitoylation and N-linked glycosylation of SARS-CoV E protein is not required for viroporin activity

4.2.1. Palmitoylation of SARS-CoV E protein

To gain further information regarding the relationships between the structure and function of the SARS-CoV E protein, we examined possible post-translational modifications of this protein.

Many virus membrane-embedded proteins are post-translationally modified by the covalent attachment of palmitates to cysteine residues located in domains close to the lipid bilayer. The MHV and IBV E proteins were reported to be palmitoylated (Corse and Machamer, 2002; Yu *et al*., 1994). In our study, SARS-CoV E protein was found to have several species ranging from 14 kDa to 18 kDa when expressed in mammalian cells. The

presence of three cysteine residues clustered in the regions flanking the hydrophobic domain of SARS-CoV E protein led us to look for acylation of this protein. Consistent with our assumption, palmitoylation was found at all the three cysteine residues. However, removal of palmitates did not change the Golgi localization pattern and showed no obvious effect on membrane-permeabilizing activity.

Lipid modification by palmitates had been reported for a number of viral envelope proteins, including the hemagglutinin (HA) and M2 protein of influenza A virus (Melkonian *et al*., 1999, Schroeder *et al*., 2005, Sugrue *et al*., 1990; Veit *et al*., 1991; Zhang *et al*., 2000), the 6K protein of Sindbis (Gaedigk-Nitschko and Schlesinger, 1990a; Gaedigk-Nitschko *et al*., 1990b), the gp160 protein of HIV-1 (Rousso *et al*., 2000), and the envelope protein of murine leukemia virus (Li *et al*., 2002). It has been noted that palmitoylation of these viral envelope proteins usually takes place on cysteine residues located within the transmembrane domain or in the cytoplasmic tail close to this domain (Bhattacharya *et al*., 2004, Hausmann *et al*., 1998, Schmidt *et al*., 1988 and Veit *et al*., 1989). This thioester linkage of fatty acids to viral envelope proteins is a post-translational event that takes place in the *cis* or medial Golgi after exit from the ER. It usually occurs after oligomerization but prior to acquisition of endo H (endo-β-*N*-acetylglucosaminidase H) resistance (Bonatti *et al*., 1989 and Veit and Schmidt, 1993).

Palmitoylation of viral proteins plays a considerable role in virus infectivity, virion assembly and release. Each virus has unique dependence on this modification. For example, in the influenza virus, palmitoylation of the HA protein enhanced its association with lipid rafts. Removal all three palmitoylation sites on HA was shown to dramatically

decrease HA incorporation into virions (Melkonian *et al*., 1999 and Zhang *et al*., 2000). In HIV-1, removal of both palmitoylation sites of gp160 resulted in the decrease of gp160 association with lipid rafts, low levels of gp160 incorporating into virion as well as a decrease in viral infectivity (Rousso *et al*., 2000). Palmitoylation of the murine leukemia virus envelope protein was critical for its association with lipid rafts and cell surface expression (Li *et al*., 2002). Palmitoylation of the Rous sarcoma virus transmembrane glycoprotein was required for protein stability and virus infectivity (Ochsenbauer-Jambor *et al*., 2001).

The functional role of palmitoylation of SARS-CoV E protein is unknown. However, it is reasonable to assume that this lipid modification may act to position the cytoplasmic tails of E protein at juxtamembrane location, thereby contributes to membrane anchoring that is secondary to protein transmembrane spans. The abolishment of membrane-permeabilizing activity in Em6 could give some clues for the functional role of palmitates. The palmitate adducts may also alter E protein transport in the cellular exocytic pathway, assist in clustering the E protein into lipid microdomain, and enforce membrane anchoring. Palmitoylation seems to be a general feature for coronavirus E protein as IBV and MHV E proteins are also found to be palmitoylated. Recently, palmitoylation of MHV S protein was found to be essential for virus assembly and play an essential role in creating viral membrane protein interactions required for particle infectivity using both pharmacologic and molecular genetic approaches (Thorp *et al*., 2006). These approaches should also help to clarify the role of palmitoylation of the coronavirus E protein in virus life cycle.

4.2.2. N-linked glycosylation of SARS-CoV E protein

N-linked glycosylation is another common modification for virus envelope proteins. It presents on the surface of the enveloped viruses and for this reason it is supposed to be important for the generation of their bioactive conformation and can have effects on receptor binding, fusion activity, and antigenic properties of the virus. In the early secretory pathway, the glycans also play a role in protein folding, quality control and certain sorting events.

Two of the three coronavirus membrane-associated structural proteins, M and S, have been shown to be modified by either N- or O-linked glycosylation (Nal *et al*., 2005). The fourth membrane-associated structural protein, the hemagglutinin-esterase (HE), in some coronaviruses is also a glycoprotein. So far, the E protein is an apparent exception. For SARS-CoV E protein, it contains two predicted N-linked glycosylation site, N48 and N66, with the consensus sequence Asn-X-Ser/Thr. The minimum distance between a functional C-terminal glycosylation acceptor site and the luminal end of the transmembrane domain is 12-13 residues (Nilsson and Von, 1993), suggesting that only the most C-proximal asparagine residue out of the two potential sites in the SARS-CoV E protein can be glycosylated. Consistent with this observation it was demonstrated that the SARS-CoV E protein was modified by N-linked glycosylation. Mutagenesis studies present in this study confirmed that only N66 is modified. N-linked glycosylation seems not to affect the membrane association and membrane-permeabilizing activity of the SARS-CoV E protein. To further characterize the functional significance of this modification, it would be interesting to test whether N-linked glycosylation of SARS-

CoV E protein can be detected in virus-infected cells and in purified virions. As N66 residue is not conserved in the E protein of other coronaviruses, it is likely that this modification may render unique feature to the SARS-CoV E protein.

Neither the palmitoylation nor the N-linked glycosylation was essential for the ion channel activity of E protein. Similarly, none of the post-translational modifications was important for the ion channel activity of the well characterized viroporin M2 (Holsinger *et al*., 1995). These observations indicated that viroporin needed minimal structural requirements for its function. This notion was reinforced by the finding that a 40 amino acid polypeptide corresponding to the N-terminal hydrophobic domain inserted into planar lipid bilayers and promoted the formation of channels (Wilson *et al*., 2004). Therefore, if there is a role for the post-translational modifications of the E protein described here in the life cycle of the virus, it would most probably be in the formation of infectious virions. This possibility remains to be determined.

4.3. The role of SARS-CoV E protein in virus life cycle

SARS-CoV E protein is not only viroporin but also a viral structural glycoprotein. Recently, another SARS-CoV structural glycoprotein, 3a, was also reported to be endowed with ion channel activity (Lu *et al*, 2006). In our study, 3a was neglected as it did not cause obvious inhibition of *E. coli* growth and its membrane-permeabilizing activity to hygromycin B was weaker than E protein.

Three groups of virus-encoded proteins were found to be able to enhance cell membrane permeability: viroporins, pore-forming glycoproteins, and proteases. Among

them, viroporin and glycoprotein are pore-forming proteins associated with membrane, whereas protease may induce effects on membrane permeability by degradation of one or more proteins involved in maintenance of the plasma membrane architecture. There are several virus glycoproteins known to increase cell membrane permeability. Examples are HIV-1 transmembrane glycoprotein gp41 (Arroyo *et al*., 1995; Chernomordik *et al*., 1994), HCV structural glycoprotein E1 (Ciccaglione *et al*., 1998), rotavirus nonstructural glycoprotein NSP4 (Newton *et al*., 1997) and outer glycoprotein VP7 (Charpilience *et al*., 1997), vaccinia virus integral membrane glycoprotein A38L (Sanderson *et al*., 1996), and Semliki forest virus E1 glycoprotein (Nieva *et al*., 2004). These glycoproteins are integral membrane proteins and can form a physical pore upon oligomerization. Domains adjacent to the transmembrane region could have motifs designed to destabilize membrane structure. Usually the size of these glycoproteins is bigger than viroporin.

In viruses that lack the typical viroporin, viroporin function could be replaced by these pore-forming glycoproteins. Those viruses that code for a viroporin may also contain a glycoprotein with the capacity to alter membrane permeability. For example, in HIV-1, both viroporin Vpu and glycoprotein gp41 can enhance membrane permeability. In Semliki forest virus, the 6K protein was identified as viroporin and another protein E1 was membrane-active glycoprotein (Nieva *et al*., 2004). In HCV, the p7 protein with 63 aa was characterized as a viroporin responsible for the calcium selectivity and was essential for infectivity of HCV (Sakai, *et al*., 2003; Premkumar, *et al*., 2004), whereas the glycoprotein E1, a structural protein of 383 aa, could also enhance membrane permeability in *E. coli* cells (Ciccaglione, *et al*., 1998, 2001). Most membrane-active

glycoproteins are associated with virion, while viroporins can be a component of the virion, such as influenza A virus M2, or an accessory protein, such as HIV-1 Vpu. Usually, virion-associated viroporin and glycoprotein can provoke both early and late membrane modification, but viroporin excluded by virion can only perform its function at late stage since as it requires gene expression.

SARS-CoV is another virus that encodes more than one membrane-active protein. Both the SARS-CoV E and 3a proteins are glycosylated and embedded in the virion envelope, it is difficult to give a definition of which one is viroporin and which one belongs to membrane-active glycoprotein. According to their size, E protein is more consistent with the definition of viroporin.

Why does SARS-CoV contain two different ion channel proteins? What are the different roles of E and 3a ion channels during virus life cycle? What has been known is only their different ion selectivity. E protein prefers sodium while 3a prefers potassium (Wilson *et al.,* 2004; Lu *et al*, 2006). It is not known yet whether E and 3a protein induce membrane permeability at early or late stage. Recently, an attenuated E protein deleted SARS-CoV with similar morphology as the recombinant wild-type virus was recovered (DeDiego *et al.,* 2007). The recovered E protein deletion mutant grew in Vero E6, Huh-7 and CaCo-2 cells to titers 20, 200 and 200-folder lower that the recombinant wild-type virus (DeDiego *et al.,* 2007), indicating E protein is integral parts of the viral life cycle and promote efficient viral replication. This finding also suggested that although SARS-CoV E protein has effect on virus growth, it is not essential for virus replication. There

might be factors that complement the role of E protein in SARS-CoV. Is 3a the possible complement factor for E protein? This need to be further investigated.

The E protein was also shown to be non-essential gene for the group 2 MHV coronavirus (Kuo and Master, 2003). The E protein deleted mutant MHV virus with aberrant and heterogeneous in virion morphology was recovered, which produced tiny plaque compared to wild-type MHV and showed low growth rate and low infectious titer (Kuo & Masters, 2003). In contrast, two independent reverse genetic experiments demonstrated that, for TGEV, the E protein deletion was lethal. Viable virus could be recovered only if E protein was provided *in trans* (Curtis *et al.,* 2002; Ortego *et al.,* 2002). One possible reason for this discordance is, in SARS-CoV and MHV, the pivotal role of E proteins can be substituted by other factors, whereas in TGEV, there is no such factor to substitute the role of E protein. Alternatively, the TGEV E protein play more important role in virus life cycle than SARS-CoV and MHV E proteins.

Recently, it has been shown that E proteins from group 2, BCoV and SARS-CoV, as well as the group 3 IBV can substitute for the E protein of MHV easily and enhance replication of recombinant MHV. The group 1 TGEV E protein became functional in recombinant MHV after acquisition particular mutations (Kuo *et al.,* 2007). This work supports that E proteins from different coronaviruses play certain common role in virus life cycle that can substitute each other.

What's the role does E protein play in coronavirus life cycle? The earliest investigations for the E protein significance demonstrated that co-expression of MHV E

and M proteins were necessary and sufficient for VLP formation and release from cells (Bos *et al*., 1996; Vennema *et al*., 1996). It was subsequently shown that E proteins from BCoV, TGEV, IBV and SARS-CoV were conformed the same rule (Baudoux *et al*., 1998; Corse and Machamer, 2000; Corse and Machamer, 2003; Mortola and Roy, 2004). Conversely, the single expression of either IBV or MHV E protein led to the formation and cellular export of E protein-containing vesicles, indicating E protein could act independently of M protein (Corse and Machamer, 2000; Maeda *et al*., 1999). Likewise, the expression of MHV E protein has been shown to give rise to intracellular clusters of convoluted membrane structures (Raamsman *et al*., 2000) that strongly resemble those seen in coronavirus-infected cells (David-Ferreira and Manaker, 1965). These observations suggested that the principal role of E protein is to induce membrane curvature in the budding compartment. It is conceivable that one function of E protein is to potentiate the kinetics of virion assembly.

Another function of coronavirus E protein is ion channel activity. What's the main role of ion channel function of E protein in virus life cycle? For the well defined ion channel influenza A virus M2 protein, it acts at two different stages during virus infection: at early stage, M2 protein allows the entry of protons into virions, promoting virus uncoating in endosomes (Mould *et al*., 2000); at late stage, M2 protein shunts the pH gradient of the *trans*-Golgi apparatus to prevent premature conformational change of the HA protein (Lamb *et al*., 1994). The information available about coronavirus E protein at this time is not sufficiently complete to allow us to understand how this ion channel function affects virus entry, uncoating, replication, assembly, and release. Undoubtedly,

ion channel activity of E protein is very important to virus replication and release as the ion channel inhibitor HMA was found to inhibit budding or release of the parent coronaviruses in culture cells (Wilson *et al*., 2006).

4.4. The impact of this study

The E protein of coronavirus has important but poorly defined role in coronavirus biology. The overall objective of this study was to characterize the SARS-CoV E protein. In this study, SARS-CoV E protein was found to possess viroporin activity. The existence of viroporin has been reported for many viruses but not for coronavirus until our paper published (Liao *et al.,* 2004). It is a very important finding in coronavirus.

Viroporin is attractive targets for antiviral action, as they have very high specific activity. A single blocking molecule can prevent the flow of millions of ion through a single ion channel protein. The fact that some compounds such as amiloride derivatives or amantadine are able to block influenza a virus M2 protein, HIV-1 Vpu protein and HCV p7 protein suggests the possibility of finding additional selective agents toward viroporin function. Inhibiting viroporin activity would lead to diminished virus production. This alone might be sufficient for the immune system to eradicate the virus infection. In fact, M2 protein inhibitor amantadine and its derivative rimantadine have been proven to be effective drugs in humans for the prevention of influenza, and have been widely used in the influenza therapy.

For coronavirus viroporin, amiloride derivative HMA has been found to inhibit the HCoV-229E and MHV E protein ion channel conductance in lipid bilayer and inhibit

budding or release of the parent coronaviruses in cultured cells in a subsequent study (Wilson *et al*., 2006). SARS-CoV E protein inhibitor can also be screened by the same method (Wilson *et al*., 2006). Our finding of SARS-CoV E protein viroporin activity would shed light on the searching for compounds toward SARS-CoV E protein and open a door for SARS therapy.

In this study, SARS-CoV E protein was characterized as an oligomeric integral membrane protein that mainly localized to the Golgi apparatus. Palmitoylation and glycosylation of SARS-CoV were also first reported to this protein. All these findings would help people to better understand the function and structure this protein.

4.5. Future direction

4.5.1. Direct measurement of the ion channel activity of SARS-CoV E protein in mammalian cells.

In this study, evidence that the SARS-CoV E protein may have the ion channel activity was obtained by the measurement of cell membrane permeability to hygromycin B upon expressing the E protein in cells. The idea that the SARS-CoV E protein could form a pore was reinforced by the finding of the synthetic full length E protein or the first 40 aa of the E protein could be incorporated into the planar lipid bilayers and promoted the formation of sodium selective channels in a separate study (Wilson *et al*., 2004). Therefore, the ion channel activity of this protein has been so far measured by indirect measurement *in vivo* or direct measurement *in vitro*. Direct measurement of its ion channel activity in mammalian cells is necessary. The ion channel current in cells

expressing SARS-CoV E protein will be measured using the whole cell version of the patch clamp technique.

4.5.2. Identification of the active oligomeric structure of the SARS-CoV E protein ion channel

SARS-CoV E protein could form dimers, trimers, tetramers and pentamers. However, a plausible ion channel model for the full length E protein is still lacking although it was predicted that E protein forms pentamers by α-helix (Torres *et al.,* 2006). To determine the active oligomers, the E protein will be purified and mixed with microsomal membrane. The ion channel structure of the E protein will be examined by transmission electron microscopy (TEM) following by immunogold labeling, and will be further characterized by solid state NMR experiments.

4.5.3. Identification of the gating mechanism of the SARS-CoV E protein ion channel

In general, ion channels are selective for a given ion and do not permit the passage of other ions or molecules. Moreover, the gating of these channels is regulated. The gating mechanism of influenza A virus M2 has been well characterized. Therefore, another essential point that needs to be established is whether SARS-CoV E protein forms pores allowing the passage of specific ions with a controlled gating mechanism. The gating mechanism of the SARS-CoV E protein ion channel will be analyzed by systematic mutagenesis. A better understanding of the ion channel gating mechanism will help to screen anti-viroporin drugs.

4.5.4. Characterization of the role of SARS-CoV E protein in virus life cycle

Research on viroporins is usually directed at two directions. First, expression of them individually in mammalian cells to analyze their effects on cultured cells. Alternatively, construction of recombinant virus with mutations in these proteins demonstrates their impacts on virus life cycle. Despite all experimental evidence for ion channel-like activity of E protein, all the knowledge about channel activity is still a consequence of the expression of E protein in particular cells. In this respect, deletion or systematic mutation of E protein could be introduced into the SARS-CoV genome to characterize the role of SARS-CoV E protein in virus life cycle.

4.5.5. Searching for drugs that block SARS-CoV E protein ion channel activity

Heamethylene amiliride (HMA), an drug that blocks HIV-1 Vpu and HCV p7 ion channels, also blocks the HCoV-229 E and MHV E protein ion channels and inhibits the replication of the parental coronaviruses in cultured cells (Wilson *et al*., 2006). Amantadine, another drug blocks influenza A virus M2 ion channel and inhibits influenza A virus replication, is widely used in the anti-viral therapy. Viroporin represents a promising target for developing antiviral drug. The searching for drugs towards SARS-CoV E protein would open another door for the anti-SARS therapy. The anti-viroporin drug will also be useful for evaluating the mode of action of E protein.

Cited Literature

Agirre, A., Barco, A., Carrasco, L., and Nieva, J. B. 2002. Viroporin-mediated membrane permeabilization. *J. Biol. Chem.* **277**, 40434–40441.

Aldabe, R., Barco, A., and Corrasco, L. 1996. Membrane permeabilization by poliovirus proteins 2B and 2BC, *J. Biol. Chem.* **271**, 23134–23137.

Alvarez, E., Girones, N., and Davis, R. J. 1989. Intermoleculardisulfide bonds are not required for the expression of the dimeric state and functional activity of the transferrin receptor. *EMBO J*. **8,** 2231-2240.

An, S., Chen. C. J., Yu, X., Leibowitz, J. L., and Makino, S. 1999. Induction of apopotosis in murine coronavirus-infected cultured cells and demonstration of E protein as an apoptosis inducer. *J. Virol*. **73,** 7853-7859.

Arbely, E., Khattari, Z., Brotons, G., Akkawi, M., Salditt, T., and Arkin, I. T. 2004. A highly unusual palindromic transmembrane helical hairpin formed by SARS coronavirus E protein. *J. Mol. Biol.* **341,** 769-779.

Arden, K. E., Nissen, M. D., Sloots, T. P. and Mackay, I. M. 2005. New human coronavirus, HCoV-NL63, associated with severe lower respiratory tract disease in Australia. *J. Med. Virol.* **75,** 455-462.

Arroyo, J., Boceta, M., Gonzalez, M. E., Michel, M., and Carrasco, L. 1995. Membrane permeabilization by different regions of the human immunodeficiency virus type 1 transmembrane glycoprotein gp41. *J. Virol*. **69,** 4095-4102.

Bastien, N., Anderson, K., Hart, L., Van Caeseele, P., Brandt, K., Milley, D., Hatchette, T., Weiss, E. C., and Li, Y. 2005a. Human coronavirus NL63 infection in Canada. *J. Infect. Dis.* **191,** 503-506.

Bastien, N., Robinson, J. L., Tse, A., Lee, B. E., Hart, L., and Li, Y. 2005b. Human coronavirus NL-63 infections in children: a 1-year study. *J. Clin. Microbiol.* **43,** 4567-4573.

Baudoux, P., Carrat, C., Besnardeau, L., Charley, B., and Laude, H. 1998. Coronavirus pseudoparticles formed with recombinant M and E proteins induce α interferon synthesis by leukocytes. *J. VIrol*. **72,** 8636-8643.

Berger, A., Drosten, C. H., Doerr, H.W., Sturmer, M., and Preiser, W., 2004. Severe acute respiratory syndrome (SARS)—paradigm of an emerging viral infection. *J. Clin. Virol.* **29**, 13–22.

Bhattacharya, J., Peters, P. J., and Clapham, P. R. 2004. Human immunodeficiency virus type 1 envelope glycoproteins that lack cytoplasmic domain cysteines: impact on association with membrane lipid rafts and incorporation onto budding virus particles. *J. Virol.* **78,** 5500-5506.

Bijlmakers, M. J., and Marsh, M. 2003. The on-off story of protein palmitoylation. *Trends in Cell Biol.* **13**, 32-42.

Blanco, R., Carrasco, L., and Ventoso, I. 2003. Cell killing by HIV-I protease. *J. Biol. Chem.* **278,** 1086-1093.

Bodelon, G., Labrada, L., Martinez-Costas, J., and Benavente, J. 2002. Modification of late membrane permeability in avian reovirus-infected cells. *J. Biol. Chem.* **227**, 17789–17796.

Bonatti, S., Migliaccio, G., and Simons, K. 1989. Palmitoylation of viral membrane glycoproteins takes place after exit from the endoplasmic reticulum. *J. Biol. Chem.* **264**, 12590-12595.

Bos, E. C., Luytjes, W., van der Meulen, H. V., Koerten, H. K., and Spaan, W. J. 1996. The production of recombinant infectious DI-particles of a murine coronavirus in the absence of helper virus. *Virology*. **218,** 52-60.

Bour, S., and Strebel, K. 1996. The human immunodeficiency virus (HIV) type 2 envelope protein is a functional complement to HIV type 1 Vpu that enhances particle release of heterologous retroviruses. *J. Virol.* **70,** 8285-8300.

Brian, D. A., Hague, B. G., and Kienzle, T. E. 1995. The coronavirus hemagglutinin esterase glycoprotein. *In* "The *coronaviridae*" (S. G. Siddell, ed.). Plenum Press, New York. pp. 165-179.

Brown, T. D. K., and Brierly, I. 1995. The coronavirus nonstructural proteins. In: Siddell, S.G. (Ed.). The Coronaviridae. Plenum Press, New York, NY, pp.191–217.

Buchholz, U. J., Finke, S., and Conzelmann, K. K. 1999. Generation of bovine respiratory syncytial virus (BRSV) from cDNA: BRSV NS2 is not essential for virus replication in tissue culture, and the human RSV leader region acts as a functional BRSV genome promoter. *J. Virol.* **73,** 251-259.

Chan, W. S., Wu, C., Chow, S. C., Cheung, T., To, K. F., Leung, W. K., Chan, P. K., Lee, K. C., Ng, H. K., Au, D. M., and Lo, A. W. 2005. Coronaviral hypothetical and structural proteins were found in the intestinal surface enterocytes and pneumocytes of severe acute respiratory syndrome (SARS). *Mod. Pathol.* **18,** 1432–1439.

Carrasco, L., Perez, L., Irurzun, A., Lama, J., Martinez-Abarca, F., Rodriguez, P., Guinea, R., Castrillo, J. L., Sanz, M. A., and Ayala, M. J. 1995. Modification of membrane permeability by animal viruses. *Adv. Virus Res.* **45**，61–112.

Casais, R., Davies, M., Cavanagh, D., and Britton, P. 2005. Gene 5 of the avian coronavirus infectious bronchitis virus is not essential for replication, *J. Virol.* **79,** 8065–8078.

Castrucci, M. R., Hughes, M., Calzoletti, L., Donatelli, I., Wells, K., Takada, A., and Kawaoka, Y. 1997. The cysteine residues of the M2 protein are not required for influenza A virus replication. *Virology.* **238,** 128-134.

Charley, B., and Laude, H. 1988. Induction of α interferon by transmissible gastroenteritis coronavirus: Role of transmembrane glycoprotein E1. *J. Virol.* **62,** 8-11.

Charpilienne, A., Abad, M. J., Michelangeli, F., Alvarado, F., Vasseur, M., Cohen, J., and Ruiz, M. C. 1997. Solubilized and cleaved VP7, the outer glycoprotein of rotavirus, induces permeabilization of cell membrane vesicles. *J. Gen. Virol.* **78,** 1367-1371.

Chen, H., Wurm, T., Britton, P., Brooks, G., and Hiscox, J. A. 2002. Interaction of the coronavirus nucleoprotein with nucleolar antigens and the host cell. *J. Virol.* **76,** 5233-5250.

Chernomordik, L., Chanturiya, A. N., Suss-Toby, E., Nora, E., and Zimmerberg, J. 1994. An amphipathic peptide from the C-terminal region of the human immunodeficiency virus envelope glycoprotein causes pore formation in membranes. *J. Virol.* **68,** 7115-7123.

Chiu, S. S., Chan, K. H., Chu, K. W., Kwan, S. W., Guan, Y., Poon, L. L., and Peiris, J. S. 2005. Human coronavirus NL63 infection and other coronavirus infections in children hospitalized with acute respiratory disease in Hong Kong, China. *Clin. Infect. Dis.* **40,** 1721-1729.

Chow, S. C., Ho, C. Y., Tam, T. T., Wu, C., Cheung, T., Chan, P. K., Ng, M. H., Hui, P. K., Ng, H. K., Au, D. M., and Lo, A. W., 2006. Specific epitopes of the structural and hypothetical proteins elicit variable humoral responses in SARS patients. *J. Clin. Pathol.* **59,** 468–476.

Christian, M. D., Poutanen, S. M., Loutfy, M. R., Muller, M. P., and Low, D. E., 2004. Severe acute respiratory syndrome. *Clin. Infect. Dis.* **38,** 1420–1427.

Cinatl Jr., J., Michaelis, M., Hoever, G., Preiser, W., and Doerr, H. W. 2005. Development of antiviral therapy for severe acute respiratory syndrome. Antiviral Res. **66,** 81–97.

Ciccaglione, A. R., Marcantonio, C., Costantino, A., Equestre, M., Geraci, A., and Rapicetta, M. 1998. Hepatitis C virus E1 protein induces modification of membrane permeability in *E. coli* cells. *Virology.* **250,** 1-8.

Ciccaglione, A.R., Costantino, A., Marcantonio, C., Equestre, M., Geraci, A., and Rapicetta, M. 2001. Mutagenesis of hepatitis C virus E1 protein affects its membrane-permeabilizing activity. *J. Gen. Virol.* **82,** 2243-2250.

Corse, E., and Machamer, C. E. 2001. Infectious bronchitis virus E protein is targeted to the Golgi complex and directs release of virus-like particles. *J. Virol.* **74**, 4319-4326.

Corse, E., and Machamer, C. E. 2002. The cytoplasmic tail of infectious bronchitis virus E protein directs Golgi targeting. *J. Virol.* **76**, 1273-1284.

Corse, E., and Machamer, C. E. 2003. The cytoplasmic tails of infectious bronchitis virus E and M proteins mediate their interaction. *Virology.* **312**, 25-34.

Curtis, K. M., Yount, B., and Baric, R. S. 2002. Heterologous gene expression from transmissible gastroenteritis virus replicon particles. J. Virol. 76, 1422-1434.

David-Ferreira, J. F., and Manaker, R. A. 1965. An electron microscope study of the development of mouse hepatitis virus in tissue culture cells. *J. Cell. Biol.* **24,** 57-78.

DeDiego, M. L, Alvarez, E., Almazan, F., Rejas, M. T., Lamirande, E., Roberts, A., Shieh, W. J., Zaki, S. R., Subbarao, K., and Enjuanes, L. 2007. A severe acute respiratory syndrome coronavirus that lacks the E gene is attenuated in vitro and in vivo. *J. Virol.* **81,** 1701-1713.

de Haan, C. A. M., Masters, P. S., Shen, X., Weiss, S and Rottier, P. J. M. 2002. The

group - specific murine coronavirus genes are not essential, but their deletion, by reverse genetics, is attenuating in the natural host, *Virology*. **296,** 177–189.

de Hann, C. A. M., de Wit, M., Kou, L., Montalto-Morrison, C., Haagmans, B. L., Weiss, S. R., Masters, P. S., and Rottier, P. J. 2003. The glycosylation status of the murine hepatitis coronavirus M protein affects the interferogenic capacity of the virus *in vitro* and its ability to replicate in the liver but not the brain. *Virology*. **312,** 395-406.

de Hann, C. A. M., and Rottier, P. J. M. 2005. Molecular interactions in the assembly of coronaviruses. *Adv. Virus Res.* **64,** 165-229.

Delmas, B., and Laude, H. 1990. Assembly of coronavirus spike protein into trimers and its role in epitope expression. *J. Virol*. **64,** 5367-5375.

Doms, R. W, Lamb, R. A, Rose, J. K, and Helenius, A. 1993. Folding and assembly of viral membrane proteins. *Virology*. **193,** 545-562.

Donnelly, C. A., Fisher, M. C., Fraser, C., Ghani, A. C., Riley, S., Ferguson, N. M., and Anderson, R. M., 2004. Epidemiological and genetic analysis of severe acute respiratory syndrome. *Lancet. Infect. Dis*. **4,** 672–683.

Drisdel, R.C., and Green, W.N. 2004. Labeling and quantifying sites of protein palmitoylation. *Biotechniques.* **36,** 276-285.

Drosten, C., Gunther, S., Preiser, W., van der Werf, S., Brodt, H. R., Becker, S., Rabenau, H., Panning, M., Kolesnikova, L., Fouchier, R.A., Berger, A., Burguiere, A. M., Cinatl, J., Eickmann, M., Escriou, N., Grywna, K., Kramme, S., Manuguerra, J. C., Muller, S., Rickerts, V., Sturmer, M., Vieth, S., Klenk, H. D., Osterhaus, A. D., Schmitz, H., and Doerr, H.W. 2003. Identification of a novel coronavirus in patients with severe acute respiratory syndrome. *N. Engl. J. Med*. **348,** 1967-1976.

Dunphy, J. T., Schroeder, H., Leventis, R., Greentree, W. K., Knudsen, J. K., Silvius, J. R., and Linder, M. E. 2000. Differential effects of acyl-CoA binding protein on

enzymatic and non-enzymatic thioacylation of protein and peptide substrates. *Biochim. Biophys. Acta.* **1485,** 185-198.

Ebihara, T., Endo, R., Ma, X., Ishiguro, N., and Kikuta, H. 2005. Detection of human coronavirus NL63 in young children with bronchiolitis. *J. Med. Virol.* **75,** 463-465.

Eickmann, M., Becker, S., Klenk, H. D., Doerr, H. W., Stadler, K., Censini, S., Guidotti, S., Masignani, V., Scarselli, M., Mora, M., Donati, C., Han, J. H., Song, H. C., Abrignani, S., Covacci, A., and Rappuoli, R. 2003. Phylogeny of the SARS coronavirus. *Science.* **302,** 1504-1505.

Engel, J. P. 1995. Virus upper respiratory infections. *Semin. Respir. Infect.* **10,** 3-13.

Estola, T. 1970. Coronaviruses, a new group of animal RNA viruses. *Avian. Dis*. **14,** 330-336.

Ewart, G. D., Sutherland, T., Gage, P. W., and Cox, G. B. 1996. The Vpu protein of human immunodeficiency virus type 1 forms cation-selective ion channels. *J. Virol*. **70,** 7108-7115.

Ewart, G. D., Mills, K., Cox, G. B., and Gage, P. W. 2002. Amiloride derivatives block ion channel activity and enhancement of virus-like particle budding caused by HIV-1 protein Vpu. *Eur. Biophys. J*. **31,** 26-35.

Fielding, B. C., Tan, Y. -J., Shuo, S., Tan, T. H. P., Ooi, E. -E., Lim, S. G., Hong, W., and Goh, P. -Y., 2004. Characterization of a unique group-specific protein (U122) of the severe acute respiratory syndrome (SARS) coronavirus. *J. Virol.* **78,** 7311–7318.

Fielding, B. C., Gunalan, V., Tan, T. H. P., Chou, C. -F., Shen, S., Khan, S., Lim, S. G., Hong, W., and Tan, Y.-J., 2006. Severe acute respiratory syndrome coronavirus protein 7a interacts with hGST. *Biochem. Biophys. Res. Commun*. **343**, 1201–1208.

Fischer, F., Peng, D., Hingley, S.T., Weiss S.R., and Masters, P.S. 1997. The internal open reading frame within the nucleocapsid gene of mouse hepatitis virus encodes a structural protein that is not essential for viral replication, *J. Virol.* **71,** 996–1003.

Fischer, F, Stegen, C. F., Masters, P. S., and Samsonoff, W. A. 1998. Analysis of constructed E gene mutants of mouse hepatitis virus confirms a pivotal role for E protein in coronavirus assembly. *J. Virol.* **72**, 7885-7894.

Fischer, W. B., and Sansom, M. S. P. 2002. Viral ion channels: structure and function. *Biochim. et biophys.* **1561,** 27-45.

Fischer, W. B. 2003. Vpu from HIV-1 on an atomic scale: experiments and computer simulations. *FEBS. Lett.* **552,** 39-46.

Fuerst, T.R., Niles, E.G., Studier, F.W., and Moss, B. 1986. Eukaryotic transient-expression system based on recombinant vaccinia virus that synthesizes bacteriophage T7 RNA polymerase. *Proc. Natl. Acad. Sci. USA*. **83,** 8122-8126.

Fujiki, Y., Hubbard, A. L., Fowler, S., and lazarow, P. B. 1982. Isolation of intracellular membranes by means of sodium carbonate treatment: Application to endoplasmic reticulum. *J. Cell. Biol.* **93**, 97-102.

Gaedigk-Nitschko, K., and Schlesinger, M. J. 1990a. The sindbis virus 6K protein can be detected in virions and is acylated with fatty acids. *Virology.* **175,** 274-281.

Gaedigk-Nitschko, K., Ding, M. X., Levy, M. A., and Schlesinger, M. J. 1990b. Site-directed mutations in the sindbis virus 6K protein reveal sites for fatty acylation and the underacylated protein affects virus release and virion structure *Virology*. **175**. 282-291.

Geng, H., Liu, Y. M., Chan, W. S., Lo, A. W., Au, D. M., Waye, M.M., and Ho, Y. Y., 2005. The putative protein 6 of the severe acute respiratory syndrome-associated coronavirus: expression and functional characterization. *FEBS. Lett.* **579,** 6763–6768.

Goebel, S. J., Taylor, J., and Masters, P. S. 2004. The 3' cis-acting genomic replication element of the severe acute respiratory syndrome coronavirus can function in the murine coronavirus genome. *J. Virol.* 78, 7846-7851.

Godet, M., Haridon, R., Vautherot, J. F., and Laude, H. 1992. TGEV coronavirus ORF4 encodes a membrane protein that is incorporated into virions. *Virology.* **188,** 666-675.

Gonzalez, M. E., and Carrasco, L. 1998. The human immunodeficiency virus type 1 Vpu protein enhances membrane permeability. *Biochemistry.* **37**, 13710–13719.

Gonzalez, M. E., and Carrasco, L. 2003. Viroporins. *FEBS. Lett.* **552**, 28–34.

Groneberg, D. A., Poutanen, S. M., Low, D. E., Lode, H., Welte, T., and Zabel, P., 2005. Treatment and vaccines for severe acute respiratory syndrome. *Lancet. Infect. Dis.* **5,** 147–155.

Guan, Y., Zheng, B. J., He, Y. Q., Liu, X. L., Zhuang, Z. X., Cheung, C. L., Luo, S. W., Li, P. H., Zhang, L. J., Guan, Y. J., Butt, K. M., Wong, K. L., Chan, K. W., Lim, W., Shortridge, K. F., Yuen, K. Y., Peiris, J. S., and Poon, L. L. 2003. Isolation and characterization of viruses related to the SARS coronavirus from animals in southern China. *Science.* **302,** 276-278.

Guan, M., Chan, K. H., Peiris, J. S., Kwan, S. W., Lam, S. Y., Pang, C. M., Chu, K. W., Chan, K. M., Chen, H. Y., Phuah, E. B., and Wong, C. J. 2004a. Evaluation and validation of an enzyme-linked immunosorbent assay and an immunochromatographic test for serological diagnosis of severe acute respiratory syndrome. *Clin. Diagn. Lab. Immunol.* **11,** 699–703.

Guan, M., Chen, H. Y., Foo, S. Y., Tan, Y. -J., Goh, P. Y., and Wee, S. H. 2004b. Recombinant protein-based enzyme-linked immunosorbent assay and immunochromatographic tests for detection of immunoglobulin G antibodies to severe acute respiratory syndrome (SARS) coronavirus in SARS patients. *Clin. Diagn. Lab. Immunol.* **11,** 287–291.

Guinea, R., and Carrasco, L. 1994. Influenza virus M2 protein modifies membrane permeability in *E. coli* cells. *FEBS. Letters.* **343,** 242-246.

Guo, J. P., Petric, M., Campbel, W., and McGeer, P..L. 2004. SARS coronavirus peptides recognized by antibodies in the sera of convalescent cases. *Virology.* **324,** 251–256.

Haijema, B. J., Volders, H., and Rottier, P. J. M. 2003. Switching species tropism: An effective way to manipulate the feline coronavirus genome. *J. Virol.* **77**, 4528–4538.

Haijema, B. J., Volders, H., and Rottier, P. J. M. 2004. Live, attenuated coronavirus vaccines through the directed deletion of group-specific genes provide protection against feline infectious peritonitis, *J. Virol.* **78**, 3863–3871.

Hanel, K., Stangler, T., Stoldt, M., and Willbold, D. 2006. Solution structure of the X4 protein coded by the SARS-related coronavirus reveals an immunoglobulin-like fold and suggests a binding activity to integrin I domains. *J. Biomed. Sci*. **23,** 1–13.

Hausmann, J., Ortmann, D., Witt, E., Veit, M., and Seidel, W. 1998. Adenovirus death protein, a transmembrane protein encoded in the E3 region, is palmitoylated at the cytoplasmic tail. *Virology.* **244**, 343-351.

Huang, C., Ito, N., Tseng, C. T., and Makino, S. 2006. Severe acute respiratory syndrome coronavirus 7a accessory protein is a viral structural protein. *J. Virol.* **80,** 7287-7294.

Helinius, A., and Simons, K. 1975. Solubilization of membrane by detergent. *Biochim. Biophys. Acta.* **415,** 29-79.

Henkel, J. R., and Weisz, O. A. 1998. Influenza virus M2 protein slows traffic along the secretory pathway. *J. Biol. Chem.* **273,** 6518-6524.

Ho, Y., Lin, P. H., Liu, C. Y. Y., Lee, S. P., and Chao, Y. C. 2004. Assembly of

human severe acute respiratory syndrome coronavirus-like particles. *Biochem. Biophys. Res Commun.* **318,** 833-838.

Hoek, L. V. D, Pyrc, K., Jebbink, M. F., Vermeulen-Oost, W., Berkhout, R. J. M., Wolthers, K. C., Wertheim-van Dillen, P. M. E., Kaandorp, J., Spaargaren, J., and Berkhout, B. 2004. Identification of a new human coronavirus. *Nat. Med.* **10,** 368 – 373.

Hofmann, H., Pyrc, K., van der Hoek, L., Geier, M., Berkhout, B., and Pohlmann, S. 2005. Human coronavirus NL63 employs the severe acute respiratory syndrome coronavirus receptor for cellular entry. *Proc. Natl. Acad. Sci. U S A*. **102,** 7988-7993.

Holmes, K. V. 2003a. SARS coronavirus: a new challenge for prevention and therapy. *J. Clin. Invest*. **111,** 1605-1609.

Holmes, K.V. 2003b. SARS-associated coronavirus. *N. Engl. J. Med.* **348,** 1948-1951.

Holsinger, L. J., and Lamb, R. A. 1991. Influenza virus M2 integral membrane protein is a homotetramer stabilized by formation of disulfide bonds. *Virology.* **183,** 32-43.

Holsinger, L. J., Shaughnessy, M. A., Micko, A., Pinto, L. H., and Lamb, R. A. 1995. Analysis of the posttranslational modifications of the influenza virus M2 protein. *J. Virol.* **69,** 1219-1225.

Hsu, K., Seharaseyon, J., Dong, P., Bour, S., and Marban, E. 2004. Mutual functional destruction of HIV-1 Vpu and host TASK-1 channel. *Mol. Cell*. **14,** 259-267.

Huang, C., Narayanan, K., Ito, N., Peters, C.J., Makino, S., 2006. Severe acute respiratory syndrome coronavirus 3a protein is released in membranous structures from 3a protein-expressing cells and infected cells. *J. Virol.* **80,** 210–217.

Ito, N, Mossel, E. C., Narayanan, K., Popov, V. L., Huang, C., Inoue, T., Peters, C. J., and Makino, S. 2005. Severe acute respiratory syndrome coronavirus 3a protein is a

viral structural protein. *J. Virol.* **79,** 3182-3186.

Jeffers, S. A., Tusell, S. M., Gillim-Ross, L., Hemmila, E. M., Achenbach, J. E., Babcock, G. J., Thomas, W. D. Jr., Thackray, L. B., Young, M. D., Mason, R. J., Ambrosino, D. M., Wentworth, D. E., Demartini, J. C., and Holmes, K. V. 2004. CD209L (L-SIGN) is a receptor for severe acute respiratory syndrome coronavirus. *Proc. Natl. Acad. Sci. U S A.* **101,** 15748-15753.

Jiang, S., He, Y., and Liu, S. 2005. SARS vaccine development. *Emerg. Infect. Dis.* **11,** 1016–1020.

Jonassen, C. M., Kofstad, T., Larsen, I. L., Lovland, A., Handeland, K., Follestad, A., and Lillehaug, A. 2005. Molecular identification and characterization of novel coronaviruses infecting graylag geese (Anser anser), feral pigeons (Columbia livia) and mallards (Anas platyrhynchos). *J. Gen. Virol.* **86,** 1597-1607.

Kan, B., Wang, M., Jing, H., Xu, H., Jiang, X., Yan, M., Liang, W., Zheng, H., Wan, K., Liu, Q., Cui, B., Xu, Y., Zhang, E., Wang, H., Ye, J., Li, G., Li, M., Cui, Z., Qi, X., Chen, K., Du, L., Gao, K., Zhao, Y. T., Zou, X. Z., Feng, Y. J., Gao, Y. F., Hai, R., Yu, D., Guan, Y., and Xu, J. 2005. Molecular evolution analysis and geographic investigation of severe acute respiratory syndrome coronavirus-like virus in palm civets at an animal market and on farms. *J. Virol.* **79,** 11892–11900.

Khattari, Z., Brotons, G., Akkawi, M., Arbely, E., Arkin, I. T., and Salditt, T. 2006. SARS coronavirus E protein in phospholipids bilayers: a X-ray scattering study. *Biophysical. J.* **90,** 2038-2050.

Kopecky-Bromberg, S.A., Martinez-Sobrido, L., and Palese, P., 2006. 7a protein of severe acute respiratory syndrome coronavirus inhibits cellular protein synthesis and activates p38 mitogen-activated protein kinase. *J. Virol.* **80,** 785–793.

Kou, L., and Masters, P. S. 2003. The small envelope protein E protein is not essential for murine coronavirus replication. *J. Virol.* **77,** 4597-4608.

Kuo, L., Hurst, K. R., and Masters, P. S. 2007. Exceptional flexibility in the sequence requirements for coronavirus small envelope protein function. *J. Virol.* **81,** 2249-2262.

Krokhin, O., Li, Y., Andonov, A., Feldmann, H., Flick, R., Jones, S., Stroeher, U., Bastien, N., Dasuri, K. V., Cheng, K., Simonsen, J. N., Perreault, H., Wilkins, J., Ens, W., Plummer, F., and Standing, K. G. 2003. Mass spectrometric characterization of proteins from the SARS virus: a preliminary report. *Mol. Cell. Proteomics.* **2,** 346-356.

Ksiazek, T.G., Erdman, D., Goldsmith, C.S., Zaki, S.R., Peret, T., Emery, S., Tong, S., Urbani, C., Comer, J.A., Lim, W., Rollin, P.E., Dowell, S.F., Ling, A.E., Humphrey, C.D., Shieh, W.J., Guarner, J., Paddock, C.D., Rota, P., Fields, B., DeRisi, J., Yang, J.Y., Cox, N., Hughes, J.M., LeDuc, J.W., Bellini, W.J. and Anderson, L.J. 2003. SARS Working Group. A novel coronavirus associated with severe acute respiratory syndrome. *N. Engl. J. Med.* **348,** 1953-1966.

Lai, M. M., and Cavanagh, D. 1997. The molecular biology of coronaviruses. *Adv. Virus Res.* **48,** 1–100.

Lama, J., and Carrasco, L. 1995. Mutations in the hydrophobic domain of poliovirus protein 3AB abrogate its permeabilizing activity. *FEBS. Lett.* **367,** 5-11.

Lama, J., and Carrasco, L. 1996. Screening for membrane-permeabilizing mutants of the poliovirus protein 3AB. *J. Gen. Virol.* **77,** 2109-2119.

Lamb, R. A., Holsinger, L. J., and Pinto, L. H. 1994. The influenza A virus AM2 ion channel protein and its role in the influenza virus life cycle. In: Wimmer, E., editor. *Receptor-mediated virus entry into cells.* Cold Spring Harbor, N. Y.: Cold Spring Harbor Press; 303-321.

Landecker, H. 2000. Immortality, In Vitro: A history of the HeLa cell line. Indiana. Uni. Press. 53-74. Lau, S. K., Woo, P. C., Li, K. S., Huang, Y., Tsoi, H. W., Wong, B. H., Wong, S. S., Leung, S. Y., Chan, K. H., and Yuen, K. Y. 2005. Severe acute respiratory syndrome coronavirus-like virus in Chinese horseshoe bats. *Proc. Natl. Acad. Sci.* U S A. **102,** 14040-14045.

Laude, H., Gelfi, J., Lavenant, L., and Charley, B. 1992. Single amino acid changes in the viral glycoprotein M affect induction of α interferon by the coronavirus transmissible gastroenteritis virus. *J. Virol.* **66,** 743-749.

Laude, H., and Masters, P. S. 1995. The coronavirus nucleocapsid protein. *In* "The *coronaviridae*" (S. G. Siddell, ed.), *Plenum Press, New York*. pp. 141-163.

Law, P. T., Wong, C. H., Au, T. C., Chuck, C. P., Kong, S. K., Chan, P. K., To, K. F., Lo, A. W., Chan, J. Y., Suen, Y. K., Chan, H. Y., Fung, K. P., Waye, M. M., Sung, J. J., Lo, Y. M., and Tsui, S. K., 2005. The 3a protein of severe acute respiratory syndrome-associated coronavirus induces apoptosis in Vero E6 cells. *J. Gen. Virol***. 86,** 1921–1930.

Leventis, R., Juel, G., Knudsen, J. K., and Silvius, J. R. 1997. Acyl-CoA binding proteins inhibit the nonenzymic S-acylation of cysteinyl-containing peptide sequences by long-chain acyl-CoAs. *Biochemistry.* **36,** 5546-5553.

Liang, G., Chen, Q., Xu, J., Liu, Y., Lim, W., Peiris, J. S., Anderson, L. J., Ruan, L., Li, H., Kan, B., Di, B., Cheng, P., Chan, K. H., Erdman, D. D., Gu, S., Yan, X., Liang, W., Zhou, D., Haynes, L., Duan, S., Zhang, X., Zheng, H., Gao, Y., Tong, S., Li, D., Fang, L., Qin, P., and Xu, W. 2004. Laboratory diagnosis of four recent sporadic cases of community-acquired SARS, Guangdong Province, China. *Emerg. Infect. Dis.* **10,** 1774–1781.

Liao, Y., Lescar, J., Tam, J. P., and Liu, D. X. 2004. Expression of SARS coronavirus envelope protein in *Escherichia coli* cells alters membrane permeability. *Biochem. Biophys. Res. Commun.* **325**, 374-380.

Liao, Y., Yuan, Q., Torres, J., Tam, J. P. and Liu, D. X. 2006. Biochemical and functional characterization of the membrane association and membrane permeabilizing activity of the acute respiratory syndrome coronavirus envelope protein. *Virology.* **349,** 264-275.

Li, F. Q., Xiao, H., Tam, J. P. and Liu, D. X. 2005. Sumoylation of the nucleocapsid protein of severe acute respiratory syndrome coronavirus. *FEBS. Lett.* **579,** 2387-96.

Li, M., Yang, C., Tong, S., Weidmann, A., and Compans, R. W. 2002. Palmitoylation of the murine leukemia virus envelope protein is critical for lipid raft association and surface expression. *J. Virol*. **76,** 11845-11852.

Li, W., Moore, M. J., Vasillieva, N., Sui, J., Wong, S. K. Berne, M. A., Somasundaran, M., Sullivan, J. L., Luzuriaga, K., Greenough, T. C., Choe, H. and Farzan, M. 2003. Angiotensin-converting enzyme 2 is a functional receptor for the SARS coronavirus. *Nature.* **426,** 450-454.

Li , W., Shi, Z., Yu, M., Ren, W., Smith, C., Epstein, J. H., Wang, H., Crameri, G., Hu, Z., Zhang, H., Zhang, J., McEachern, J., Field, H., Daszak, P., Eaton, B. T., Zhang, S. and Wang, L. F. 2005. Bats are natural reservoirs of SARS-like coronaviruses. *Science.* **310,** 676-679.

Lim, K. P., and Liu, D. X. 2001. The missing link in coronavirus assembly. *J. Biol. Chem.* **276**, 17515–17523.

Lin, Y., Yan, X., Cao, W., Wang, C., Feng, J., Duan, J., and Xie, S. (2004). Probing the structure of the SARS coronavirus using scanning electron microscopy. *Antiviral Ther.* **9,** 287-289.

Liu, D. X., and Inglis, S. C. 1991. Association of the infectious bronchitis virus 3c protein with the virion envelope. *Virology.* **185**, 911–917.

Liu, D. X., Cavanagh, D., Green, P., and Inglis, S. C. 1991. A polycistronic mRNA specified by the coronavirus infectious bronchitis virus. *Virology.* **184,** 531-544.

Lu, W., Zheng, B. J., Xu, K., Schwarz, W., Du, L., Wong, C. K., Chenm J., Duan, S., Deubel, V., and Sun, B. 2006. Severe acute respiratory syndrome-associated coronavirus 3a protein forms an ion channel and modulates virus release. *Proc. Natl. Acad. Sci. U S A*. **103,** 12540-12545.

Madan, V., Garcia, M. J., Sanz, M. A., and Carrasco, L. 2005. Viroporin activity of murine hepatitis virus E protein. *FEBS. Lett*. **579**, 3607-3612.

Maeda, J., Maeda, A., and Makino, S. 1999. Release of coronavirus E protein in membrane vesicles from virus-infected cells and E protein-expressing cells. *Virology.* **263,** 265-272.

Marra, M. A., Jones, S. J, Astell, C. R, Holt, R. A, Brooks-Wilson, A., Butterfield, Y. S., Khattra, J., Asano, J. K., Barber, S. A., Chan, S.Y, Cloutier, A., Coughlin, S. M., Freeman, D., Girn, N., Griffith, O. L., Leach, S. R., Mayo, M., McDonald, H., Montgomery, S. B., Pandoh, P. K., Petrescu, A. S., Robertson, A. G., Schein, J. E., Siddiqui, A., Smailus, D. E., Stott, J. M., Yang, G. S., Plummer, F., Andonov, A., Artsob, H., Bastien, N., Bernard, K., Booth, T. F., Bowness, D., Czub, M., Drebot, M., Fernando, L., Flick, R., Garbutt, M., Gray, M., Grolla, A., Jones, S., Feldmann, H., Meyers, A., Kabani, A., Li, Y., Normand, S., Stroher, U., Tipples, G. A., Tyler, S., Vogrig, R., Ward, D., Watson, B., Brunham, R. C., Krajden, M., Petric, M., Skowronski, D. M, Upton, C., and Roper, R.L. 2003. The Genome Sequence of the SARS-Associated coronavirus. *Science.* **300**, 1399–1404.

Marassi, F. M., Ma, C., Gratkowski, H., Straus, S. K., Strebel, K., Oblatt-Montal, M., Montal, M., and Opella, S. J. 1999. Correlation of the structural and functional domains in the membrane protein Vpu from HIV-1. *Proc. Natl. Acad. Sci.* U S A. **25,** 14336-14341.

Martina, B. E., Haagmans, B. L., Kuiken, T., Fouchier, R. A., Rimmelzwaan, G. F., Van Amerongen, G., Peiris, J. S., Lim, W., and Osterhaus, A. D. 2003. Virology: SARS virus infection of cats and ferrets. *Nature.* **425,** 915.

Masters, J. R. 2002. HeLa cells 50 years on: the good, the bad and the ugly. *Nature Rev.s Cancer.* **2,** 315-319.

Mehmel, M., Rothermel, M., Meckel, T., van Etten, J. L., Moroni, A., and Thiel, G. 2003. Possible function for virus encoded K+ channel Kcv in the replication of chlorella virus PBCV-1. *FEBS. Lett.* **552,** 7-11.

Melkonian, K. A., Ostermeyer, A. G., Chen, J. Z., , Roth, M. G., and Brown, D. A. 1999. Role of lipid modifications in targeting proteins to detergent-resistant membrane rafts. Many raft proteins are acylated, while few are prenylated. *J. Biol. Chem.* **274,** 3910-3917.

Moes, E., Vijgen, L., Keyaerts, E., Zlateva, K., Li, S., Maes, P., Pyrc, K., Berkhout, B., van der Hoek, L., and van Ranst, M. 2005. A novel pancoronavirus RT-PCR assay: frequent detection of human coronavirus NL63 in children hospitalized with respiratory tract infections in Belgium. *BMC. Infect. Dis.* **5,** 6.

Montal, M. 2003. Structure-function correlates of Vpu, a membrane protein of HIV-1. *FEBS. Lett.* **552,** 47-53.

Mortola, E., and P. Joy. 2004. Efficient assembly and release of SARS coronavirus-like particles by a heterologous expression system. *FEBS Lett.* **576,** 174-178.

Mould, J. A., Drury, J. E., Frings, S. M., Kaupp, U. B., Pekosz, A., Lamb, R. A., and Pinto, L. H. 2000. Permeation and activation of the M2 ion channel of influenza A virus. *J. Biol. Chem.* **275,** 31038-31050.

Nal, B., Chan, C., Kien, F., Siu, L., Tse, J., CHu, K., Kam, J., Staropoli, I., Crescenzo-Chaigne, B., Escriou, N., van der Werf, S., Yuen, K. Y., and Altmeyer, R. 2005. Differential maturation and subcellular localization of sever respiratory syndrome conronavirus surface proteins S, M and E. *J. Gen. Virol*. **86,** 1423-1434.

Navas-Martin, S. R., and Weiss, S. 2004. Coronavirus replication and pathogenesis:

Implications for the recent outbreak of severe acute respiratory syndrome (SARS), and the challenge for vaccine development. *J. Neurovirol.* **10,** 75-85.

Nelson, C. A., Pekosz, A., Lee, C. A., Diamond, M. S., and Fremont, D. H., 2005. Structure and intracellular targeting of the SARS-coronavirus ORF 7a accessory protein. *Structure.* **13,** 75–85.

Newton, K., Meyer, J. C., Bellamy, A. R., and Taylor, J. A. 1997. Rotavirus nonstructural glycoprotein NSP4 alters plasma membrane permeability in mammalian cells. *J. Virol.* **71,** 9458-9465

Nie, Q. H., Luo, X. D., and Hui, W. L. 2003. Advances in clinical diagnosis and treatment of severe acute respiratory syndrome. *World. J. Gastroenterol.* **9,** 1139-1143.

Nieva, J. L., Sanz, M. A., and Carrasco, L. 2004. Membrane-permeabilizing motif in Semliki forest virus E1 glycoprotein. *FEBS. Lett.* **576,** 417-22.

Nilsson, I. M., and Von, H. G. 1993. Determination of the distance between the oligosaccharyltransferase active site and the endoplasmic reticulum membrane. *J. Biol. Chem.* **268,** 5798-5801.

Ochsenbauer-Jambor, C., Miller, D. C., Roberts, C. R., Rhee, S. S., and Hunter, E. 2001. Palmitoylation of the Rous sarcoma virus transmembrane glycoprotein is required for protein stability and virus infectivity. *J. Virol*. **75**, 11544-11554.

Okada, A., Miura, T., and Takeuchi, H. 2001. Protonation of Histidine-Tryptophan interaction in the activation of the M2 ion channel from influenza A virus. *Biochemistry.* **40,** 6053-6060.

Ontiveros, E., Kuo, L., Masters, P. S., and Perlman, S. 2001. Inactivation of expression of gene 4 of mouse hepatitis virus strain JHM does not affect virulence in the murine CNS, *Virology.* **289**, 230–238.

Oostra, M., de Haan, C. A., de Groot, R. J., and Rottier, P. J., 2006. Glycosylation of the severe acute respiratory syndrome coronavirus triple-spanning membrane proteins 3a and M. *J. Virol.* **80,** 2326–2336.

Opstelten, D. J., Rammsman, M. J., Wolfs, K., Horzinek, M. C., and Rottier, P. J. 1995. Envelope glycoprotein interactions in coronavirus assembly. *J. Cell Biol.* **131,** 339-349.

Ortego, J., Escors, D., Laude, H., and Enjuanes, L. 2002. Generation of a replication-competent, propagation-deficient virus vector based on the transmissible gastroenteritis coronavirus genome. *J. Virol.* **76,** 11518-11529.

Ortego, J., Sola, I., Almazan, F., Ceriani, J.E., Riquelme, C., Balasch, M., Plana, J. and Enjuanes, L. 2003. Transmissible gastroenteritis coronavirus gene 7 is not essential but influences *in vivo* virus replication and virulence. *Virology*. **308,** 13–22.

Osterhaus, A. D., Fouchier, R. A., and Kuiken, T. 2004. The aetiology of SARS: Koch's postulates fulfilled. *Philos. Trans. R. Soc. Lond. B. Biol. Sci*. **359,** 1081–1082.

Pavlovic, D., Neville, D. C. A., Argaud, O., Blumberg, B., Dwek, R. A., Fischer, W. B., and Zitzmann, N. 2003. The hepatitis C virus P7 forms an ion channel that is inhibited by long-alkyl-chain iminosugar derivatives. *Proc. Natl. Acad. Sci. U S A.* **100**, 6104–6108.

Peiris, J. S., Laim S. T., Poon, L. L., Guan, Y., Yam, L. Y., Lim, W., Nicholls, J., Yee, W. K., Yan, W. W., Cheung, M. T., Cheng, V. C., Chan, K. H., Tsang, D. N., Yung, R. W., Ng, T. K., and Yuen, K. Y. SARS study group. 2003a. Coronavirus as a possible cause of severe acute respiratory syndrome. *Lancet.* **361,** 1319-1325.

Peiris, J. S., Yuen, K. Y., Osterhaus, A. D., and Stohr, K. 2003b. The severe acute respiratory syndrome. *N. Engl. J. Med.* **349,** 2431-2441.

Peiris, J. S., Guan, Y., and Yuen, K.Y. 2004. Severe acute respiratory syndrome. *Nat. Med.* **10 (Suppl.),** S88–S97.

Pewe, L., Zhou, H., Netland, J., Tangudu, C., Olivares, H., Shi, L., Look, L., Gallagher, T., and Perlman, S., 2005. A severe acute respiratory syndrome associated coronavirus-specific protein enhances virulence of an attenuated murine coronavirus. *J. Virol.* **79,** 11335–11342.

Pinto, L. H., Holsinger, L. J., and Lamb, R. A. 1992. Influenza virus M2 protein has ion channel activity. *Cell.* **59**, 517–528.

Ponimaskin, E., and Schmidt, M. F. G. 1998. Domain-structure of cytoplasmic border region is main determinant for palmitoylation of influenza virus hemagglutinin (H7). *Virology*. **249,** 325-335.

Poon, L. L., Guan, Y., Nicholls, J. M., Yuen, K. Y., and Peiris, J. S. 2004. The aetiology, origins, and diagnosis of severe acute respiratory syndrome. *Lancet Infect. Dis.* **4,** 663–671.

Premkumar, A., Wilson, L., Ewart, G. D., and Gage, P. W. 2004. Cation-selective ion channels formed by p7 of hepatitis C virus are blocked by hexamethylene amiloride. *FEBS. Lett.* **557,** 99-103.

Pyrc, K., Jebbink, M. F., Berkhout, B. and van der Hoek, L. 2004. Genome structure and transcriptional regulation of human coronavirus NL63. *Virol. J.* **17**, 1-7.

Qiu, M., Shi, Y., Guo, Z., Chen, Z., He, R., Chen, R., Zhou, D., Dai, E., Wang, X., Si, B., Song, Y., Li, J., Yang, L., Wang, J., Wang, H., Pang, X., Zhai, J., Du, Z., Liu, Y., Zhang, Y., Li, L., Wang, J., Sun, B., and Yang, R. 2005. Antibody responses to individual proteins of SARS coronavirus and their neutralization activities. *Microb. Infect.* **7,** 882– 889.

Resh, M. D. 1999. Fatty acylation of proteins: new insights into membrane targeting of myristoylated and palmitoylated proteins. *Biochim. Biophys. Acta.* **1451,** 1-16.

Rota, P. A., Oberste, M. S., Monroe, S. S., Nix, W. A., Campagnoli, R., Icenogle, J.

P., Penaranda, S., Bankamp, B., Maher, K., Chen, M. H., Tong, S., Tamin, A., Lowe, L., Frace, M., DeRisi, J. L., Chen, Q., Wang, D., Erdman, D. D., Peret, T. C., Burns, C., Ksiazek, T. G., Rollin, P. E., Sanchez, A., Liffick, S., Holloway, B., Limor, J., McCaustland, K., Olsen-Rasmussen, M., Fouchier, R., Gunther, S., Osterhaus, A. D., Drosten, C., Pallansch, M. A., Anderson, L. J., and Bellini, W. J. 2003 Characterization of a novel coronavirus associated with severe acute respiratory syndrome. *Science.* **300,** 1394–1399.

Rottier, P. J. M. 1995. The coronavirus membrane glycoprotein. *In* "The coronaviridae" (S. G SIddell, ed.). *Plenum, New York*. pp. 115-139.

Rousso, I., Mixon, M. B., Chen, B. K., and Kim, P. S. 2000. Palmitoylation of the HIV-1 envelope glycoprotein is critical for viral infectivity. *Proc. Natl. Acad. Sci.* **97**, 13523-13525.

Ruan, Y. J., Wei, C. L., Ee, A. L., Vega, V. B., Thoreau, H., Su, S. T., Chia, J. M., Ng, P., Chiu, K. P., Lim, L., Zhang, T., Peng, C. K., Lin, E. O., Lee, N. M., Yee, S. L., Ng, L. F., Chee, R. E., Stanton, L. W., Long, P. M., and Liu, E. T. 2003. Comparative full length genome sequence analysis of 14 SARS coronavirus isolates and common mutations associated with putative origins of infection. *Lancet.* **361,** 1779-1785.

Sakaguchi, T., Tu, Q., Pinto, L. H., and Lamb, R. A. 1997. The active oligmeric state of the minimalistic influenza virus M2 ion channel is a tetramer. *Proc. Natl. Acad. Sci. USA*. **94,** 5000-5005.

Sakai, A., Claire, M. S., Faulk, K., Govindarajan, S., Emerson, S. U., Purcell, R. H., and Bukh, J. 2003. The p7 polypeptide of hepatitis C virus is critical for infectivity and contains functionally important genotype-specific sequences. *Proc. Natl. Acad. Sci. USA*. **100,** 11646-11651.

Sanderson, C. M., Parkinson, J. E., Hollinshead, M., and Smith, G. L. 1996. Overexpression of the vaccinia virus A38L integral membrane protein promotes Ca2+ influx into infected cells. *J. Virol.* **70,** 905-914.

Sanz, M. A., Perez, L., and Carrasco, L. 1994. Semliki forest virus 6K protein modifies membrane permeability after inducible expression in *Escherichia coli* cells. *J. Biol. Chem.* **269**, 12106–12110.

Schlesinger, M. J., Veit, M., and Schmidt, M. F. G. 1993. Palmitoylation of cellular and viral proteins. *In* Lipid Modifications of Proteins. M. J. Schlesinger, editor. *CRC Press, Boca Raton*, FL. 1-19.

Schwarz, B., Routledge, E., and Siddell, S. G. 1990. Murine coronavirus nonstructural protein ns2 is not essential for virus replication in transformed cells. *J. Virol.* **64**, 4784–4791.

Schweizer, A., Rohrer, J., and Kornfeld, S. 1995. Determination of the structural requirements for palmitoylation of p63. *J. Biol. Chem.* **270,** 9638-9644.

Schmidt, M., Schmidt, M. F. G., and Rott, R. 1988. Chemical identification of cysteine as palmitoylation site in a transmembrane protein (Semliki forest virus E1). *J. Biol. Chem.* **263,** 18635-18639.

Schroeder, C., Heider, H., Moncke-Buchner, E., and Lin, T. I. 2005. The influenza virus ion channel and maturation cofactor M2 is a cholesterol-binding protein. *Eur Biophys J.* **34,** 52-66.

Schubert, U., Ferrer-Montiel, A. V., Oblatt-Montal, M., Henklein, P., Strebel, K., and Montal, M. 1996. Identification of an ion channel activity of the Vpu transmembrane domain and its involvement in the regulation of virus release from HIV-1-infected cells. *FEBS. Lett*. **398**, 12-18.

Sefton, B. M., and Buss, J. E. 1987. The covalent modification of eukaryotic proteins with lipid. *J. Cell Biol.* **104,** 1449-1453.

Shen, S., Lin, P. S., Chao, Y.C., Zhang, A., Yang, X., Lim, S. G., Hong, W., and Tan, Y. J. 2005. The severe acute respiratory syndrome coronavirus 3a is a novel structural

protein. *Biochem. Biophys. Res. Commun*. **330,** 286–292.

Siddell, S. G., 1995. The Coronaviridae. *Plenum Press, New York, USA*.

Shimbo, K., Brassard, D. L., Lamb, R. A., and Pinto, L. H. 1995. Viral and cellular small integral membrane proteins can modify ion channels endogenous to Xenopus oocytes. *Biophys. J.* **69,** 1819-1829.

Snijder, E. J, Bredenbeek, P. J, Dobbe, J. C, Thiel V., Ziebuhr, J., Poon, L. L, Guan, Y., Rozanov, M., Spaan, W. J., and Gorbalenya, A.E. 2003. Unique and conserved features of genome and proteome of SARS-coronavirus, an early split-off from the coronavirus group 2 lineage. *J. Mol. Biol.* **331,** 991-1004.

Song, H. D., Tu, C. C., Zhang, G. W., Wang, S. Y., Zheng, K., Lei, L. C., Chen, Q. X., Gao, Y. W., Zhou, H. Q., Xiang, H., Zheng, H. J., Chern, S. W., Cheng, F., Pan, C. M., Xuan, H., Chen, S. J., Luo, H. M., Zhou, D. H., Liu, Y. F., He, J. F., Qin, P. Z., Li, L. H., Ren, Y. Q., Liang, W. J., Yu, Y. D., Anderson, L., Wang, M., Xu, R. H., Wu, X. W., Zheng, H. Y., Chen, J. D., Liang, G., Gao, Y., Liao, M., Fang, L., Jiang, L. Y., Li, H., Chen, F., Di, B., He, L. J., Lin, J. Y., Tong, S., Kong, X., Du, L., Hao, P., Tang, H., Bernini, A., Yu, X. J., Spiga, O., Guo, Z. M., Pan, H. Y., He, W. Z., Manuguerra, J. C., Fontanet, A., Danchin, A., Niccolai, N., Li, Y. X., Wu, C. I., and Zhao, G. P. 2005. Cross-host evolution of severe acute respiratory syndrome coronavirus in palm civet and human. *Proc. Natl. Acad. Sci. U S A*. **102,** 2430–2435.

Sperry, S. M., Kazi, L., Graham, R. L., Baric, R. S., Weiss S. R., and Denison, M. R. 2005. Single-amino-acid substitutions in open reading frame (ORF) 1b-nsp14 and ORF 2a proteins of the coronavirus mouse hepatitis virus are attenuating in mice. *J. Virol.* **79**, 3391–3400.

Spiro, R. G. 2002. Protein glycosylation: nature, distribution, enzymatic formation and disease implications of glycopeptide bond. *Glycobiol*. **12,** 43R-53R.

Sunstrom, N. A., Premkumar, L. S., Premkumar, A., Ewart, G., Cox, G. B., and Gage, P. W. 1996. Ion channels formed by NB, an influenza B virus protein. *J. Membr. Biol.*

150, 127-132.

Sugrue, R. J., Belshe, R. B., and Hay, A. J. 1990. Palmitoylation of the influenza a virus M2 protein. *Virology*. **179,** 51-56.

Surjit, M., Lium B., Jameelm S., Chow V.T., and Lal, S. K. 2004. The SARS coronavirus nucleocapsid protein induces actin reorganization and apoptosis in COS-1 cells in the absence of growth factors. *Biochem. J.* **383,** 13-18.

Surjit, M., Liu, B., Chow, V. T., and Lal, S. K. 2006. The nucleocapsid protein of severe acute respiratory syndrome-coronavirus inhibits the activity of cyclin-cyclin-dependent kinase complex and blocks S phase progression in mammalian cells. *J. Biol. Chem.* **281,** 10669-10681.

Suzuki, A., Okamoto, M., Ohmi, A., Watanabe, O., Miyabayashi, S. and Nishimura, H. 2005. Detection of human coronavirus-NL63 in children in Japan. *Pediatr. Infect. Dis. J.* **24,** 645-646.

Takeuchi, H., Okada, A., and Miura, T. 2003. Roles of the histidine and tryptophan side chains in the M2 proton channel from influenza A virus. *FEBS. Lett.* **552,** 35-38.

Tan, Y. J., Fielding, B. C., Goh, P. Y., Shen, S., Tan, T. H. P., Lim, S. G., and Hong, W. 2004a. Overexpression of 7a, a protein specifically encoded by the severe acute respiratory syndrome coronavirus, induces apoptosis via a caspase-dependent pathway. *J. Virol.* **78,** 14043–14047.

Tan, Y. J., Goh, P. Y., Fielding, B. C., Shen, S., Chou, C.-F., Fu, J. L., Leong, H. N., Leo, Y. S., Ooi, E. E., Ling, A. E., Lim, S. G., and Hong, W. 2004b. Profiles of antibody responses against SARS-coronavirus recombinant proteins and their potential use as diagnostic markers. *Clin. Diagn. Lab. Immunol*. **11,** 362–371.

Tan, Y. J., Teng, E., Shen, S., Tan, T. H. P., Goh, P.Y., Fielding, B. C., Ooi, E. E., Tan, H. C., Lim, S. G., and Hong, W. 2004c. A novel SARS coronavirus protein, U274, is transported to the cell surface and undergoes endocytosis. *J. Virol.* **78,** 6723–

6734.

Tan, Y. J., Lim, S. G., and Hong, W. 2005. Characterization of viral proteins encoded by the SARS-coronavirus genome. *Antiviral Res.* **65,** 69–78.

Tan, Y. J., Lim, S. G., and Hong, W. 2006. Understanding the accessory viral proteins unique to the severe acute respiratory syndrome (SARS) coronavirus. *Antiviral Res.* **72,** 78-88.

Tang, Y., Zaitseva, F., Lamb, R. A., and Pinto, L. H. 2002. The gate of the influenza virus M2 proton channel is formed by a single tryptophan residue. *J. Virol.* **277,** 39880-39886.

Thiel, V., Ivanov, K. A., Putics, A., Hertzig, T., Schelle, B., Bayer, S., Weißbrich, B., Snijder, E. J., Rabenau, H., Doerr, H. W., Gorbalenya, A. E., and Ziebuhr, J. 2003. Mechanisms and enzymes involved in SARS coronavirus genome expression. *J. Gen. Virol.* **84**, 2305-2315.

Tiganos, E., Friborg, J., Allain, B., Daniel, N. G., Yao, X. J., and Cohen, E. A. 1998. Structural and functional analysis of the membrane-spanning domain of the human immunodeficiency virus type 1 Vpu protein. *Virology*. **251,** 96-107.

Thorp, E. B., Boscarino, J. A., Logan, H. L., Goletz, J. T., and Gallagher, T. M. 2006. Palmitoylations on murine coronavirus spike proteins are essential for virion assembly and infectivity. *J. Virol.* **80,** 1280-1289.

Torres, J., Wang, J., Parthasarathy, K., and Liu, D. X. 2005. The transmembrane oligomers of coronavirus protein E. *Biophys. J.* **88**, 1283-1290.

Torres, J., Parthasarathy, K., Lin, X., Saravanan, R., and Liu, D. X. 2006. Model of a putative pore: the pentameric α-helical bundle of SARS coronavirus E protein in lipid bilayers. *Biophys. J.* 91, 938-947.

Tsui, P. T., Kwok, M. L., Yuen, H., and Lai, S.T. 2003. Sever acute respiratory

syndrome: clinical outcome and prognostic correlates. *Emerg. Infect. Dis.* **9,** 1064-1069.

Tung, F. Y. T, Abraham, S., Sethna, M., Hung, S. L, Sethna, P., Hogue, B. G., and Brian, D. A. 1992. The 9-kDa hydrophobic protein encoded at the 3' end of the porcine transmissible gastroenteritis coronavirus genome is membrane-associated. *Virology.* **186,** 676-683.

Tyrrell, D. A., Cohen, S., and Schlarb, J. E. 1993. Signs and symptoms in common colds. *Epidemiol. Infect*. **111,** 143-156.

United Nations World Health Organization: Coronavirus never before seen in humans is the cause of SARS, New York. 16 April 2006. URL Accessed 5 July 2006.

Vabret, A., Mourez, T., Gouarin, S., Petitjean, J., and Freymuth, F. 2003. An outbreak of coronavirus OC43 respiratory infection in Normandy, France. *Clin. Infect. Dis.* **36,** 985-989.

Vabret, A., Mourez, T., Dina, J., van der Hoek, L., Gouarin, S., Petitjean, J., Brouard, J. and Freymuth, F. 2005. Human coronavirus NL63, France. *Emerg. Infect. Dis*. **11,** 1225-1229.

van Elden, L. J., van Loon, A. M., van Alphen, F., Hendriksen, K. A., Hoepelman, A. I., van Kraaij, M. G., Oosterheert, J. J., Schipper, P., Schuurman, R., and Nijhuis, M. 2004. Frequent detection of human coronaviruses in clinical specimens from patients with respiratory tract infection by use of a novel real-time reverse-transcriptase polymerase chacin reaction. *J. Infect. Dis.* **189,** 652-657.

van Valen., Leigh, M., and Maiorana, V. C. 1991. HeLa, a new microbial species. *Evolutionary Theory*. **10,** 71-74.

Veit, M., Schmidt, F. G., and Rott, R. 1989. Different palmitoylation of paramyxovirus glycoproteins. *Virology*. **168**, 173-176.

Veit, M., Klenk, H. D., Kendal, A., and Rott, R. 1991. The M2 protein of influenza A virus is acylated. *J. Gen. Virol*. **72,** 1461-1465.

Veit, M., and. Schmidt, M. F. G. 1993. Timing of palmitoylation of influenza virus hemagglutinin. *FEBS. Lett*. **336**, 243-247.

Vennema, H., Godeke, G. J., Rossen, J. W., Voorhout, W. F., Horzinek, M. C., Opstelten, D. J., and Rottier, P. J. 1996. Nucleocaspid-independent assembly of coronavirus-like particles by co-expression of viral envelope protein genes. *EMBO J.* **15,** 2020-2028.

Wang, C., Takeuchi, K., Pinto, L. H., and Lamb, R. A. 1993. Ion channel activity of influenza A virus M2 protein: Characterization of Amamtadine block. *J. Virol.* **67,** 5585-5594.

Wang, M., Yan, M., Xu, H., Liang, W., Kan, B., Zheng, B., Chen, H., Zheng, H., Xu, Y., Zhang, E., Wang, H., Ye, J., Li, G., Li, M., Cui, Z., Liu, Y. F., Guo, R. T., Liu, X. N., Zhan, L. H., Zhou, D. H., Zhao, A., Hai, R., Yu, D., Guan, Y., and Xu, J., 2005. SARS-CoV infection in a restaurant from palm civet. *Emerg. Infect. Dis.* **11,** 1860-1865.

Weiss, S. R., Zoltick, P. W., and Leibowitz, J. L. 1993. The ns 4 gene of mouse hepatitis virus (MHV), strain A 59 contains two ORFs and thus differs from ns 4 of the JHM and S strains. *Arch. Virol.* **129**, 301–309.

Weiss, S. R., and Navas-Martin, S. 2005. Coronavirus pathogenesis and the emerging pathogen severe acute respiratory syndrome coronavirus. *Microbiol. Mol. Biol. Rev.* **69,** 635–664.

Willey, R. L., Maldarelli, F., Martin, M. A., and Strebel, K. 1992a. Human immunodeficiency virus type 1 Vpu protein regulates the formation of intracellular gp160-CD4 complexes. *J. Virol.* **66,** 226-234.

Willey, R. L., Maldarelli, F., Martin, M. A., and Strebel, K. 1992b. Human immunodeficiency virus type 1 Vpu protein induces rapid degradation of CD4. *J. Virol.* **66,** 7193-7200.

Wilson, L., McKinlay, C., Gage, P., and Ewart, G. 2004. SARS coronavirus E protein forms cation-selective ion channels. *Virology.* **330**, 322-331.

Wilson, L, Gage, P., and Ewart, G. 2006. Hexamethylene amiloride blocks E protein ion channels and inhibits coronavirus replication. *Virology.* **353,** 294-306.

Woo, P. C. Y., Lau, S. K. P., Chu, C. M., Chan, K. H., Tsoi, H. W., Huang, Y., Wong, B. H. L., Poon, R. W. S., Cai, J. J., Luk, W. K., Poon, L. L. M., Wong, S. S. Y., Guan, Y., Peiris, J. S. M., and Yuen, K. Y. 2005a. Characterization and Complete Genome Sequence of a Novel Coronavirus, Coronavirus HKU1, from Patients with Pneumonia. *J. Virol.* **79**, 884-895.

Woo, P. C., Lau, S. K., Huang, Y., Tsoi, H. W., Chan, K. H. and Yuen, K. Y. 2005b. Phylogenetic and recombination analysis of coronavirus HKU1, a novel coronavirus from patients with pneumonia. *Arch Virol.* **150,** 2299-2311.

Yamada, Y. K., Yabe, M., Ohtsuki, T., and Taguchi, F. 2000. Unique N-linked glycosylation of murine coroanvirus MHV-2 membrane protein at the conserved O-linked glycosylation site. *Virus Res.* **66,** 49-154.

Yang, C., Spies, C. P., and Compans, R. W. 1995. The human and simian immunodeficiency virus envelope glycoprotein transmembrane subunits are palmitoylated. *Pro. Natl. Acad. Sci. U. S. A.* **92**, 9871-9875.

Yang, Y., Xiong, Z., Zhang, S., Yan, Y., Nguyen, J., Ng, B., Lu, H., Brendese, J., Yang, F., Wang, H., and Yang, X. F. 2005. Bcl-xL inhibits T-cell apoptosis induced by expression of SARS coronavirus E protein in the absence of growth factors. *J. Biochem.* **392,** 135-143.

Ying, W., Hao, Y., Zhang, Y. Peng, W., Qin, E., Cai, Y., Wei, K., Wang, J., Chang, G., Sun, W., Dai, S., Li, X., Zhu, Y., Li, J., Wu, S., Guo, L., Dai, J., Wang, J., Wan, P., Chen, T., Du, C., Li, D., Wan, J., Kuai, X., Li, W., Shi, R., Wei, H., Cao, C., Yu, M., Liu, H., Dong, F., Wang, D., Zhang, X., Qian, X., Zhu, Q., and He, F. 2004. Proteomic analysis on structural proteins of severe acute respiratory syndrome coronavirus. *Proteomics.* **4,** 492–504.

Yokomori, K., and Lai, M. M. C. 1991. Mouse hepatitis virus S RNA sequence reveals that nonstructural proteins ns4 and ns5a are not essential for murine coronavirus replication. *J. Virol.* **65**, 5605–5608.

Youn, S., Leibowitz, J. L., and Collisson, E. W. 2005. *In vitro* assembled, recombinant infectious bronchitis viruses demonstrate that the 5a open reading frame is not essential for replication. *Virology.* **332**, 206–215.

Yount, B., Roberts, R. S., Sims, A. C., Deming, D., Frieman, M. B., Sparks, J., Denison, M. R., Davis, N., and Baric, R. S. 2005. Severe acute respiratory syndrome coronavirus group-specific open reading frames encode nonessential functions for replication in cell cultures and mice. *J. Virol.* **79,** 14909-14922.

Yu, X., Bi, W., Weiss, S. R., and Leibowitz, J. L. 1994. Mouse hepatitis virus gene 5b protein is a new virion envelope protein. *Virology.* **202,** 1018-1023.

Yu, C. J., Chen, Y. C., Hsiao, C. H., Kuo, T. C., Chang, S. C., Lu, C. Y., Wei, W. C., Lee, C. H., Huang, L. M., Chang, M. F., Ho, H. N., and Lee, F. J. S. 2004. Identification of a novel protein 3a from severe acute respiratory syndrome coronavirus. *FEBS. Lett.* **565,** 111–116.

Yuan, Q., Liao, Y., Torres, J., Tam, J. P., and Liu, D. X. 2006. Biochemical evidence for the presence of mixed membrane topologies of the severe acute respiratory syndrome coronavirus envelope protein expressed in mammalian cells. *FEBS. Lett.* **580,** 3192-3200.

Yuan, X., Li, J., Shan, Y., Yang, Z., Zhao, Z., Chen, B., Yao, Z., Dong, B., Wang, S.,

Chen, J., and Cong, Y. 2005a. Subcellular localization and membrane association of SARS-CoV 3a protein. *Virus Res.* **109**, 191-202.

Yuan, X., Shan, Y., Zhao, Z., Chen, J., and Cong, Y. 2005b. G0/G1 arrest and apoptosis induced by SARS-CoV 3b protein in transfected cells. *J. Virol.* **2,** 66.

Yuan, X., Yao, Z., Shan, Y., Chen, B., Yang, Z., Wu, J., Zhao, Z., Chen, J., and Cong, Y. 2005c. Nucleolar localization of non-structural protein 3b, a protein specifically encoded by the severe acute respiratory syndrome coronavirus. *Virus Res.* **114,** 70–79.

Yuan, X., Shan, Y., Yao, Z., Li, J., Zhao, Z., Chen, J., and Cong, Y. 2006a. Mitochondrial location of severe acute respiratory syndrome coronavirus 3b protein. *Mol. Cells.* **21,** 186-191.

Yuan, X., Wu, J., Shan, Y., Yao, Z., Dong, B., Chen, B., Zhao, Z., Wang, S., Chen, J., and Cong, Y. 2006b. SARS coronavirus 7a protein blocks cell cycle progression at G0/G1 phase via the cyclin D3/pRb pathway. *Virology*. **346,** 74-85.

Zeng, R., Yang, R. F., Shi, M. D., Jiang, M. R., Xie, Y. H., Ruan, H. Q., Jiang, X. S., Shi, L., Zhou, H., Zhang, L., Wu, X. D., Lin, Y., Ji, Y. Y., Xiong, L., Jin, Y., Dai, E. H., Wang, X. Y., Si, B. Y., Wang, J., Wang, H. X., Wang, C. E., Gan, Y. H., Li, Y. C., Cao, J. T., Zuo, J. P., Shan, S. F., Xie, E., Chen, S. H., Jiang, Z. Q., Zhang, X., Wang, Y., Pei, G., Sun, B., and Wu, J. R., 2004. Characterization of the 3a protein of SARS-associated coronavirus in infected Vero E6 cells and SARS patients. *J. Mol. Biol.* **341,** 271–279.

Zhang, J., Pekosz, A., and Lamb, R. A. 2000. Influenza virus assembly and lipid raft microdomains: a role for the cytoplasmic tails of the spike glycoproteins. *J. Virol.* **74,** 4634-4644.

Zhu, R. N., Qian, Y., Zhao, L. Q., Deng, J., Wang, F., and Liao, B. 2006. Human coronavirus-NL63 was detected in specimens from children with acute respiratory infection in Beijing. *China Zhonghua Er Ke Za Zhi*. **44,** 202-205.

Ziebuhr, J. 2004. Molecular biology of severe acute respiratory syndrome coronavirus. *Curr. Opin. Microbiol.* **7,** 412–419.

Publications

1. Liu, D. X., Yuan, Q., and **Liao, Y.** 2007. Coronavirus envelope protein: A small membrane protein with multiple functions. *Cell Mol Life Sci.* May 29; [Epub ahead of print]

2. Yuan, Q., **Liao, Y.,** Torres, J., Tam, J. P., and Liu, D. X. 2006. Biochemical evidence for the presence of mixed membrane topologies of the severe acute respiratory syndrome coronavirus envelope protein expressed in mammalian cells. *FEBS. Letter.* 580(13): 3192-3200.

3. **Liao, Y.,** Yuan, Q., Torres, J., Tam, J. P., and Liu, D. X. 2006. Biochemical and functional characterization of the membrane association and membrane permeabilizing activity of the severe acute respiratory syndrome coronavirus envelope protein. *Virology.* 349:264-275.

4. **Liao, Y.,** Tam, J. P., and Liu, D. X. 2006. Viroporin activity of SARS-CoV E protein. *Adv. Exp. Med. Biol*. 581: 199-202.

5. Wang, X. X., **Liao, Y.,** Wong, S. M., and Liu, D. X. 2006. Identification and characterization of a unique ribosomal frameshifting signal in SARS-CoV ORF 3a. *Adv. Exp. Med. Biol*. 581: 89-92.

6. **Liao, Y.,** Lescar, J., Tam, P. J., and Liu, D. X. 2004. Expression of SARS-coronavirus envelope protein in *Escherichia coli* cells alters membrane permeability. *BBRC*. 325: 374-380.

Available online at www.sciencedirect.com
SCIENCE DIRECT®
Biochemical and Biophysical Research Communications 325 (2004) 374–380
BBRC
www.elsevier.com/locate/ybbrc

Expression of SARS-coronavirus envelope protein in *Escherichia coli* cells alters membrane permeability

Y. Liao[a], J. Lescar[a], J.P. Tam[a], D.X. Liu[a,b,*]

[a] *School of Biological Science, Nanyang Technological University, 61 Biopolis Drive, Proteos, Singapore 138673, Singapore*
[b] *Institute of Molecular and Cell Biology, 61 Biopolis Drive, Proteos, Singapore 138673, Singapore*

Received 27 September 2004

Abstract

To promote viral entry, replication, release, and spread to neighboring cells, many cytolytic animal viruses encode proteins responsible for modification of host cell membrane permeability and for formation of ion channels in host cell membranes during their life cycles. In this study, we show that the envelope (E) protein of severe acute respiratory syndrome-associated coronavirus can induce membrane permeability changes when expressed in *Escherichia coli*. E protein expressed in bacterial and mammalian cells under reducing conditions existed as monomers, but formed homodimer and homotrimer under non-reducing conditions. Site-directed mutagenesis studies revealed that two cysteine residues of the E protein were essential for oligomerization, leading to induction of membrane permeability. This is the first report demonstrating that a coronavirus-encoded protein could modify membrane permeability in *E. coli* cells.

Keywords: Severe acute respiratory syndrome coronavirus; Envelope protein; Membrane permeability; *Escherichia coli*; E protein; Oligomerization; Viroporin

A novel coronavirus was identified as the causative agent of the recent epidemic of severe acute respiratory syndrome (SARS) [18]. Similar to other coronaviruses, SARS coronavirus (SARS-CoV) is an enveloped virus with a single strand, positive-sense RNA genome of 29.7 kb in length. Upon virus entry into cells, a 3′-coterminal nested set of 9 mRNAs is produced [20]. The genome-length mRNA, mRNA1, expresses two overlapping replicase proteins in the form of polyproteins 1a and 1a/b. The polyproteins are subsequently processed into at least 16 putative nonstructural proteins (NSP1–NSP16) by virus-encoded proteinases [20]. The mature proteins comprise proteinases, RNA-dependent RNA polymerase, and helicase, involved in the genomic and subgenomic RNA synthesis. The four structural proteins, arranged in the order 5′-S-E-M-N-3′, are encoded by subgenomic mRNA 2, 4, 5, and 9, respectively. In addition, eight putative nonstructural proteins, 3a, 3b, 6, 7a, 7b, 8a, 8b, and 9b, are encoded by mRNA3, 6, 7, 8, and 9, respectively [20]. They are unique proteins of SARS-CoV and very little is known about the functions of these nonstructural proteins [18,20].

Coronavirus infection of cultured cells causes typical cytopathic effects (CPEs), including rounding-up and fusion of the infected cells, detachment of cells from the culture dishes, cell lysis, and death [13]. Among them, formation of giant syncytial cells is the hallmark of early CPE in cells infected with most coronaviruses. The prominent CPE in cells infected with SARS-CoV, however, is rounding up of the infected cells, cell detachment, and lysis [9]. Typically, two types of membrane active proteins are able to modify membrane

* Corresponding author. Fax: +65 67791117.
E-mail address: dxliu@imcb.a-star.edu.sg (D.X. Liu).

0006-291X/$ - see front matter © 2004 Elsevier Inc. All rights reserved.
doi:10.1016/j.bbrc.2004.10.050

permeability, leading to lysis of virus-infected cells [4,7]. The first type of these membrane active proteins is the viral proteins with fusogenic activity. One example of such proteins is the hepatitis C virus (HCV) E1 protein [5]. The second type is a group of small, hydrophobic proteins termed viroporins [4,7].

Viroporins are small, highly hydrophobic viral proteins that could interact with cellular membranes and modify membrane permeability to ions or other small molecules. In this manner, viroporins disorganize the membrane, cause cell lysis, and facilitate the release of viral progeny. This group of viral proteins is usually expressed at late stages of the infection cycles, forming hydrophilic pores in the plasma membrane and inducing a general increase in permeability to ions and small molecules, but not to macromolecules [4,7]. Viroporins have been found in many viruses, such as HCV p7 protein [8,15], human immunodeficiency virus type 1 (HIV-1) Vpu [6], influenza A virus M2 [16], hepatitis A virus 2B [10], Semliki Forest virus 6K [19], picornavirus 2B [1,2,11], and avian reovirus p10 protein [3].

In this study, we aimed to identify and characterize SARS-CoV proteins that may induce membrane permeability upon expression in bacterial cells. Among five proteins tested, the E protein can obviously enhance membrane permeability to *o*-nitrophenyl-β-D-galactopyranoside (ONPG), a β-galactosidase substrate, and hygromycin B (HB), an antibiotic which can inhibit protein synthesis. Analysis of the E protein expressed in bacterial and mammalian cells demonstrated that the protein may form homodimer and homotrimer, and site-directed mutagenesis studies revealed that two cysteine residues of the E protein located at amino acid positions 40 and 44 are essential for the formation of oligomers and for induction of membrane permeability in *Escherichia coli* cells. These results together with the predicted structural similarity with known membrane-permeable proteins of other viruses suggest that the E protein might be a putative viroporin.

Experimental procedures

Transient expression of SARS-CoV sequence in mammalian cells. HeLa cells were grown at 37 °C in 5% CO_2 and maintained in Glasgow's modified Eagle's medium supplemented with 10% fetal calf serum.

SARS-CoV sequences were placed under the control of a T7 promoter and transiently expressed in mammalian cells using a vaccinia virus-T7 expression system. Briefly, 60–80% confluent monolayers of HeLa cells grown on 35-mm dishes (Falcon) were infected with 10 plaque-forming units/cell of a recombinant vaccinia virus (vTF7-3) that expresses T7 RNA polymerase. Two hours later, cells were transfected with 5 μg of plasmid DNA mixed with transfection reagent (DOTAP) according to the instructions of the manufacturer (Roche). The transfection mixture was replaced with fresh culture medium 6 h post-transfection. Cells were harvested and stored at −80 °C.

Expression of proteins in E. coli. Plasmids were transformed into *E. coli* strain BL21 (DE3). A single colony was grown in LB medium overnight and then diluted 100-fold in LB medium or M9 medium supplemented with 0.2% glucose. When the absorbance of the cultures reached 0.6 at 600 nm, 1 mM IPTG was added to the medium to induce protein synthesis.

At indicated times post-induction, the cell density of bacterial cultures was determined by measuring the light scattering at 600 nm.

Western blot analysis. Total protein from bacterial or HeLa cells was lysed with 2× SDS loading buffer (with or without 200 mM DTT) plus 10 mM of iodoacetamide and subjected to SDS–PAGE. Proteins were transferred to PVDF membrane (Stratagene) and blocked overnight at 4 °C in blocking buffer (5% fat free milk powder in TBST buffer (20 mM Tris–HCl (pH 7.4), 150 mM NaCl, and 0.1% Tween 20). The membrane was incubated with a 1:1000 diluted primary antibody in blocking buffer for 1 h at room temperature. After washing three times with TBST, the membrane was incubated with 1:2000 diluted anti-mouse IgG conjugated with horseradish peroxidase (DAKO) in blocking buffer for 1 h at room temperature. After washing for three times with TBST, the polypeptides were detected with a chemiluminescence detection kit (ECL, Amersham Biosciences) according to the instructions of the manufacturer.

β-Galactosidase and hygromycin B assays. To measure the entry of ONPG into bacterial cells, 1 ml of bacterial cultures was removed at indicated times post-induction. After centrifugation, cells were resuspended in 1 ml of fresh M9 medium containing 2 mM ONPG, a β-galactosidase substrate. Cells were incubated for 10 min at 30 °C, and the reaction was stopped by addition of 0.4 ml of 1 M sodium carbonate. Samples were centrifuged, and the absorbance at 420 nm was measured to estimate the cleavage of ONPG.

To detect the entry of HB into bacterial cells, 1 mM of HB was added to the medium 50 min post-induction. After incubation for 30 min, 1 μCi of [^{35}S]methionine per ml was added to the medium and incubated at 37 °C for 15 min. The bacterial cells were then harvested and subjected to SDS–PAGE. The proteins were detected by autoradiography.

Polymerase chain reaction and site-directed mutagenesis. Amplification of the respective template DNAs with appropriate primers was performed with pfu DNA polymerase (Strategene) under the standard buffer conditions with 2 mM $MgCl_2$. The PCR conditions were 35 cycles of 94 °C for 45 s, 50–58 °C for 45 s, and 72 °C for 45 s to 2 min. The annealing temperature and extension time were subjected to adjustments according to the melting temperatures of the primers used and the lengths of the PCR fragments synthesized. Site-directed mutagenesis was carried out with two rounds of PCR and two pairs of primers.

Construction of plasmids. Plasmids pET24-E, pET24-3a, pET24-3b, pET24-6, pET24-7a, and pET24-HCVE1 were constructed by cloning an *Nde*I/*Xho*I-digested PCR fragment into *Nde*I/*Xho*I-digested pET24a vector. All the constructs have a His tag fused to the 3′ end of the genes. The two primers for SARS E protein are: 5′-CGGGATA TCCCATATGTACTCATTCGTTTCGGAA-3′ and 5′-CGGAATT CTTACTCGAGGACCAGAAGATCAGGAACTCC-3′. The two primers for SARS 3a protein are: 5′-CGGGATATCCCATATGGA TTTGTTTATGAGATTT-3′ and 5′-CGGAATTCTTACTCGAGC AAAGGC-ACGCTAGTAGTTCGT-3′. The two primers for SARS 3b protein are: 5′-CGGGATATCCCATATGATGCCAACTACTT TGTTT-3′ and 5′-CGGAATTCTTACTCGAGACGTACCTGTTTC TTCCGAA-A-3′. The two primers for SARS 6 protein are: 5′-CGGGATATCCCATATGTTTCATCTTGTTGACTTC-3′ and 5′-CGGAATTCTTACTCGAGTGGATAATCTAACTCCATAGG-3′. The two primers for SARS 7a protein are: 5′-CGGGATATCCCAT ATGAAAATTATTCTCTTCCTG-3′ and 5′-CGGAATTCTTACT CGAGTTCTGTCTTTCTCTTAATGGT-3′. The two primers for HCV E1 protein are: 5′-CGGGATATCCCATATGTACCAAGTGC GCAATTCCTCG-3′ and 5′-CCGGAATTCTTAGCGGCCGCCGC GTCGACGCCGGCAAATAG-3′.

Modification of membrane permeability by the expression of E protein

To test if the observed inhibition of bacterial growth by the expression of E and 7a proteins is caused by the modification of membrane permeability, HB, an antibiotic which can inhibit host cell protein synthesis but is normally impermeable to cells within a short period of time, was added to the culture medium after induction of protein expression with IPTG. When the cell membrane permeability is altered, it can translocate into cells to block cellular protein translation. Cells were metabolically labeled with [^{35}S]methionine for 15 min after addition of HB. Expression of SARS-CoV E protein allows the entry of HB to cells, as host protein synthesis was completely blocked (Fig. 2A, lanes 1 and 2). Similar inhibitory effect on host protein synthesis was observed in bacterial cells expressing the positive control protein, HCV E1 protein (Fig. 2A, lanes 5 and 6). No obvious effect on membrane permeability was observed in cells expressing 7a protein (Fig. 2A, lanes 3 and 4).

To further confirm the observation that expression of SARS-CoV E protein can induce changes in membrane permeability, entry of ONPG into bacterial cells was analyzed. ONPG, a substrate of β-galactosidase, is normally excluded by the membrane of intact cells. Entry of ONPG into bacterial cells was easily monitored by measuring its conversion to a colored compound by the β-galactosidase activity present in bacterial cells. As shown in Fig. 2B, induction of the expression of E protein caused a clear increase in the entry of ONPG into cells. These results confirm that expression of SARS-CoV E protein could increase membrane permeability in bacterial cells.

Oligomerization of E protein

We next tested if E protein could form oligomers by analysis of the E protein expressed in bacteria and mammalian cells on both reducing and non-reducing SDS–PAGE gels. After induction with IPTG, the bacterial cells were harvested and lysed with the protein loading buffer plus 10 mM of iodoacetamide to irreversibly block the free cysteinyl thiols to form disulfide bonds. Under such conditions, electrophoresis of the bacterially expressed E protein on reducing SDS–PAGE gel showed the detection of a 9.3 kDa band, representing the monomer of the E protein (Fig. 3, lane 2). In addition to the 9.3-kDa protein band, analysis of the same sample on non-reducing SDS–PAGE gel showed the detection of a protein band migrating at the position of 27 kDa (Fig. 3, lane 1), representing a putative homotrimer of the E protein.

The E protein was then expressed in HeLa cells. To detect the protein expression, an 11-amino-acid Flag tag was fused to the N-terminus of the E protein. Analysis of the E protein expressed in HeLa cell on reducing SDS–PAGE gel showed the detection of the 9.3-kDa monomer (Fig. 3, lane 4). Both the 9.3-kDa monomer and the 27-kDa trimer were observed under non-reducing conditions (Fig. 3, lane 3).

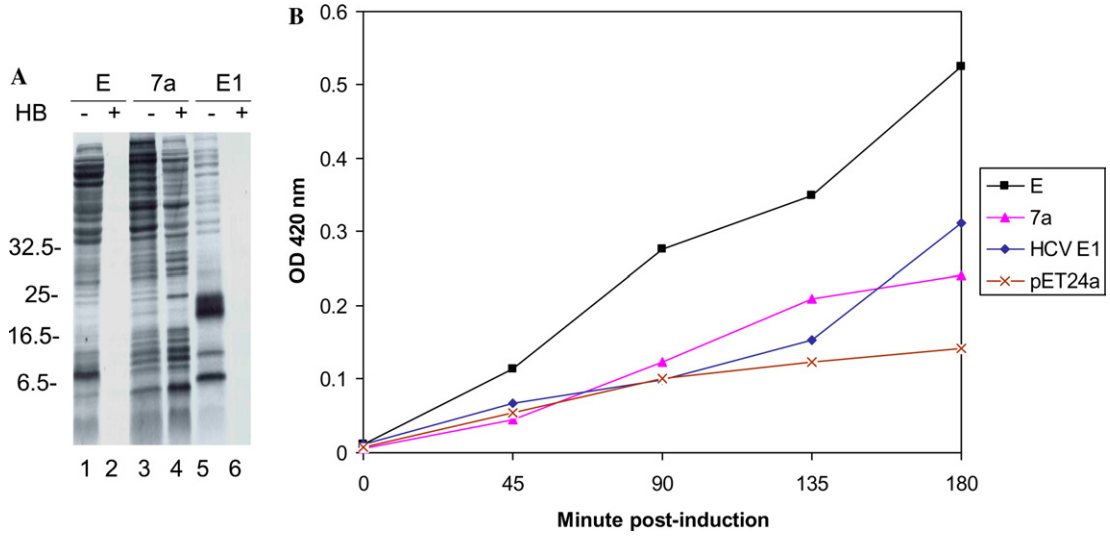

Fig. 2. Modification of membrane permeability by SARS-CoV E protein. (A) Entry of HB into bacterial cells. BL21 (DE3) cells transformed with pET24-E, pET24-7a, and pET24-HCVE1 were induced with 1 mM IPTG. At 1 h post induction, 2 mM HB was added. After incubation for 15 min, proteins were metabolically labeled with [^{35}S]methionine for 15 min. Cell extracts were analyzed by SDS–15% PAGE. Cells carrying pET24-HCVE1 were used as positive control. Numbers on the left indicate molecular masses in kiloDaltons. (B) Entry of ONPG into bacterial cells. BL21 (DE3) cells carrying pET24-E, pET24-7a, pET24-HCVE1, and pET24a were induced with 1 mM IPTG. Two millimolar ONPG was added at the indicated times and incubated at 30 °C for 10 min. The β-galactosidase activity was determined by measuring the absorbance at 420 nm. Cells carrying pET24-HCVE1 were used as positive control and cells carrying pET24a were used as negative control.

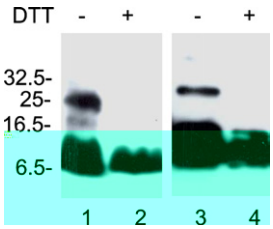

Fig. 3. Oligomerization of SARS-CoV E protein. The His-tagged E protein expressed in bacteria (lanes 1 and 2) and the flag-tagged E protein expressed in HeLa cells were separated on SDS–15% polyacrylamide gels under reducing (lanes 2 and 4) and non-reducing (lanes 1 and 3) conditions. Polypeptides were transferred to PVDF membrane and probed with anti-His (lanes 1 and 2) and anti-Flag (lanes 3 and 4) monoclonal antibodies, respectively. After incubation with horseradish peroxidase-conjugated anti-mouse IgG, the E protein was detected by a chemiluminescence detection kit. Numbers on the left indicate molecular masses in kiloDaltons.

Occasionally, a protein band migrating between the 9.3-kDa monomer and the 27-kDa trimer could be detected when the E protein expressed in both bacterial and mammalian cells was analyzed under non-reducing conditions (Fig. 3, lanes 1 and 3; and see Fig. 4B). It may represent dimerization of the E protein. These results suggest that the E protein may form homo-dimers and trimers in both bacterial and mammalian cells.

The essential roles of two cysteine residues of E protein in its modification of membrane permeability and oligomerization in E. coli cells

Examination of the amino acid sequence of E protein showed that the protein contains three cysteine residues at amino acid positions 40 (C1), 43 (C2), and 44 (C3), respectively. To analyze the involvement of these cysteine residues in the oligomerization of E protein, site-directed mutagenesis of these cysteine residues to alanine either individually or in combination of two or three was made to generate five mutants (M1–M5). Mutant M1 contains mutation at the C1 position, M2 at C2, and M3 at C3. M4 contains mutations at both the C1 and C2 positions, and M5 contains mutations at all three positions. These mutants were then expressed in *E. coli* BL21 (DE3). As can be seen in Fig. 4A, expression of wild type E protein and mutant M2 showed obvious induction of membrane permeability, as significant inhibition of protein synthesis by HB was observed (lanes 1 and 2; and lanes 5 and 6). Expression of mutants M1, M3, M4, and M5 showed no obvious increase of membrane permeability to HB (Fig. 4A, lanes 3, 4, and 7–12), indicating that these mutations may abolish the function of E protein in its induction of membrane permeability in bacterial cells. These results demonstrate that C1 and C3 residues are crucial for the function of E protein.

Analysis of the expression of wild type and mutant E protein was then carried out to see if the two cysteine

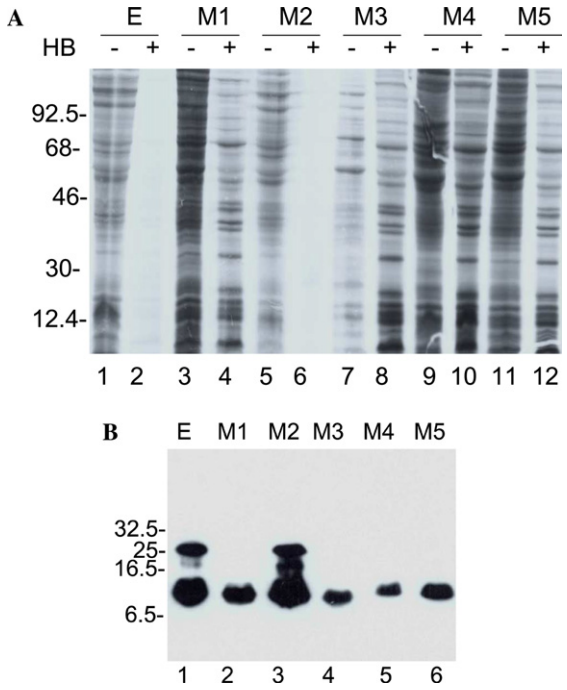

Fig. 4. Mutational analysis of the role of three cysteine residues of E protein in its modification of membrane permeability and oligomerization. (A) Entry of HB into bacterial cells expressing wild type and mutant E proteins. BL21 (DE3) cells transformed with pET24-E, pET24-M1, pET24-M2, pET24-M3, pET24-M4, and pET24-M5 were induced with 1 mM IPTG. At 1 h post-induction, 2 mM HB was added. After incubation for 15 min, proteins were metabolically labeled with [^{35}S]methionine for 15 min. Cell extracts were analyzed by SDS–15% polyacrylamide gel. Numbers on the left indicate molecular mass in kiloDaltons. (B) Oligomerization of wild type and mutant E protein. The His-tagged wild type and mutant E proteins expressed in BL21 (DE3) were separated on SDS–15% polyacrylamide gels under non-reducing conditions. Polypeptides were transferred to PVDF membrane and probed with anti-His monoclonal antibody. After incubation with horseradish peroxidase-conjugated anti-mouse IgG, the E protein was detected by a chemiluminescence detection kit. Numbers on the left indicate molecular masses in kiloDaltons.

residues are involved in the formation of the oligomers. As shown in Fig. 4B, both the 9.3-kDa monomer and the 27-kDa homotrimer were detected in bacterial cells expressing wild type E protein and M2 under non-reducing conditions (lanes 1 and 3). Only the 9.3-kDa monomer was detected in bacterial cells expressing M1, M3, M4, and M5 under the same non-reducing conditions (Fig. 4B, lanes 2, 4, 5, and 6). As mentioned, a protein band of approximately 18 kDa migrating between the 9.3-kDa monomer and the 27-kDa homotrimer was detected in cells expressing both wild type E protein and M2 (Fig. 4B, lanes 1 and 3). These results confirm that the two cysteine residues are involved in oligomerization of the E protein by formation of interchain disulfide bonds.

Cytolytic animal viruses encode small hydrophobic integral membrane proteins to modify host cell membrane permeability during their infection cycles. These

proteins contain at least one transmembrane domain that interacts with and expands the lipid bilayer, and could form hydrophilic pores in the membrane by oligomerization, with hydrophilic residues presumably facing the aqueous lumen of the pore [4,7]. The hydrophilic channels would allow low molecular weight hydrophilic molecules across the membrane barrier, leading to the disruption of membrane potential, collapse of ionic gradients, and release of essential compounds from the cell. Alterations in ion concentration, such as enhancing the intracellular concentration of sodium ions, in the cytoplasm of virus-infected cells at the beginning of viral protein synthesis would favor virus replication. This would promote translation of viral versus cellular mRNAs, as translation of mRNAs from many cytolytic animal viruses is fairly resistant to high sodium concentrations. In contrast, high sodium concentrations are inhibitory to the translation of most cellular mRNAs [4,7]. Progressive membrane damage during viral replication cycles would also result in cell lysis, promote virus release, and facilitate virus spread to surrounding cells. Disruption of the function of viroporins would therefore abrogate viral infectivity, rendering this group of viral proteins suitable targets for the development of antiviral drugs.

Is the SARS-CoV E protein a viroporin? Data presented in this study demonstrated that expression of E protein in bacteria inhibits bacterial growth, increase the entry of ONPG and HB into bacterial cells. Furthermore, the protein could form homo-dimers and trimers by interchain disulfide bonds in both bacterial and mammalian cells. These observations support that SARS-CoV E protein might function as a viroporin. Further studies are required to address if similar modification of membrane permeability can be observed in other systems, including yeast and mammalian cells.

Coronavirus E protein is a minor virion component [14]. It plays an essential role in virion assembly and morphogenesis [12]. Computer-aided programs predict that SARS-CoV E protein may contain a putative α-helical transmembrane domain from amino acids 11–33. Similar to other viroporins, SARS-CoV E protein also contains some hydrophilic residues in the helical region. These functional and structural features resemble the influenza virus M2 protein, the best characterized ion-channel forming viroporin with four α-helices and a tetrameric quaternary structure [17]. If the SARS-CoV E protein were proved to be able to form ion channels in cellular membranes, it would open a way to design anti-SARS therapeutic approaches.

Is induction of membrane permeability a general feature of coronavirus E protein? Although the E proteins from different coronaviruses share a low homology in their primary amino acid sequences, the general structural features consisting of an α-helical transmembrane domain are conserved. It suggests that the E protein may play very similar roles, including induction of host cell membrane permeability changes critical for the replication of coronaviruses. Comparative studies of E proteins from different coronavirus would help delineate the molecular and structural basis of their modification of membrane permeability and potential pore-forming activities.

Acknowledgments

This work was supported by grants from Nanyang Technological University (SUG15/02) and from the Biomedical Research Council (BMRC 03/1/22/17/220), Agency for Science Technology and Research, Singapore.

References

[1] A. Agirre, A. Barco, L. Carrasco, J.B. Nieva, Viroporin-mediated membrane permeabilization, J. Biol. Chem. 277 (2002) 40434–40441.
[2] R. Aldabe, A. Barco, L. Corrasco, Membrane permeabilization by poliovirus proteins 2B and 2BC, J. Biol. Chem. 271 (1996) 23134–23137.
[3] G. Bodelon, L. Labrada, J. Martinez-Costas, J. Benavente, Modification of late membrane permeability in avian reovirus-infected cells, J. Biol. Chem. 227 (2002) 17789–17796.
[4] L. Carraso, L. Perez, A. Irurzun, J. Lama, F. Martinez-Abarca, P. Rodriguez, R. Guinea, J.L. Castrillo, M.A. Sanz, M.J. Ayala, Modification of membrane permeability by animal viruses, Adv. Virus Res. 45 (1995) 61–112.
[5] A.R. Ciccaglione, C. Marcantonio, A. Costantino, M. Equestre, A. Geraci, M. Rapicetta, Hepatitis C virus E1 protein induces modification of membrane permeability in *E. coli* cells, Virology 250 (1998) 1–8.
[6] M.E. Gonzalez, L. Carrasco, The human immunodeficiency virus type 1 vpu protein enhances membrane permeability, Biochemistry 37 (1998) 13710–13719.
[7] M.E. Gonzalez, L. Carrasco, Viroporins, FEBS Lett. 552 (2003) 28–34.
[8] S.D.C. Griffin, L.P. Beales, D.S. Clarke, O. Worsfold, S.D. Evans, J. Jaeger, M.P.G. Harris, D.J. Rowlands, The p7 protein of hepatitis C virus forms an ion channel that is blocked by the antiviral drug, Amantadine, FEBS 535 (2003) 34–38.
[9] T.G. Ksiazek, D. Erdman, C.S. Goldsmith, S.R. Zaki, T. Peret, S. Emery, S. Tong, C. Urbani, J.A. Comer, W. Lim, P.E. Rollin, S.F. Dowell, A.E. Ling, C.D. Humphrey, W.J. Shieh, J. Guarner, C.D. Paddock, P. Rota, B. Fields, J. DeRisi, J.Y. Yang, N. Cox, J.M. Hughes, J.W. LeDuc, W.J. Bellini, L.J. Anderson and SARS Working Group, A novel coronavirus associated with severe acute respiratory syndrome, N. Engl. J. Med. 348 (2003) 1953–1966.
[10] M. Jecht, C. Probst, V. Gauss-Muller, Membrane permeability induced by Hepatitis A virus proteins 2B and 2BC and proteolytic processing of HAV 2BC, Virology 252 (1998) 218–227.
[11] J. Lama, L. Carrasco, Expression of poliovirus nonstructural proteins in *Escherichia coli* cells, J. Biol. Chem. 267 (1992) 15932–15937.
[12] K.P. Lim, D.X. Liu, The missing link in coronavirus assembly, J. Biol. Chem. 276 (2001) 17515–17523.
[13] C. Liu, H.Y. Xu, D.X. Liu, Induction of caspase-dependent apoptosis in cultured cells by the avian coronavirus infectious bronchitis virus, J. Virol. 75 (2001) 6402–6409.

[14] D.X. Liu, S.C. Inglis, Association of the infectious bronchitis virus3c protein with the virion envelope, Virology 185 (1991) 911–917.
[15] D. Pavlovic, D.C.A. Neville, O. Argaud, B. Blumberg, R.A. Dwek, W.B. Fischer, N. Zitzmann, The hepatitis C virus forms an ion channel that is inhibited by long-alkyl-chain iminosugar derivatives, Proc. Natl. Acad. Sci. USA 100 (2003) 6104–6108.
[16] L.H. Pinto, L.J. Holsinger, R.A. Lamb, Influenza virus M2 protein has ion channel activity, Cell 59 (1992) 517–528.
[17] L.H. Pinto, R.A. Lamb, viral ion channels as models for ion transport and targets for antiviral drug action, FEBS Lett. 560 (2004) 1–2.
[18] P.A. Rota, M.S. Oberste, S.S. Monroe, W.A. Nix, R. Campagnoli, J.P. Icenogle, S. Penaranda, B. Bankamp, K. Maher, M.-H. Chen, S. Tong, A. Tamin, L. Lowe, M. Frace, J.L. DeRisi, Q. Chen, D. Wang, D.D. Erdman, T.C.T. Peret, C. Burns, T.G. Ksiazek, P.E. Rollin, A. Sanchez, S. Liffick, B. Holloway, J. Limor, K. McCaustland, M. Olsen-Rasmussen, R. Fouchier, S. Gunther, A.D.M.E. Osterhaus, C. Drosten, M.A. Pallansch, L.J. Anderson, W.J.. Bellini, Characterization of a novel coronavirus associated with severe acute respiratory syndrome, Science 300 (2003) 1394–1399.
[19] M.A. Sanz, L. Perez, L. Carrasco, Semliki forest virus 6K protein modifies membrane permeability after inducible expression in *Escherichia coli* cells, J. Biol. Chem. 269 (1994) 12106–12110.
[20] V. Thiel, K.A. Ivanov, A. Putics, T. Hertzig, B. Schelle, S. Bayer, B. Weißbrich, E.J. Snijder, H. Rabenau, H.W. Doerr, A.E. Gorbalenya, J. Ziebuhr, Mechanisms and enzymes involved in SARS coronavirus genome expression, J. Gen. Virol. (2003).

Available online at www.sciencedirect.com
SCIENCE DIRECT®
Virology 349 (2006) 364–275
VIROLOGY
www.elsevier.com/locate/yviro

Biochemical and functional characterization of the membrane association and membrane permeabilizing activity of the severe acute respiratory syndrome coronavirus envelope protein

Y. Liao [a], Q. Yuan [a], J. Torres [a], J.P. Tam [a], D.X. Liu [a,b,*]

[a] School of Biological Science, Nanyang Technological University, 60 Nanyang Drive, Singapore 637551, Singapore
[b] Institute of Molecular and Cell Biology, 61 Biopolis Drive, Proteos, Singapore 138673, Singapore

Received 1 November 2005; returned to author for revision 7 December 2005; accepted 21 January 2006
Available online 28 February 2006

Abstract

A diverse group of cytolytic animal viruses encodes small, hydrophobic proteins to modify host cell membrane permeability to ions and small molecules during their infection cycles. In this study, we show that expression of the SARS-CoV E protein in mammalian cells alters the membrane permeability of these cells. Immunofluorescent staining and cell fractionation studies demonstrate that this protein is an integral membrane protein. It is mainly localized to the ER and the Golgi apparatus. The protein can be translocated to the cell surface and is partially associated with lipid rafts. Further biochemical characterization of the protein reveals that it is posttranslationally modified by palmitoylation on all three cysteine residues. Systematic mutagenesis studies confirm that the membrane permeabilizing activity of the SARS-CoV E protein is associated with its transmembrane domain.

Keywords: SARS-CoV; E protein; Membrane association; Permeabilizing activity; Palmitoylation

Introduction

The causative agent of severe acute respiratory syndrome (SARS) was identified to be a novel coronavirus (SARS-CoV), an enveloped virus with a single strand, positive-sense RNA genome of 29.7 kb in length (Rota et al., 2003). In SARS-CoV-infected cells, a 3′-coterminal nested set of nine mRNA species, including the genome-length mRNA, mRNA 1, and eight subgenomic mRNAs (mRNA 2–mRNA 9), is produced (Thiel et al., 2003). Four structural proteins, spike (S), membrane (M), envelope (E), and nucleocapsid (N), arranged in the order 5′-S-E-M-N-3′, are encoded by subgenomic mRNA 2, 4, 5, and 9, respectively. In addition, 3a protein, a recently identified minor structural protein, is encoded by the first ORF of subgenomic mRNA3 (Ito et al., 2005; Yuan et al., 2005).

A group of small, highly hydrophobic viral proteins, termed viroporin, has been identified in diverse viral systems. These include the HCV p7 protein (Pavlovic et al., 2003), human immunodeficiency virus type 1(HIV-1) Vpu (Gonzalez and Carrasco, 1998; Schubert et al., 1996), influenza A virus M2 (Pinto et al., 1992), hepatitis A virus 2B (Jecht et al., 1998), semliki forest virus 6K (Sanz et al., 1994), picornavirus 2B (Agirre et al., 2002; Aldabe et al., 1996), chlorella virus PBCV-1 Kcv (Mehmel et al., 2003), and avian reovirus p10 protein (Bodelon et al., 2002). These proteins contain at least one transmembrane domain that interacts with and expands the lipid bilayer. The transmembrane domain could form hydrophilic pores in the membrane by oligomerization (Carrasco et al., 1995; Gonzalez and Carrasco, 2003). The hydrophilic channels would allow low molecular weight hydrophilic molecules to across the membrane barrier, leading to the disruption of membrane potential, collapse of ionic gradients, and release of essential compounds from the cell. Alterations in ion concentration would promote translation of viral versus cellular mRNAs, as translation of mRNAs from many cytolytic animal viruses is fairly resistant to high sodium concentrations

* Corresponding author. Institute of Molecular and Cell Biology, 61 Biopolis Drive, Proteos, Singapore 138673, Singapore.
E-mail address: dxliu@imcb.a-star.edu.sg (D.X. Liu).

0042-6822/$ - see front matter © 2006 Elsevier Inc. All rights reserved.
doi:10.1016/j.virol.2006.01.028

(Carrasco et al., 1995; Gonzalez and Carrasco, 2003). Progressive membrane damage during viral replication cycles would also result in cell lysis, promote viral budding and release, and facilitate virus spread to surrounding cells. Therefore, disruption of the function of viroporins could abrogate viral infectivity, rendering these proteins as suitable targets for the development of antiviral drugs.

Coronavirus E protein is a minor structural protein (Liu and Inglis, 1991; Yu et al., 1994). It plays essential roles in virion assembly, budding, morphogenesis, and regulation of other cellular functions (Corse and Machamer, 2001, 2002; Fischer et al., 1998; Lim and Liu, 2001). In a recent study, we demonstrated that the SARS-CoV E protein could obviously enhance the membrane permeability of bacterial cells to *o*-nitrophenyl-β-D-galactopyranoside and hygromycin B, suggesting that the protein may function as a viroporin (Liao et al., 2004). Similar observations were recently reported on mouse hepatitis virus E protein (Madan et al., 2005). In a separate study, the transmembrane domain of the protein was indeed shown to be able to form a cation channel on artificial membrane (Wilson et al., 2004). Molecular simulation and in vitro oligomerization studies indicate that this domain could form stable pentamers (Torres et al., 2005). In this study, we show that the expression of SARS-CoV E protein alters membrane permeability of mammalian cells. This membrane permeabilizing activity is associated with the transmembrane domain. Unlike in bacterial cells, mutations of the three cysteine residues alone do not obviously affect the membrane permeabilizing activity of the protein. Further biochemical characterization of the E protein shows that it is an integral membrane protein, and is posttranslationally modified by palmitoylation on all three cysteine residues.

Results

Alteration of membrane permeability to hygromycin B upon expression of SARS-CoV E protein in HeLa Cells

To test if the SARS-CoV E protein could affect the membrane permeability of mammalian cells, the Flag-tagged E protein was expressed in HeLa cells. At 12 h posttransfection, cells were treated with two different concentrations of hygromycin B for 30 min, and then radiolabeled with [^{35}S] methionine–cysteine for 3 h. Cell extracts were prepared and the expression of E protein was detected by immunoprecipitation with anti-Flag antibody under mild washing conditions. As shown in Fig. 1, extracts prepared from cells without treatment with hygromycin B showed the detection of the E protein and some other cellular proteins. In cells treated with 1 and 2 mM of hygromycin B, the expression of the E protein was reduced to 6 and 2%, respectively (Fig. 1). However, in cells transfected with the SARS-CoV N protein, a similar amount of the N protein was detected in cells both treated and untreated with hygromycin B (Fig. 1). The expression of the N protein was marginally reduced to 90 and 85%, respectively (Fig. 1). These results confirm that expression of E protein in mammalian cells alters the membrane permeability of these cells to hygromycin B.

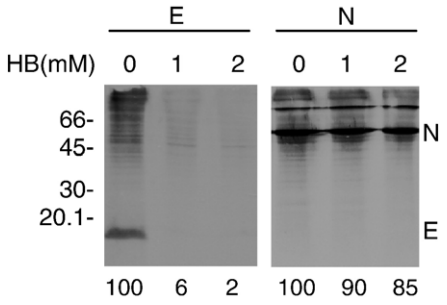

Fig. 1. Modification of the membrane permeability of mammalian cells by SARS-CoV E protein. HeLa cells expressing the Flag-tagged E protein were treated with 0, 1, and 2 mM of hygromycin B for 30 min at 12 h posttransfection (lanes 1, 2, and 3), and radiolabeled with [^{35}S] methionine–cysteine for 3 h. Cell lysates were prepared and the expression of E protein was detected by immunoprecipitation with anti-Flag antibody under mild washing conditions. Polypeptides were separated by SDS-PAGE and visualized by autoradiography. Cells expressing SARS-CoV N proteins were included as negative control (lanes 4, 5, and 6). The expression of N protein was detected by immunoprecipitation with polyclonal anti-N antibodies. The percentages of E and N proteins detected in the presence of hygromycin B were determined by densitometry and indicated at the bottom. Numbers on the left indicate molecular masses in kilodaltons.

Effects of mutations of the three cysteine residues on the membrane permeabilizing activity of the SARS-CoV E protein

SARS-CoV E protein contains three cysteine residues at amino acid positions 40, 43, and 44, respectively. These residues are located 3–7 amino acids downstream of the C-terminal residue of the transmembrane domain (Fig. 2). The first and third cysteine residues, at amino acid positions 40 and 44, respectively, were previously shown to play certain roles in oligomerization of the E protein (Liao et al., 2004). They may also be involved in the E protein-induced alteration of membrane permeability in bacterial cells (Liao et al., 2004). To systematically test the effects of these residues on the expression, posttranslational modification, folding, oligomerization, and the membrane-permeabilizing activities of E protein, seven mutants, C40-A, C43-A, C44-A, C40/44-A, C40/43-A, C43/44-A, and C40/43/44-A, with mutations of the three cysteine residues to alanine either individually or in combination of two or three, were made by site-directed mutagenesis (Fig. 2). Western blotting analysis of cells expressing wild type and most mutant constructs showed specific detection of three species migrating at the range of molecular masses from 14 to 18 kDa under reducing conditions and representing three isoforms of the E protein (Fig. 3a). These isoforms may be derived from posttranslational modification of the protein. The apparent molecular masses of these isoforms on SDS-PAGE are significantly larger than the calculated molecular mass of approximately 10 kDa for the Flag-tagged E protein.

In the membrane permeability assay shown in Fig. 3b, 0.5 and 1 mM of hygromycin B were used. The use of lower concentrations of hygromycin B is to ensure the detection of subtle changes on membrane permeability induced by the mutant constructs. Meanwhile, SARS-CoV N protein was cotransfected into HeLa cell together with wild type and mutant

```
                1         10        20        30        40        50        60        70
E               MYSFVSEETGTLIVNSVLLFLAFVVFLLVTLAILTALRLCAYCCNIVNVSLVKPTVYVYSRVKNLNSSEGVPDLLV
C40-A           ----------------------------------------A---------------------------------
C43-A           ----------------------------------------A---------------------------------
C44-A           ----------------------------------------A---------------------------------
C40/44-A        ----------------------------------------A---A-----------------------------
C40/43-A        ----------------------------------------A--A-----------------------------
C43/44-A        ----------------------------------------AA----------------------------------
C40/43/44-A     ----------------------------------------A--AA----------------------------------
Em1             ----------------EK-E-----------------------------------------------------------
Em2             ------------------------E-KE-----------------------------------------------------
Em3             ----------------EK-----E-KE-----------------------------------------------------
Em4             ----------------EKEKEKE--------------------------------------------------------
Em5             --------------E----------------------------------------------------------------
Em6             ----------------EKEKEKE--------------A--AA----------------------------------
```

Fig. 2. Amino acid sequences of wild type and mutant SARS-CoV E protein. The putative transmembrane domain is underlined, and the three cysteine residues are in bold. Also indicated are the amino acid substitutions in each mutant construct.

E proteins to aid assessment of the inhibitory effect of protein synthesis by hygromycin B. Expression of wild type and mutant E protein showed that similar levels of inhibition of protein synthesis by hygromycin B were obtained (Fig. 3b). When 0.5 and 1 mM of hygromycin B were added to the culture medium, wild type and mutant E constructs render similar levels of inhibition to the expression of both N and E proteins (Fig. 3b). These results suggest that, contrary to the previous results observed in bacterial cells, these cysteine residues do not render significant effects on the membrane permeabilizing activity of the E protein. The reason for this discrepancy is uncertain, but it may reflect differences in posttranslational modifications, membrane association, subcellular localization, and translocation of the E protein in prokaryotic and eukaryotic cells.

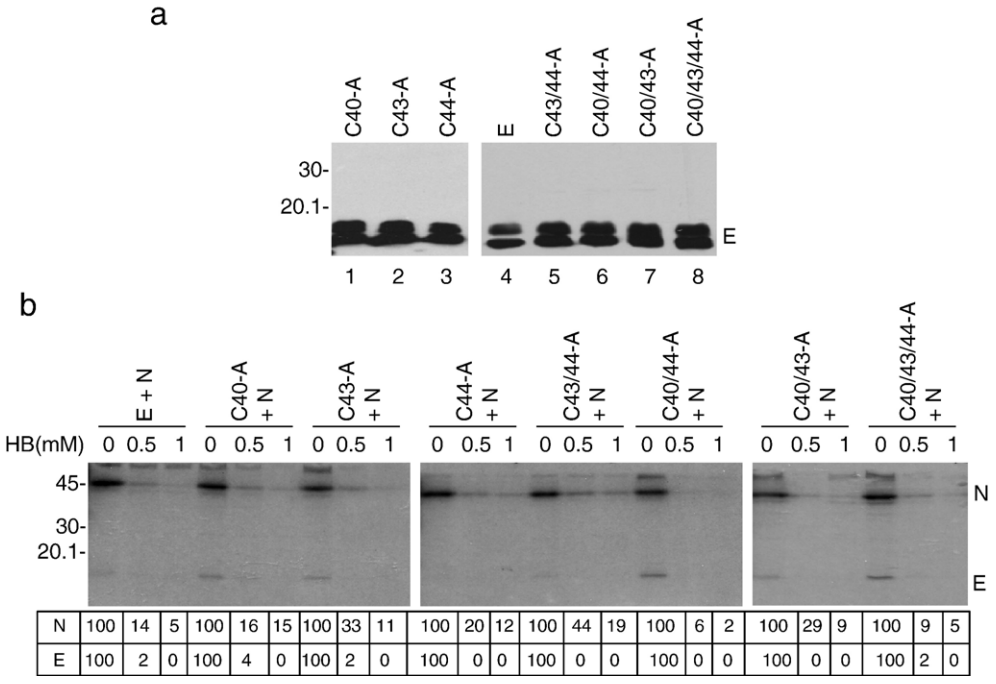

N	100	14	5	100	16	15	100	33	11	100	20	12	100	44	19	100	6	2	100	29	9	100	9	5
E	100	2	0	100	4	0	100	2	0	100	0	0	100	0	0	100	0	0	100	0	0	100	2	0

Fig. 3. Mutational analysis of the three cysteine residues of SARS-CoV E protein. (a) HeLa cells were transfected with the Flag-tagged wild type and seven mutant E constructs containing mutations of either a single (C40-A, C43-A, and C44-A), combination of two (C40/43-A, C40/44-A, and C43/44-A) or all three (C40/43/44-A) cysteine residues. Cell lysates were prepared at 24 h posttransfection, polypeptides were separated by SDS-PAGE and analyzed by Western blot using the anti-Flag antibody. Numbers on the left indicate molecular masses in kilodaltons. (b) Entry of hygromycin B into HeLa cells expressing wild type and mutant E proteins. HeLa cells expressing the Flag-tagged wild type E (lanes 1, 2, and 3) and seven cysteine to alanine mutation constructs (lanes 4–24) were treated with 0, 0.5, and 1 mM of hygromycin B for 30 min at 12 h posttransfection, and radiolabeled with [^{35}S] methionine–cysteine for 3 h. Cell lysates were prepared and the expression of E protein was detected by immunoprecipitation with anti-Flag antibody under mild washing conditions. SARS-CoV N protein was coexpressed with wild type and mutant E protein, and the expression of N protein was detected by immunoprecipitation with polyclonal anti-N antibodies. Polypeptides were separated by SDS-PAGE and visualized by autoradiography. The percentages of E and N proteins detected in the presence of hygromycin B were determined by densitometry and indicated at the bottom. Numbers on the left indicate molecular masses in kilodaltons.

Effects of mutations introduced into the transmembrane domain on the membrane permeabilizing activity of the SARS-CoV E protein

SARS-CoV E protein contains an unusually long putative transmembrane domain of 29 amino acid residues with a high leucine/isoleucine/valine content (55.17%) (Arbely et al., 2004). Recent molecular simulation and biochemical evidence showed that this domain may be involved in the formation of ion channel by oligomerization (Torres et al., 2005). Mutations of the putative transmembrane domain were therefore carried out to study its functions in membrane association and permeabilizing activity of the E protein. As shown in Fig. 2, four mutants, Em1, Em2, Em3, and Em4, were initially made by mutation of 3–7 leucine/valine residues to charged amino acid residues in the transmembrane domain. Two more mutants, Em5 and Em6, were subsequently made. Em5, which contains mutation of N15 to E, was constructed based on the molecular simulation studies showing that this residue may be essential for oligomerization of the protein (Fig. 2) (Torres et al., 2005). Em6 was made by combination of the Em4 and C40/43/44-A (Fig. 2). Expression of these mutants showed the detection of polypeptides with apparent molecular masses ranging from 10 to 18 kDa (Fig. 4a). Interestingly, mutations introduced into Em2, Em3, EM4, and Em6 significantly change the migration rate of the corresponding mutant E protein on SDS-PAGE. The apparent molecular mass of these mutants is approximately 10 kDa, which is consistent with the predicted molecular weight for the Flag-tagged E protein (Fig. 4a). The fact that substitutions of the hydrophobic amino acid residues in the transmembrane domain of the E protein with charged amino acids significantly alter the migrating properties of the E protein in SDS-PAGE may reflect the changes in overall conformation and membrane association of these mutants compared to wild type E protein.

In the hygromycin B permeability assays, cells transfected with Em1, Em2, and Em5 constructs showed a similar degree of inhibition on protein synthesis as in cells expressing wild type E protein (Fig 4b). In cells expressing Em3 and Em4, much less inhibition of protein synthesis by hygromycin B was observed compared to cells expressing wild type E protein (Fig. 4b). No obvious inhibition of protein synthesis was observed in cells expressing Em6 and N protein (Fig. 4b). These results confirm that the transmembrane domain is essential for the membrane permeabilizing activity of the protein, and further suggest that dramatic mutations of the transmembrane domain are required to disrupt this function. The combination of mutations in the transmembrane domain and the three cysteine residues abolishes the membrane permeabilizing activity of E protein, suggesting that these cysteine residues and may play certain roles in the membrane association and permeabilizing activity of the E protein.

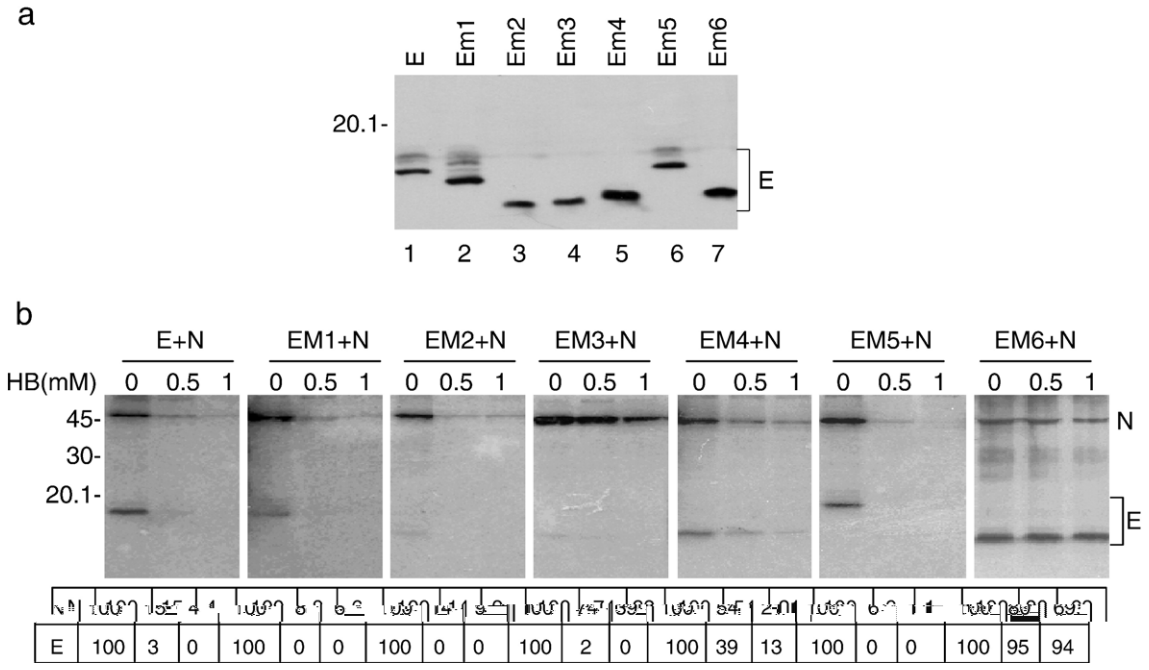

Fig. 4. Mutational analysis of the transmembrane domain of SARS-CoV E protein. (a) HeLa cells were transfected with the Flag-tagged wild type and six mutant constructs containing mutations in the transmembrane domain of the E protein. Cell lysates were prepared 24 h posttransfection, polypeptides were separated by SDS-PAGE and analyzed by Western blot using the anti-Flag antibody. Numbers on the left indicate molecular masses in kilodaltons. (b) Entry of hygromycin B into HeLa cells expressing wild type and mutant E proteins. HeLa cells expressing the Flag-tagged wild type E (lanes 1, 2, and 3) and six mutant E constructs (lanes 4–21), respectively, were treated with 0, 0.5, and 1 mM of hygromycin B for 30 min at 12 h posttransfection, and radiolabeled with [^{35}S] methionine–cysteine for 3 h. Cell lysates were prepared and the expression of E protein was detected by immunoprecipitation with anti-Flag antibody under mild washing conditions. SARS-CoV N protein was coexpressed with wild type and mutant E protein, and the expression of N protein was detected by immunoprecipitation with polyclonal anti-N antibodies. Polypeptides were separated by SDS-PAGE and visualized by autoradiography. The percentages of E and N proteins detected in the presence of hygromycin B were determined by densitometry and indicated at the bottom. Numbers on the left indicate molecular masses in kilodaltons.

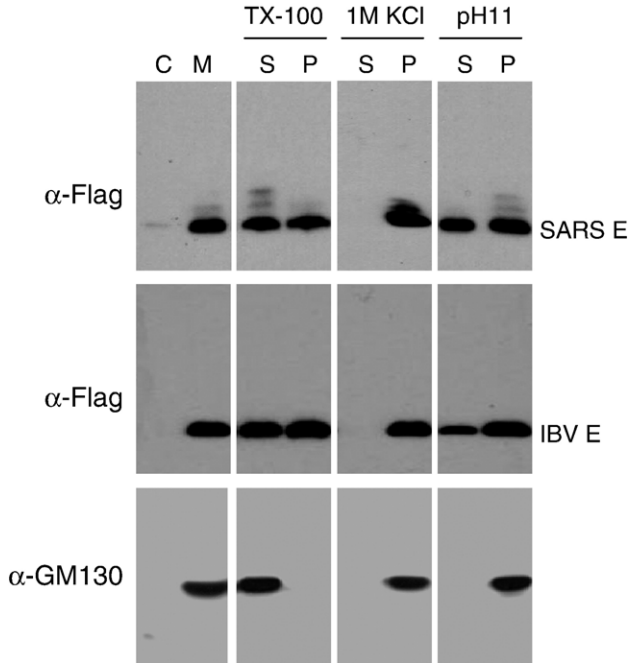

Fig. 5. Determination of SARS-CoV E protein as an integral membrane protein. HeLa cells expressing the Flag-tagged SARS-CoV and IBV E proteins, respectively, were harvested at 12 h posttransfection, broken by 20 stokes with a Dounce cell homogenizer, and fractionated into cytosol (C) and membrane (M) fractions after removal of cell debris and nuclei. The membrane fraction was treated with 1% Triton X-100, 100 mM Na_2CO_3 (pH 11), and 1 M KCl, respectively, and further fractionated into soluble (S) and pellet (P) fractions. Polypeptides were separated by SDS-PAGE and analyzed by Western blot using either anti-Flag antibody or anti-GM130 antibody (Abcam). Numbers on the left indicate molecular masses in kilodaltons.

Membrane association of SARS-CoV E protein

To characterize the membrane association property of the SARS-CoV E protein, HeLa cells expressing the Flag-tagged E protein were fractionated into membrane and cytosol fractions, and the presence of the E protein in each fraction was analyzed by Western blot. As shown in Fig. 5, the protein was almost exclusively located in the membrane fraction. Western blot analysis of the same fractions with anti-GM130 antibody (Abcam) showed the detection of an unknown host protein of approximately 60 kDa that is exclusively located in the membrane fraction (Fig. 5). Similarly, fractionation of HeLa cells expressing the Flag-tagged IBV E protein also showed exclusive detection of the protein in the membrane fraction (Fig. 5).

The membrane fraction was then treated with either 1% Triton X-100, 100 mM Na_2CO_3 pH 11 (high pH), or 1 M KCl (high salt), and centrifuged to separate the soluble contents (S) from the pellets (P). Treatment of the membrane fraction with 1 M KCl showed that both SARS-CoV and IBV E proteins were solely detected in the pellets (Fig. 5). Treatment of the same membrane pellets with 1% Triton X-100 and high pH led to the detection of the E proteins in both the supernatants and the pellets (Fig. 5). As an integral membrane protein control, anti-GM130 antibodies detected the protein exclusively in the supernatants after treatment of the membrane fraction with Triton X-100 (Fig. 5). In samples treated with both high pH and high salt, the protein was detected in the pellets only (Fig. 5), confirming that the procedures and conditions used to fractionate the cell lysates and to treat the membrane fractions are appropriate.

Oligomerization of SARS-CoV E protein

Oligomerization of viroporin is thought to be critical for the formation and expansion of the hydrophilic pore in the lipid bilayers. To determine the oligomerization status of the SARS-CoV E protein, the E protein with a His-tag at the C-terminus was expressed in insect cells using a baculovirus expression system and purified by Ni-NTA purification system. The purified E protein was concentrated and subjected to cross-linking with three different concentrations of glutaraldehyde, a short self-polymerizing reagent that reacts with lysine, tyrosine, histidine, and tryptophan. Cross-linking with glutaraldehyde showed the detection of dimer, trimer, tetramer, pentamer, and other higher-order oligomers/aggregates of the E protein under either non-reducing (Fig. 6, lanes 1–3) or reducing (Fig. 6, lanes 4–6) conditions. It was noted that more higher-order oligomers/aggregates were detected under non-reducing conditions when higher concentrations of the cross-linking reagent were used (Fig. 6, lanes 1–3). These results indicate that both interchain disulfide bond formation and hydrophobic interaction are contributing to the oligomerization of the E protein. More detailed characterization of the oligomerization status of the SARS-CoV E protein was hampered by the low expression efficiency of the protein in the system.

Palmitoylation of SARS-CoV E protein

The E protein from coronavirus MHV and IBV was previously shown to undergo modification by palmitoylation

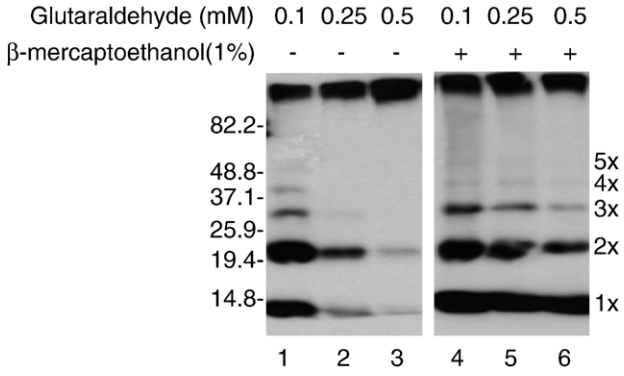

Fig. 6. Oligomerization of SARS-CoV E protein. The His-tagged E protein expressed in Sf9 insect cells was purified using Ni-NTA purification system (Qiagen), and incubated with three different concentrations of glutaraldehyde (0.1, 0.25, and 0.5 mM) for 1 h at room temperature. The reaction was quenched by adding 100 mM glycine. Polypeptides were separated on SDS-15% polyacrylamide gel in the presence or absence of 1% β-mercaptoethanol, and analyzed by Western blot with anti-His antibody. Different oligomers of the E protein are indicated on the right. Numbers on the left indicate molecular masses in kilodaltons.

(11, 43). To verify if SARS-CoV E protein is palmitoylated, two independent experiments were performed. First, treatment of the E protein with 1M hydroxylamine showed the reduced detection of the more slowly migrating isoforms (Fig. 7a, lanes 1 and 2). As a control, treatment of the IBV E protein with the same reagent abolished the detection of upper bands (Fig. 7a, lanes 3 and 4). Second, the three cysteine residues in combinations of two or all three were mutated to alanine (Fig. 2). Wild type and mutant E proteins were then expressed in HeLa cells and labeled with [^{3}H] palmitic acid or [^{35}S] methionine–cysteine. As shown in Fig. 7b, wild type and all mutant E proteins were efficiently labeled with [^{35}S] methionine–cysteine (Fig. 7b, upper panel). In cells labeled with [^{3}H] palmitate, wild type and the three mutants with mutations of different combinations of two cysteine residues (C40/44-A, C40/43-A and C43/44-A) were efficiently detected (Fig. 7b, lower panel, lanes 1–4). However, the construct with mutation of all three cysteine residues (C40/43/44-A) was not labeled (Fig. 7b, lower panel, lane 5). As a positive control, the IBV E protein was also efficiently labeled by [^{3}H] palmitate (Fig. 7b, lower panel, lane 6). These results confirm that SARS-CoV E protein is modified by palmitoylation at all three cysteine residues.

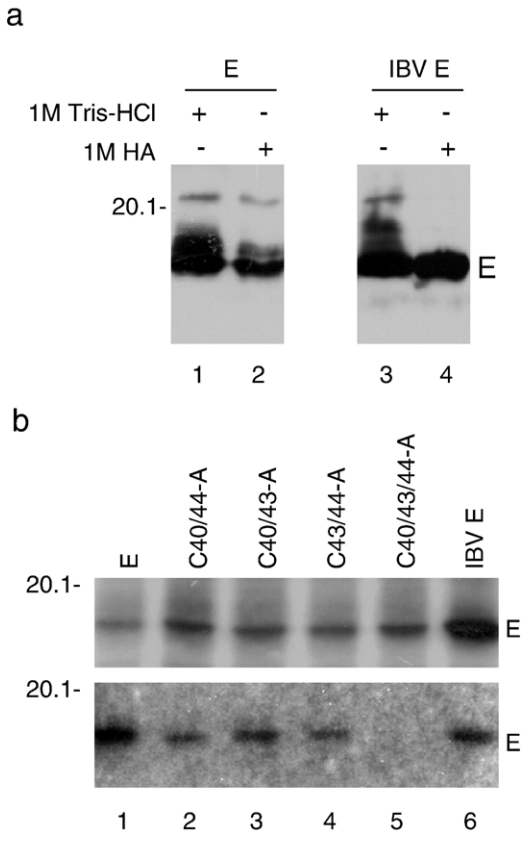

Fig. 7. Palmitoylation of SARS-CoV E protein. (a) Total cell lysates prepared from HeLa cells expressing the Flag-tagged SARS-CoV E protein (lanes 1 and 2) and IBV E protein (lanes 3 and 4) were treated either with 1 M Tris–HCl (lanes 1 and 3) or 1M hydroxylamine (lanes 2 and 4). Polypeptides were separated by SDS-PAGE and analyzed by Western blot using the anti-Flag antibody. Numbers on the left indicate molecular masses in kilodaltons. (b) HeLa cells expressing the Flag-tagged wild type SARS-CoV E protein (lane 1), mutant C40/44-A (lane 2), C40/44-A (lane 3), C43/44-A (lane4), C40/43/44-A (lane 5), and IBV E protein (lane 6) were radiolabeled with [^{35}S] methionine–cysteine (upper panel) and [^{3}H] palmitic acid (lower panel). Cell lysates were prepared and subjected to immunoprecipitation with anti-Flag antibody. Polypeptides were separated by SDS-PAGE and visualized by autoradiography. Numbers on the left indicate molecular masses in kilodaltons.

Mutational analysis of the subcellular localization and membrane association property of SARS-CoV E protein

To further analyze the membrane association properties of the E protein, its subcellular localization was studied by indirect immunofluorescence. HeLa cells overexpressing the Flag-tagged E protein were fixed with 4% paraformaldehyde at 12 h postinfection and stained with anti-Flag monoclonal antibody (Fig. 8a). In cells permeabilized with 0.2% Triton X-100, the Flag-tagged E protein is mainly localized to the perinuclear regions of the cells (Fig. 8a, panel A). The staining patterns largely overlap with calnexin, an ER resident protein (panels B and C). It was also noted that some granules and punctated staining patterns are not well merged with the calnexin staining patterns. They may represent aggregates of the E protein.

The exact subcellular localization of a coronavirus E protein is an issue of debate in the current literature (Corse and Machamer, 2003). Although clear ER localization of the coronavirus IBV E protein was observed at early time points in a time course experiment using an overexpression system (Lim and Liu, 2001), no such localization patterns were observed as reported by Corse and Machamer (2003). To clarify that the above observed ER localization pattern may be due to the high expression level of the protein in HeLa cells using the vaccinia/T7 system, the subcellular localization of the SARS-CoV E protein in another cell type with lower expression efficiency of the protein was carried out. As shown in Fig. 8a, expression of the Flag-tagged SARS-CoV in BHK cells stably expressing the T7 RNA polymerase (Buchholz et al., 1999) showed that the protein exhibits typical Golgi localization patterns (panels D–F). Expression of the untagged SARS-CoV E protein in the same cell type also shows very similar Golgi localization patterns as the Flag-tagged protein (Fig. 8a, panels G–I). These results suggest that the predominant ER localization patterns in HeLa cells observed above may be due to the cell type used and the very high expression levels of the protein in individual cells with the vaccinia/T7 expression system.

The subcellular localization of wild type and six mutants, Em1, Em2, Em3, Em4, Em5, and Em6, was then studied in BHK cells. The localization patterns of Em1, Em2, and Em5 were similar to wild type E protein, showing predominant Golgi localization patterns (Fig. 8b). In cells expressing Em3 and Em4, more diffuse staining patterns throughout the cytoplasm were observed (Fig. 8b). It suggests that these mutations may change the membrane association properties of the protein, leading to the alteration of the subcellular localization of the

protein. In cells expressing Em6, a diffuse localization pattern was observed (Fig. 8b).

The membrane association properties of wild type and mutant E proteins were further confirmed by fractionation of HeLa cells expressing E protein into membrane and cytosol fractions, and the presence of E protein in each fraction was analyzed by Western blot. As shown in Fig. 8c, 95.28% of wild type E protein was detected in the membrane fraction. The percentages of the mutant E protein detected in the similarly prepared membrane fraction were 93.67% for Em1, 89.85% for Em2, 62.60% for Em3, 58.58%for Em4, 93.64% for Em5, and 55.46% for Em6 (Fig. 8c).

Partial association of SARS-CoV E protein with lipid rafts

To test if the E protein may be associated with lipid rafts, the low-density, detergent-insoluble membrane fraction was isolated from HeLa cells overexpressing the SARS-CoV E protein. As shown in Fig. 9, the majority of the E protein was detected at the bottom fractions (lanes 9–11). However, a certain proportion of E protein associated with lipid rafts was detected in fractions 3, 4, and 5 (Fig. 9, lanes 3–5). As a marker for lipid rafts, the GM1 was detected in fractions 4 and 5 (Fig. 9, lanes 3 and 4).

Discussion

All coronaviruses encode a small hydrophobic envelope protein with essential functions in virion assembly, budding, and morphogenesis (Corse and Machamer, 2001, 2002; Fischer et al., 1998; Lim and Liu, 2001). In a previous study, the SARS-CoV E protein was shown to obviously enhance the membrane permeability of bacterial cells to *o*-nitrophenyl-β-D-galactopyranoside and hygromycin B (Liao et al., 2004). In this study, we show that this protein can also alter membrane permeability of mammalian cells to the general translation inhibitor, hygromycin B. Evidence present further demonstrates that the SARS-CoV E protein is an integral membrane protein, and its membrane-permeabilizing activity is associated with the transmembrane domain. The

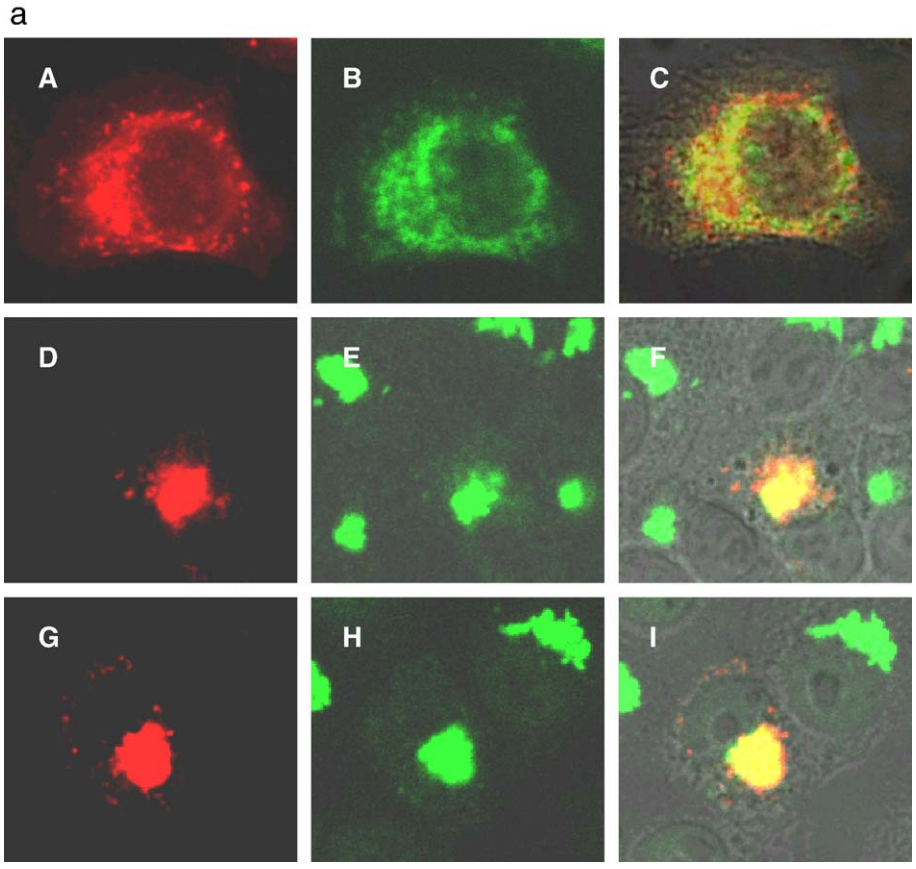

Fig. 8. Subcellular localization and membrane association of wild type and mutant SARS-CoV E protein. (a) HeLa cells expressing the Flag-tagged E protein (A–C), and BHK cells expressing the Flag-tagged (D–F) and untagged (G–I) SARS-CoV E were stained with either anti-Flag (A–F) or anti-E (G–I) antibodies at 12 h posttransfection after permeabilizing with 0.2% Triton X-100. The same HeLa cells were also stained with anti-calnexin antibody (B), and the same BHK cells were also stained with anti-p230 trans Golgi antibodies (panels E and H). Panels C, F, and I show the overlapping images. (b) BHK cells expressing the Flag-tagged wild type (E) and mutant E protein (Em1, Em2, Em3, Em4, Em5, and Em6) were stained with anti-Flag antibody at 12 h posttransfection after permeabilizing with 0.2% Triton X-100. (c) HeLa cells expressing the Flag-tagged wild type and mutant E protein were harvested at 12 h posttransfection, broken by 20 stokes with a Dounce cell homogenizer, and fractionated into cytosol (C) and membrane (M) fractions after removal of cell debris and nuclei. Polypeptides were separated by SDS-PAGE and analyzed by Western blot using the anti-Flag antibody. The percentages of E protein detected in the membrane fraction were determined by densitometry and indicated on the right. Numbers on the left indicate molecular masses in kilodaltons.

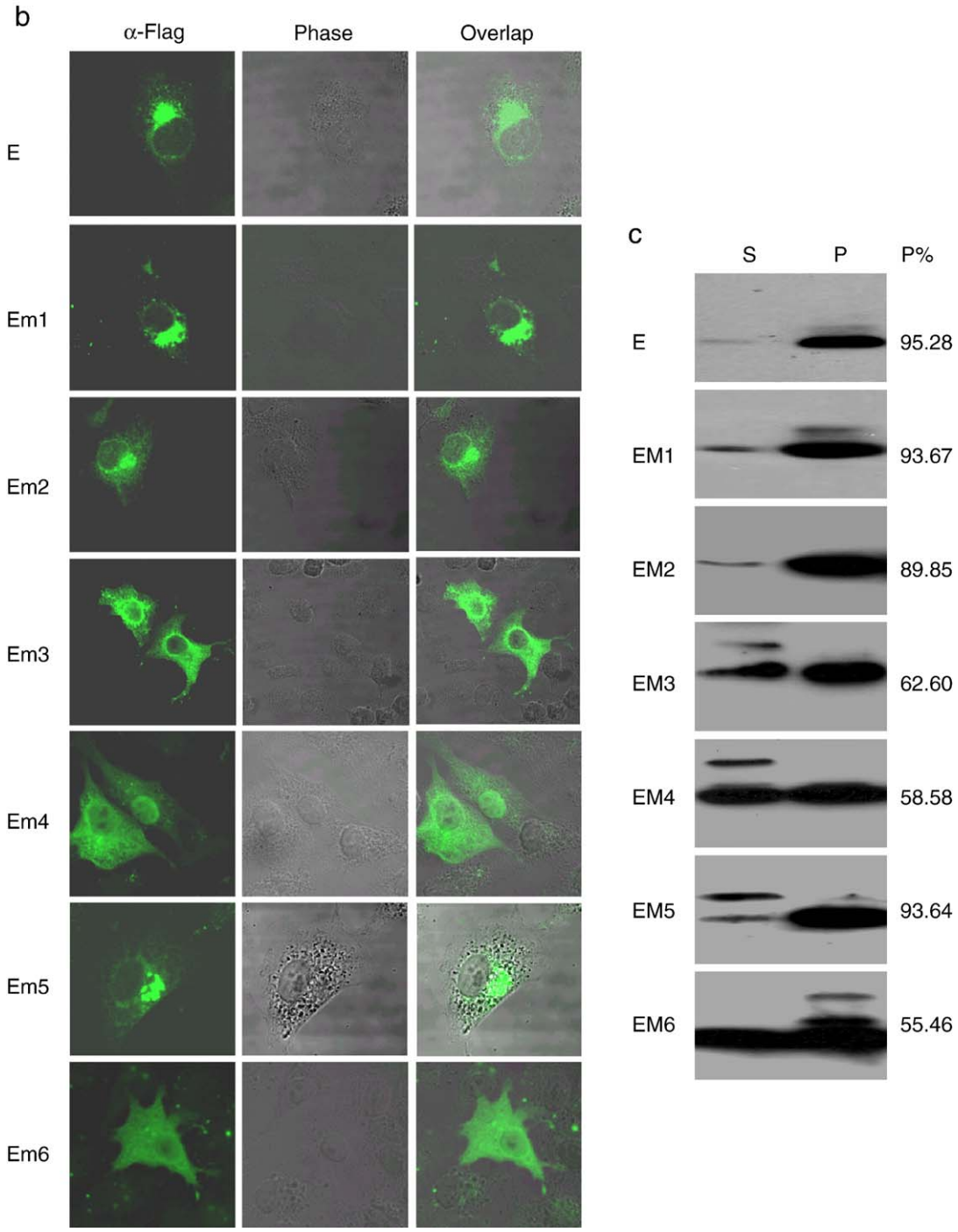

Fig. 8 (*continued*).

protein is posttranslationally modified by palmitoylation on all the three cysteine residues.

SARS-CoV E protein contains a putative long transmembrane domain of 29 amino acid residues (Arbely et al., 2004). In a recent report, Arbely et al. (2004) showed that the protein might have a highly unusual topology, consisting of a short transmembrane helical hairpin that forms an inversion about a previously unidentified pseudo-center of symmetry. This hairpin structure could deform lipid bilayers and cause tabulation (Arbely et al., 2004). The full-length and N-terminal 40 amino acid region were shown to be able to form cation-selective ion channels on artificial lipid bilayers (Wilson et al., 2004). By using molecular simulation and synthetic peptide approaches, it was shown that the transmembrane domain of E protein could form ion channels by homooligomerization into stable dimers, trimers, and pentamers (Torres et al., 2005). The mutagenesis data present in this study showed that introduction of radical mutations to the transmembrane domain is required to block the membrane-permeabilizing activity of the protein.

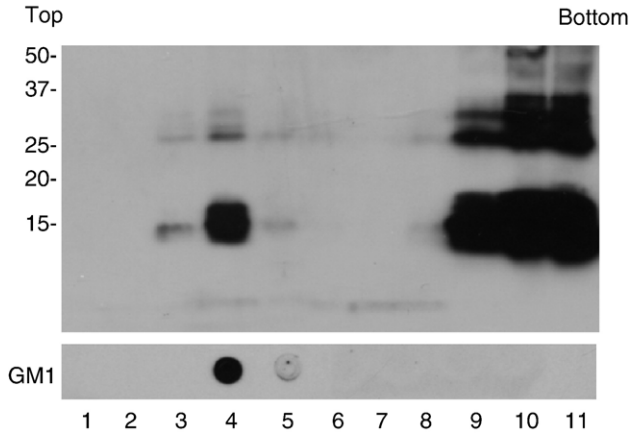

Fig. 9. Association of SARS-CoV E protein with lipid rafts. HeLa cells expressing the Flag-tagged SARS E protein were lysed with 1% Triton, and centrifuged to remove insoluble material and nuclei. The supernatants were fractionated by ultracentrifugation with a sucrose gradient, and 11 fractions were collected. The presence of the SARS-CoV E protein in each fraction was analyzed by Western blot using anti-Flag antibody, and the presence of GM1 was determined by dot blot. Numbers on the left indicate molecular masses in kilodaltons.

Mutations introduced into the transmembrane domain of SARS-CoV E protein in Em2 as well as in Em3 and Em4 drastically change the migration properties of the E protein in SDS-PAGE (Fig. 4a). It suggests that these mutations would have significantly altered the overall folding, hydrophobicity, and membrane association properties of the E protein. However, this mutant shows very similar properties in subcellular localization, membrane association, and membrane-permeabilizing activity as wild type E protein. The high tolerance of E protein to such dramatic mutations indicates that maintenance of these properties would be essential for the functionality of E protein in coronavirus life cycles. This possibility would warrant more systematic studies by using an infectious clone system.

The first and third Cys residues of the E protein were previously shown to play important roles in oligomerization and modification of membrane permeability in bacterial cells (Liao et al., 2004). The protein could form homodimers and trimers by interchain disulfide bonds in both bacterial and mammalian cells (Liao et al., 2004). In this study, mutation of all the three cysteine residues did not obviously affect the membrane-permeabilizing activity of the E protein. Instead, these residues could affect the membrane association of the protein as they were shown to be modified by palmitoylation. Examples of palmitoylation of viral and cellular proteins on multiple cysteine residues include influenza virus HA protein, members of seven transmembrane domains containing G-protein-coupled receptors (CCR5 and endothelin B receptor, etc.), and other cellular proteins (Bijlmakers and Marsh, 2003).

Lipid modification by palmitic acid has been reported for a number of viral envelope proteins, including the hemagglutinin (HA) and M2 protein of influenza virus (Melkonian et al., 1999; Schroeder et al., 2004; Veit et al., 1991; Zhang et al., 2000), gp160 of HIV-1 (Rousso et al., 2000), and Env protein of murine leukemia virus (Li et al., 2002). The E protein of coronavirus mouse hepatitis virus and IBV was also reported to be palmitoylated (Corse and Machamer, 2001). It has been noted that palmitoylation of viral envelope proteins usually takes place on cysteine residues located within the transmembrane domain or in the cytoplasmic tail close to this domain (Bhattacharya et al., 2004; Hausmann et al., 1998; Schmidt et al., 1988; Veit et al., 1989). This thioester linkage of fatty acids to viral envelope proteins is a posttranslational event that takes place in the *cis* or medial Golgi after exit from the ER and after oligomerization but prior to acquisition of endo H (endo-β-*N*-acetylglucosaminidase H) resistance (Bonatti et al., 1989; Veit and Schmidt, 1993). Palmitoylation of viral proteins plays a considerable role in virus infectivity, virion assembly, and release. For example, palmitoylation of the HA protein of influenza virus enhances its association with lipid rafts (Melkonian et al., 1999; Zhang et al., 2000); palmitoylation of the HIV-1 envelope glycoprotein is critical for viral infectivity (Rousso et al., 2000); palmitoylation of the murine leukemia virus envelope protein is critical for its association with lipid rafts and cell surface expression (Li et al., 2002); palmitoylation of the Rous sarcoma virus transmembrane glycoprotein is required for protein stability and virus infectivity (Ochsenbauer-Jambor et al., 2001). The observed palmitoylation of the SARS-CoV E protein may play certain roles in its cell surface expression and association with lipid rafts.

In this study, we show that radical mutations introduced into the transmembrane domain of the SARS-CoV E protein could neither totally block the membrane-permeabilizing activity nor completely disrupt the membrane association properties of the protein, unless the three cysteine residues were simultaneously mutated. This may reflect the relatively low sensitivity of the hygromycin B assays used to detect the membrane-permeabilizing activity of the protein. Alternatively, it suggests that the palmitoylated mutant E protein may be still tightly associated with cellular membrane, as palmitoylation of the protein would help target the protein to the cellular membrane. This membrane association could, in turn, cause membrane damage, leading to the increased membrane permeability to hygromycin B.

Subcellular fractionation and biochemical characterization studies demonstrated that, similar to the IBV E protein, the SARS-CoV E protein behaves as an integral membrane protein. However, it was consistently observed that, under the experimental conditions used, certain proportions of both SARS-CoV and IBV E proteins associated with cellular membranes were resistant to 1% Triton X-100, while some of the membrane-associated proteins can be released from the membrane pellets by treatment with high pH. Two possibilities are considered. First, as observed in this study, SARS-CoV E protein is partially associated with lipid rafts. This may render the protein resistant to the treatment by Triton X-100. Second, immunofluorescent staining of cells expressing the E protein showed the detection of the protein with punctated staining patterns at both cell surface and intracellular structures. It would suggest that the protein may form aggregates. These aggregates

may be cofractionated with the membrane-associated E protein and can be released by high pH but are resistant to the detergent treatment.

Cell surface expression is a prerequisite for SARS-CoV E protein to alter the membrane permeability of the cells. Over the course of this study, it was consistently observed that SARS-CoV E protein exhibits much weaker cell surface staining than the IBV E protein even in cells overexpressing the protein (data not shown). This may reflect the unique topology of the SARS-CoV E protein on cellular membranes. This possibility is currently under investigation.

Material and methods

Polymerase chain reaction and site-directed mutagenesis

Amplification of respective template DNAs with appropriate primers was performed with Pfu DNA polymerase (Strategene) with 2 mM $MgCl_2$. The PCR conditions were 35 cycles of 94 °C for 45 s, 46–58 °C for 45 s, and 72 °C for 30 s. The annealing temperature and extension time were subjected to adjustments according to the melting temperatures of the primers used and the lengths of the PCR fragments synthesized.

Site-directed mutagenesis was carried out with two rounds of PCR and two pairs of primers (Liu et al., 1997).

Transient expression of SARS-CoV sequence in mammalian cells

HeLa cells were grown at 37 °C in 5% CO_2 and maintained in Glasgow's modified Eagle's medium supplemented with 10% fetal calf serum. SARS-CoV E and mutants were placed under the control of a T7 promoter and transiently expressed in mammalian cells using a vaccinia virus-T7 expression system. Briefly, 60–80% confluent monolayers of HeLa cells grown on dishes (Falcon) were infected with 10 plaque-forming units/cell of a recombinant vaccinia virus (vTF7-3) that expresses T7 RNA polymerase. Two hours later, cells were transfected with plasmid DNA mixed with Effectene according to the instructions of the manufacturer (Qiagen). Cells were harvested at 12 to 24 h posttransfection.

Western blot analysis

Total proteins extracted from HeLa cells were lysed with 2× SDS loading buffer in the presence of 200 mM DTT plus 10 mM of iodoacetamide and subjected to SDS-PAGE. Proteins were transferred to PVDF membrane (Stratagene) and blocked overnight at 4 °C in blocking buffer (5% fat free milk powder in PBST buffer). The membrane was incubated with 1:2000 diluted primary antibodies in blocking buffer for 2 h at room temperature. After washing three times with PBST, the membrane was incubated with 1:2000 diluted anti-mouse or anti-rabbit IgG antibodies conjugated with horseradish peroxidase (DAKO) in blocking buffer for 1 h at room temperature. After washing for three times with PBST, the polypeptides were detected with a chemiluminescence detection kit (ECL, Amersham Biosciences) according to the instructions of the manufacturer.

Metabolic radiolabeling, immunoprecipitation, and SDS-PAGE

Permeability of the plasma membrane of cells expressing SARS-CoV E or mutants to hygromycin B was determined as described below. Briefly, HeLa cells in 100 mm dish were transfected with plasmids described as above, the cells were pretreated with different concentrations of hygromycin B (Sigma) for 30 min in methionine–cysteine free medium at 12 h posttransfection, and then 25 μCi/ml of [^{35}S] methionine–cysteine (Amersham) was added to the culture medium. The cells were incubated at 37 °C for 3 h in the presence or absence of hygromycin B, harvested, and lysed in 1× radioimmune precipitation assay buffer (RIPA) containing 1.0 mM phenylmethylsulfonyl fluoride and 10 μg/ml each of aprotinin and leupeptin (Roche Applied Science). The cell extracts were clarified for 10 min at 13,000 rpm at 4 °C, and the proteins were immunoprecipitated with appropriate antibodies for 1 h at 4 °C, incubated with 20 μl of protein A-agarose overnight at 4 °C, and washed three times with RIPA. The proteins were analyzed by 15% SDS-PAGE.

For palmitoylation assay, HeLa cells in 60mm dish were labeled with 1 mCi/ml of [9, 10-^{3}H] palmitic acid (50Ci/mmol; Amersham) for 10 h at 4 h posttransfection. A duplicate dish of cells was labeled with 25 μCi/ml of [^{35}S] methionine–cysteine (Amersham) for 10 h at 4 h posttransfection. Cells were harvested and proteins were immunoprecipitated as described above.

Expression and purification of the SARS-CoV E protein expressed in insect cells

A cDNA fragment covering the SARS-CoV E protein with a His-tag at the C-terminus was cloned to the transfer vector pVL1392 (Pharmingen). A recombinant baculovirus expressing the His-tagged SARS-CoV E protein was generated by cotransfection of the pVL1392-E-His construct together with Baculogold DNA (Pharmingen) into Sf9 cells according to the instruction of the manufacturer. Fresh Sf9 cells were infected with the recombinant virus and harvested at 72 h postinfection. The His-tagged E protein was purified using Ni-NTA purification system (Qiagen) according to the instruction of the manufacturer.

Cross-linking experiment

The His-tagged E protein was incubated with 0.1, 0.25, and 0.5 mM glutaraldehyde at room temperature for 1 h. The reaction was quenched by adding 100 mM glycine. Polypeptides were separated on SDS-15% polyacrylamide gel in the presence or absence of 1% β-mercaptoethanol, and analyzed by Western blot with anti-His antibody.

Indirect immunofluorescence

HeLa cells expressing E protein or various mutants were fixed with 4.0% paraformaldehyde for 10 min at 16 h post-transfection, washed three times with 1× PBS, permeabilized with 0.2% Triton X-100 for 10 min at room temperature, and washed three times with 1× PBS. Rabbit anti-E antibodies were used to detect E protein and mutants, and mouse anti-calnexin monoclonal antibodies (Abcam) were used to detect calnexin, an ER marker. Mouse anti-Flag monoclonal antibodies were also used to detect Flag-tagged E protein and mutants.

Subcellular fractionation

HeLa cells were resuspended in hypotonic buffer (1 mM Tris–HCl pH 7.4, 0.1 mM EDTA, 15 mM NaCl) containing 2 μg of leupeptin per ml and 0.4 mM phenylmethylsulfonyl fluoride and broken by 20 strokes with a Dounce cell homogenizer. Cell debris and nuclei were removed by centrifugation at 1500 × *g* for 10 min at 4 °C. The cytosol fraction and membrane fraction (postnuclear fraction) were separated by ultracentrifugation through a 6% sucrose cushion at 150,000×*g* for 30 min at 4 °C. Membrane pellets were resuspended in hypotonic buffer, treated with 1% Triton X-100, 100 mM Na_2CO_3 or 1 M KCl for 30 min, and further fractionated into supernatant (S) and pellet (P) fractions by ultracentrifugation at 150,000 × *g* for 30 min at 4 °C.

Isolation of low-density detergent-insoluble membrane fractions on flotation gradients

HeLa cells expressing the Flag-tagged SARS-C0V E from two 10 cm dishes were washed twice with ice-cold PBS and lysed on ice for 30 min in 1 ml of 1% Triton X-100 TNE lysis buffer (25 mM Tris–HCl pH 7.5, 150 mM NaCl, 5 mM EDTA) supplemented with protease inhibitor cocktail (Roche). The cell lysates were homogenized with 25 strokes using a Dounce homogenizer and centrifuged at 3000 × *g* at 4 °C for 5 min to remove insoluble materials and nuclei. The supernatants were mixed with 1 ml of 80% sucrose in lysis buffer, placed at the bottom of a ultracentrifuge tube, overlaid with 6 ml of 30% and 3 ml of 5% sucrose in TNE lysis buffer, and ultracentrifuged at 38,000 rpm at 4 °C in a SW41 rotor (Beckman) for 18 h. After centrifugation, 11 fractions (1 ml each) were collected from the top to the bottom and analyzed immediately by Western blot or stored at −80 °C.

Construction of plasmids

Plasmid pFlagE was constructed by cloning an *Eco*RV- and *Eco*RI-digested PCR fragment into *Eco*RV- and *Eco*RI-digested pFlag. The Flag tag is fused to the N-terminal end of the E protein. The two primers used are: 5′-CGGGATATCCTACTCATTCGTTT CGGAA-3′ and 5′-CCGGAATTCTTAGACCAGAAGATCAGGAAC-3′. Mutations were introduced into the E gene by two rounds of PCR. The PCR amplified fragments were cloned into *Eco*RV- and *Eco*RI-digested pFlag. All plasmids and the introduced mutations were confirmed by automated DNA sequencing.

Acknowledgments

This work was supported by the Agency for Science Technology and Research, Singapore and a grant the Biomedical Research Council (BMRC 03/1/22/17/220).

References

Agirre, A., Barco, A., Carrasco, L., Nieva, J.B., 2002. Viroporin-mediated membrane permeabilization. J. Biol. Chem. 277, 40434–40441.

Aldabe, R., Barco, A., Corrasco, L., 1996. Membrane permeabilization by poliovirus proteins 2B and 2BC. J. Biol. Chem. 271, 23134–23137.

Arbely, E., Khattari, Z., Brotons, G., Akkawi, M., Salditt, T., Arkin, I.T., 2004. A highly unusual palindromic transmembrane helical hairpin formed by SARS coronavirus E protein. J. Mol. Biol. 341, 769–779.

Bhattacharya, J., Peters, P.J., Clapham, P.R., 2004. Human immunodeficiency virus type 1 envelope glycoproteins that lack cytoplasmic domain cysteines: impact on association with membrane lipid rafts and incorporation onto budding virus particles. J. Virol. 78, 5500–5506.

Bijlmakers, M.-J., Marsh, M., 2003. The on–off story of protein palmitoylation. Trends Cell Biol. 13, 32–42.

Bodelon, G., Labrada, L., Martinez-Costas, J., Benavente, J., 2002. Modification of late membrane permeability in avian reovirus-infected cells. J. Biol. Chem. 227, 17789–17796.

Bonatti, S., Migliaccio, G., Simons, K., 1989. Palmitoylation of viral membrane glycoproteins takes place after exit from the endoplasmic reticulum. J. Biol. Chem. 264, 12590–12595.

Buchholz, U.J., Finke, S., Conzelmann, K.K., 1999. Generation of bovine respiratory syncytial virus (BRSV) from cDNA: BRSV NS2 is not essential for virus replication in tissue culture, and the human RSV leader region acts as a functional BRSV genome promoter. J. Virol. 73, 251–259.

Carrasco, L., Perez, L., Irurzun, A., Lama, J., Martinez-Abarca, F., Rodriguez, P., Guinea, R., Castrillo, J.L., Sanz, M.A., Ayala, M.J., 1995. Modification of membrane permeability by animal viruses. Adv. Virus Res. 45, 61–112.

Corse, E., Machamer, C.E., 2001. Infectious bronchitis virus E protein is targeted to the Golgi complex and directs release of virus-like particles. J. Virol. 74, 4319–4326.

Corse, E., Machamer, C.E., 2002. The cytoplasmic tail of infectious bronchitis virus E protein directs Golgi targeting. J. Virol. 76, 1273–1284.

Corse, E., Machamer, C.E., 2003. The cytoplasmic tails of infectious bronchitis virus E and M proteins mediate their interaction. Virology 312, 25–34.

Fischer, F., Stegen, C.F., Masters, P.S., Samsonoff, W.A., 1998. Analysis of constructed E gene mutants of mouse hepatitis virus confirms a pivotal role for E protein in coronavirus assembly. J. Virol. 72, 7885–7894.

Gonzalez, M.E., Carrasco, L., 1998. The human immunodeficiency virus type 1 vpu protein enhances membrane permeability. Biochemistry 37, 13710–13719.

Gonzalez, M.E., Carrasco, L., 2003. Viroporins. FEBS Lett. 552, 28–34.

Hausmann, J., Ortmann, D., Witt, E., Veit, M., Seidel, W., 1998. Adenovirus death protein, a transmembrane protein encoded in the E3 region, is palmitoylated at the cytoplasmic tail. Virology 244, 343–351.

Ito, N., Mossel, E.C., Narayanan, K., Popov, V.L., Huang, C., Inoue, T., Peters, C.J., Makino, S., 2005. Severe acute respiratory syndrome coronavirus 3a protein is a viral structural protein. J. Virol. 79, 3182–3186.

Jecht, M., Probst, C., Gauss-Muller, V., 1998. Membrane permeability induced by Hepatitis A virus proteins 2B and 2BC and proteolytic processing of HAV 2BC. Virology 252, 218–227.

Li, M., Yang, C., Tong, S., Weidmann, A., Compans, R.W., 2002. Palmitoylation of the murine leukemia virus envelope protein is critical for lipid raft association and surface expression. J. Virol. 76, 11845–11852.

Liao, Y., Lescar, J., Tam, J.P., Liu, D.X., 2004. Expression of SARS-coronavirus envelope protein in *Escherichia coli* cells alters membrane permeability. Biochem. Biophys. Res. Commun. 325, 374–380.

Lim, K.P., Liu, D.X., 2001. The missing link in coronavirus assembly. J. Biol. Chem. 276, 17515–17523.

Liu, D.X., Inglis, S.C., 1991. Association of the infectious bronchitis virus3c protein with the virion envelope. Virology 185, 911–917.

Liu, D.X., Xu, H.Y., Brown, T.D.K., 1997. Proteolytic processing of the coronavirus infectious bronchitis virus 1a Polyprotein: identification of a 10-kilodalton polypeptide and determination of its cleavage sites. J. Virol. 71, 1814–1820.

Madan, V., Garcia, M.J., Sanz, M.A., Carrasco, L., 2005. Viroporin activity of murine hepatitis virus E protein. FEBS Lett. 579, 3607–3612.

Mehmel, M., Rothermel, M., Meckel, T., Van Etten, J.L., Moroni, A., Thiel, G., 2003. Possible function for virus encoded K+ channel Kcv in the replication of chlorella virus PBCV-1. FEBS Lett. 552, 7–11.

Melkonian, K.A., Ostermeyer, A.G., Chen, J.Z., Roth, M.G., Brown, D.A., 1999. Role of lipid modifications in targeting proteins to detergent-resistant membrane rafts. Many raft proteins are acylated, while few are prenylated. J. Biol. Chem. 274, 3910–3917.

Ochsenbauer-Jambor, C., Miller, D.C., Roberts, C.R., Rhee, S.S., Hunter, E., 2001. Palmitoylation of the Rous sarcoma virus transmembrane glycoprotein is required for protein stability and virus infectivity. J. Virol. 75, 11544–11554.

Pavlovic, D., Neville, D.C.A., Argaud, O., Blumberg, B., Dwek, R.A., Fischer, W.B., Zitzmann, N., 2003. The hepatitis C virus forms an ion channel that is inhibited by long-alkyl-chain iminosugar derivatives. Proc. Natl. Acad. Sci. 100, 6104–6108.

Pinto, L.H., Holsinger, L.J., Lamb, R.A., 1992. Influenza virus M2 protein has ion channel activity. Cell 59, 517–528.

Rota, P.A., Oberste, M.S., Monroe, S.S., Nix, W.A., Campagnoli, R., Icenogle, J.P., Penaranda, S., Bankamp, B., Maher, K., Chen, M.H., Tong, S., Tamin, A., Lowe, L., Frace, M., DeRisi, J.L., Chen, Q., Wang, D., Erdman, D.D., Peret, T.C., Burns, C., Ksiazek, T.G., Rollin, P.E., Sanchez, A., Liffick, S., Holloway, B., Limor, J., McCaustland, K., Olsen-Rasmussen, M., Fouchier, R., Gunther, S., Osterhaus, A.D., Drosten, C., Pallansch, M.A., Anderson, L.J., Bellini, W.J., 2003. Characterization of a novel coronavirus associated with severe acute respiratory syndrome. Science 300, 1394–1399.

Rousso, I., Mixon, M.B., Chen, B.K., Kim, P.S., 2000. Palmitoylation of the HIV-1 envelope glycoprotein is critical for viral infectivity. Proc. Natl. Acad. Sci. 97, 13523–13525.

Sanz, M.A., Perez, L., Carrasco, L., 1994. Semliki forest virus 6K protein modifies membrane permeability after inducible expression in *Escherichia coli* cells. J. Biol. Chem. 269, 12106–12110.

Schmidt, M., Schmidt, M.F.G., Rott, R., 1988. Chemical identification of cysteine as palmitoylation site in a transmembrane protein (Semliki forest virus E1). J. Biol. Chem. 263, 18635–18639.

Schroeder, C., Heider, H., Moncke-Buchner, E., Lin, T.I., 2004. The influenza virus ion channel and maturation cofactor M2 is a cholesterol-binding protein. Eur. Biophys. J. 34, 52–66.

Schubert, U., Ferrer-Montiel, A.V., Oblatt-Montal, M., Henklein, P., Strebel, K., Montal, M., 1996. Identification of an ion channel activity of the Vpu transmembrane domain and its involvement in the regulation of virus release from HIV-1-infected cells. FEBS Lett. 398, 12–18.

Thiel, V., Ivanov, K.A., Putics, A., Hertzig, T., Schelle, B., Bayer, S., Weißbrich, B., Snijder, E.J., Rabenau, H., Doerr, H.W., Gorbalenya, A.E., Ziebuhr, J., 2003. Mechanisms and enzymes involved in SARS coronavirus genome expression. J. Gen. Virol. 84, 2305–2315.

Torres, J., Wang, J., Parthasarathy, K., Liu, D.X., 2005. The transmembrane oligomers of coronavirus protein E. Biophys J. 88, 1283–1290.

Veit, M., Schmidt, M.F.G., 1993. Timing of palmitoylation of influenza virus hemagglutinin. FEBS Lett. 336, 243–247.

Veit, M., Schmidt, F.G., Rott, R., 1989. Different palmitoylation of paramyxovirus glycoproteins. Virology 168, 173–176.

Veit, M., Klenk, H.D., Kendal, A., Rott, R., 1991. The M2 protein of influenza A virus is acylated. J. Gen. Virol. 72, 1461–1465.

Wilson, L., McKinlay, C., Gage, P., Ewart, G., 2004. SARS coronavirus E protein forms cation-selective ion channels. Virology 330, 322–331.

Yu, X., Bi, W., Weiss, S.R., Leibowitz, J.L., 1994. Mouse hepatitis virus gene 5b protein is a new virion envelope protein. Virology 202, 1018–1023.

Yuan, X., Li, J., Shan, Y., Yang, Z., Zhao, Z., Chen, B., Yao, Z., Dong, B., Wang, S., Chen, J., Cong, Y., 2005. Subcellular localization and membrane association of SARS-CoV 3a protein. Virus Res. 109, 191–202.

Zhang, J., Pekosz, A., Lamb, R.A., 2000. Influenza virus assembly and lipid raft microdomains: a role for the cytoplasmic tails of the spike glycoproteins. J. Virol. 74, 4634–4644.

FEBS Letters 580 (2006) 3192–3200

Biochemical evidence for the presence of mixed membrane topologies of the severe acute respiratory syndrome coronavirus envelope protein expressed in mammalian cells

Q. Yuan[a], Y. Liao[a], J. Torres[a], J.P. Tam[a], D.X. Liu[a,b,*]

[a] *School of Biological Science, Nanyang Technological University, 60 Nanyang Drive, Singapore 637551, Singapore*
[b] *Institute of Molecular and Cell Biology, 61 Biopolis Drive, Proteos, Singapore 138673, Singapore*

Received 3 March 2006; revised 18 April 2006; accepted 26 April 2006

Available online 4 May 2006

Edited by Hans-Dieter Klenk

Abstract **Coronavirus envelope (E) protein is a small integral membrane protein with multi-functions in virion assembly, morphogenesis and virus–host interaction. Different coronavirus E proteins share striking similarities in biochemical properties and biological functions, but seem to adopt distinct membrane topology. In this report, we study the membrane topology of the SARS-CoV E protein by immunofluorescent staining of cells differentially permeabilized with detergents and proteinase K protection assay. It was revealed that both the N- and C-termini of the SARS-CoV E protein are exposed to the cytoplasmic side of the membranes ($N_{cyto}C_{cyto}$). In contrast, parallel experiments showed that the E protein from infectious bronchitis virus (IBV) spanned the membranes once, with the N-terminus exposed luminally and the C-terminus exposed cytoplasmically ($N_{exo(lum)}$-C_{cyto}). Intriguingly, a minor proportion of the SARS-CoV E protein was found to be modified by N-linked glycosylation on Asn 66 and inserted into the membranes once with the C-terminus exposed to the luminal side. The presence of two distinct membrane topologies of the SARS-CoV E protein may provide a useful clue to the pathogenesis of SARS-CoV.**

Keywords: SARS-CoV; Envelope protein; Membrane topology

1. Introduction

The acute respiratory syndrome coronavirus (SARS-CoV) is an enveloped virus with a single strand, positive-sense RNA genome of 29.7 kb in length. Similar to other coronaviruses, its envelope typically contains three major structural proteins: spike (S), membrane (M) and envelope (E), with functions including recognition of target cells and fusion, interaction with other viral components, and involvement in virion assembly and budding.

All coronavirus E proteins are small integral membrane proteins with a long hydrophobic stretch from 25 to 30 residues [2,4,26]. They vary in size from 76 to 109 amino acids. The protein is associated with the ER and Golgi complex, and can be translocated to the surface of the infected cells [4,16,23,26,27]. Functionally, coronavirus E protein plays a pivotal role in viral morphogenesis, assembly and budding. Co-expression of mouse hepatitis virus (MHV) E and M was shown to result in the production of virus-like particles, roughly the same size and shape as virions [18,31]. The same phenomena were also observed in other coronaviruses, such as SARS-CoV and infectious bronchitis virus (IBV) [5,9]. When the E protein was expressed in mammalian cells on its own, the E-containing vesicles can be produced and released to the culture medium [5,19]. Furthermore, MHV and SARS-CoV E proteins were shown to induce apoptosis [1,32]. More recently, the SARS-CoV E protein was found to permeabilize bacterial cells as well as to form pores in artificial membranes [14,15,31]. It was also reported that MHV E protein could modify the membrane permeability in both *Escherchia coli* and mammalian cells [18].

Despite the similarities in biochemical properties and biological functions, the E protein from different coronaviruses shares very low homology in the primary amino acid sequence [18]. Another striking feature is that different coronavirus E proteins assume distinct membrane topologies. Based on cell surface staining with a C-terminus-specific antibody, transmissible gastroenteritis virus (TGEV) E protein was demonstrated to have a $C_{exo}N_{cyto}$ membrane topology [8]. The IBV E protein is accessible to a C-terminus-specific antibody in the presence of either digitonin or Triton X-100 but is accessible to an N-terminus-specific antibody only in the presence of Triton X-100, suggesting that IBV E protein may possess an $N_{exo}C_{cyto}$ topology [4]. Immunofluorescence analysis of cells expressing MHV E protein demonstrated that its transmembrane domain spans the lipid bilayer twice, indicating that both the N- and C-terminal regions are exposed to the cytoplasm ($N_{cyto}C_{cyto}$) [20,26]. The putative transmembrane domain of SARS-CoV E protein has been reported to adopt a highly unusual topology, consisting of a very short transmembrane helical hairpin [2], with Phe23 as the center of inversion of the hairpin. This residue was suggested to be located at the center of the bilayer [2], although a more recent report places this residue adjacent to the polar head groups of the lipids [11]. However, in silico [28] and in vitro NMR and infrared dichroic data (unpublished results) are in contrast with this model and are consistent with a normal transmembrane helix. In addition, the membrane orientation of the protein is yet to be determined.

In this report, the membrane topology of SARS-CoV E protein was determined by immunofluorescent staining of cells differentially permeabilized with detergents and by limited proteinase K digestion of microsomal membranes. These studies have revealed that both the N- and C-terminal regions of

*Corresponding author. Fax: +65 67791117.
E-mail address: dxliu@imcb.a-star.edu.sg (D.X. Liu).

0014-5793/$32.00
doi:10.1016/j.febslet.2006.04.076

the protein are located in the cytoplasm ($N_{cyto}C_{cyto}$). However, a minor proportion of the protein is found to be posttranslationally modified by N-linked glycosylation on the asparagine 66 residue. It suggests that a certain proportion of the protein may also adopt either an $N_{cyto}C_{exo}$ or $N_{exo}C_{exo}$ topology. This is the first coronavirus E protein with two distinct membrane topologies.

2. Material and methods

2.1. Polymerase chain reaction and site-directed mutagenesis

Amplification of respective template DNAs with appropriate primers was performed with Pfu DNA polymerase (Strategene) with 2 mM $MgCl_2$. The PCR conditions were 35 cycles of 94 °C for 45 s, 46–58 °C for 45 s, and 72 °C for 30 s. The annealing temperature and extension time were subjected to adjustments according to the melting temperatures of the primers used and the lengths of the PCR fragments synthesized.

Site-directed mutagenesis was carried out with two rounds of PCR and two pairs of primers.

2.2. Transient expression of SARS-CoV sequence in mammalian cells

HeLa cells were grown at 37 °C in 5% CO_2 and maintained in Glasgow's modified Eagle's medium supplemented with 10% fetal calf serum. SARS-CoV E and mutants were placed under the control of a T7 promoter and transiently expressed in mammalian cells using a vaccinia virus/T7 expression system described by Fuerst et al. [7]. Briefly, 60–80% confluent monolayers of HeLa cells grown on dishes (Falcon) were infected with 10 plaque-forming units/cell of a recombinant vaccinia virus (vTF7-3) that expresses T7 RNA polymerase. Two hours later, cells were transfected with plasmid DNA mixed with Effectene according to the instructions of the manufacturer (Qiagen). Cells were harvested at 12–24 h post-transfection.

2.3. Western blot analysis

Total proteins extracted from HeLa cells were lysed with 2× SDS loading buffer in the presence of 200 mM DTT plus 10 mM of iodoacetamide and subjected to SDS–PAGE. Proteins were transferred to PVDF membrane (Stratagene) and blocked overnight at 4 °C in blocking buffer containing 5% fat free milk powder in PBST buffer pH 7.5 (80 mM Na_2HPO_4,20 mM NaH_2PO_4,100 mM NaCl, 0.1% Tween 20). The membrane was incubated with 1:2000 diluted primary antibodies in blocking buffer for 2 h at room temperature. After washing three times with PBST, the membrane was incubated with 1:2000 diluted anti-mouse or anti-rabbit IgG antibodies conjugated with horseradish peroxidase (DAKO) in blocking buffer for 1 h at room temperature. After washing for three times with PBST, the polypeptides were detected with a chemiluminescence detection kit (ECL, Amersham Biosciences) according to the instructions of the manufacturer.

2.4. Indirect immunofluorescence

HeLa cells expressing Flag-tagged SARS-CoV or IBV E protein were fixed with 4% paraformaldehyde for 10 min at 16 h post-transfection, washed three times with 1× PBS, permeabilized with 0.2% Triton X-100 for 10 min at room temperature, and washed three times with 1× PBS. Monoclonal anti-Flag antibody was used to detect E protein and mutants. To selectively permeabilize the plasma membrane, HeLa cells were fixed with 4% paraformaldehyde for 10 min and permeabilized with 5 μg of digitonin per ml for 5 min at room temperature. Staining was as described above. Images were collected with a META 510 confocal laser-scanning microscope (Zeiss).

2.5. Glycosylation study of E protein

HeLa cells expressing E protein were treated with glycoprotein denaturing buffer (0.5% SDS and 1% β-mercaptoethanol) at 100 °C for 10 min. The denatured proteins were incubated with 1 μl glycosidase PNGaseF (Research Biolabs) in the reaction buffer (50 mM sodium phosphate, pH 7.5) supplemented with 1% NP40 at 37 °C for 1 h. The deglycosylated proteins were analyzed by western blot.

2.6. Subcellular fractionation

HeLa cells were resuspended in hypotonic buffer (1 mM Tris–HCl, pH 7.4, 0.1 mM EDTA, 15 mM NaCl) containing 2 μg of leupeptin per ml and 0.4 mM phenylmethylsulfonyl fluoride (PMSF) and broken by 20 strokes with a Dounce cell homogenizer. Cell debris and nuclei were removed by centrifugation at $1500 \times g$ for 10 min at 4 °C. The cytosol fraction and membrane fraction (postnuclear fraction) were separated by ultracentrifugation through a 6% sucrose cushion at $150000 \times g$ for 30 min at 4 °C. Membrane pellets were resuspended in hypotonic buffer, treated with 1% Triton X-100, 100 mM Na_2CO_3 or 1 M KCl for 30 min, and further fractionated into supernatant (S) and pellet (P) fractions by ultracentrifugation at $150000 \times g$ for 30 min at 4 °C.

2.7. Proteinase K protection assay

HeLa cells grown in 60 mm dishes were transfected with SARS-CoV E and IBV E tagged with the Flag epitope at either N- or C-terminus, respectively, by using the vaccinia/T7 virus (vTF7-3) system. After incubation for 18 h, the cells were washed twice with ice-cold PBS, scraped off the dish, and homogenized with 20 strokes in a tight-fitting Dounce homogenizer. Nuclei were removed by centrifugation at 1200 rpm for 15 min at 4 °C. Individual samples with the tagged SARS-CoV E or IBV E proteins were split into three microcentrifuge tubes. One tube was taken as control, the remaining two tubes in the absence or presence of 1% Triton X-100 were subjected to 20 μg/ml proteinase K digestion for 40 min on ice. The reaction was stopped by adding 4 mM PMSF. The samples were incubated at 100 °C for 15 min in the Laemmli sample buffer and then analyzed on SDS–PAGE.

2.8. Metabolic radiolabeling, immunoprecipitation and SDS–PAGE

HeLa cells in 100 mm dish were transfected with appropriate plasmid DNA, treated with different concentrations of hygromycin B (Sigma) for 30 min in methionine/cysteine free medium at 12 h post-transfection, and 25 μCi/ml of [^{35}S] methionine/cysteine (Amersham) were added to the culture medium. The cells were incubated at 37 °C for 3 h in the presence or absence of hygromycin B, harvested and lysed in RIPA buffer containing 1.0 mM PMSF and 10 μg/ml each aprotinin and leupeptin (Roche Applied Science). The cell extracts were clarified at 13000 rpm at 4 °C for 10 min, and the proteins were immunoprecipitated with appropriate antibodies for 1 h at 4 °C, incubated with 20 μl of protein A–agarose overnight at 4 °C, and washed three times with RIPA buffer. The proteins were analyzed by 15% SDS–PAGE.

2.9. Construction of plasmids

Plasmid Flag-SARS E, which covers the SARS-CoV E sequence, was constructed by cloning an *Eco*RV-/*Eco*RI-digested PCR fragment into *Eco*RV-/*Eco*RI-digested pKT0-Flag. The PCR fragment was generated using primers 5′-GCAAGATATCCTACTCATTCGTTTCGGAA-3′ and 5′-CCGGAATTCTTAGACCAGAAGATCAG-3′. Plasmid SARS E-Flag was created by cloning a *Bgl*II-/*Eco*RI-digested PCR fragment into *Bgl*II-/*Eco*RI-digested pKT0. The PCR fragment was generated using primers 5′-TGGAAGATCTCCACCATGTACTCATTCGTT TCGGAA-3′ and 5′-CGGAATTCTTACTTGTCATCGTCGTCCTTGTAATCGACCAGAAG ATCAGGAA-3′. Plasmid Flag-IBV E was generated by cloning an *Eco*RV-/*Eco*RI-digested PCR fragment into *Eco*RV-/*Eco*RI-digested pKT0-Flag. The two primers used to generate the PCR fragment are 5′-GCAAGATATCCAATTTATTGAATAAGTCG-3′ and 5′-CCGGAATTC TCA AGAG TACAATTTGTC-3′. Plasmid IBV E-Flag was created by cloning a *Bgl*II-/*Eco*RI-digested PCR fragment into *Bgl*II-/*Eco*RI-digested pKT0. The PCR fragment was generated using primers 5′-TGGAAGATCTCCACCATGAATTTATTGAATAA-3′ and 5′-CCGGAATTCTCACTTGTCA TCGTCGTCCTTGTAATCAGAG-TACAATTTGTCTCG-3′. Plasmid pKT-SARS E was constructed by cloning a *Bgl*II-/*Eco*RI-digested PCR fragment into *Bgl*II-/*Eco*RI-digested pKT0. The PCR fragment was generated using primers 5′-TGGAAGATCTCCACCAT GTACTCATTCGTTTCGGAA-3′ and 5′-CCGGAATTCTTAGACCAGAAGATCAG-3′. Plasmid pKT-IBV E was constructed by cloning a *Bgl*II-/*Eco*RI-digested PCR fragment into *Bgl*II-/*Eco*RI-digested pKT0. The PCR fragment was generated using primers 5′-TGGAAGAT CTCCACCATGAATTTATT GAATAA-3′ and 5′-CCGGAATTCTCAAGAGTACAATTTG TC-3′. The underlined nucleotides represent the restriction sites introduced into each primer.

Mutations were introduced into the SARS-CoV E gene by two rounds of PCR. The PCR amplified fragments were cloned into *Eco*RV- and *Eco*RI-digested pFlag. All plasmids and the introduced mutations were confirmed by automated DNA sequencing.

3. Results

3.1. Prediction of the hydrophobicity and membrane topology of SARS-CoV E protein

The hydrophobicity of the SARS-CoV E protein is shown as a Kyte–Doolittle hydropathy plot in Fig. 1B. The protein is largely hydrophobic in the region from amino acids 9 to 59. In both N- and C-terminal regions, some hydrophilic amino acid stretches were found.

Three computer programs, i.e., TMHMM [13], HMMTOP [29], and MEMSAT [10], were used to predict the membrane topology of the SARS-CoV E protein. All three programs predicted that SARS-CoV E protein contains one transmembrane domain. Both TMHMM and MEMSAT predicted that SARS-CoV E protein may assume an $N_{cyto}C_{exo}$ topology, whereas HMMTOP indicated that SARS-CoV E protein may adopt a $C_{cyto}N_{exo}$ topology.

3.2. Analysis of the membrane topology of SARS-CoV E protein by immunofluorescence microscopy

To test these predictions and to experimentally determine the membrane topology of the SARS-CoV E protein, both SARS-CoV and IBV E proteins were tagged with Flag at N- and C-termini, respectively, and expressed in HeLa cells. Cells were then permeabilized with either 0.5% Triton X-100 or 5 μg/ml digitonin, and the expression of the Flag-tagged E protein was detected by indirect immunofluorescent staining using anti-Flag monoclonal antibody. Treatment of cells with digitonin at low concentrations selectively permeabilizes the plasma membrane but leaves the intracellular membranes intact, while Triton X-100 treatment permeabilizes both plasma and intracellular membranes [25]. If the Flag tag is exposed to the cytoplasmic side, the epitope can be recognized by anti-Flag antibody after digitonin treatment. On the other hand, if the Flag tag is exposed luminally, the epitope cannot be recognized by the anti-Flag antibody after digitonin treatment. It can only be recognized after Triton X-100 treatment.

As shown in Fig. 2, clear detection of the N- and C-terminally tagged SARS-CoV E protein at perinuclear regions was obtained in HeLa cells permeabilized with either 0.5% Triton X-100 or 5 μg/ml digitonin (Fig. 2), suggesting that both N- and C-termini of the protein may be located in the cytoplasmic side. However, in cells expressing the N-terminally tagged IBV E protein, expression of the protein was observed in cells permeabilized with 0.5% Triton X-100 only (Fig. 2). No detection of the protein expression in cells permeabilized with 5 μg/ml digitonin was obtained (Fig. 2). It is also noted that no significant difference in the staining intensity was observed between cells treated with digitonin and Triton X-100. In cells expressing the C-terminally tagged IBV E protein, the protein was detected in cells permeabilized under either condition (Fig. 2). These results are consistent with the topology of IBV E protein established before [4], and justify the experimental conditions used. As a control, PDI, a host protein residing in the ER lumen, was detected in cells permeabilized with 0.5% Triton X-100, but was not detected in cells permeabilized with 5 μg/ml digitonin (Fig. 2), confirming that the ER membrane was still intact after treatment with digitonin (Fig. 2). Taken together, these results indicate that both the N- and C-termini of the SARS-CoV E protein may be located in the cytoplasmic side of the cell, whereas IBV E protein adopts an $N_{exo}C_{cyto}$ topology.

3.3. Analysis of the membrane topology of SARS-CoV E protein by differential permeabilization of the plasma membrane and limited proteinase K treatment

The topology of SARS-CoV E protein on cellular membranes was further analyzed by limited proteinase K digestion

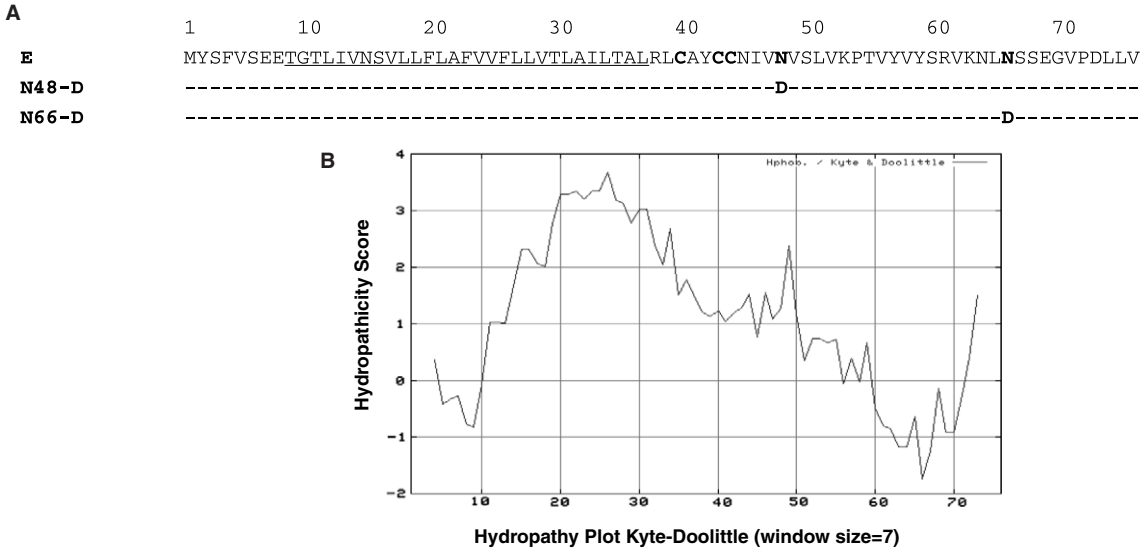

Fig. 1. Diagram of wild type and mutant SARS-CoV E constructs, and hydrophathicity score of SARS-CoV E protein. (A) Amino acid sequences of wild type and mutant SARS-CoV E protein. The amino acid sequence of the putative transmembrane domain is underlined, the three cysteine residues and the two potential glycosylation sites are indicated in bold. Also shown are the mutations introduced into each of the mutant constructs. (B) The hydropathy profile of SARS-CoV E protein determined by Kyte and Doolittle with a 7-residue window. It displays the highly hydrophobic character of this protein.

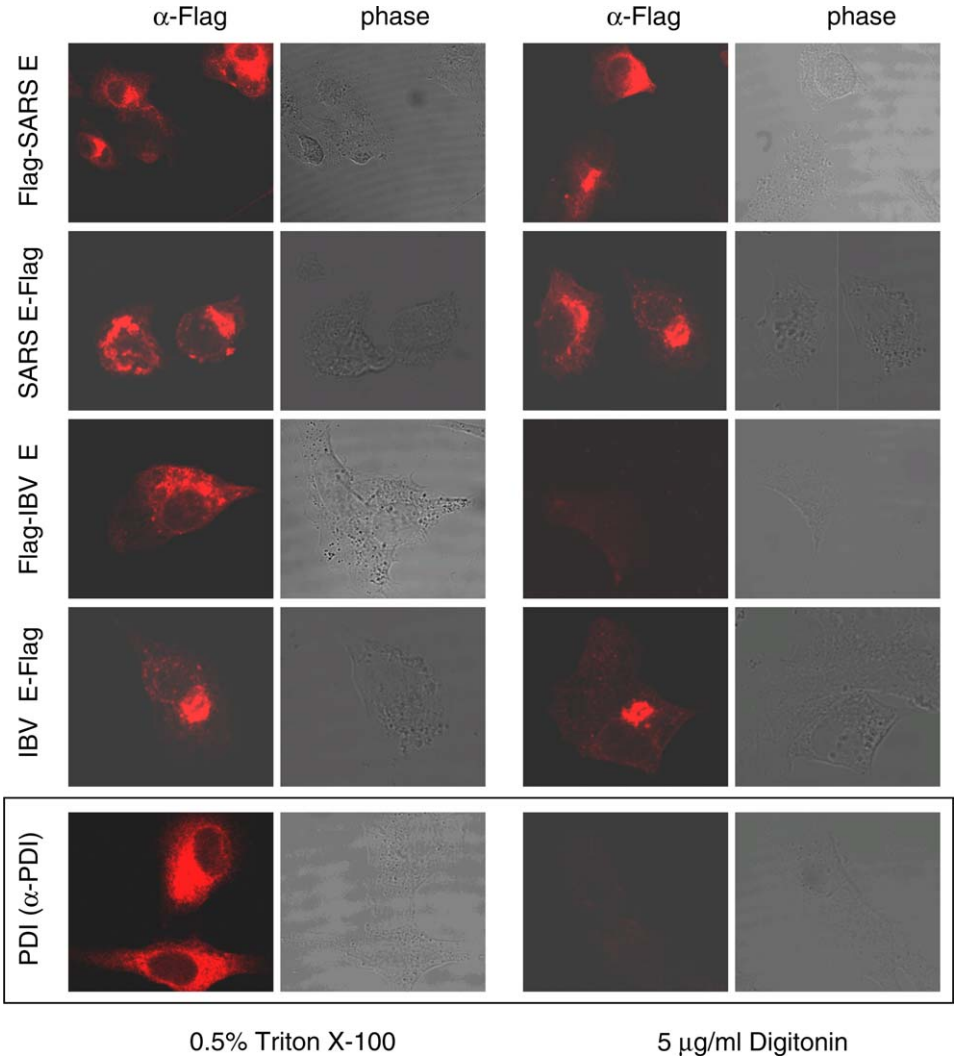

Fig. 2. Cytoplasmic exposure of the Flag epitope tagged at the N- and C-terminus of the SARS-CoV E protein and the C-terminus of the IBV E protein. HeLa cells expressing Flag-SARS E, SARS E-Flag, Flag-IBV E and IBV E-Flag, respectively, were permeabilized using either 5 μg/ml digitonin or 0.5% Triton X-100 and immunostained with anti-Flag antibody as the primary antibody and TRITC-conjugated anti-mouse IgG antibody as the secondary antibody. Untransfected HeLa cells were treated with digitonin or Triton X-100 and immunostained with anti-PDI antibody and TRITC-labeled anti-rabbit IgG secondary antibody.

of the membrane fraction prepared from cells expressing the N- or C-terminally tagged E protein. Digestion with the non-specific proteinase K would degrade proteins (or a portion of the protein) protruding from the exterior face of the microsomal membranes, while proteins (or a portion of the protein) orientated towards the lumen are protected. For this purpose, HeLa cells expressing the Flag-tagged SARS-CoV E protein at either N- or C-terminus were broken by homogenization, and the membrane fraction was collected. The membrane fraction was then divided into three aliquots: one was treated with both 1% Triton X-100 and 20 μg/ml proteinase K, one treated with 20 μg/ml proteinase K only, and one without any treatment. The total proteins were then separated by SDS–PAGE and analyzed by Western blot with anti-Flag antibody. As shown in Fig. 3, efficient detection of both N- and C-terminally tagged SARS-CoV E protein was obtained from the untreated membrane fraction (Fig. 3, lanes 1 and 4). Upon treatment of the membrane fraction with 20 μg/ml proteinase K in the presence of 1% Triton X-100, no detection of the SARS-CoV E protein was observed from cells expressing either the N- or C-terminally tagged E protein (Fig. 3, lanes 3 and 6), demonstrating that treatment with proteinase K led to the removal of the Flag tag from either terminus of the SARS-CoV E protein. Similar results were observed after treatment of the membrane fraction with 20 μg/ml proteinase K in the absence of 1% Triton X-100 (Fig. 3, lanes 2 and 5). However, prolonged exposure of the same gel showed detection of minor amounts of the E protein in the same fractions (data not shown).

In cells expressing the N- and C-terminally tagged IBV E protein, the protein was clearly detected in the membrane fraction without treatment with Triton X-100 and proteinase K (Fig. 3, lanes 7 and 10). Treatment of the membrane fraction with 20 μg/ml proteinase K resulted in the detection of a fragment of approximately 10 kDa representing the N-terminal region of the IBV E protein (Fig. 3, lane 8). Upon treatment of the membrane fraction with 1% Triton X-100 and 20 μg/ml proteinase K, the IBV E protein was no longer detected (Fig. 3, lane 9). In cells expressing the C-terminally tagged

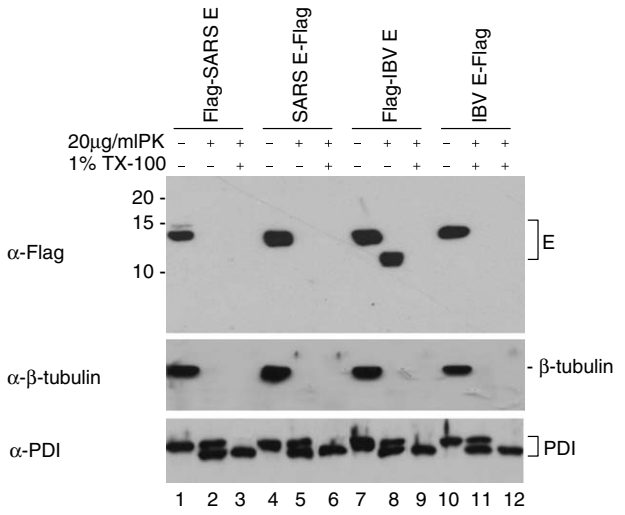

Fig. 3. Limited proteinase K digestion of microsomal membranes prepared from cells expressing the SARS-CoV and IBV E protein tagged with the Flag epitope at the N- and C-termini, respectively. Intact microsomes were isolated from cells expressing Flag-SARS E, SARS E-Flag, Flag-IBV E and IBV E-Flag, and subjected to digestion by proteinase K in the absence (lanes 2, 5, 8, 11) or presence (lanes 3, 6, 9, 12) of Triton X-100. The proteinase K-treated samples were separated on SDS–17.5% polyacrylamide gel and analyzed by Western blot. PDI (an ER luminal protein) was detected by anti-PDI antibody (Santa Cruz), and β-tubulin (a cytosolic protein) was detected by anti-β-tubulin antibody (Santa Cruz). Numbers on the left indicate molecular masses in kilodaltons.

IBV E protein, the protein was not detected after treatment of the membrane fraction with proteinase K in the presence or absence of Triton X-100 (Fig. 3, lanes 10–12). Consistent with the immunofluorescence data, these results reinforce the conclusion that the N-terminus of the IBV E protein was located in the lumen of the ER and the Golgi apparatus.

As an internal control for the integrity of microsomal membranes after limited proteolytic digestion, the detection of PDI was included in the experiment. As shown in Fig. 3, the full-length PDI was detected in the membrane fraction before and after treatment with 20 μg/ml proteinase K in the absence of 1% Triton X-100 (lanes 1, 2, 4, 5, 7, 8, 10 and 11). In addition, a shorter form of the protein was also detected in the membrane fraction after treatment with 20 μg/ml proteinase K in the absence of 1% Triton X-100 (lanes 2, 5, 8 and 11). In the presence of 1% Triton X-100, treatment of the membrane fraction with proteinase K showed that no full-length PDI was detected (Fig. 3, lanes 3, 6, 9 and 12). However, the shorter form of PDI was still detected (Fig. 3, lanes 3, 6, 9 and 12), suggesting that it may represent a proteinase K-resistant fragment of PDI. The fact that the shorter form of PDI was detected in the membrane fraction after treatment with 20 μg/ml proteinase K in the absence of 1% Triton X-100 suggests that the procedure used to prepare the membrane fraction may result in partial disruption of the microsomes. In the same experiment, β-tubulin was also included as an internal control for the degradation of cytosolic proteins. The protein was degraded by the treatment with 20 μg/ml proteinase K in the presence or absence of Triton X-100 (Fig. 3). Together with the immunofluorescence studies, these results confirm that both the N-terminus and C-terminus of SARS-CoV E are cytosolic with an orientation of $N_{cyto}C_{cyto}$.

3.4. Glycosylation of SARS-CoV E protein

Examination of the SARS-CoV E protein sequence showed the presence of two potential N-linked glycosylation sites on asparagine 48 (N48) and 66 (N66) (Fig. 1A). If the protein adopted a sole $N_{cyto}C_{cyto}$ topology, glycosylation at the two positions would not occur. However, multiple bands were usually detected when the protein was expressed in different systems, suggesting that it may undergo posttranslational modifications. To address the possibility that the protein may be modified by N-linked glycosylation, mutations were introduced into the E protein to change the predicted N-linked glycosylation sites from asparagine to aspartic acid. Two mutants, N48-D and N66-D, were generated and expressed (Fig. 1A). Western blot analysis of cells expressing wild type and the N48-D mutant showed the detection of three bands on an SDS–17.5% polyacrylamide gel (Fig. 4A, lanes 1 and 2). These may represent three isoforms of the E protein. In cells expressing the N66-D mutant, only two bands were detected; the most slowly migrating species of the three isoforms was not observed (Fig. 4A, lane 3).

To analyze further the N-linked glycosylation of the E protein, cells expressing wild type (Fig. 5B, lanes 1 and 2) and mutant E (Fig. 4B, lanes 3–6) were lysed. The total cell lysates were first treated with the N-linked glycosidase PNGaseF, and analyzed by Western blot with anti-E polyclonal antibodies. In cells expressing wild type and the N48-D mutant E protein, the protein was separated into two major bands in the gel system used (Fig. 4B, lanes 1 and 3). Treatment of the same total cell lysates led to the removal of the upper band (Fig. 4B, lanes 2 and 4), confirming that it represents the glycosylated form of the protein. In this gel system, the two unglycosylated isoforms of wild type SARS-CoV E protein were not well separated, so three major bands were detected with Flag-SARS E but only two major bands detected with wild type SARS-CoV E. In addition, a minor species of approximately 20 kDa, representing the dimeric form of the protein, was observed in cells expressing the two constructs (Fig. 4B, lanes 1–4). In cells expressing the N66-D mutant, the glycosylated form was not detected either before or after treatment with PNGaseF (Fig. 4B, lanes 5 and 6). Interestingly, in cells expressing this mutant E protein, more dimeric form and a species representing trimers of the E protein were detected (Fig. 4B, lanes 5 and 6). It suggests that this mutant E protein tends to form multimers or aggregates. As a control, cells expressing IBV E protein were treated with the same glycosidase. The protein was detected as a single band in total cell lysates with or without PNGaseF treatment (Fig. 4B, lanes 7 and 8). In cells expressing the Flag-tagged E protein, this treatment resulted in the disappearance of the most slowly migrating species of the three isoforms (Fig. 4B, lanes 9 and 10), further confirming that it is the glycosylated form of the E protein. It was noted that the pattern of the Flag-tagged E protein present in this figure was different from that in Fig. 3. This is because that much more materials were loaded and prolonged electrophoresis of the gel was applied in order to separate well and to detect clearly the minor glycosylated form of the protein. These results demonstrate that a minor proportion of the SARS-CoV E protein is modified by N-linked glycosylation and the N66 residue is the site for this modification. More importantly, it suggests that this portion of the SARS-CoV E protein would assume a different membrane topology from the majority of

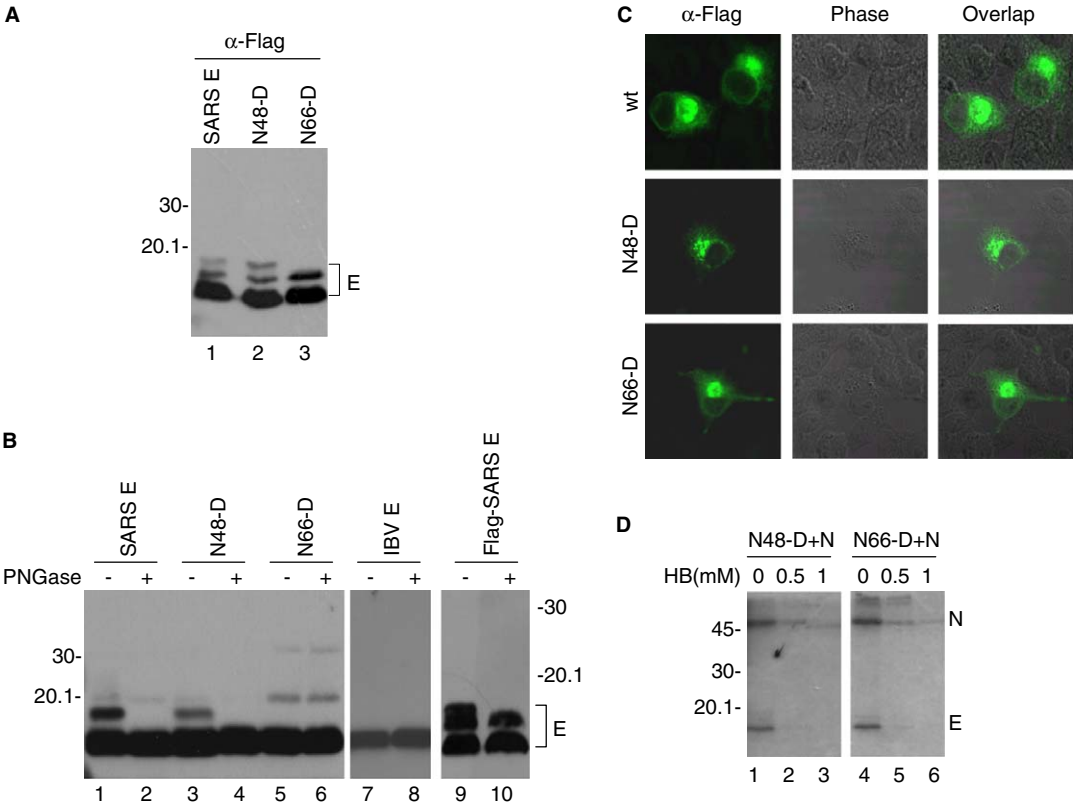

Fig. 4. N-linked glycosylation of SARS-CoV E protein. (A) HeLa cells were transfected with the Flag-tagged wild type (lane 1) and three mutant constructs containing mutations of the N48 (lane 2) and N66 (lane 3). Cell lysates were prepared 24 h posttransfection, polypeptides were separated by SDS–PAGE and analyzed by Western blot using the anti-Flag antibody. Numbers on the left indicate molecular masses in kilodaltons. (B) Total cell lysates prepared from HeLa cells expressing wild type SARS-CoV E (lanes 1 and 2), N48-D (lanes 3 and 4), N66-D (lanes 5 and 6), wild type IBV E (lanes 7 and 8) and the Flag-tagged SARS-CoV E (lanes 9 and 10) were treated either with (lanes 2, 4, 6, 8 and 10) or without (lanes 1, 3, 5, 7, and 9) PNGase F. Polypeptides were separated by SDS–PAGE and analyzed by Western blot using anti-SARS-CoV E antibodies (lanes 1–6), anti-IBV E (lanes 7 and 8) or anti-Flag (lanes 9 and 10). Numbers on the left indicate molecular masses in kilodaltons. (C) Subcellular localization of the Flag-tagged wild type SARS-CoV E, N48-D and N66-D. BHK cells expressing the Flag-tagged wild type and mutant E protein were stained with anti-Flag antibodies at 12 h posttransfection after permeabilizing with 0.2% Triton X-100. (D) Entry of hygromycin B into HeLa cells expressing wild type and mutant E proteins. HeLa cells expressing N48-D (lanes 1–3) and N66-D (lanes 4–6), respectively, were treated with 0, 0.5 and 1 mM of hygromycin B for 30 min at 12 h posttransfection, and radiolabelled with [^{35}S] methionine–cysteine for 3 h. Cell lysates were prepared and the expression of E protein was detected by immunoprecipitation with anti-Flag antibody under mild washing conditions. SARS-CoV N protein was co-expressed with wild type and mutant E protein, and the expression of N protein was detected by immunoprecipitation with polyclonal anti-N antibodies. Polypeptides were separated by SDS–PAGE and visualized by autoradiography. Numbers on the left indicate molecular masses in kilodaltons.

the E protein, i.e., the C-terminal region of the protein would be located in the lumen of the ER and the Golgi apparatus.

The effects of these mutations on the subcellular localization of E protein were then analyzed. As shown in Fig. 4C, expression of the Flag-tagged SARS-CoV E protein in BHK cells stably expressing the T7 RNA polymerase [3] showed that the protein mainly located in the perinuclear region. The two mutant proteins also displayed very similar localization patterns (Fig. 4C). These results demonstrated that mutation of the glycosylation site of the protein does not affect the membrane association and subcellular localization patterns of the protein.

As the N66-D mutant tends to form multimers or aggregates, it would be interesting to test if this mutation could affect the membrane-permeabilizing activity of the SARS-CoV E protein. For this purpose, the Flag-tagged constructs were expressed in HeLa cells. At 12 h post-transfection, cells were treated with two different concentrations of hygromycin B for 30 min, and then radiolabeled with [^{35}S] methionine–cysteine for 3 h. Cell extracts were prepared and the expression of E protein was detected by immunoprecipitation with anti-Flag antibody. As shown in Fig. 4D, this mutation did not obviously affect the membrane-permeabilizing activity of the E protein. A very similar degree of inhibition of protein synthesis was observed in cells expressing both N-48-D and N-66-D constructs (Fig. 4D).

3.5. Cell surface expression of the SARS-CoV E protein

Immunofluorescent staining of cells expressing the Flag-tagged SARS-CoV E protein at either N- or C-terminus was then carried out to test if the E protein translocated to the cell surface could be accessed by the antibody. As shown in Fig. 5, immunofluorescent staining of HeLa cells expressing the N-terminally Flag-tagged IBV E using anti-Flag antibody exhibit typical cell surface staining. In cells expressing SARS-CoV E protein with the Flag epitope tagged at either N- or C-terminus, no cell with obvious positive staining was detected (Fig. 5). However, cells with a few fluorescent dots on the surface were consistently observed (Fig. 5).

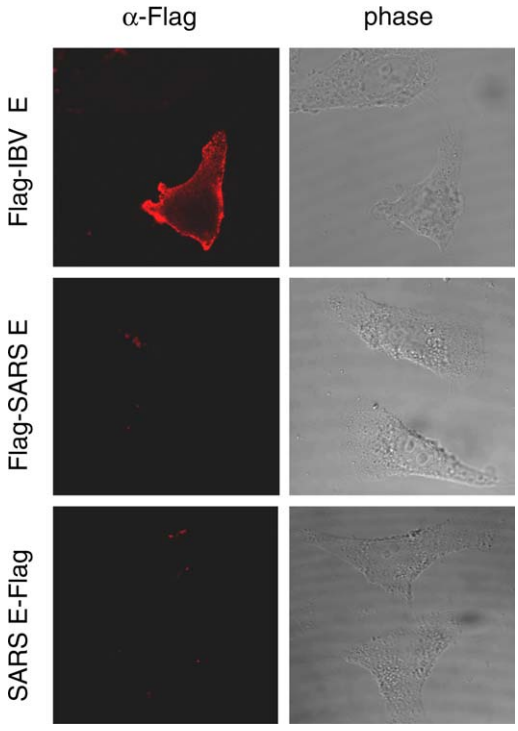

Fig. 5. Surface staining of HeLa cells expressing the SARS-CoV E protein with Flag tagged at the N- and C-terminus, respectively, and IBV E protein with the Flag tagged at the N-terminus. HeLa cells expressing Flag-SARS E, SARS E-Flag and Flag-IBV E, respectively, were immunostained with anti-Flag antibody as the primary antibody and TRITC-conjugated anti-mouse IgG antibody as the secondary antibody.

4. Discussion

Coronaviruses encode a small integral membrane protein that is associated with the viral envelope and plays important functions in virion assembly and morphogenesis [19,30]. Recently, the E protein from SARS-CoV and MHV was shown to enhance the membrane permeability of bacterial and mammalian cells to small molecules [14,15,18]. SARS-CoV E protein contains a putative long transmembrane domain of 29 amino acid residues. Based on the distribution of the charged amino acids flanking the transmembrane domain and the recent observation that the E protein is palmitoylated on all three cysteine residues [15], the protein may insert into the ER and Golgi membranes with an $N_{exo(lum)}C_{cyto}$ orientation. In vitro results reported by Arbely et al. suggest that the transmembrane domain of SARS-CoV may adopt a highly unusual topology, consisting of a short transmembrane helical hairpin that forms an inversion about a previously unidentified pseudo-centre of symmetry [2], although this is in contrast with simulation results based on phylogenetic data [28]. In the present study, the membrane topology of the SARS-CoV E protein is systematically studied with N- and C-terminally Flag-tagged SARS-CoV E protein. As the Flag tag does not affect the release of E-containing vesicles and virus-like particles (data not shown), and the permeabilizing activity of the protein, it is assumed that the Flag-tagged E protein is functionally active. Immunofluorescent staining of cells differentially permeabilized with detergents and proteinase K protection assay revealed that both the N- and C-termini of the SARS-CoV E protein are exposed to the cytoplasmic side of the membranes ($N_{cyto}C_{cyto}$) (see Fig. 6A). Two potential forms are proposed (Fig. 6A, forms (1) and (2)). Based on Arbely et al. [2], the SARS-CoV E protein may assume the form (1) topology. However, we cannot rule out the possibility that the protein may cross the membrane twice and assume the form (2) topology, based on our biophysical and molecular simulation data [28]. Consistent with previous studies, parallel experimental data presented in this study demonstrated that the IBV E protein spans the membranes once with the N-terminus exposed luminally and the C-terminus exposed cytoplasmically ($N_{exo(lum)}C_{cyto}$) (see Fig. 6A).

Interestingly, a small proportion of the SARS-CoV E protein was shown to be modified by N-linked glycosylation on the asparagine 66 residue. Glycosylation of the C-terminal region of the E protein was an unexpected finding, since no proteinase K-protected fragment was detected in the limited proteinase K assay. Nevertheless, the detection of the N-linked glycosylation at the C-terminal region and the inefficient synthesis of the glycosylated form suggest that the SARS-CoV E protein may have an alternative membrane topology. Two possible models for this alternative membrane topology of the SARS-CoV E protein were proposed (Fig. 6B). In the first case, the protein may span the membranes once with an $N_{cyto}C_{exo(lum)}$ orientation (Fig. 6B). Alternatively, both N- and C-termini may be exposed to the luminal side of the membranes ($N_{exo(lum)}C_{exo(lum)}$) (Fig. 6B). Once again, two potential forms are proposed (Fig. 6B, form (1) and (2)). At present, we

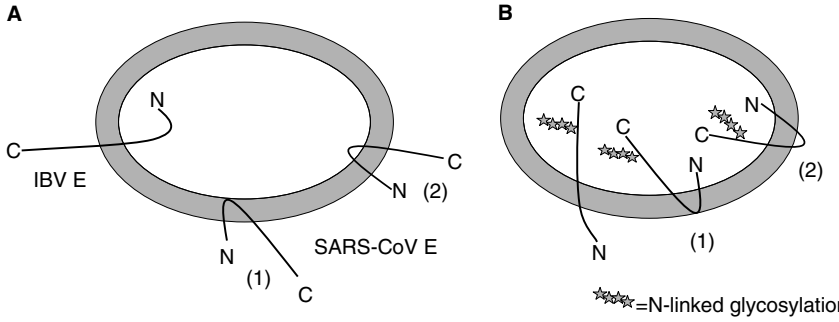

Fig. 6. Proposed membrane topologies of the unglycosylated form of the SARS-CoV E (A), the IBV E (A), and the glycosylated form of the SARS-CoV E protein (B). N and C represent the N- and C-termini of the proteins, respectively. The two potential forms of SARS-E when both the N- and C-terminal ends are located in the same side of the membrane are indicated by (1) and (2). The Asn-linked high mannose carbohydrate modification is shown at the C terminus of the two proposed forms by stars.

cannot sort out which form is more likely the membrane topology for this portion of the E protein, as neither the full-length nor a shorter form of the protein was detected in the limited proteinase K assay probably due to the reason that only a very small proportion of protein assumes this topology.

It is therefore established that the majority of the SARS-CoV E protein is inserted into cellular membranes with an $N_{cyto}C_{cyto}$ topology, but a small proportion of the protein is modified by N-linked glycosylation and inserted into the membranes with the C-terminus exposed to the luminal side. There are a few examples of viral proteins that adopt more than one membrane topology. These include the transmissible gastroenteritis coronavirus membrane protein [6], the fusion protein F from the Newcastle disease virus [21] and the adenovirus E3, a 6.7K protein [22]. As coronavirus E protein including SARS-CoV E protein is a multi-functional protein, it would be important to establish whether different topological forms are responsible for a distinct function. The SARS-CoV E protein was found to interact with Bcl-xL [32]. As this interaction was mediated by the C-terminal BH_3-like region of the E protein, it would require that the C-terminal part of the protein is exposed to the cytoplasm [32]. The C-terminal tail of the IBV E protein is important for its interaction with the M protein during virus budding [5]. It is therefore likely that the $N_{cyto}C_{cyto}$ form of the E protein may be the form that accomplishes these functions.

In the limited proteinase digestion assay, a proteinase K-resistant fragment of PDI was consistently observed. The same fragment as well as some smaller fragments was observed when PDI expressed in *E. coli* was treated with proteinase K [12], confirming that it represents a proteinase K-resistant fragment of PDI. The smaller fragments were not detected in this study may be due to fact that the antibody used was raised against the middle region of PDI from amino acids 211 to 370 only.

Most coronavirus E proteins could be translocated to the cell surface to facilitate budding and release of progeny viruses [16,17,19,27]. Recently, the E protein of SARS-CoV and MHV was found to modify membrane permeability, allowing entry of small molecules into cells and leading to cell lysis [14,15,18,31]. As cell surface expression of E protein would be essential for this function, it is quite certain that SARS-CoV must be translocated to the cell surface. In this study, however, we were unable to detect efficiently cell surface expression of the SARS-CoV E protein in cells expressing the protein under non-permeabilizing conditions. This would be an additional line of evidence that indirectly supports the conclusion that the majority of the SARS-CoV E protein adopts an $N_{cyto}C_{cyto}$ topology in cells. Interestingly, a few fluorescent dots were consistently observed in non-permeabilized cells expressing the protein. We are currently unclear if these represent the minor proportion of the SARS-CoV E protein that expresses on the cell surface and with both N- and C-termini located outside the cells.

Two of the three coronavirus membrane-associated structural proteins, M and S, are posttranslationally modified by either N- or O-linked glycosylation [23]. The fourth membrane-associated structural protein, the hemagglutinin-esterase (HE), in some coronaviruses is also a glycoprotein [23]. So far, the E protein is an apparent exception. In this study, we show that the SARS-CoV E protein is also modified by N-linked glycosylation. In N-linked glycosylation, the oligosaccharides are added to specific asparagine residues in the consensus sequence Asn-X-Ser/Thr. The minimum distance between a functional C-terminal glycosylation acceptor site and the luminal end of the transmembrane domain is 12–13 residues [24], suggesting that only the most C-proximal asparagine residue out of the two potential sites in the SARS-CoV E protein can be glycosylated. Consistent with this observation, mutagenesis studies present in this paper confirmed that only N66 is modified. Furthermore, we also show that a potential N-linked glycosylation site in the N-terminal region of the IBV E protein (N6), which is 6 amino acids upstream of the transmembrane domain, was not modified, although the N-terminal region of this protein is exposed to the luminal side of the membranes.

N-linked glycosylation affects most of the proteins present on the surface of the enveloped viruses. For this reason, it is likely to play a major role in the stability, antigenicity and other biological functions of the modified viral envelope proteins. In the early secretory pathway, the glycans also play a role in protein folding, quality control and certain sorting events. However, N-linked glycosylation seems not to affect the membrane-association and membrane-permeabilizing activity of the SARS-CoV E protein. To further characterize the functional significance of this modification, it would be interesting to test if N-linked glycosylation of SARS-CoV E protein can also be detected in virus-infected cells and in purified virions. As the N66 residue is not conserved in the E protein of other coronaviruses, it is likely that this modification may render unique features to the SARS-CoV E protein. Further exploration of the functions and effects of this modification on SARS-CoV E protein using an infectious cloning system may shed new light on the molecular biology and pathogenesis of SARS-CoV.

Acknowledgement: This work was supported by the Agency for Science Technology and Research, Singapore and a grant from the Biomedical Research Council (BMRC 03/1/22/17/220).

References

[1] An, S., Chen, C.J., Yu, X., Leibowitz, J.L. and Makino, S. (1999) Induction of apoptosis in murine coronavirus-infected cultured cells and demonstration of E protein as an apoptosis inducer. J. Virol. 73, 7853–7859.
[2] Arbely, E., Khattari, Z., Brotons, G., Akkawi, M., Salditt, T. and Arkin, I.T. (2004) A highly unusual palindromic transmembrane helical hairpin formed by SARS coronavirus E protein. J. Mol. Biol. 341, 769–779.
[3] Buchholz, U.J., Finke, S. and Conzelmann, K.K. (1999) Generation of bovine respiratory syncytial virus (BRSV) from cDNA: BRSV NS2 is not essential for virus replication in tissue culture, and the human RSV leader region acts as a functional BRSV genome promoter. J. Virol. 73, 251–259.
[4] Corse, E. and Machamer, C.E. (2000) Infectious bronchitis virus E protein is targeted to the Golgi complex and directs release of virus-like particles. J. Virol. 74, 4319–4326.
[5] Corse, E. and Machamer, C.E. (2003) The cytoplasmic tails of infectious bronchitis virus E and M proteins mediate their interaction. Virology 312, 25–34.
[6] Escors, D., Camafeita, E., Ortego, J., Laude, H. and Enjuanes, L. (2001) Organization of two transmissible gastroenteritis coronavirus membrane protein topologies within the virion and core. J. Virol. 75, 12228–12240.
[7] Fuerst, T.R., Niles, E.G., Studier, F.W. and Moss, B. (1986) Eukaryotic transient-expression system based on recombinant vaccinia virus that synthesizes bacteriophage T7 RNA polymerase. Proc. Natl. Acad. Sci. USA 83, 8122–8126.
[8] Godet, M., L'Haridon, R., Vautherot, J.F. and Laude, H. (1992) TGEV corona virus ORF4 encodes a membrane protein that is incorporated into virions. Virology 188, 666–675.

[9] Ho, Y., Lin, P.H., Liu, C.Y., Lee, S.P. and Chao, Y.C. (2004) Assembly of human severe acute respiratory syndrome coronavirus-like particles. Biochem. Biophys. Res. Commun. 318, 833–838.
[10] Jones, D.T., Taylor, W.R. and Thornton, J.M. (1994) A model recognition approach to the prediction of all-helical membrane protein structure and topology. Biochemistry 33, 3038–3049.
[11] Khattari, Z., Brotons, G., Akkawi, M., Arbely, E., Arkin, I.T. and Salditt, T. (2005) SARS coronavirus E protein in phospholipid bilayers: a X-ray scattering study. Biophysical. J. BioFAST, doi:10.1529/biophysj.105.072892.
[12] Koivunen, P., Salo, K.E., Myllyharju, J. and Ruddock, L.W. (2005) Three binding sites in protein-disulfide isomerase cooperate in collagen prolyl 4-hydroxylase tetramer assembly. J. Biol. Chem. 280, 5227–5235.
[13] Krogh, A., Larsson, B., Von, H.G. and Sonnhammer, E.L. (2001) Predicting transmembrane protein topology with a hidden Markov model: application to complete genomes. J. Mol. Biol. 305, 567–580.
[14] Liao, Y., Lescar, J., Tam, J.P. and Liu, D.X. (2004) Expression of SARS-coronavirus envelope protein in *Escherichia coli* cells alters membrane permeability. Biochem. Biophys. Res. Commun. 325, 374–380.
[15] Liao, Y., Yuan, Q., Torres, J., Tam, J.P. and Liu, D.X. (2006) Biochemical and functional characterization of the membrane association and permeabilizing activity of the severe acute respiratory syndrome coronavirus envelope protein. Virology, [Epub ahead of print].
[16] Lim, K.P. and Liu, D.X. (2001) The missing link in coronavirus assembly: retention of the avian coronavirus infectious bronchitis virus envelope protein in the pre-Golgi compartments and physical interaction between the envelope and membrane proteins. J. Biol. Chem. 276, 17515–17523.
[17] Liu, D.X. and Inglis, S.C. (1991) Association of the infectious bronchitis virus 3c protein with the virion envelope. Virology 185, 911–917.
[18] Madan, V., Garcia, M.J., Sanz, M.A. and Carrasco, L. (2005) Viroporin activity of murine hepatitis virus E protein. FEBS Lett. 579, 3607–3612.
[19] Maeda, J., Maeda, A. and Makino, S. (1999) Release of coronavirus E protein in membrane vesicles from virus-infected cells and E protein-expressing cells. Virology 263, 265–272.
[20] Maeda, J., Repass, J.F., Maeda, A. and Makino, S. (2001) Membrane topology of coronavirus E protein. Virology 281, 163–169.
[21] McGinnes, L.W., Reitter, J.N., Gravel, K. and Morrison, T.G. (2003) Evidence for mixed membrane topology of the newcastle disease virus fusion protein. J. Virol. 77, 1951–1963.
[22] Moise, A.R., Grant, J.R., Lippe, R., Gabathuler, R. and Jefferies, W.A. (2004) The adenovirus E3-6.7K protein adopts diverse membrane topologies following posttranslational translocation. J. Virol. 78, 454–463.
[23] Nal, B., Chan, C., Kien, F., Siu, L., Tse, J., Chu, K., Kam, J., Staropoli, I., Crescenzo-Chaigne, B., Escriou, N., van der, W.S., Yuen, K.Y. and Altmeyer, R. (2005) Differential maturation and subcellular localization of severe acute respiratory syndrome coronavirus surface proteins S, M and E. J. Gen. Virol. 86, 1423–1434.
[24] Nilsson, I.M. and Von, H.G. (1993) Determination of the distance between the oligosaccharyltransferase active site and the endoplasmic reticulum membrane. J. Biol. Chem. 268, 5798–5801.
[25] Plutner, H., Davidson, H.W., Saraste, J. and Balch, W.E. (1992) Morphological analysis of protein transport from the ER to Golgi membranes in digitonin-permeabilized cells: role of the P58 containing compartment. J. Cell Biol. 119, 1097–1116.
[26] Raamsman, M.J., Locker, J.K., de Hooge, A., de Vries, A.A., Griffiths, G., Vennema, H. and Rottier, P.J. (2000) Characterization of the coronavirus mouse hepatitis virus strain A59 small membrane protein E. J. Virol. 74, 2333–2342.
[27] Smith, A.R., Boursnell, M.E., Binns, M.M., Brown, T.D. and Inglis, S.C. (1990) Identification of a new membrane-associated polypeptide specified by the coronavirus infectious bronchitis virus. J. Gen. Virol. 71, 3–11.
[28] Torres, J., Wang, J., Parthasarathy, K. and Liu, D.X. (2005) The transmembrane oligomers of coronavirus protein E. Biophys. J. 88, 1283–1290.
[29] Tusnady, G.E. and Simon, I. (1998) Principles governing amino acid composition of integral membrane proteins: application to topology prediction. J. Mol. Biol. 283, 489–506.
[30] Vennema, H., Godeke, G.J., Rossen, J.W., Voorhout, W.F., Horzinek, M.C., Opstelten, D.J. and Rottier, P.J. (1996) Nucleocapsid-independent assembly of coronavirus-like particles by co-expression of viral envelope protein genes. EMBO J. 15, 2020–2028.
[31] Wilson, L., McKinlay, C., Gage, P. and Ewart, G. (2004) SARS coronavirus E protein forms cation-selective ion channels. Virology 330, 322–331.
[32] Yang, Y., Xiong, Z., Zhang, S., Yan, Y., Nguyen, J., Ng, B., Lu, H., Brendese, J., Yang, F., Wang, H. and Yang, X.F. (2005) Bcl-xL inhibits T-cell apoptosis induced by expression of SARS coronavirus E protein in the absence of growth factors. Biochem. J. 392, 135–143.